Università della Calabria

Facoltà di Farmacia e Scienze della Nutrizione e della Salute

Dipartimento Farmaco-Biologico (MED/05 PATOLOGIA CLINICA)

Dottorato di Ricerca in "Biochimica Cellulare ed Attività dei Farmaci in Oncologia" (XXIV ciclo)

Molecular Mechanisms of FXR-mediated Growth Inhibition in Hormone-dependent Cancers

Docente Tutor
Prof.ssa Stefania Catalano

Dottorando
Dott. Salvatore Panza

Coordinatore
Prof. Diego Sisci

Anno Accademico 2010-2011

INDEX

Scientific Publication

1. Barone I, Catalano S, Gelsomino L, Marsico S, Giordano C, **Panza S**, Bonofiglio S, Bossi G, Covington KR, Fuqua S, and Andò S. Leptin as a novel mediator of tumor/stroma interaction promoter the invasive growth of breast cancer cells. Cancer Research. Revision.

2. Giordano C, Catalano S, **Panza S**, Vizza D, Barone I, Bonofiglio D, Gelsomino L,Rizza P, Fuqua S, Andò S. Farnesoid X receptor inhibits tamoxifen-resistant MCF-7 breast cancer cell growth through downregulation of HER2 expression. Oncogene. 2011 Sep 29;30(39):4129-40.

3. De Amicis F, Guido C, Perrotta I, Avena P, **Panza S**, Andò S, Aquila S. Conventional progesterone receptors (PR) B and PRA are expressed in human spermatozoa and may be involved in the pathophysiology of varicocoele: a role for progesterone in metabolism. Int J Androl. 2011 Oct;34(5 Pt 1):430-45.

4. Guido C, Perrotta I, **Panza S**, Middea E, Avena P, Santoro M, Marsico S, Imbrogno P, Andò S, Aquila S. Human sperm physiology: estrogen receptor alpha (ERα) and estrogen receptor beta (ERβ) influence sperm metabolism and may be involved in the pathophysiology of varicocele associated male infertility. J Cell Physiol. 2011 Dec;226(12):3403-12.

5. Catalano S, Malivindi R, Giordano C, Gu G, **Panza S**, Bonofiglio D, Lanzino M, Sisci D, Panno ML, Andò S. Farnesoid X receptor, through the binding with steroidogenic factor 1-responsive element, inhibits aromatase expression in tumor Leydig cells. J Biol Chem. 2010 Feb 19;285(8):5581-93.

6. Aquila S, Guido C, Laezza C, Santoro A, Pezzi V, **Panza S**, Andò S, Bifulco M. A new role of anandamide in human sperm: focus on metabolism. J Cell Physiol. 2009 Oct;221(1):147-53.

INTRODUCTION

The Farnesoid X Receptor (FXR) is an adopted member of the metabolic nuclear receptor (NR) superfamily, members of which are highly expressed in liver, intestine, kidney and adrenals (Forman, BM *et al.* 1995; Otte, K. *et al.* 2003). FXR was first isolated from a rat-liver cDNA library and named after its weak activation by supraphysiological concentrations of farnesol, an intermediate in the mevalonate biosynthetic pathway (Forman, BM *et al.* 1995). Shortly after its discovery, specific Bile Acids (BAs) that both bind to the ligand-binding domain (LBD) of the receptor and activate the transcription of FXR target genes were identified (Makishima, M. *et al.* 1999; Wang, H. *et al.* 1999). Subsequent studies have led to the identification of potent synthetic FXR agonists (Maloney, PR *et al.* 2000; Downes, M. *et al.* 2003), including GW4064, 6-ethyl chenodeoxycholic acids (6-ECDCAs) and fexaramine. Taking advantage of the availability of FXR-deficient mice (Sinal, CJ *et al.* 2000), studies with these ligands have demonstrated a critical role for FXR in regulating cholesterol and BA homeostasis (Maloney, PR *et al.* 2000; Sinal, CJ *et al.* 2000).

FXR shares the common modular structure of all members of the metabolic-NR superfamily; this structure includes a highly conserved DNA-binding domain (DBD) in the N-terminal region and a moderately conserved LBD in the C-terminal region (Pellicciari, R. *et al.* 2005). The ligand-independent activation function-1 (AF-1) and ligand-dependent activation function-2 (AF-2) are located in the N-terminal and C-terminal regions, respectively. Two cysteine-coordinated Zn^{2+} finger motifs located in the DBD are directly involved in DNA binding and dimerization. The E region is also involved in dimerization and coregulator interaction (Figure 1).

Figure 1. General structure of a nuclear receptor. A typical nuclear receptor is composed of several functional domains. The variable NH2-terminal region (A/B) contains the ligand-independent AF-1 transactivation domain. The conserved DNA-binding domain (DBD), or region C, is responsible for the recognition of specific DNA sequences. A variable linker region (D) connects the DBD to the conserved E region that contains the ligand-binding domain (LBD) as well as the dimerization surface and the ligand-dependent AF-2 within the C-terminal portion of the LBD.

There are two known FXR genes, which are commonly referred to as FXRα and FXRβ. FXRα is conserved from humans to fish (teleost fish, *Fugu rubripes*) (Maglich, JM *et al.* 2003). The single FXRα gene in humans and mice encodes four FXRα isoforms (FXRα1, FXRα2, FXRα3 and FXRα4) as a result of the use of different promoters and alternative splicing of the RNA (Huber, RM *et al.* 2002; Zhang, Y. *et al.* 2003). (Figure 2).

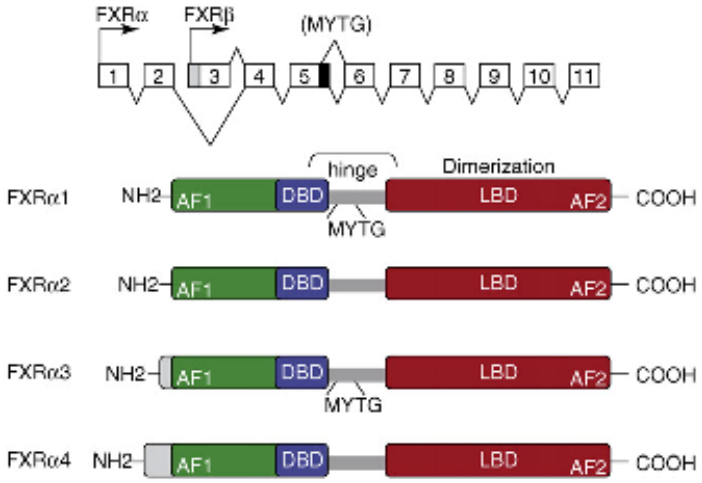

Figure 2. Schematic representation of the exon–intron organization of FXRα gene and relative protein isoforms. Distinct FXRα isoforms are generated by alternative promoter usage (arrows) and splicing (linked exons). FXRα1 and FXRα3 have an insertion of four amino acids (MYTG) in the hinge-domain region; this insertion is generated by the alternative splicing of the 12 bp at the 30 end of exon 5.

FXRα3 and FXRα4 possess an extended N terminus, which encompasses the poorly defined AF-1. In addition, FXRα1 and FXRα3 have an insert of four amino acids (MYTG) immediately adjacent to the DNA-binding domain in a region referred to as the 'hinge domain' (Figure 2).

The second FXR gene, FXRβ, encodes a functional member of the nuclear receptor family in rodents, rabbits and dogs, but is a pseudogene in human and primates (Otte, K. *et al.* 2003). FXRβ has been proposed to be a lanosterol sensor, although its physiological function remains unclear. FXRα is expressed mainly in the liver, intestine, kidney and adrenal gland, with much lower levels in adipose tissue (Forman, BM *et al*. 1995; Huber, RM *et al.* 2002; Zhang, Y. *et al*. 2003).

Like many other non-steroid hormone nuclear receptors, regulates the expression of a wide variety of target genes involved in bile acid, lipid and glucose metabolism by binding either as monomer or as a heterodimer with the Retinoid X Receptor (RXR) to FXR response element (FXREs) (Song, CS *et al.* 2001; Ananthanarayanan, M. *et al.* 2001).

FXR is an obligate partner of the 9-cis-retinoic acid receptor (RXR). The FXR/RXR heterodimer binds DNA sequences composed of two inverted repeats (IR) (AGGTCA hexanucleotide core motif spaced by one nucleotide), and can be activated by ligands for both receptors (BAs and/or 9-cis-retinoic acid). Upon ligand binding, FXR undergoes conformational changes to release corepressors such as NCor (nuclear co-repressor) and recruit coactivators such as SRC-1 (steroid receptor coactivator-1), PRMT-1 (protein arginine(R)methyl transferase-1), CARM-1 (coactivator-associated arginine(R) methyltransferase-1), PGC1α (peroxisome-proliferator-receptor (PPAR)-γ coactivator- 1a) and DRIP-205 (vitamin-D-receptor-interacting protein-205) (Figure 3) (Pellicciari, R. *et al* 2005; Rizzo, G. *et al.* 2005). The mechanism(s) that regulate recruitment of these coactivators by FXR ligands and the relevance of these molecules to the regulation of specific genes by FXR ligands is still unknown.

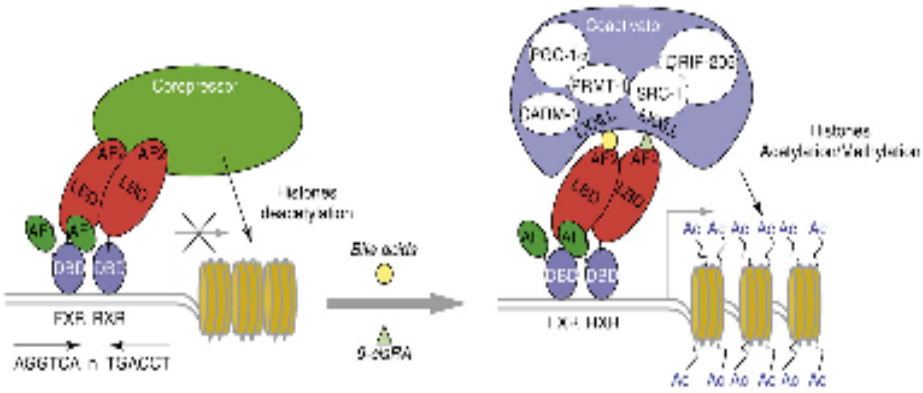

Figure 3. Coactivator and corepressor complexes are involved in FXR activation and repression, respectively. In the absence of ligand, the FXR heterodimer is associated with corepressor complexes, which recruit histone-deacetylase activities. Deacetylation of histone tails leads to chromatin compactation and transcriptional repression. Receptor activation causes the release of the corepressor complex and the AF-2-dependent recruitment of a coactivator complex that contains at least a p160 coactivator (such as SRC-1). These proteins possess histone-acetyltransferase activity that allows chromatin decompactation and gene activation. Multiple protein–protein interactions exist among the FXR and other coactivators such as PRMT-1 (protein arginine(R) methyl transferase-1) and CARM-1 (coactivator-associated arginine methyltransferase-1), which induce histone methylation, and PGC-1α (ppar-gamma coactivator-1α) and DRIP-205 (vitamin-D-receptor-interacting protein-205).

IR-1 is the primary binding sequence for FXR. FXR regulates human intestinal bile acid binding protein (IBABP), small heterodimer partner (SHP), bile salt export pump (BSEP), BA-CoA:amino acid *N*-acetyltransferase (BAT) (Shibata, M. *et al.* 1998) and phospholipid transfer protein (PLTP) via IR-1 elements in the promoters of these genes (Grober, J. *et al.* 1999; Urizar, NL *et al.* 2000). Besides IR-1, other FXREs include IR-0, direct repeat (DR), everted repeat (Huang, W. *et al.* 2006) of the core motif separated by eight nucleotides (ER-8) and monomeric binding sites (Song, CS *et al.* 2001; Laffitte, BA *et al.* 2000; Claudel, T. *et al.* 2002) (Figure 4).

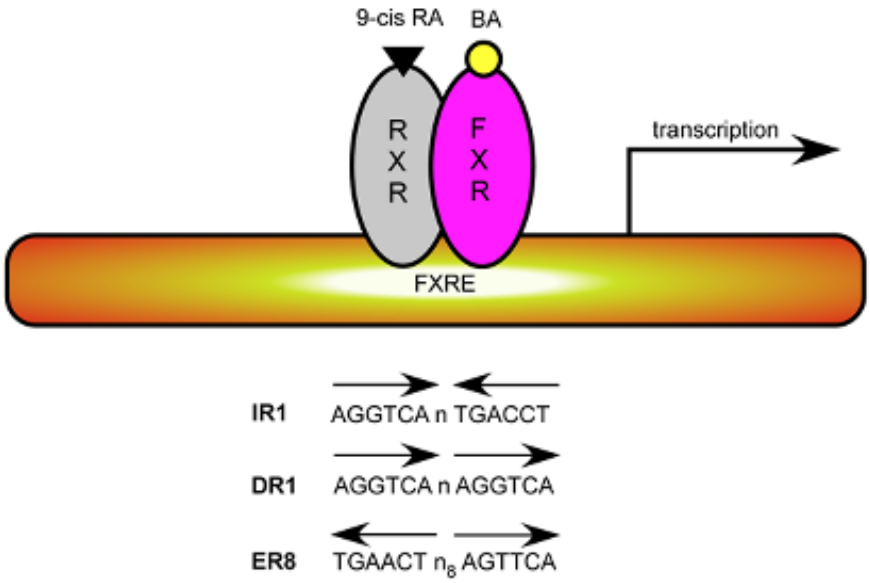

Figure 4. Upon ligand binding, FXR binds to FXR response elements (FXRE) of its target genes as a heterodimer with RXR. Examples of consensus sequences are shown.

By binding to FXREs, FXR regulates many genes belonging to different metabolic pathways. Activation of FXR modulates the expression of different groups of genes involved in BA homoeostasis, lipid metabolism, and glucose balance (Figure 5). FXR is the primary sensor of BAs. FXR activates the expression of short heterodimer partner (SHP) which interacts with other nuclear

receptors preventing their activation (Goodwin, B. *et al.* 2000; Claudel, T. *et al.* 2002; Seol, W. *et al.* 1996).

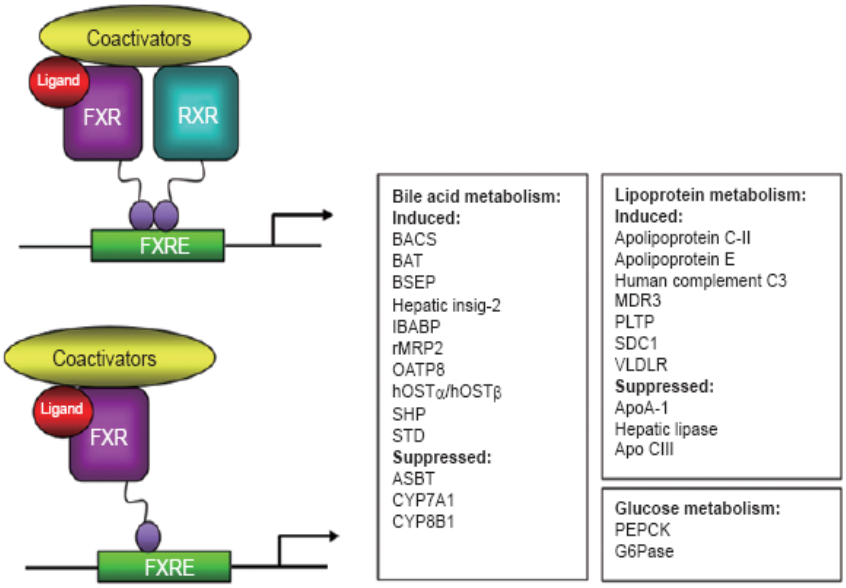

Figure 5. FXR regulates a large number of target genes involved in bile acid, lipoprotein and glucose metabolisms. FXR binds to DNA either as a heterodimer with RXR or as a monomer to regulate the expression of various genes. (Wang, YD *et al.* 2008)

Although FXR was originally identified in hepatocyte homeostasis, it has become increasingly clear that this nuclear receptor system is important in a number of different cell type and mediates diverse functions including its control in regulating cell growth and carcinogenesis (Wang, H. *et al.* 2008; Modica, S. *et al.* 2008). For instance, it has been demonstrated that FXR activation inhibits breast cancer cell proliferation and negatively regulates aromatase activity reducing local estrogen production which sustains tumor growth and progression (Swales, KE *et al.* 2006). In contrast, other authors have reported that FXR activation stimulates MCF-7 cell proliferation (Journe, F. *et al.* 2008). However, the functions of bile acid sensor FXR, in breast cancer tissue, are still not completely understood and there are no data regarding its role in endocrine resistant breast cancer phenotype.

Breast cancer evolution and progression are deeply influenced by both estrogen receptor (ER) and growth factor receptor signaling. In recent years, the field of cancer therapy has witnessed the emergence of multiple targeted strategies that

inhibit specific key molecules and pathways important for tumor growth and progression. Among them, endocrine therapy to block ER activity and signaling, the first targeted therapy in oncology, is still the most successful systemic therapy in the management of ER-positive breast cancer.

Therapeutic strategies directed at inhibiting the action of ERα using antiestrogens, such as Tamoxifen (Tam), or reducing estrogen levels using aromatase inhibitors, are the standard therapies offered to women with ERα-positive cancer. However, not all patients who have ER positive tumors respond to endocrine therapies (termed de novo resistance), and a large number of patients who do respond will eventually develop disease progression or recurrence while on therapy (acquired resistance).

Multiple mechanisms are responsible for the development of endocrine resistance. Among these are the loss of ERα expression or function (Encarnacion, CA *et al.* 1993), alterations in the balance of regulatory cofactors, increased oncogenic kinase signaling (Blume-Jensen, P. and Hunter, T. 2001), and altered expression of growth factor signaling pathways (Arpino, G. *et al.* 2004; Schiff, R. *et al.*, 2004; Sabnis, GJ *et al.* 2005; Staka, CM *et al.* 2005). For instance, several preclinical and clinical studies suggest that both *de novo* and acquired resistance to Tam in breast cancers can be associated with elevated levels of the membrane tyrosine kinase HER2 (c-ErbB2, Her2/neu) (Chung, YL *et al.*, 2002; Meng, S. *et al.* 2004; Shou, J. *et al.* 2004; Gutierrez, MC *et al.* 2005).

The HER2 gene codes for a 185 kDa receptor, a member of the EGFR family of transmembrane tyrosine kinases, which also includes HER3 and HER4, mainly involved in signal transduction pathways that regulate cell growth and differentiation (Figure 6). This receptor has no ligand of its own, but is activated by hetero-oligomerization with other ligand-activated receptors (Yarden, Y. 2001). The HER2 gene is amplified and/or overexpressed in 20-25% of ERα-positive breast cancers (Slamon, DJ *et al.* 1989), and clinical observations indicate that tumors with high levels of HER2 have poor outcome when treated with Tam (Osborne, CK *et al.* 2003; Kirkegaard, T. *et al.* 2007).

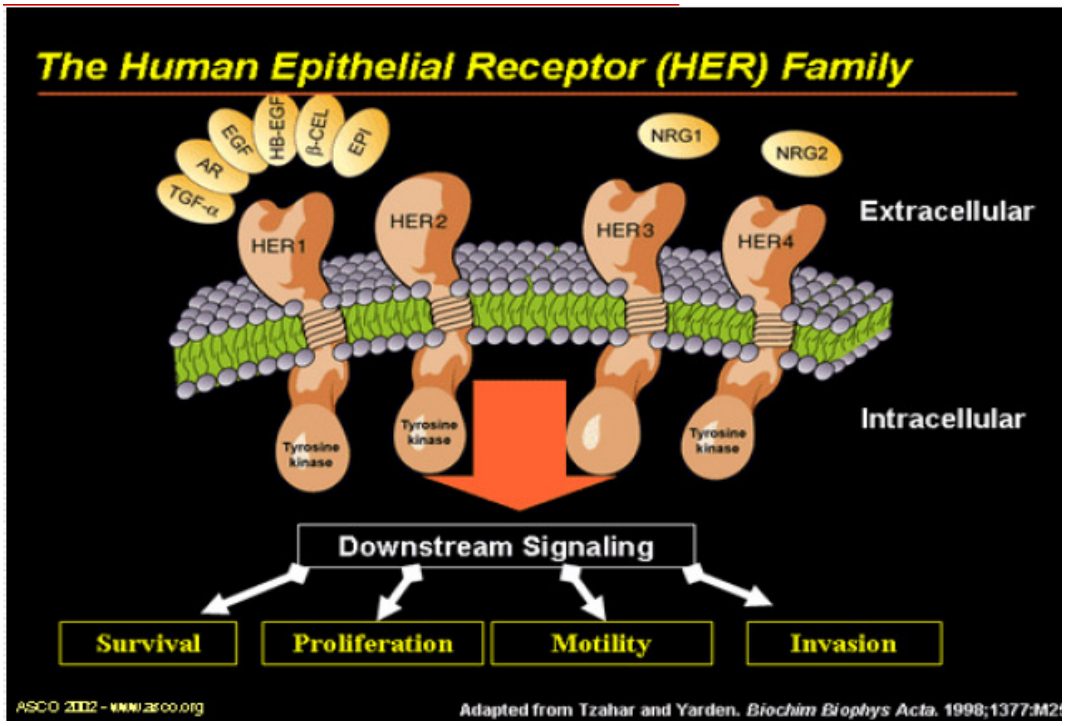

Figure 6. Schematic representation of the Human Epithelial Receptor (HER) Family.

The mechanisms by which HER2 overexpression mediates Tam resistance result from an intimate crosstalk between ERα and growth factor receptors kinase cascades, such as Ras/MAPK signaling, that in turn can promote growth and

progression in breast cancer cells, negating the inhibitory effects of Tam on nuclear ERα activity (Arpino, G. *et al.* 2008). HER2 overexpression is not attributed solely to amplification of the HER2 gene copy number, but can also occur from a single-copy gene due to deregulation events at the transcriptional level (Hurst, HC 2001). Thus an analysis of new mechanisms controlling HER2/neu receptor gene expression could be important to enhance strategies to reverse Tam resistance in breast cancer patients.

On the basis of all these observations, in the first part of our study, we investigated whether activated FXR may modulate the growth of human MCF-7 Tam-resistant breast cancer cells, a model that was developed to mimic *in vitro* the occurrence of acquired Tam resistance.

More recently, FXR was identified in normal rodent testis and in Leydig tumor cell lines (Catalano, S. *et al.* 2010). Leydig cell tumors comprise about 3% of all testicular neoplasms. Although rare, they are the most common tumors of the gonadal stroma (Hawkins, C. *et al.* 1996). In most cases, Leydig cell tumors are benign, however, if the tumor is malignant, no effective treatments are currently available.

We previously demonstrated that FXR activation exerts anti-proliferative effects on tumor Leydig cells at least in part through an inhibition of estrogen-dependent cell growth. Indeed, we evidenced, in rat tumor Leydig cells R2C that chenodeoxycholic acid (CDCA) and a synthetic agonist GW4064 downregulate aromatase expression at both mRNA and protein levels, together with the inhibition of its enzymatic activity (Catalano, S. *et al.* 2010). Thus, in the second part of the present study we evaluated whether FXR ligands can inhibit tumor Leydig cell growth using xenografts model and elucidated the possible molecular mechanism underlying these effects.

MATERIALS AND METHODS

Reagents and Antibodies

Dulbecco's Modified Eagle's Medium (DMEM), Nutrient Mixture F-10 Ham, L-glutamine, penicillin, streptomycin, fetal bovine serum (FBS), horse serum (HS), MTT, 4-Hydroxytamoxifen, CDCA and EGF were from Sigma (Milan, Italy), GW4064 by Tocris. TRIzol by Invitrogen (Carlsbad, CA,). FuGENE 6 by Roche Applied Science (Indianapolis, IN, USA). TaqDNA polymerase, RETROscript kit, Dual Luciferase kit, TNT master mix, and NF-kB protein were from Promega (Madison, WI). SYBR Green Universal PCR Master Mix by Biorad (Hercules, CA, USA). Antibodies against FXR, EGFR, β-Actin, Cyclin D1, p65, Lamin B, p53, p21, PARP, by Santa Cruz Biotechnology (Santa Cruz, CA), MAPK, phosphorylated p42/44 MAPK (Thr^{202}/Tyr^{204}), phosphorylated HER2 (Tyr^{1248}) from Cell Signaling Technology (Beverly, MA), HER2 from NeoMarker (Fremont, CA), antibody against Aromatase by Serotec (Raleigh, NC, USA). ECL system and Sephadex G-50 spin columns from Amersham Biosciences (Buckinghamshire, UK). [γ^{32}P]ATP from PerkinElmer (Wellesley, MA, USA).

Plasmids

The plasmid pNeuLite containing promoter region of human HER2/neu was kindly provided by Dr. Mien-Chie Hung (University of Texas M.D. Anderson Cancer Center, Houston, TX, USA). The FXR responsive reporter gene (FXRE-IR1) and FXR-DN (dominant negative) expression plasmids were provided from Dr. T.A. Kocarek (Institute of Environmental Health Sciences, Wayne State University, USA) (Kocarek, TA *et al.* 2002). FXR expression plasmid was provided from Dr. D.J. Mangelsdorf (Southwestern Medical Center, TX, USA).

The deletion of AP-1 sequence in the promoter construct was generated by PCR using as template the pNeulite plasmid with the following primers: forward 5'-GATAAGTGTGAGAACGGCTGCAGGC- 3' and reverse 5'-GGGCAGATCTGGTTTTCCGGTCCCAATGGA- 3'. The amplified DNA fragment was digested with BglII and KpnI and ligated into pGL2-Basic vector.

The resulting plasmid encoding the HER2 promoter containing the desired deletion was designated ΔAP-1. The desired deletion was confirmed by DNA sequencing.

The p53 promoter-luciferase reports, constructed using pGL2 for cloning of p53-1 and -6, and TpGL2 for p53-13 and -14 were kindly provided by Dr. Stephen H. Safe (Texan A&M University, College Station, TX). The constructs used were generated by Safe (Qin, C. *et al.* 2002) from the human p53 gene promoter as follows: p53-1 (containing the -1800 to + 12 region), p53-6 (containing the -106 to + 12 region), p53-13 (containing the -106 to - 40 region) and p53-14 (containing the -106 to - 49 region).

Site-directed mutagenesis

The pNeulite promoter plasmid-bearing NF-kB–responsive element mutated site (NF-kB mut) was created by site-directed mutagenesis using Quick Change kit (Stratagene, La Jolla, CA) according to manufacturer's method. We used as template the pNeulite plasmid and the following mutagenic primers (mutations are shown as lowercase letters): 5'-AGAGAGGGAGAAAGTGAAGCTaatcGTTGCCGACTCCCAGACTTCG- 3' and 5'-CGAAGTCTGGGAGTCGGCAACgattAGCTTCACTTTCTCCCTCTCT-3'. The desired mutation was confirmed by DNA sequencing.

Cell culture

Breast cancer epithelial cell line MCF-7 were cultured in DMEM medium containing 10% FBS, 1% L-glutamine, 1% Eagle's nonessential amino acids, and 1 mg/ml penicillin-streptomycin at 37 °C with 5% CO_2 air. MCF-7 TR1 and MCF-7 TR2 cells were generated in the laboratory of Dr. Fuqua. Cells were cultured in MEM with 10% FBS, 6 ng/ml insulin, penicillin (100 U/ml), streptomycin (100 μg/ml), and adding 4-hydroxytamoxifen in 10-fold increasing concentrations every 4 weeks. Cells were thereafter routinely maintained with 10^{-6} M (MCF-7 TR1) and 10^{-7}M (MCF-7 TR2) of 4-hydroxytamoxifen.

SKBR3 cells were cultured in phenol red-free RPMI medium containing 10% FBS, 1% L-glutamine, 1% Eagle's nonessential amino acids, and 1 mg/ml penicillin-streptomycin.

MCF-10A normal breast epithelial cells were grown in Dulbecco's modified Eagle's medium-F12 plus glutamax containing 5% horse serum, 1 mg/ml penicillin-streptomycin, 0.5 μg/ml hydrocortisone, and 10 μg/ml insulin.

MCF-7/HER2-18 were kindly provided by Dr. Schiff (Baylor College of Medicine, Houston, TX, USA) and maintained in DMEM with 10% FBS, 6 ng/ml insulin, penicillin (100 U/ml), streptomycin (100 μg/ml), 0.4% Geneticin, (Shou, J. *et al.* 2004).

Rat Leydig tumor cells (R2C) were cultured in Ham/F-10 supplemented with 15% HS, 2.5% FBS, and 1 mg/ml penicillin-streptomycin.

Before each experiment, cells were grown in phenol red-free media, containing 5% charcoal-stripped foetal bovine serum (cs-FBS) for 2 days and then treated as described.

Cell proliferation assays

MTT anchorage-dependent growth assay. Cell viability was determined by using 3-(4,5-Dimethylthiazol-2-yl)-2,5-Diphenyltetrazolium Bromide Analysis. MCF-7, MCF-7 TR1, MCF-10 and SKBR3 cells (20000/well) were treated with Tamoxifen (Tam), Chenodeoxycholic acid (CDCA), GW4064 and Epidermal Growth Factor (EGF) as indicated. At the end of the incubation with different treatments, 3-[4,5-dimethylthiazol-2-yl]-2,5-diphenyltetrazolium bromide (MTT) was added to each well and incubated at 37 °C and 5% CO_2 for 2h followed by medium removal and solubilisation in 500 μl DMSO. The resulting colour change was read at 570 nm and calculated as absorbance above background. The absorbance readings of a minimum of three experiments, contained 4 different doses of CDCA and GW4064 in triplicate, was combined for IC50 calculations using GraphPad Prism 4 (GraphPad Software, Inc., San Diego, CA). Briefly, values were log-trasformed, then normalized, and nonlinear regression analysis was used to generate a sigmoidal dose-respose curve to calculate IC50 values for each cell line. In a set of experiments cells were transiently transfected with the FXR-DN plasmid for 24h before starting with the treatments.

Anchorage-independent soft agar growth assays. Cells (25000/well) were plated in 4 ml of 0.35% agarose with 5% charcoal-stripped FBS in phenol red-free media, in a 0.7% agarose base in six-well plates. Two days after plating, media containing control vehicle or treatments was added to the top layer, and the media was replaced every two days. After 14 days, 150 µl of MTT was added to each well and allowed to incubate at 37°C for 4h. Plates were then placed in 4°C overnight and colonies > 50 µm diameter from triplicate assays were counted. Data are the mean colony number of three plates and representative of two independent experiments analyzed for statistical significance ($p<0,05$) using a two-tailed student's Test, performed by Graph Pad Prism 4. Standard deviations are shown.

R2C Xenograft Models

The experiments in vivo were done in 45 days old nude mice (nu/nu Swiss; Charles River, Milan, Italy). At day 0 mice were inoculated with R2C cells (1.0 x 10^5 mice) into the intrascapular region. GW4064 treatment was started 12 days later after tumors established. GW4064 was delivered daily to the animals by i.p. injection using corn oil as carrier. The treatment was done for 13 days. Tumor growth was followed twice a week by calliper measurements along two orthogonal axes: length (L) and width (W). The tumor volume (V) was estimated by the following formula: $V= L \times (W)^2/2$. At the time of killing, 25 days, tumors were dissected out from the neighboring connective tissue, frozen in nitrogen, and stored at -80 °C. All the procedures involving animals and their care have been conducted in conformity with the institutional guidelines at the Laboratory of Molecular Oncogenesis, Regina Elena Cancer Institute in Rome.

Immunoprecipitation and immunoblot analysis

MCF-7, MCF-7 TR1, SKBR3 and R2C cells were grown to 50–60% confluence and treated as indicated before lysis in 500µl of 50 mM Tris-HCl, 150 mM NaCl, 1% NP-40, 0.5% sodium deoxycholate, 2 mM sodium fluoride, 2 mM EDTA, 0.1% SDS, containing a mixture of protease inhibitors (aprotinin, phenylmethylsulfonyl fluoride, and sodium orthovanadate) for protein extraction. The nuclear protein were lysed with the buffer containing 20 mM HEPES pH 8,

0.1 mM EDTA, 5 mM $MgCl_2$, 0.5 M NaCl, 20% glycerol, 1% NP-40, inhibitors (as above). For coimmunoprecipitation experiments, we used 1 mg of nuclear protein extract and 2 μg of FXR polyclonal antisera overnight, followed by protein A/G precipitation with rotation at 4°C for 2h.

Frozen tumors from each of the different treatment groups were manually homogenized in lysis buffer supplemented with 10% glycerol, and protease inhibitor (0.1 mM Na_3VO_4, 1% PMSF, 20 μg/ml aprotinin)). Tumor lysates were collected, sonicated (5× for 5 s on ice), and microcentrifuged at 14000×*g* for 20 min at 2°C. Supernatants of the lysates were aliquoted and stored at −80°C.

Equal amounts of cell extract and immunoprecipitated proteins were resolved under denaturing conditions by electrophoresis in 8% to 10% polyacrylamide gels containing SDS (SDS-PAGE), and transferred to nitrocellulose membranes by electroblotting. After blocking the transferred nitrocellulose membranes were incubated with primary antibodies overnight at 4°C. The antigen-antibody complex was detected by incubation of the membranes with peroxidase-coupled goat anti-mouse, goat anti-rabbit, donkey anti-goat, and revealed using the ECL System. To ensure equal loading all membranes were stripped and incubated with anti Lamin B antibody for nuclear extracts or anti β-Actin antibodies for total extracts. The bands of interest were quantified by Scion Image laser densitometry scanning program.

RT-PCR and Real-time RT-PCR assays

Total RNA was extracted from cells using TRIzol reagent and the evaluation of FXR gene expression was performed by the reverse transcription-PCR method using a RETROscript kit. The cDNAs obtained were amplified by PCR using the following primers:

FXR	Forward 5'-CGAGCCTGAAGAGTGGTACTGTC-3'
	Reverse 5'-CATTCAGCCAACATTCCCATCTC-3'
36B4	Forward 5'-CTCAACATCTCCCCCTTCTC-3'
	Reverse 5'-CAAATCCCATATCCTCGT-3'
L19	Forward 5'-GAAATCGCCAATGCCAACTC-3'
	Reverse 5'-ACCTTCAGGTACAGGCTGTG-3'

p53 Forward 5’ -CAAGTCTGTTATGTGCACGTACTCA-3’
Reverse 5’-AACTGCACAGGGCATGTCTTC-3’

$p21^{WAF1/Cip1}$ Forward 5’-AGCAAAGTATGCCGTCGTCT-3’
Reverse 5’-ACACGCTCCCAGACGTAGTT-3’

The PCR was performed for 35 cycles for hFXR (94°C 1 min, 65°C 1 min, 72°C 1 min); 18 cycles for 36 B4 (94 °C for 1 min, 58 °C for 1 min, and 72 °C for 1 min); 25 cycles for L19 (94°C 1 min, 60°C 1 min, and 72°C 2 min); 25 cycles for p53 (94 °C for 1 min, 61 °C for 1 min, and 72 °C for 1 min); 22 cycles for $p21^{WAF1/Cip1}$ (94 °C for 1 min, 57 °C for 1 min, and 72 °C for 1 min), in the presence of 1µl of first strand cDNA, 1µM each of the primers, 0.5mM dNTP, *Taq* DNA polymerase (2 units/tube), and 2.2 mM MgCl in a final volume of 25µl.

Analysis of HER2 gene expression was performed by Real-time reverse transcription–PCR. Total RNA (2µg) was reverse transcribed with the RETROscript kit; cDNA was diluted 1:3 in nuclease-free water and 5µl were analysed in triplicates by real-time PCR in an iCycler iQ Detection System (Bio-Rad, USA) using SYBR Green Universal PCR Master Mix with 0.1 mmol/l of each primer in a total volume of 30µl reaction mixture following the manufacturer’s recommendations. Negative control contained water instead of first strand cDNA was used. Each sample was normalized on its GAPDH mRNA content. Primers used for the amplification were:

HER2 Forward 5’-CACCTACAACACAGACACGTTTGA-3’
Reverse 5’-GCAGACGAGGGTGCAGGAT-3’

GAPDH Forward 5’-CCCACTCCTCCACCTTTGAC-3’
Reverse 5’-TGTTGCTGTAGCCAAATTCGTT-3’

Each sample was normalized on its GAPDH mRNA content. The relative gene expression levels were normalized to a calibrator that was chosen to be the basal, untreated sample. Final results were expressed as n-fold differences in gene expression relative to GAPDH mRNA and calibrator, calculated using the ΔCt method as follows:

$$\text{n-fold}=2^{-(\Delta Ctsample-\Delta Ctcalibrator)}$$

where ΔCt values of the sample and calibrator were determined by subtracting the average Ct value of the GAPDH mRNA reference gene from the average Ct value of the gene analysed.

Transient transfection assay

MCF-7 and MCF-7 TR1 cells were transiently transfected using the FuGENE 6 reagent with FXR reporter gene (FXRE-IR1) in the presence or absence of FXR-DN plasmid. After transfection cells were treated with different doses of CDCA. In a set of experiments cells were transfected with different HER2 promoter constructs for 24h followed by treatment with CDCA 50μM for 6h. Empty vectors were used to ensure that DNA concentrations were constant in each transfection.

R2C cells were transiently transfected using the FuGENE 6 reagent with different constructs p53 promoter-luciferase reporter gene (p53-1, p53-6, p53-13, p53-14). After transfection, R2C cells were treated with GW4064 3 μM for 24 h.

TK Renilla luciferase plasmid was used to normalize the efficiency of the transfection. Firefly and Renilla luciferase activities were measured by Dual Luciferase kit. The firefly luciferase data for each sample were normalized based on the transfection efficiency measured by Renilla luciferase activity.

Electrophoretic mobility shift assay (EMSA)

Nuclear extracts from MCF-7 and MCF-7 TR1 cells, treated or not for 3h with CDCA 50μM, were prepared as previously described (Andrews NC, *et al.* 1991). The probe was generated by annealing single-stranded oligonucleotides, labeled with [γ^{32}P] ATP using T4 polynucleotide kinase, and purified using Sephadex G50 spin columns. The DNA sequences used as probe or as cold competitors are the following (nucleotide motifs of interest are underlined and mutations are shown as lowercase letters): NF-kB, 5'-AAGTGAAGCTGGGAGTTGCCGACTCCCAGA-3'; mutated NF-kB, 5'-AAGTGAAGCTaatcGTTGCCGACTCCCAGA-3'. *In vitro* transcribed and translated FXR protein was synthesized using the T7 polymerase in the rabbit reticulocyte lysate system. The protein-binding reactions were carried out in 20μL

of buffer [20 mmol/L HEPES (pH 8), 1 mmol/L EDTA, 50 mmol/L KCl, 10 mmol/L DTT, 10% glycerol, 1 mg/mL BSA, 50 μg/mL poly(dI/dC)] with 50,000 cpm of labelled probe, 20 μg of nuclear proteins from cells or an appropriate amount of NF-kB or FXR proteins and 5 μg of poly(dI-dC). The mixtures were incubated at room temperature for 20 min in the presence or absence of unlabeled competitor oligonucleotides. For experiments involving anti- NF-kB (p65) antibody, the reaction mixture was incubated with this antibody at 4°C for 12h before addition of labelled probe. The entire reaction mixture was electrophoresed through a 6% polyacrylamide gel in 0.25x Tris borate-EDTA for 3 h at 150 V.

Chromatin immunoprecipitation assay

MCF-7 and MCF-7 TR1 cells were treated with CDCA 50 μM or left untreated for 1 h and then DNA/protein complexes were cross-linked with 1% formaldehyde at 37°C for 10 min and sonicated. Supernatants were immunocleared with salmon sperm DNA/protein A agarose for 1h at 4°C. The precleared chromatin was immunoprecipitated with specific anti- NF-kB (p65) or anti polymerase II antibodies. A normal mouse serum IgG was used as negative control. Pellets were washed, eluted with elution buffer (1% SDS, 0.1 M $NaHCO_3$) and digested with proteinase K. DNA was obtained by phenol/chloroform/isoamyl alcohol extractions and precipitated with ethanol. A 5μl volume of each sample and input were used for real time PCR using the primers flanking NF-kB sequence in the human HER2 promoter region: 5'-TGAGAACGGCTGCAGGCAAC-3' and 5'-CCCACCAACTGCATTCCAA-3'. PCR reactions were performed in the iCycler iQ Detection System, using SYBR Green Universal PCR Master Mix, in a total volume of 50μL as described above. Final results were calculated using the ΔCt method as explained above, using input Ct values instead of the GAPDH mRNA. The basal sample was used as calibrator.

DNA Fragmentation

DNA fragmentation was determined by gel electrophoresis. R2C cells were grown in 10 cm dishes to 70% confluence and exposed to treatments. After 24h cells were collected and washed with PBS and pelleted at 1800 rpm for 5 minutes. The

samples were resuspended in 0.5 ml of extraction buffer (50 mmol/L Tris-HCl, pH 8; 10 mmol/L EDTA, 0.5% SDS) for 20 min in rotation at 4°C. DNA was extracted three times with phenol-chloroform and one time with chloroform. The aqueous phase was used to precipitate nucleic acids with 0.1 volumes of 3M sodium acetate and 2.5 volumes cold ethanol overnight at −20°C. The DNA pellet was resuspended in 15 μl of H2O treated with RNase A for 30 minutes at 37°C. The absorbance of the DNA solution at 260 and 280 nm was determined by spectrophotometry. The extracted DNA (40μg/lane) was subjected to electrophoresis on 1.5% agarose gels. The gels were stained with ethidium bromide and then photographed.

TUNEL assay

Apoptosis was determined by enzymatic labelling of DNA strand breaks using terminal deoxynucleotidyl transferase-mediated deoxyuridine triphosphate nick endlabeling (TUNEL). TUNEL labelling was conducted using APO-BrdUTM TUNEL Assay Kit (Invitrogen) and performed according to the manufacturer's instructions. Briefly, cells were trypsinized after treatments and resuspended in 0.5 ml of PBS.

After fixation with 1% paraformaldehyde for 15 min on ice, cells were incubated on ice-cold 70% ethanol overnight. After washing twice with washing buffer for 5 min, the labelling reaction was performed using terminal deoxynucleotidyl transferase endlabeling cocktail for each sample and incubated for 1h at 37°C.

After rinsing, cells were incubated with antibody staining solution with Alexa Fluor 488 dye-labeled anti-BrdU for 30 min at room temperature. Subsequently 0.5 mL of propidium iodide/RNase A buffer was added for each sample. Cells were incubated 30 min at room temperature, protected from light, analyzed and photographed by using a fluorescent microscope

Histologic Analysis

Tumor, livers, lung, spleens, and kidneys were fixed in 4% formalin, sectioned at 5 μm, and stained with hematoxylin and eosin Y (Bio-Optica, Milan, Italy).

Immunofluorescence study

Tumor section were incubated with anti-Aromatase (4°C/overnight) and with rhodamine-conjugated secondary antibody (30min/room temperature). IgG primary antibody as negative control. 4´,6-Diamidino-2-phenylindole (DAPI, Sigma) staining for nuclei detection. Fluorescence was photographed using OLYMPUS BX51 microscope.

Statistical analyses

Each datum point represents the mean ± S.D. of three different experiments. Data were analyzed by Student's t test using the GraphPad Prism 4 software program. $P<0.05$ was considered as statistically significant.

AIM 1

May activated FXR modulate MCF-7 tamoxifen-resistant breast cancer cell growth ?

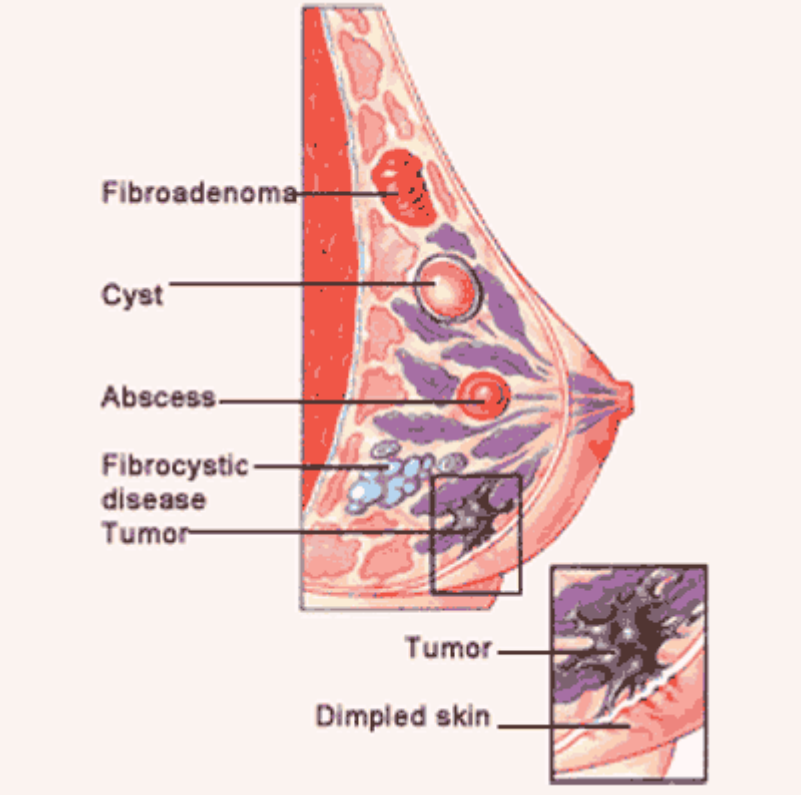

RESULTS

Characterization of MCF-7 and MCF-7 TR1 cells.

To well characterize the antiestrogen-resistant phenotype that frequently develops in breast cancer patients receiving tamoxifen, we used Tamoxifen-Resistant breast cancer cells (MCF-7 TR1), generated by long-term exposure to 4-OH-TAM (Tam). The resistant phenotype was confirmed evaluating, by MTT assay, in tamoxifen-sensitive MCF-7 and tamoxifen-resistant MCF-7 TR1 breast cancer cells, the means of growth curve in the presence of Tam 1μM of. As expected, we found that the MCF-7 cells showed significantly decrease in viability upon Tam treatment compared to control, whereas antiestrogen treatment had no effect on cell viability of MCF-7 TR1 cells, over a period of 8 days (Figure 1A).

Acquired resistance to Tam has been associated with elevated levels of the membrane tyrosine kinase HER2 (Knowlden, JM *et al*. 2003; Nicholson, RI *et al.* 2004; Gutierrez, MC *et al.* 2005). In agreement with these reports, we found a marked increase in the levels of total HER2 protein content in Tam-resistant MCF-7 TR1 compared with MCF-7 cells, whereas no differences were seen in the expression of EGFR and ERα (Figure 1B).

We therefore evaluated anchorage-independent growth of MCF-7 and MCF-7 TR1 cells after treatment with herceptin, a humanized monoclonal antibody directed against the extracellular domain of HER2, in the presence or not of EGF. Herceptin had no effect on MCF-7 growth, whereas significantly inhibited anchorage-independent growth of MCF-7 TR1 cells in basal conditions as well as upon EGF treatment (Figure 1C). These data confirm that the HER2 overexpression found in the MCF-7 TR1 cells renders them more sensitive to the inhibitory effect of this selective HER2-targeted agent.

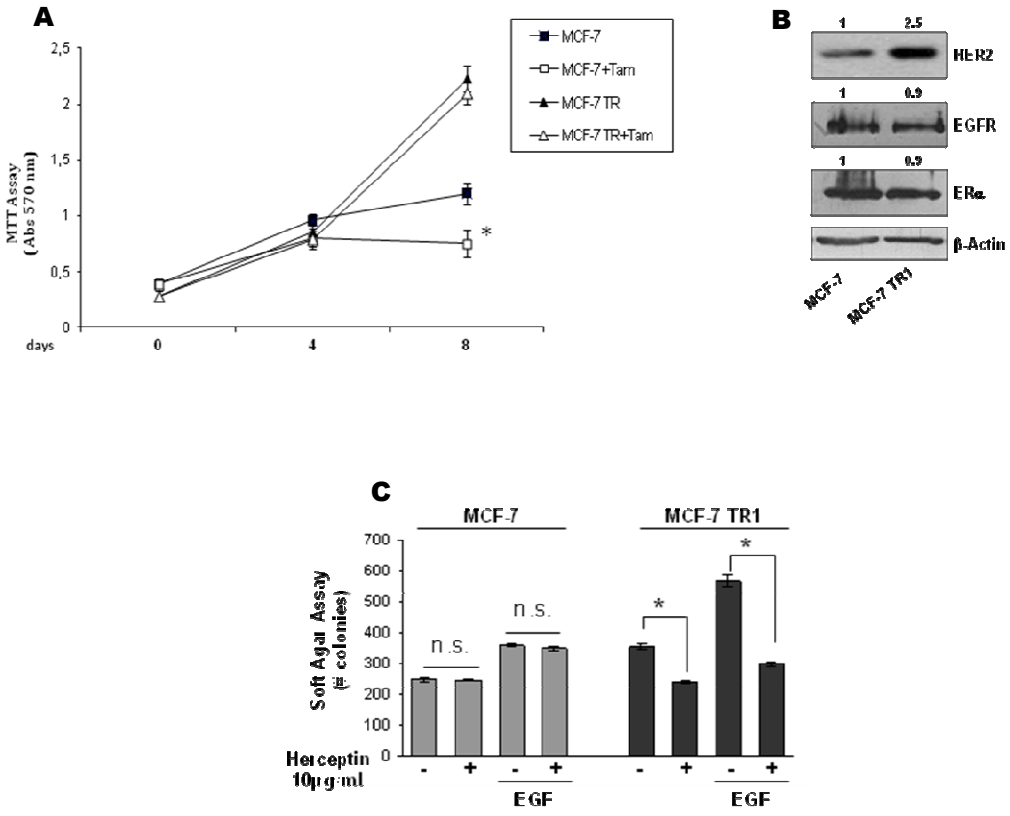

Figure 1. Characterization MCF-7 and MCF-7 TR1. (A) MTT proliferation assay of MCF-7 and MCF-7 TR1 cells treated with vehicle or Tam 1μM for 4 and 8 days. The results are expressed as the mean absorbance (570 nm) ± SD (standard deviation) of triplicate wells and are representative of three separate experiments. (B) Western blot analysis of HER2, EGFR, ERα in total protein extracts from MCF-7 and MCF-7 TR1 cells; β-Actin was used as loading control. (C) Soft-agar growth assay in MCF-7 and MCF-7 TR1 cells plated in 0.35% agarose and treated with EGF 100 ng/ml in the presence or absence of herceptin (10 μg/ml). After 14 days of growth, colonies >50 μm diameter were counted. n.s., nonsignificant; *P<0.05 compared with vehicle or EGF. Numbers on top of the blots represent the average fold change versus control of MCF-7 cells normalized for β-Actin.

FXR expression in Tam-resistant breast cancer cells

Next, we evaluated the expression of FXR in MCF-7 and MCF-7 TR1 cells. Our results revealed the presence of FXR mRNA (Figure 2A, upper panel) and protein (Figure 2A, lower panel) in both MCF-7 and MCF-7 TR1 cells. To assess the ability of FXR to be transactivated by CDCA, we transiently transfected cells with an FXR-responsive reporter gene (FXRE-IR1) followed by treatment with increasing doses of CDCA.

The specificity of the system was tested by co-transfecting the cells with a dominant negative FXR (FXR-DN) plasmid. As shown in Figure 2B, CDCA treatment induced a dose-dependent FXR activation in both cell lines and expression of the FXR-DN completely abrogated the CDCA induced transactivation.

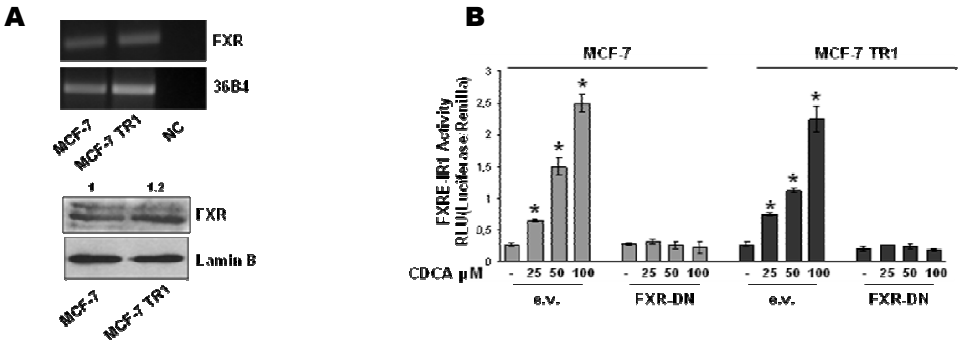

Figure 2. Expression of FXR in breast cancer cells. (A) Total RNA was extracted from MCF-7 and MCF-7 TR1 cells, reverse transcribed and cDNA was subjected to PCR using primers specific for FXR or 36B4 (upper panel). NC: negative control, RNA sample without the addition of reverse transcriptase. Nuclear proteins were extracted from MCF-7 and MCF-7 TR1 and then western blotting analysis was performed using anti-FXR antibody. Lamin B was used as loading control (lower panel). (B) MCF-7 and MCF-7 TR1 cells were transiently transfected with a FXR-responsive reporter gene (FXRE-IR1), with either empty vector (e.v.) or FXR-DN expression plasmid. After transfection, cells were treated for 24h with vehicle (-) or increasing doses of CDCA (25–50–100 μM) and then luciferase activity was measured. Results represent the mean ± S.D. of three different experiments each performed in triplicate. *P<0.05 compared with vehicle. Numbers on top of the blots represent the average fold change versus control of MCF-7 cells normalized for β-Actin.

FXR activation inhibits Tam-resistant breast cancer cell growth

We examined, by MTT growth assays, the effects of increasing doses of CDCA and GW4064. Treatment with both ligands reduced cell proliferation in a dose dependent manner in MCF-7 and MCF-7 TR1 cells, whereas had no effects on normal breast epithelial cells MCF-10A (Figures 3A and B).

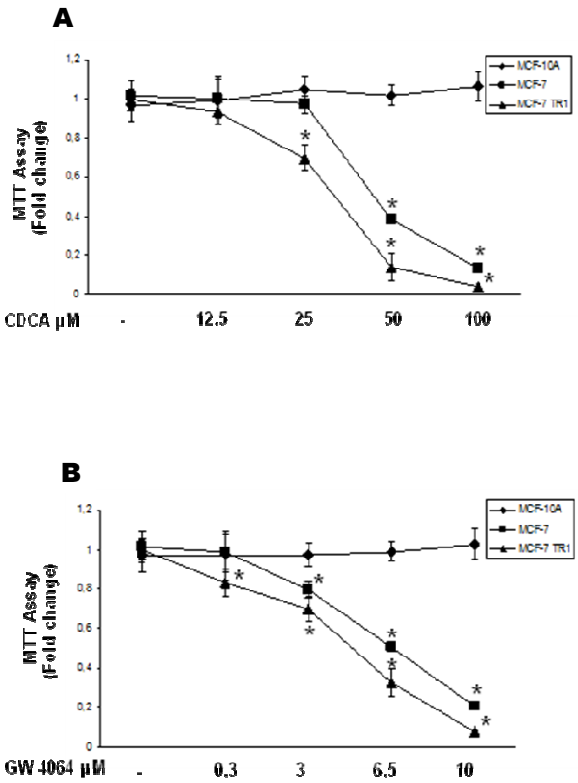

Figure 3. FXR ligands effects on breast cancer cells proliferation. MTT growth assays in MCF-10A, MCF-7 and MCF-7 TR1 cells treated with vehicle (-) or increasing doses of CDCA (12.5–25–50–100 µM) (A) or GW4064 (0.3–3–6.5–10 µM) (B) for 7 days. Cell proliferation is expressed as fold change ± S.D. relative to vehicle-treated cells and is representative of three different experiments each performed in triplicate. *P<0.05 compared with vehicle.

Similar results in growth inhibition were also obtained in another Tam-resistant breast cancer cell line termed MCF-7 TR2 (Figures 4A and B).

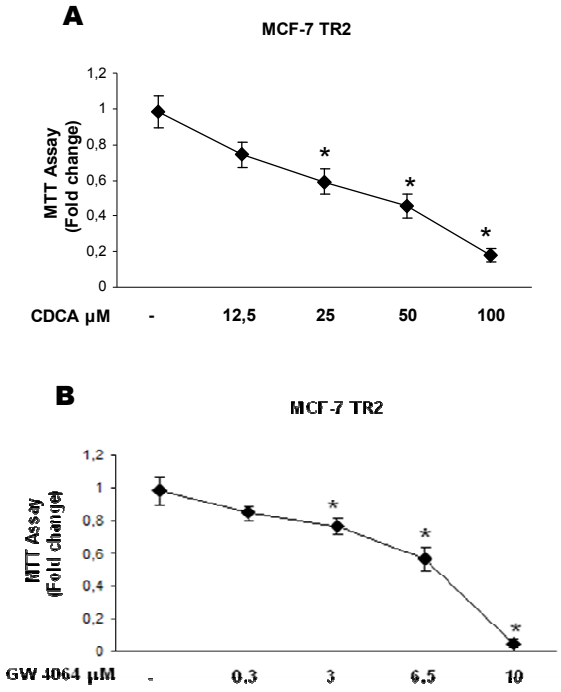

Figure 4. FXR ligands inhibit MCF-7 TR2 cell growth. MTT growth assays in MCF-7 TR2 cells treated with vehicle (-) or increasing doses of CDCA (12,5-25-50-100 µM) (A) or GW4064 (0,3-3-6,5-10 µM) (B) for 7 days. Cell proliferation is expressed as fold change ± SD relative to vehicle treated cells, and is representative of three different experiments each performed in triplicate. *P<0.05 compared with vehicle.

It is worth noting that the inhibitory effects exerted by FXR ligands on cell proliferation were significant at lower dose in MCF-7 TR1 cells compared with MCF-7 cells, as evidenced by half-maximal inhibitory concentration (IC50) values (Table 1).

Cell lines	IC_{50} (mmol/l) CDCA	95% confidence interval	P	IC_{50} (μmol/l) GW4064	95% confidence interval	P
MCF-7	46	42.2–50.1		6.04	5.44–6.70	
MCF-7 TR1	31	28.6–33.9	0.0001	4.47	3.6–5.49	0.008

Table 1. IC_{50} of CDCA and GW4064 for MCF-7 and MCF-7 TR1 cells on anchorage-dependent growth**.** Abbreviations: CDCA, chenodeoxycholic acid; IC_{50}, half-maximal inhibitory concentration.

The antiproliferative effects exerted by CDCA were completely reversed in the presence of a FXR-DN plasmid, supporting the specific involvement of the FXR (Figure 5).

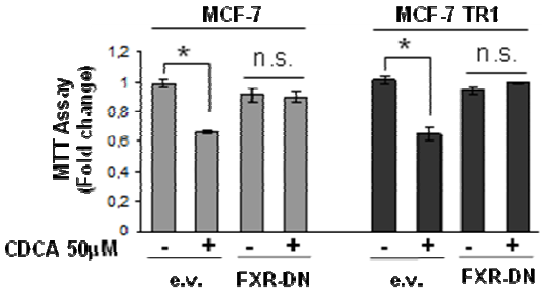

Figure 5. FXR mediates inhibitions effects on breast cancer cell growth. MCF-7 and MCF-7 TR1 cells, transiently transfected with either empty vector (e.v.) or FXR-DN vector plasmids, were treated with vehicle (-) or CDCA 50 μM for 4 days before testing cell viability using MTT assay. Results are expressed as fold change ± S.D. relative to vehicle-treated cells and are representative of three different experiments each performed in triplicate. *P<0.05 compared with vehicle.

Next, we tested the effects of CDCA in the presence of Tam on cell growth (Figure 6A). As expected, with anti-estrogen treatment, cell viability was significantly reduced in MCF-7 cells, whereas MCF-7 TR1 cells growth was unaffected, confirming the Tam-resistant phenotype. Interestingly, combined treatment with CDCA and Tam reduced growth of MCF-7 TR1 cells compared with treatment with Tam alone, but showed no additive effects in MCF-7 cells (Figure 6A). The ability of CDCA and Tam to inhibit Tam-resistant growth was also confirmed using anchorage-independent growth assays (Figure 6B). These results suggest that FXR activation can interfere with the cellular mechanisms by which MCF-7 TR1 cells escape antihormonal treatments.

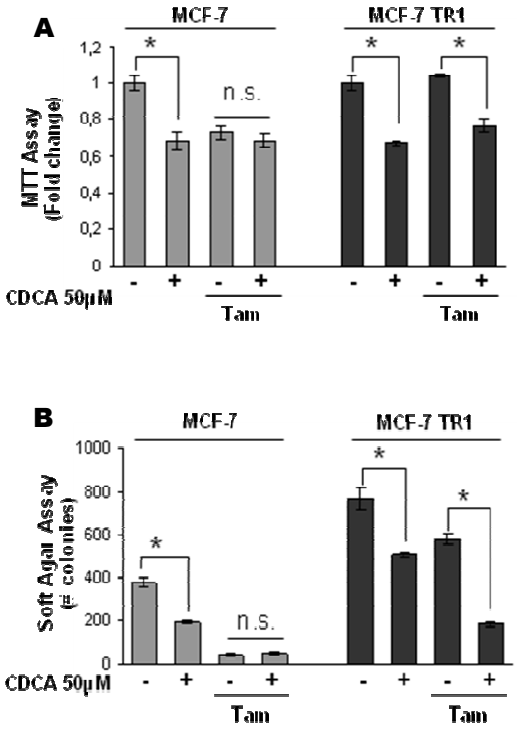

Figure 6. Effects of FXR ligand on tamoxifen-resistant breast cancer cells. (A) MTT growth assay in MCF-7 and MCF-7 TR1 cells treated with vehicle (-) or CDCA 50 µM in the presence or not of Tam 1 µM for 4 days. Results are expressed as fold change ± S.D. relative to vehicle-treated cells and are representative of three different experiments each performed in triplicate. (B) Soft-agar growth assay in MCF-7 and MCF-7 TR1 cells plated in 0.35% agarose and treated as indicated above. After 14 days of growth, colonies >50 µm diameter were counted. n.s. (non significant); *P<0.05 compared with vehicle or Tam.

CDCA reduces HER2 expression and signaling in MCF-7 TR1 cells

To understand the mechanisms associated with CDCA mediated inhibition of Tam-resistant growth in breast cancer cells, we evaluated the possible role of FXR ligands in modulating HER2 expression. As shown in Figure 7A, treatment with CDCA downregulated HER2 protein expression in both cell lines, but with higher reduction seen in MCF-7 TR1 cells. Similar results were also observed after treatment with GW4064. In the presence of an FXR-DN the HER2 downregulation was completely abrogated, confirming FXR involvement in CDCA-induced effects on HER2 (Figure 7B). Next, we questioned whether these HER2-decreased levels could modify the responsiveness of breast cancer cells after growth factor stimulation. Thus, we investigated the effects of short-term stimulation with EGF, in the presence of CDCA treatment, on phosphorylation levels of HER2 and MAPK, the main downstream effectors of the growth factor signaling. EGF treatment increased phosphorylation of both HER2 and MAPK, even though in higher extent in MCF-7 TR1 cells.

However, pretreatment with CDCA reduced EGF induced phosphorylation of HER2 in both cell lines and drastically prevented MAPK activation in MCF-7 TR1 cells (Figure 7C). No differences were found in EGFR expression upon CDCA treatment (Figure 7D), confirming that activated FXR specifically target HER2 expression in breast cancer cells.

A reduction in HER2 levels was also found upon CDCA treatment in MCF-7 TR2 cells (Figure 7E).

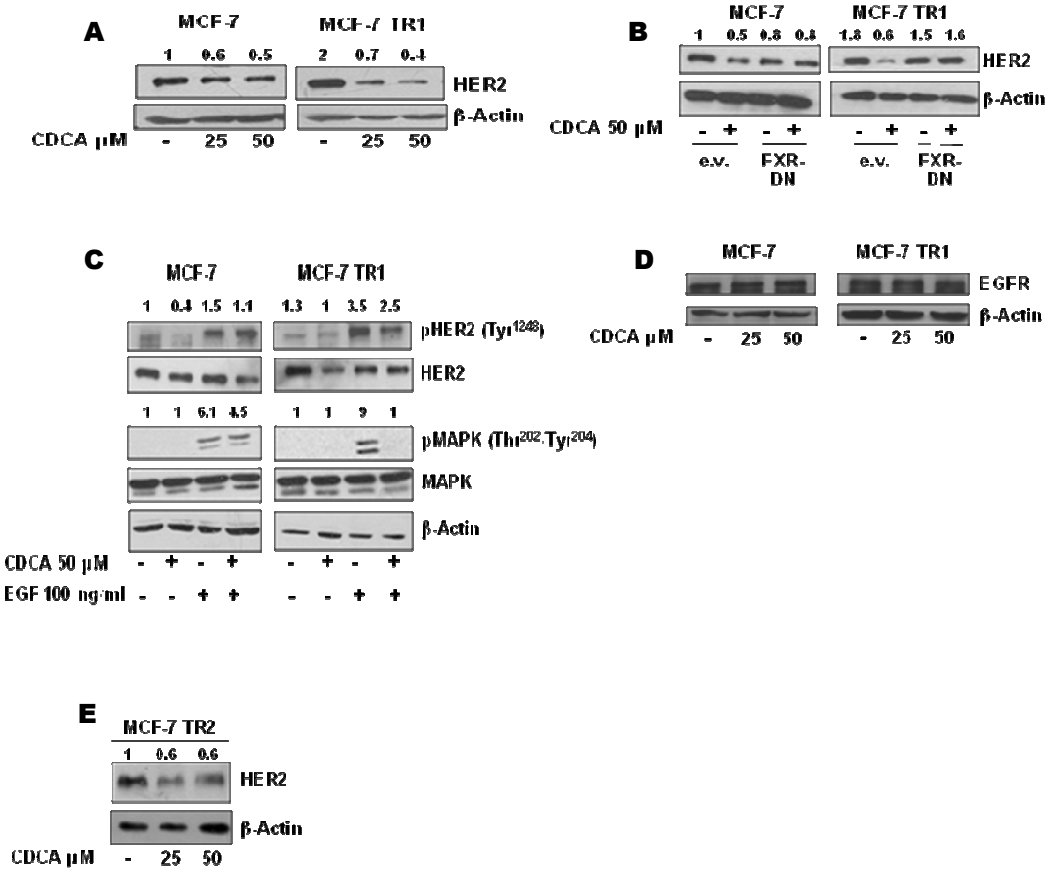

Figure 7. Effects of CDCA on HER2 expression and its transduction pathways in MCF-7 and MCF-7 TR1 cells. (A) MCF-7 and MCF-7 TR1 cells were treated for 24h with vehicle (-) or CDCA 25 and 50 µM before lysis. Equal amounts of total cellular extract were analyzed for HER2 levels by western blotting. β-Actin was used as loading control. (B) Cells were transiently transfected with either empty vector (e.v.) or FXR-DN plasmids and then treated with vehicle (-) or CDCA 50 µM for 24h and HER2 levels were evaluated by western blotting. β-Actin was used as loading control. (C) Immunoblot analysis showing phosphorylated HER2 (pHER2 Tyr1248) and MAPK (pMAPK Thr202/Tyr204), total HER2, total MAPK in MCF-7 and MCF-7 TR1 cells pretreated for 24h with CDCA 50 µM and then treated for 10 min with EGF 100 ng/ml. β-Actin was used as loading control. (D) MCF-7 and MCF-7 TR1 cells were treated for 24h with vehicle (-) or CDCA 25 and 50µM before lysis. Equal amounts of total cellular extract were analyzed for EGFR levels by Western blotting. β-Actin was used as loading control. (E) MCF-7 TR2 cells were treated for 24h with vehicle (-) or CDCA 25 and 50µM before lysis. Equal amounts of total cellular extract were analyzed for HER2 levels by Western blotting. β-Actin was used as loading control. Numbers on top of the blots represent the average fold change versus control of MCF-7 cells normalized for β-Actin.

In addition, data obtained from MTT (Figure 8A) as well as soft-agar (Figure 8B) growth assays revealed that CDCA treatment inhibited EGF-induced growth by 70% in anchorage-dependent and 50% in anchorage-independent assays in MCF-7 TR1 cells. CDCA was less effective in MCF-7 cells. These results well correlated with the downregulatory effect of CDCA on EGF induced cyclin D1 expression, particularly in MCF-7 TR1 cells (Figure 8C).

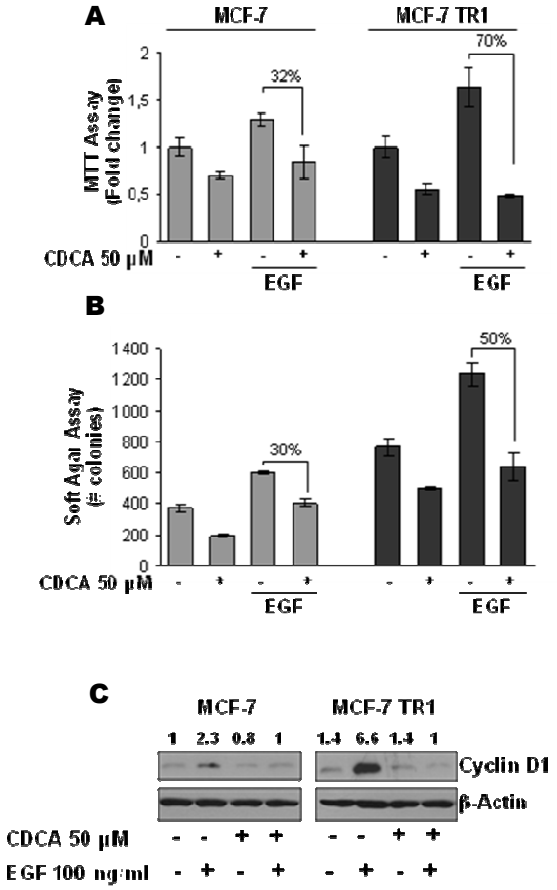

Figure 8. CDCA reverses EGF-induced growth in breast cancer cells. MTT growth assay (A) and soft-agar assay (B) in cells treated with CDCA 50 µM with or without EGF 100 ng/ml for 4 days and 14 days, respectively. The MTT assay results are expressed as fold change ± S.D. relative to vehicle-treated cells and are representative of three different experiments each performed in triplicate. The soft-agar assay values are represented as a mean of colonies number >50 µm diameter counted at the end of assay. Percentages of inhibition induced by CDCA versus EGF treatment alone are shown. (C) Cells were treated for 24h with vehicle (-) or EGF 100 ng/ml in the presence or not of CDCA 50 µM before lysis and then cellular extracts were analyzed for cyclin D1 levels by western blot analysis. β-Actin was used as loading control. Numbers on top of the blots represent the average fold change versus control of MCF-7 cells normalized for β-Actin.

Activated FXR inhibits the binding of NF-kB to HER2 promoter region

To explore whether HER2 downregulation relies on transcriptional mechanisms, we evaluated, using realtime reverse transcription (RT)-PCR, HER2 mRNA levels after treatment with CDCA for different times.

Exposure to CDCA exhibited a time-dependent reduction in HER2 mRNA levels in both MCF-7 and MCF-7 TR1 cells (Figure 9A). Also, transcriptional activity of a reporter plasmid containing the human HER2 promoter region (pNeuLite) was significantly reduced with CDCA treatment in both cell lines (Figures 9C and D).

The human HER2 promoter contains multiple consensus sites for several transcription factors, including Sp1, as well as activator protein (AP)-1 and NF-kB, the well known effectors of FXR transrepression (He, F. *et al.* 2006; Vavassori, P. *et al.* 2009) (Figure 4b). To identify the region within the HER2 promoter responsible for CDCA inhibitory effects, HER2 promoter-deleted construct (-232 pNeuLite) activity was tested (Figure 9B).

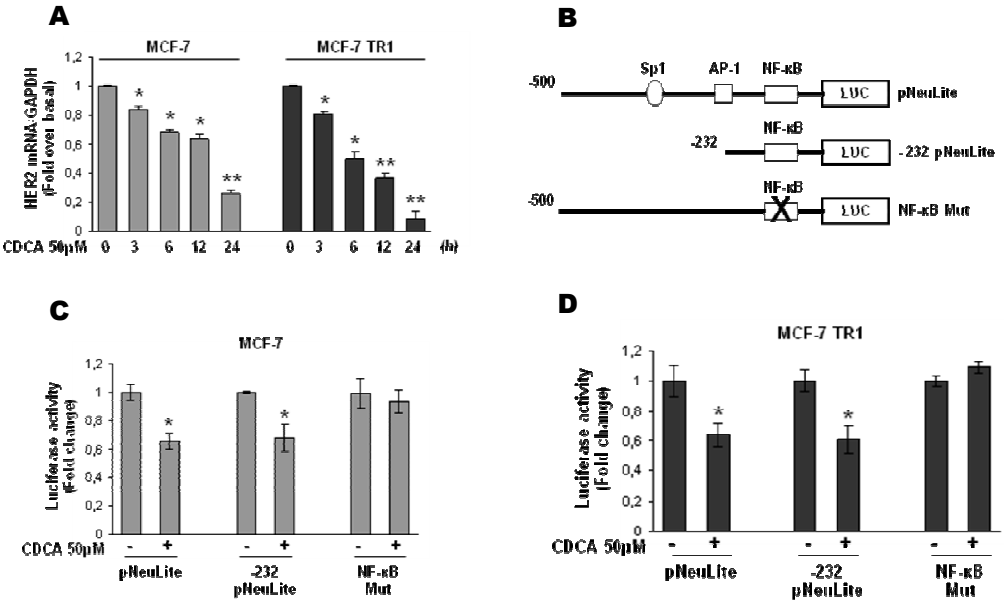

Figure 9. Effects of CDCA on human HER2 promoter activity. (A) mRNA HER2 content, evaluated by real-time RT–PCR, after treatment with vehicle or CDCA 50 μM, as indicated. Each sample was normalized to its GAPDH mRNA content. *P<0.05 and **P<0.001 compared with vehicle. (B) Schematic map of the human HER2/neu promoter region constructs used in this study. All of the promoter constructs contain the same 3' boundary. The 5' boundaries of the promoter fragments varied from -500 (pNeuLite) to -232 (-232 pNeuLite). A mutated NF-kB-binding site is present in NF-kB mut construct. HER2 transcriptional activity in MCF-7 (C) and MCF-7 TR1 (D) cells transfected with promoter constructs are shown. After transfection, cells were treated in the presence of vehicle (-) or CDCA 50 μM for 6h. The values represent the means ± S.D. of three different experiments each performed in triplicate. *P<0.05 compared with vehicle.

We observed that the responsiveness to CDCA was still maintained, suggesting that the region from -232 to + 1 containing the NF-kB motif might be involved in transrepression mechanisms exerted by activated FXR (Figures 9C and D). Thus, we performed site directed mutagenesis on the NF-kB domain (NF-kB Mut) within the HER2 promoter (Figure 9B). Mutation of this domain abrogated CDCA effects (Figures 9C and D). These latter results demonstrate that the integrity of NF-kB-binding site is necessary for FXR modulation of HER2 promoter activity in breast cancer cells. The specific role of the NF-kB motif in the transcriptional regulation of HER2 by CDCA was investigated using electrophoretic mobility shift assays. We observed the formation of a complex in nuclear extracts from MCF-7 and MCF-7 TR1 cells using synthetic oligodeoxyribonucleotides corresponding to the NF-kB motif (Figure 10A, lanes 1 and 5), which was abrogated by incubation with 100-fold molar excess of unlabeled probe (Figure 10A, lanes 2 and 6), demonstrating the specificity of the DNA-binding complex. This inhibition was no longer observed when mutated oligodeoxyribonucleotide was used as competitor (Figure 10A, lanes 3 and 7). Interestingly, treatment with CDCA strongly decreased the DNA-binding protein complex compared with control samples (Figure 10A, lanes 4 and 8). The inclusion of an anti- NF-kB antibody in the reaction immunodepleted the specific band, confirming the presence of NF-kB in the complex (Figure 10B, lanes 3 and 9). Nonspecific IgG did not affect NF-kB complex formation (Figure 10B, lanes 4 and 10). Recombinant NF-kB protein revealed a complex migrating at the same level as that of nuclear extracts from cells (Figure 10A, lane 9; Figure 10B, lanes 5 and 11). Of note, the CDCA-induced reduction in the DNA-binding complex was no longer observed utilizing as probe synthetic oligodeoxyribonucleotides corresponding to the AP-1 and Sp1 motifs. To better define the role of FXR in the inhibition of NF-kB binding on HER2 promoter, a competition assay using recombinant NF-kB protein and increasing amounts of in vitrotranslated FXR protein (1, 3 and 5 ml) was carried out. A dose-dependent reduction in the NF-kB complex was seen (Figure 10C, lanes 1–4), suggesting that physical interaction between these two transcription factors may inhibit the binding of NF-kB to human HER2 promoter region.

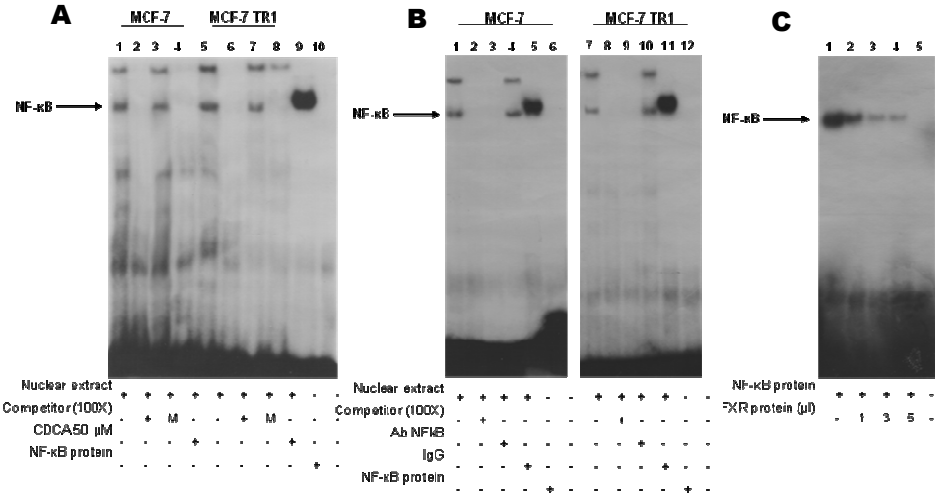

Figure 10. Electrophoretic mobility shift assay of the NF-kB-binding site in the HER2 promoter region. (A) Nuclear extracts from MCF-7 and MCF-7 TR1 cells were incubated with a double-stranded NF-kB specific sequence probe labeled with [γ^{32}P]ATP and subjected to electrophoresis in a 6% polyacrylamide gel (lanes 1 and 5). Competition experiments were performed adding as competitor a 100-fold molar excess of unlabeled probe (lanes 2 and 6) or a 100-fold molar excess of unlabeled oligonucleotide containing a mutated NF-kB RE (lanes 3 and 7). Lanes 4 and 8, nuclear extracts from CDCA (50 μM) -treated MCF-7 and MCF-7 TR1 cells, respectively, incubated with probe. Lane 9, NF-kB protein. Lane 10, probe alone. (B) Nuclear extracts from MCF-7 and MCF-7 TR1 cells were incubated with a double-stranded NF-kB specific sequence probe labeled with [γ^{32}P]ATP (lanes 1 and 7) or with a 100-fold molar excess of unlabeled probe (lanes 2 and 8). Nuclear extracts incubated with anti- NF-kB (lanes 3 and 9) or IgG (lanes 4 and 10). Lanes 5 and 11, NF-kB protein. Lanes 6 and 12, probe alone. (C) Lane 1, NF-kB protein. Lanes 2, 3 and 4, NF-kB protein incubated with increasing doses (1, 3 and 5 ml) of transcribed and translated in vitro FXR protein. Lane 5, probe alone.

To further test this possibility, we performed coimmunoprecipitation studies using nuclear protein fractions from MCF-7 and MCF-7TR1 cells treated with CDCA. As shown in Figure 11A, the formation of an FXR and NF-kB complex was detected in untreated cells, and this association was enhanced with FXR ligand treatment. Moreover, to confirm the involvement of NF-kB in CDCA mediated HER2-downregulation at the promoter level, ChIP assays were performed. Using specific antibodies against NF-kB and RNA polymerase II, protein–chromatin complexes were immunoprecipitated from cells cultured with or without CDCA for 1h. The resulting precipitated DNA was then quantified musing real-time PCR with primers spanning the NF-kB-binding element in the HER2 promoter region. NF-kB recruitment was significantly decreased upon CDCA treatment in both cell lines (Figure 11B). This result was well correlated with a lower association of RNA-polymerase II to the HER2 regulatory region (Figure 11C). To further confirm the transcriptional repression mediated by activated FXR, we also evaluated the histone deacetylase 3 association on the NF-

kB-responsive sequence within the HER2 promoter. CDCA stimulation enhanced the recruitment of histone deacetylase 3 to this NF-kB promoter site (Figure 11D).

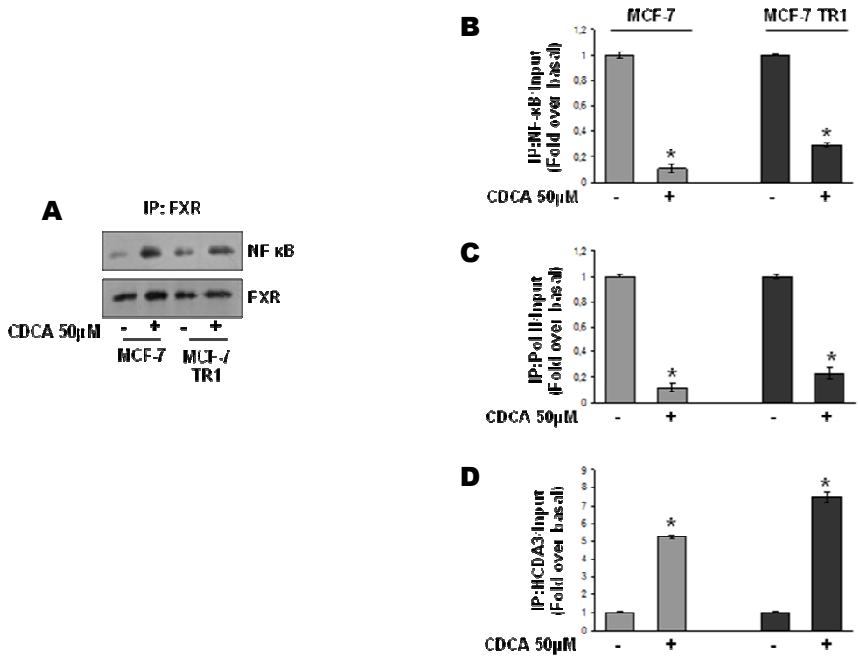

Figure 11. FXR inhibits NF-kB recruitment to HER2 promoter. (A) MCF-7 and MCF-7 TR1 cells were treated with vehicle (-) or CDCA 50 μM for 1h before lysis. FXR protein was immunoprecipitated using an anti-FXR polyclonal antibody (IP:FXR) and resolved in SDS-polyacrylamide gel electrophoresis. Immunoblotting was performed using an anti-NF-kB (p65 subunit) monoclonal antibody and anti-FXR antibody. MCF-7 and MCF-7 TR1 cells were treated in the presence of vehicle (-) or CDCA 50 μM for 1h, then crosslinked with formaldehyde, and lysed. The precleared chromatin was immunoprecipitated with anti- NF-kB (B), anti- RNA polymerase II (C) and anti- HDCA3 (D) antibodies. A 5 μl volume of each sample and input was analyzed by real-time PCR using specific primers to amplify HER2 promoter sequence, including the NF-kB site. Similar results were obtained in multiple independent experiments. *P<0.01 compared with vehicle.

HER2 downregulation underlies the ability of FXR ligands to inhibit breast cancer cell growth.

We evaluated the effects of CDCA on cell growth in the ERα-negative and HER2-overexpressing breast cancer cells SKBR3. Treatment with CDCA inhibited SKBR3 anchorage-dependent growth in a dose-dependent manner (Figure 12A) and reduced colony growth in anchorage-independent assay (Figure 12B). Indeed, we found, after 48h of treatment with CDCA, a marked decrease in both HER2 protein and mRNA levels (Figures 12C and D). In these cells, HER2 promoter activity was similarly reduced with CDCA treatment (Figure 12E).

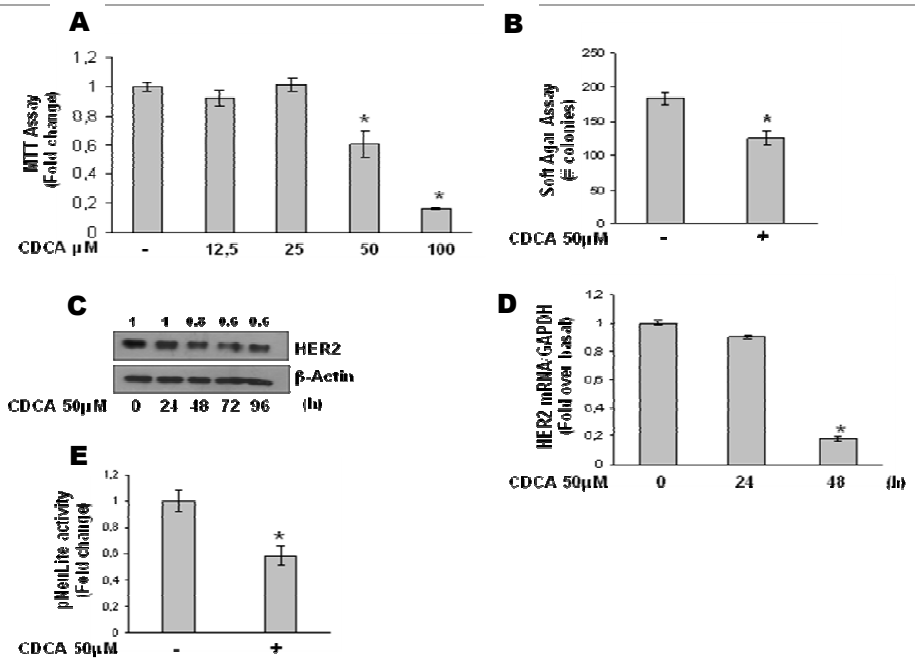

Figure 12. Effects of FXR ligand on SKBR3 breast cancer cells. (A) MTT proliferation assay of SKBR3 cells treated with vehicle (-) or increasing doses of CDCA (12,5–25–50–100 µM) for 7 days. Results are expressed as fold change ± S.D. relative to vehicle-treated cells and are representative of three different experiments each performed in triplicate. (B) Soft-agar growth assay in SKBR3 cells plated in 0.35% agarose and treated with vehicle (-) or CDCA 50 µM. After 14 days of growth, colonies >50 µm diameter were counted. (C) SKBR3 cells were treated with CDCA 50 µM as indicated before lysis. Equal amounts of total cellular extract were analyzed for HER2 levels by western blotting. β-Actin was used as loading control. Numbers on top of the blots represent the average fold change relative to control normalized for β-Actin. (D) mRNA HER2 content, evaluated by real-time RT–PCR, after treatment with CDCA 50 µM as indicated. Each sample was normalized to its GAPDH mRNA content. (E) SKBR3 cells were transiently transfected with pNeuLite construct. After transfection, cells were treated in the presence of vehicle (-) or CDCA 50 µM for 24h and the promoter activity was evaluated. The values represent the means ± S.D. of three different experiments each performed in triplicate. *P<0.05 compared with vehicle.

Finally, we explored the ability of FXR ligands to inhibit proliferation using as additional model Tam-resistant derivative cell line engineered to stably overexpress HER2 (MCF-7/HER2-18). As expected, Tam-resistant growth in these cells was not affected by both CDCA and GW4064 treatments (Figure 13).

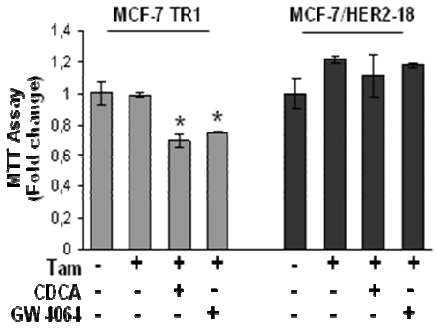

Figure 13. Effects of FXR ligands on MCF-7/her2-18 cells. MTT growth assay in MCF-7 TR1 and MCF-7/HER2-18 cells treated with vehicle (-), CDCA 50 µM and GW4064 3 µM in the presence or not of Tam 1 µM for 4 days. Results are expressed as fold change ± S.D. relative to vehicle-treated cells and are representative of three different experiments each performed in triplicate. *P<0.05 compared with Tam alone.

Altogether, these results well evidence how FXR mediated downregulation of HER2 at transcriptional level is fully responsible for inhibiting breast cancer cell Proliferation. (Figure 14)

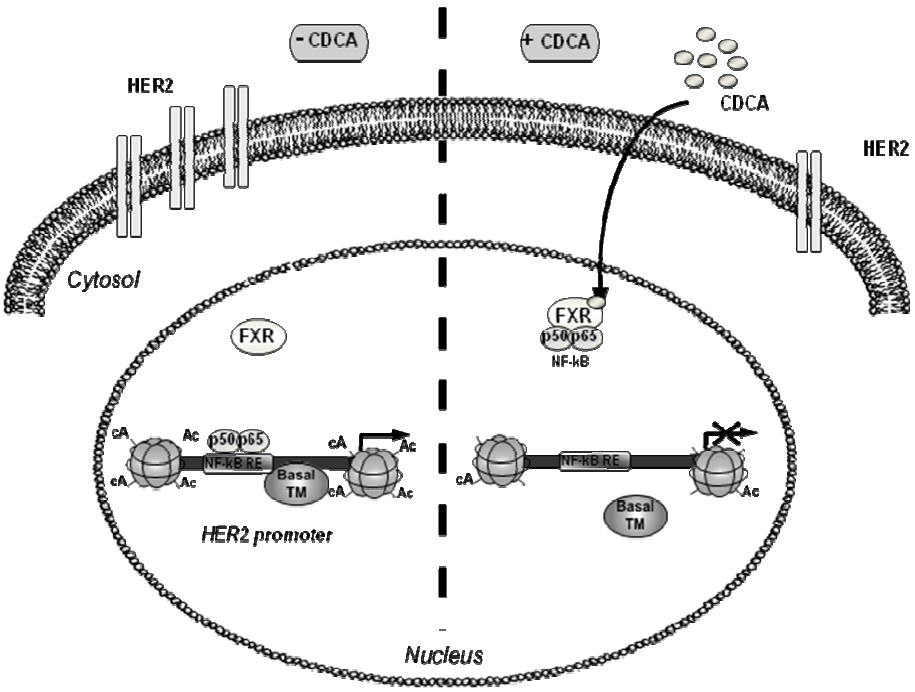

Figure 14. Proposed working model of the FXR-mediated regulation of HER2 expression in Tam-resistant breast cancer cells. In the absence of CDCA, HER2 expression is regulated by several serum factors, including NF-kB, acting through a regulatory region in HER2 promoter and enabling gene transcription. Upon CDCA treatment, FXR binds KF-kB, inhibiting is recruitment on the response element located in the proximal HER2 promoter, causing displacement of RNA polymerase II with consequent repression of HER2 expression.

AIM 2

May FXR ligands inhibit Leydig tumor cell growth in vivo ?

RESULTS

Activation of FXR Inhibits R2C tumor xenograft growth *in vivo*

Based on our previous results demonstrating that FXR activation exerts anti-proliferative effects on tumor Leydig cells *in vitro* through an inhibition of aromatase expression (Catalano, S. *et al.* 2010), we used the R2C tumor xenograft model to examine the effects of GW4064, a synthetic FXR agonist, on tumor growth *in vivo*. To this aim, we injected R2C cells into the intrascapular region of nude mice and followed tumor growth after administration of 30 and 60 mg/Kg/day GW4064.

This administration was well tolerated because no change in body weight or in food and water consumption was observed along with no evidence of reduced motor function. In addition, no significant difference in the mean weights or histological features of the major organs (liver, lung, spleen, and kidney) after sacrifice was observed between vehicle-treated mice and those that received treatment, indicating a lack of toxic effects at the dose given.

As shown in Figure 1A GW4064 (30 and 60 mg/kg day) induced regression in tumor growth. This effect was evident as early as days 6 of treatment, and tumor volumes continued to reduce over the duration of experiment. At the time of killing, 25 days, tumor size was markedly smaller in animals treated with GW4064 respect to vehicle-treated (Figure 1B).

Corresponding to their growth characteristics, histological examination of R2C xenografts by Hematoxylin & Eosin staining revealed necrotic central regions and regions of hemorrhage in GW4064-treated tumors (Figure 1C).

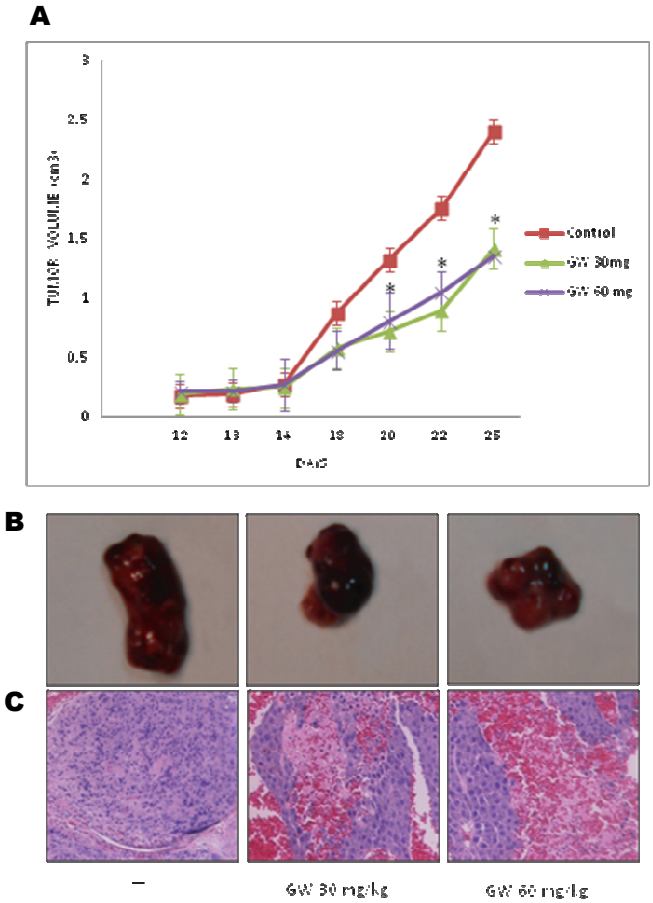

Figure 1. GW 4064 inhibits R2C tumor xenograft growth *in vivo*. (A) Tumor volume from R2C implanted in nude mice. The animals were treated with GW4064 30 mg/kg/day (n = 6), GW4064 60 mg/kg/day (n = 6), or vehicle as control (n = 6). *P<0.05, GW 4064 treated group versus control group. (B) Representative images of experimental tumor at 25 day. (C) Histological examination of R2C xenografts by Hematoxylin & Eosin staining.

In addition, in agreement with our previous *in vitro* results (Catalano, S. *et al.* 2010) in R2C xenografts a significant decrease of aromatase expression, evaluated by both western blotting and immunofluorescence analysis, was observed (Figure 2A and B). This latter result suggest that the reduced *in vivo* Leydig tumor growth is probable due at least in part to an inhibition of estrogen-dependent cell proliferation.

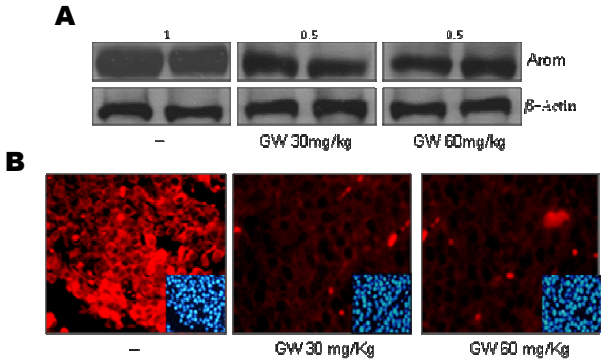

Figure 2. Effects of GW4064 on aromatase expression in R2C xenografts. (A) Total proteins extracted from R2C xenograft, treated with GW4064 (30 and 60 mg/kg), were tested for aromatase expression by immunoblot analysis. β-Actin was used as a loading control. (B) Aromatase expression was determined by immunofluorescence analysis. 4′,6-Diamidino-2-phenylindole (DAPI) staining was used to visualize the cell nucleus. Numbers on top of the blots represent the average fold change versus control of R2C xenograft normalized for β-Actin.

FXR ligands induce apoptosis *in vitro* and *in vivo.*

Since it has been shown that FXR induces apoptosis in breast and colorectal cancers (Swales, K. *et al.* 2006; Modica, S. *et al.* 2008) as well as in the vasculature (Bishop-Bailey, D. 2004) we investigated whether FXR ligands may induce cell death by apoptosis in our model system, by using different approaches. First, we evaluated the proteolysis of poly (ADP–ribose) polymerase (PARP), a known substrate of effector caspases, by western blotting analysis (Figure 3A). We found an increase in the levels of the proteolytic form of PARP (86 kDa) in R2C cells upon both chenodeoxycholic acid (CDCA 50 and 75 μM) and GW4064 (3μM) treatment. Next, we observed in the same experimental condition that FXR activation induced a marked DNA fragmentation, a diagnostic hallmark of cells undergoing apoptosis (Figure 3B). TUNEL assay showed after CDCA and GW4064 exposure a strong induction of the apoptotic cells (Figure 3C). A similar pattern of apoptotic nuclei staining was also observed in R2C xenografts following GW4064 stimulation (Figure 3D).

Taken together, these data indicate that apoptotic processes could be involved in the antiproliferative effects exerted by FXR ligands on Leydig tumor cells.

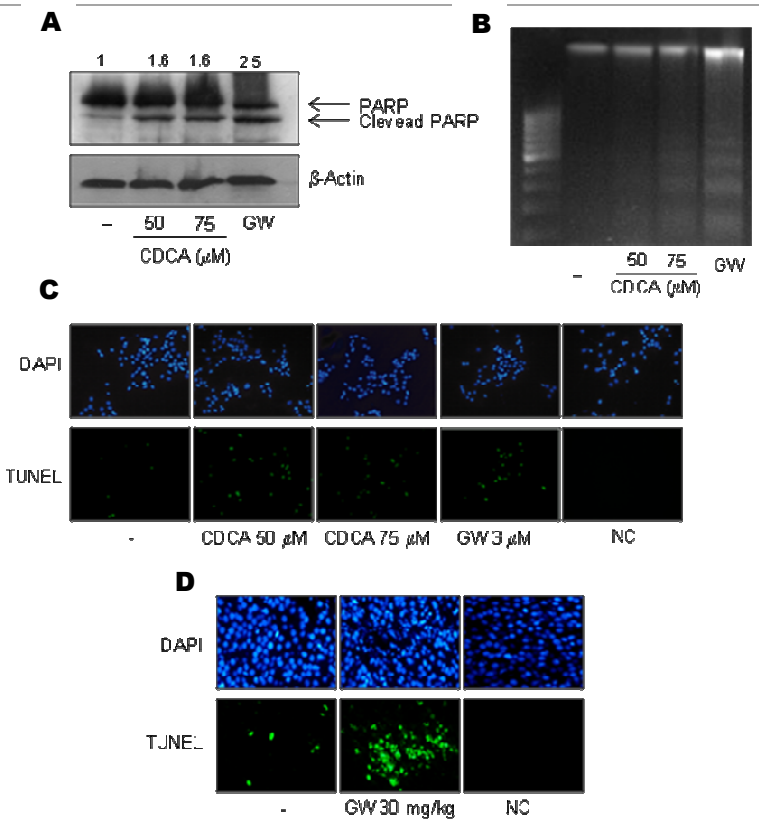

Figure 3. Induction of apoptosis by FXR ligands *in vitro* and *in vivo*. (A) Immunoblots of poly (ADP–ribose) polymerase (PARP) from extracts of R2C treated with vehicle (-) or chenodeoxycholic acid (CDCA 50 and 75 μM)) and GW4064 (3μM) for 24h. β-Actin was used as loading control. Numbers on top of the blots represent the average fold change versus control of R2C cells normalized for β-Actin. (B) DNA laddering performed in R2C cells treated with vehicle (-) or chenodeoxycholic acid (CDCA 50 and 75 μM)) and GW4064 (3μM) for 24h. TUNEL assay in R2C cells treated as in indicated for 24h (C) or in R2C xenografts (D).

Activated FXR up-Regulates p53 and p21$^{WAF1/Cip1}$ expression in R2C.

To examine the molecular mechanisms associated with the induction of apoptosis mediated by FXR ligands we evaluated, in Leydig tumor cells, the ability of CDCA and GW4064 to modulate the expression of p53, a tumor suppressor gene that plays an important role in apoptotic events (Kastan MB *et al.* 1991; Levine AJ *et al.* 1997).

As shown in Figure 4A and B FXR ligands treatment induced a significant increase in p53 protein content and mRNA levels. In addition, in the same experimental condition, we examined the expression of the p53 natural target gene p21$^{WAF1/Cip1}$. p21$^{WAF1/Cip1}$ protein and mRNA expressions were increased in all treatment compared with control (Figure 4A and B).

These results were confirmed *in vivo* since we observed a significant up-regulation in the expression of both p53 and $p21^{WAF1/Cip1}$ genes in R2C tumor xenografts (Figure 4 C and D).

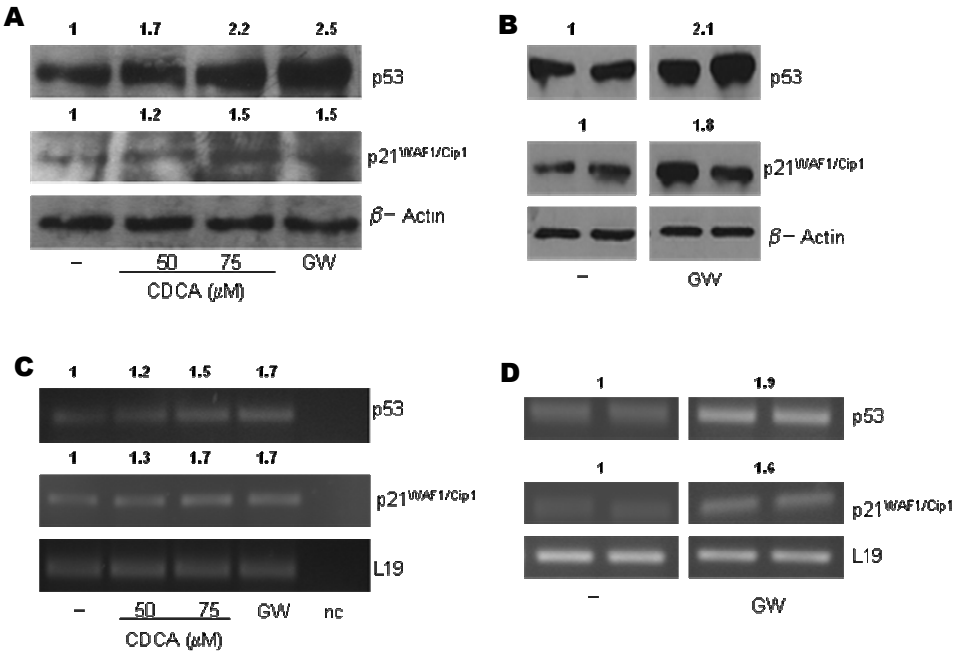

Figure 4. Up-Regulation of p53 and $p21^{WAF1/Cip1}$ Gene expression by FXR ligands *in vitro* and *in vivo*. Immunoblot of p53 and $p21^{WAF1/Cip1}$ from extracts of R2C cells treated for 24h with vehicle (-) or CDCA (50 and 75 μM) and GW4064 (3μM) for 24 h (A), or from R2C xenograft untreated or treated with GW (30 mg/kg day) (C). β-Actin was used as loading control. Total RNA from R2C cells treated as indicated (B) or from R2C xenograft (D) was reverse transcribed. cDNA was subjected to PCR using primers specific for p53, $p21^{WAF1/Cip1}$ and L19 (internal standard).

These findings suggest that p53 gene is involved in FXR-dependent apoptosis and that its modulation relies on transcriptional mechanisms.

FXR ligands transactivate p53 gene promoter

To investigate whether GW4064 is able to transactivate the p53 promoter gene, we transiently transfected R2C cells with a luciferase reporter construct (named p53-1) containing the upstream region of the p53 gene spanning from -1800 to +12 (Figure 5A). Treatment for 24h with 3 μM GW4064 significantly induced luciferase activity (Figure 5B). To identify the region within the p53 promoter responsible for its transactivation, we used constructs with deletions to different binding sites such as CTF-1 (CCAAT-binding transcription factor-1), nuclear factor-Y, NF-kB, and GC sites (Figure 5A). In transfection experiments performed using the mutants p53-6 and p53-13 encoding the regions from -106 to + 12 and from -106 to -40, respectively, the responsiveness to GW4064 was still observed (Figure 5B). In contrast, a construct encoding the sequence from -106 to -49 containing a deletion of the NF-kB domain (p53-14) the transactivation of p53 by FXR ligand was not longer noticeable (Figure 5B), suggesting that NF-kB site is required for p53 transcriptional activity. This latter result addresses that the integrity of NF-kB-binding site is necessary for FXR modulation of p53 promoter activity in Leydig tumor cells. However, additional experiments are required to better characterize the involvement of NF-kB in FXR-mediated p53 up-regulation.

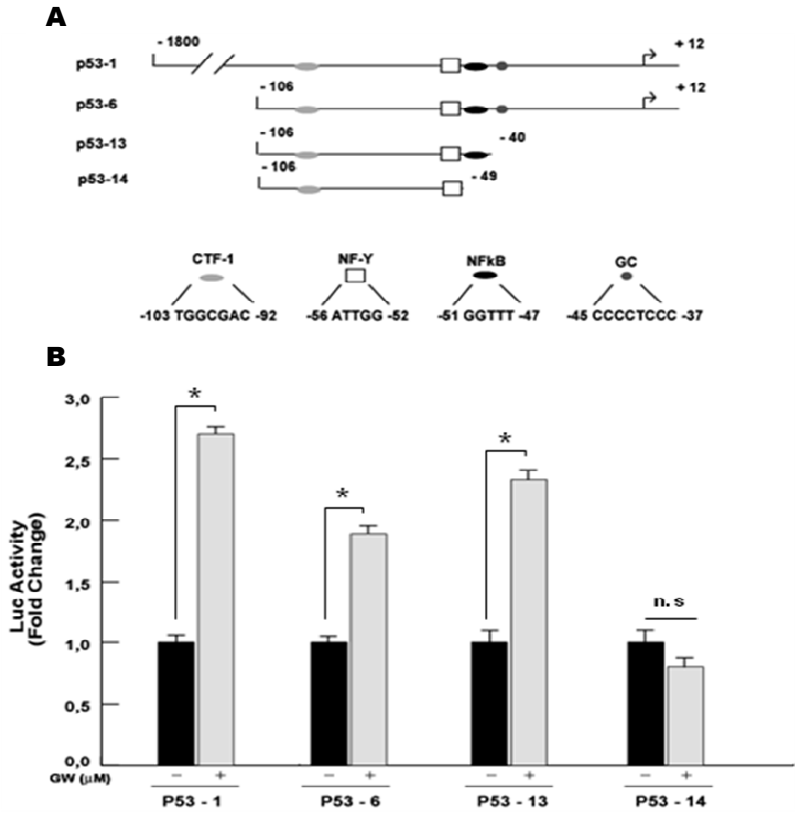

Figure 5. Effects of GW4064 on p53-gene promoter-luciferase reporter constructs in R2C cells. (A) Schematic map of the p53 promoter fragments used in this study. (B) R2C cells were transiently transfected with p53 gene promoter-luc reporter constructs (p53-1, p53-6, p53-13, p53-14) and treated for 24h with GW4064 3µM. The luciferase activities were normalized to the *Renilla* luciferase as internal transfection control and data were reported as fold change. Columns are mean ± SD of three independent experiments performed in triplicate. CTF-1, CCAAT-binding transcription factor-1; NF-Y, nuclear factor-Y. *P<0.05 compared with vehicle.

DISCUSSION

In the present study we have elucidated the molecular mechanisms through which FXR ligands exert antiproliferative effects in breast and in Leydig carcinoma cells.

In the first part of our work, we show for the first time that the activated FXR downregulates HER2 expression in ERα-positive breast cancer cells resistant to Tamoxifen (Tam). This occurs through the inhibition of NF-kB binding to its responsive element located in the human HER2 promoter region and results in a significant reduction of Tam-resistant growth.

The HER2/neu transmembrane kinase receptor is a signaling amplifier of the HER family network, as activation of membrane tyrosine receptors (EGFR, HER3 and HER4) by their respective ligands determines the formation of homodimeric and heterodimeric kinase complexes into which this receptor is recruited as a preferred partner (Yarden, Y. 2001). Multiple lines of evidences suggest a role of HER2 in the pathogenesis of breast carcinoma (Allred, DC *et al.* 1992; Glockner, S. *et al.* 2001), and clinical data suggest that breast tumors expressing elevated levels of HER2 show a more aggressive phenotype and worse outcome when treated with Tam (Arpino, G. *et al,* 2004; De Laurentiis, M. *et al.* 2005). Thus, inhibitory agents targeting HER2, such as the monoclonal antibody trastuzumab (herceptin), have been explored to improve hormonal treatment or delay emergence of endocrine resistance in estrogen-dependent breast tumors (Johnston, SR 2009). However, even though an increased response rate is obtained when trastuzumab is used in combination with chemotherapeutic agents (Seidman, AD *et al.* 2001; Slamon, DJ *et al.* 2001), patients can still develop resistance. These observations highlight the importance of discovering new therapeutic tools interfering with HER2-driven signaling to overcome therapy resistance.

We have demonstrated that treatment of breast cancer cells resistant to Tam with the FXR natural ligand CDCA resulted in a reduction of HER2 protein expression. Similar results were also obtained in the ERα-negative and HER2-

overexpressing SKBR3 breast cancer cells, suggesting that it may represent a general mechanism not related to cell specificity. Moreover, it assumes more relevance in Tam-resistant breast cancer cells, which are strongly dependent on HER2 activity for their growth. The complete abrogation of FXR-mediated HER2 downregulation with expression of an FXR-DN vector, along with the effects exerted by the synthetic FXR agonist GW4064, clearly demonstrated that activated FXR is involved in the regulation of HER2 expression. Furthermore, quantitative RT–PCR analysis demonstrated that HER2 mRNA levels were significantly decreased in both MCF-7 and MCF-7 TR1 cells treated with CDCA, suggesting that the FXR-induced HER2 downregulation arises via transcriptional mechanisms. Therefore, we focused on the molecular mechanisms by which FXR mediates repression of HER2 gene expression and on the biological consequences of FXR activation on anti-estrogen-resistant growth of breast cancer cells.

FXR acts mainly by regulating the expression of target genes by binding either as a monomer or heterodimer with the retinoid X receptor to FXR response elements (Laffitte, BA *et al.* 2000; Ananthanarayanan, M. *et al.* 2001; Claudel, T. *et al.* 2002; Kalaany, NY and Mangelsdorf, DJ 2006). Human HER2 promoter did not display any FXR response elements, thus it is reasonable to hypothesize that FXR-induced downregulation of HER2 promoter activity may occur through its interaction with other transcriptional factors. For instance, it has been described the transrepression mechanisms for FXR-mediated inhibition of endothelin-1 expression in vascular endothelial cells (He, F. *et al.* 2006). In addition, it has also been demonstrated that FXR negatively regulates IL-1β expression by stabilizing the nuclear corepressor NCoR on the NF-kB sequence within the IL-1β promoter (Vavassori, P. *et al.* 2009). Several recognition elements are present within the HER2 proximal promoter (Ishii, S. *et al.* 1987; Hurst, HC 2001) and among these functional motifs we have identified both AP-1 and NF-kB response elements as potential targets of FXR. We have demonstrated by functional studies and site-specific mutagenesis analysis that the integrity of the NF-kB sequence is a prerequisite for the downregulatory effects of the FXR ligand on HER2 promoter activity. These results were supported by electrophoretic mobility shift assays, which revealed a marked decrease in a specific DNA-binding complex in nuclear

extracts from MCF-7 and MCF-7 TR1 cells treated with CDCA. *In vitro* competition studies showed that FXR protein was able to inhibit the binding of NF-kB to its consensus site on the HER2 promoter. Furthermore, we observed a reduced recruitment of both NF-kB and RNA polymerase II in CDCA-treated cells, concomitant with an enhanced recruitment of histone deacetylase 3 supporting a negative transcriptional role for FXR in modulating HER2 expression. The physiological relevance of these effects is pointed out by proliferation studies showing that FXR activation reduced breast cancer cell growth, but did not affect the proliferation of the non-tumorogenic breast epithelial MCF-10A cell line. MCF-7 TR1 cells exhibited lower IC50 values for both ligands compared with parental MCF-7 cells, suggesting a higher sensitivity of the Tam-resistant cells to the effects of FXR ligands.

This suggestion is also well supported by the results obtained from growth assays, showing that combined treatment with CDCA and Tam significantly reduced Tam-resistant growth in MCF-7 TR1 cells, compared with Tam alone, but had no additive effects in MCF-7 parental cells. Moreover, FXR ligands failed to inhibit Tam-resistant growth in MCF-7/HER2-18 cells, in which HER2 expression is not driven by its own gene promoter activity. These latter results provided evidences that the downregulation of HER2 expression at transcriptional level underlies the ability of activated FXR to inhibit Tam-resistant growth in breast cancer cells.

Previous *in vitro* studies showed that enhanced EGFR/HER2 expression together with activation of downstream signaling pathways such as p42/44 MAPK are involved in acquired Tam resistance (Knowlden, JM *et al.* 2003; Nicholson, RI *et al.* 2004). Our studies showed that CDCA treatment significantly reduced the ability of EGF to activate its signal transduction cascade in MCF-7 TR1 cells, inhibiting both HER2 and MAPK phosphorylation. In addition, FXR activation was associated with a marked inhibition in EGF-induced growth, concomitant with a reduction in cyclin D1 expression in Tam-resistant breast cancer cells. All together these data demonstrate, as represented in Figure 14, that activated FXR, by preventing the binding of NF-kB to its response element located in the HER2 promoter sequence, abrogates HER2 expression and signaling, resulting in an inhibition of Tam-resistant growth in breast cancer cells.

Deciphering the molecular mechanisms responsible for the development of hormonal resistance is essential for establishing the most appropriate hormone agent according to tumor characteristics and for defining the optimal sequence of endocrine therapies. Moreover, this knowledge is critical for development of new therapeutic approaches able to either overcome or prevent endocrine resistance in breast cancer patients. Over the last years, significant survival benefits for breast cancer were derived from the use of combined treatment of endocrine therapies with new targeted therapies in endocrine responsive breast cancer (Johnston, SR 2009). In this scenario, the sequencing or the combination of Tam with FXR ligands may represent an important research issue to explore as an alternative therapeutic strategy to treat breast cancer patients whose tumors exploit HER2 signaling to escape Tam treatment.

In the second part of our work, we demonstrated that FXR activation suppresses Leydig carcinogenesis. We have recently reported that FXR is expressed in normal rodent testis and in a Leydig tumor cell line, where it negatively regulates expression of the enzyme aromatase that converts androgens into estrogens. FXR inhibits aromatase transcription through a mechanism that involves competition with the SF-1 receptor for binding to common nuclear response elements on the Cyp19 PII promoter. Inhibition of aromatase expression mediated by FXR ligands exerts an important role in reducing the estrogen-dependent R2C cell proliferation (Catalano, S. *et al.* 2010). However, direct evidence is missing for the *in vivo* effect of FXR activation in Leydig cancer progression.

The present study shows that FXR activation in xenograft model resulted in a marked decrease of tumor size caused by a reduction of aromatase expression and the induction of proapoptotic pathways.

The role of FXR in growth regulation, apoptosis, and cancer is still controversial. Separate studies have established both positive and negative correlations between FXR expression and cancer. An early study showed that expression of FXR was inversely related to the progression of human colorectal cancers and the degree of malignancy of colon cancer cell lines (De Gottardi, A. *et al.* 2004). Modica *et al.* evidenced that activation of FXR leads to a direct oncosuppressing activity by

blocking tumor growth in a xenografts mouse model. Activated FXR reduces proliferation and induces apoptosis in colorectal cancer cells by increasing the mRNA levels of several proapoptotic genes (Modica, S. *et al.* 2008). A recent study showed that FXR deficiency promotes cell proliferation, inflammation, and tumorigenesis in the intestine, suggesting that activation of FXR by nonbile acid ligands may protect against intestinal carcinogenesis (Maran, RR *et al.* 2009). Other studies in mice showed that FXR deficiency caused liver hyperproliferation and ultimately leads to spontaneous hepatocarcinomas (Kim, I. *et al.* 2007). Moreover, FXR agonists have been reported to inhibit aromatase expression and induce apoptosis in mammary carcinoma MCF7 and MDA-MB-468 cells (Swales, KE *et al*. 2006) suggesting that FXR activation promotes apoptosis and may have protective effects against tumorigenesis. In contrast, the FXR antagonist guggulsterone promoted apoptosis in Barrett's esophageal-derived cells (De Gottardi, A. *et al.* 2006) and inhibited proliferation, decreased migration and invasion in pancreatic cancer cells (Lee, JY *et al.* 2011).

We have found that FXR ligands induced cell apoptosis in R2C cells as evidenced by an increase in the levels of the proteolytic form of PARP, a crucial target that signals the presence of DNA damage and facilitates DNA repair. According to these findings, we evidenced upon FXR exposure a marked DNA fragmentation and, by TUNEL assay, a strong increase of the apoptotic nuclei respect to untreated cells. The *in vitro* results were also confirmed by *in vivo* studies since GW4064 treatment induced apoptosis also in R2C tumor xenografts.

A large body of evidence has suggested the straightforward role of p53 signaling in the apoptotic cascades (Haupt, S. *et al.* 2003; Schuler, M. and Green, DM 2001; Yu, J. and Zhang, Y. 2005). p53 acts as a tumor suppressor depending on its physical and functional interaction with diverse cellular proteins, like some nuclear receptors that, in turn, exert an inhibitory activity on p53 biological outcomes. Activation of p53 by UV damage or other agents/signals results in p53-mediated transcription or up-regulation of genes such as the cyclin-dependent kinase inhibitor $p21^{WAF1/Cip1}$ to induce apoptotic process, inhibiting the growth of cells with damaged DNA or cancer cells (Oren, M. *et al.* 2002; Sengupta, S. and Wasylyk, B. 2004). We have shown that FXR activation up-regulates both p53

mRNA and protein levels with a concomitant increase of $p21^{WAF1/Cip1}$ expression in R2C cells as well as in xenografts model. Functional studies evidenced the ability of activated FXR to modulate p53 promoter gene activity. Using different deletion mutants of p53 promoter gene, we have found that the FXR-mediated p53 transactivation involves the NF-kB site.

Moreover, it is important to underline that concomitant with this apoptotic event we observed, in R2C tumor xenografts treated with GW4064, a reduction of aromatase expression.

In conclusion, data from the present study demonstrate that the growth inhibition on Leydig tumor cells exerted by FXR ligands relies on two mechanisms: a reduction of aromatase expression resulting in a decrease of estrogen-dependent growth and the induction of proapoptotic pathways.

All together our findings, showing the anticancer activity of activated FXR, candidate FXR ligands as novel therapeutic tools to treat different estrogen-dependent cancers.

REFERENCES

Allred DC, Clark GM, Molina R, Tandon AK, Schnitt SJ, Gilchrist KW, Osborne CK, Tormey DC, McGuire WL. (1992). Overexpression of HER-2/neu and its relationship with other prognostic factors change during the progression of in situ to invasive breast cancer. Hum Pathol 23: 974-979.

Ananthanarayanan M, Balasubramanian N, Makishima M, Mangelsdorf DJ, Suchy FJ. (2001). Human bile salt export pump promoter is transactivated by the farnesoid X receptor/bile acid receptor. J Biol Chem 31: 28857-28865.

Andrews NC, Faller DV. (1991). A rapid micropreparation technique for extraction of DNA-binding proteins from limiting numbers of mammalian cells. Nucleic Acids Res 19: 2499.

Arpino G, Green SJ, Allred DC, Lew D, Martino S, Osborne CK. Arpino G, Elledge RM. (2004). HER-2 amplification, HER-1 expression, and tamoxifen response in estrogen receptor-positive metastatic breast cancer: a southwest oncology group study. Clin Cancer Res 17: 5670-6.

Arpino G, Wiechmann L, Osborne CK, Schiff R. (2008). Crosstalk between the estrogen receptor and the HER tyrosine kinase receptor family: molecular mechanism and clinical implications for endocrine therapy resistance. Endocr Rev 29: 217-233.

Bishop-Biley D. (2004). FXR as a novel therapeutic target for vascular disease. Drug News Perspect 17: 499-504.

Blume-Jensen P, Hunter T. (2001). Oncogenic kinase signalling. Nature 411: 355-365.

Catalano S, Malivindi R, Giordano C, Gu G, Panza S, Bonofiglio D, Lanzino M, Sisci D, Panno ML, Andò S. (2010). Farnesoid X receptor, through the binding with steroidogenic factor 1-responsive element, inhibits aromatase expression in tumor Leydig cells. J Biol Chem 285: 5581-5593.

Chung YL, Sheu ML, Yang SC, Lin CH, Yen SH. (2002). Resistance to tamoxifen-induced apoptosis is associated with direct interaction between Her2/neu and cell membrane estrogen receptor in breast cancer. Int J Cancer 97: 306-312.

Claudel T, Sturm E, Duez H, Torra IP, Sirvent A, Kosykh V, Fruchart JC, Dallongeville J, Hum DW, Kuipers F, Staels B. (2002). Bile acid-activated nuclear receptor FXR suppresses apolipoprotein A-I transcription via a negative FXR response element. J Clin Invest 7: 961-71.

De Gottardi A, Dumonceau JM, Bruttin F, Vonlaufen A, Morard I, Spahr L, Rubbia-Brandt L, Frossard JL, Dinjens WN, Rabinovitch PS, Hadengue A.

(2006). Expression of the bile acid receptor FXR in Barrett's esophagus and enhancement of apoptosis by guggulsterone in vitro. Mol Cancer 20: 5-48.

De Gottardi A, Touri F, Maurer CA, Perez A, Maurhofer O, Ventre G, Bentzen CL, Niesor EJ, Dufour JF. (2004). The bile acid nuclear receptor FXR and the bile acid binding protein IBABP are differently expressed in colon cancer. Dig Dis Sci 49: 982-9.

De Laurentiis M, Arpino G, Massarelli E, Ruggiero A, Carlomagno C, Ciardiello F, Tortora G, D'Agostino D, Caputo F, Cancello G, Montagna E, Malorni L, Zinno L, Lauria R, Bianco AR, De Placido S. (2005). A meta-analysis on the interaction between HER-2 expression and response to endocrine treatment in advanced breast cancer. Clin Cancer Res 11: 4741-4748.

Downes, M. Verdecia MA, Roecker AJ, Hughes R, Hogenesch JB, Kast-Woelbern HR, Bowman ME, Ferrer JL, Anisfeld AM, Edwards PA, Rosenfeld JM, Alvarez JG, Noel JP, Nicolaou KC, Evans RM. (2003). A chemical, genetic, and structural analysis of the nuclear bile acid receptor FXR. Mol Cell 11: 1079-1092.

Encarnacion CA, Ciocca DR, McGuire WL, Clark GM, Fuqua SA, Osborne CK. (1993). Measurement of steroid hormone receptors in breast cancer patients on tamoxifen. Breast Cancer Res Treat 26: 237-246.

Forman, BM, Goode E, Chen J, Oro AE, Bradley DJ, Perlmann T, Noonan DJ, Burka LT, McMorris T, Lamph WW, Evans RM, Weinberger C. (1995). Identification of a nuclear receptor that is activated by farnesol metabolites. Cell 81: 687-693.

Glockner S, Lehmann U, Wilke N, Kleeberger W, Langer F, Kreipe H. (2001). Amplification of growth regulatory genes in intraductal breast cancer is associated with higher nuclear grade but not with the progression to invasiveness. Lab Invest 81: 565-571.

Goodwin B, Jones SA, Price RR, Watson MA, McKee DD, Moore LB, Galardi C, Wilson JG, Lewis MC, Roth ME, Maloney PR, Willson TM, Kliewer SA. (2000). A regulatory cascade of the nuclear receptors FXR, SHP-1, and LRH-1 represses bile acid biosynthesis. Mol Cell 6: 517-526.

Grober J, Zaghini I, Fujii H, Jones SA, Kliewer SA, Willson TM, Ono T, Besnard P. (1999). Identification of a bile acid-responsive element in the human ileal bile acid-binding protein gene. Involvement of the farnesoid X receptor/9-cis-retinoic acid receptor heterodimer. J Biol Chem 42: 29749-29754.

Gutierrez MC, Detre S, Johnston S, Mohsin SK, Shou J, Allred DC, Schiff R, Osborne CK, Dowsett M. (2005). Molecular changes in tamoxifen-resistant breast cancer: relationship between estrogen receptor, HER-2, and p38 mitogen-activated protein kinase. J Clin Oncol 23: 2469-2476.

Haupt S, Berger M, Goldberg Z, Haupt Y. (2003). Apoptosis - the p53 network. J Cell Sci 15: 4077-85.

Hawkins C, Miaskowski C. (1996). Testicular cancer: a review. Oncol Nurs Forum 23: 1203-11.

He F, Li J, Mu Y, Kuruba R, Ma Z, Wilson A, Alber S, Jiang Y, Stevens T, Watkins S, Pitt B, Xie W, Li S. (2006). Downregulation of endothelin-1 by farnesoid X receptor in vascular endothelial cells. Circ Res 98: 192-199.

Huang W, Ma K, Zhang J, Qatanani M, Cuvillier J, Liu J, Dong B, Huang X, Moore DD. (2006). Nuclear receptor-dependent bile acid signaling is required for normal liver regeneration. Science 312: 233-236.

Huber RM, Murphy K, Miao B, Link JR, Cunningham MR, Rupar MJ, Gunyuzlu PL, Haws TF, Kassam A, Powell F, Hollis GF, Young PR, Mukherjee R, Burn TC. (2002). Generation of multiple farnesoid-X-receptor isoforms through the use of alternative promoters. Gene. 1-2: 35-43

Hurst HC. (2001). Update on HER-2 as a target for cancer therapy: the ERBB2 promoter and its exploitation for cancer treatment. Breast Cancer Res 3: 395-398

Ishii S, Imamoto F, Yamanashi Y, Toyoshima K, Yamamoto T. (1987). Characterization of the promoter region of the human cerbB-2 protooncogene. Proc Natl Acad Sci USA 84: 4374-4378.

Johnston SR. (2009). Enhancing the efficacy of hormonal agents with selected targeted agents. Clin Breast Cancer 9 (Suppl 1): S28-S36.

Journe F, Durbecq V, Chaboteaux C, Rouas G, Laurent G, Nonclercq D, Sotiriou C, Body JJ, Larsimont D. (2009). Association between farnesoid X receptor expression and cell proliferation in estrogen receptor-positive luminal-like breast cancer from postmenopausal patients. Breast Cancer Res 115: 523-35.

Kalaany NY, Mangelsdorf DJ. (2006). LXRS and FXR: the yin and yang of cholesterol and fat metabolism. Annu Rev Physiol 68:159-191.

Kastan MB, Onyekwere O, Sidransky D, Vogelstein B, Craig RW. (1991). Participation of p53 protein in the cellular response to DNA damage. Cancer Research 23: 6304-6311.

Kim I, Morimura K, Shah Y, Yang Q, Ward JM, Gonzalez FJ. (2007). Spontaneous hepatocarcinogenesis in farnesoid X receptor-null mice. Carcinogenesis 5: 940-6.

Kirkegaard T, McGlynn LM, Campbell FM, Muller S, Tovey SM, Dunne B, Nielsen KV, Cooke TG, Bartlett JM. (2007). Amplified in breast cancer 1 in human epidermal growth factor receptor-positive tumors of tamoxifen-treated breast cancer patients. Clin Cancer Res 13: 1405-1411.

Knowlden JM, Hutcheson IR, Jones HE, Madden T, Gee JM, Harper ME, Barrow D, Wakeling AE, Nicholson RI. (2003). Elevated levels of epidermal growth factor receptor/c-erbB2 heterodimers mediate an autocrine growth regulatory pathway in tamoxifen-resistant MCF-7 cells. Endocrinology 144: 1032-1044.

Kocarek TA, Shenoy SD, Mercer-Haines NA, Runge-Morris M. (2002). Use of dominant negative nuclear receptors to study xenobiotic-inducible gene expression in primary cultured hepatocytes. J Pharmacol Toxicol Methods 3: 177-87.

Laffitte BA, Kast HR, Nguyen CM, Zavacki AM, Moore DD, Edwards PA. (2000). Identification of the DNA binding specificity and potential target gene for the farnesoid X-activated receptor. J Biol Chem 275: 10638-10647.

Lee JY, Lee KT, Lee JK, Lee KH, Jang KT, Heo JS, Choi SH, Kim Y, Rhee JC. (2011). Farnesoid X receptor, overexpressed in pancreatic cancer with lymph node metastasis promotes cell migration and invasion. Br J Cancer 6: 1027-37.

Levine AJ. (1997). p53, the cellular gatekeeper for growth and division. Cell 3: 323-331.

Maglich JM, Caravella JA, Lambert MH, Willson TM, Moore JT, Ramamurthy L. (2003). The first completed genome sequence from a teleost fish (Fugu rubripes) adds significant diversity to the nuclear receptor superfamily. Nucleic Acids Res 31: 4051-4058

Makishima M, Okamoto AY, Repa JJ, Tu H, Learned RM, Luk A, Hull MV, Lustig KD, Mangelsdorf DJ, Shan B. (1999). Identification of a nuclear receptor for bile acids. Science 284: 13621365

Maloney PR, Parks DJ, Haffner CD, Fivush AM, Chandra G, Plunket KD, Creech KL, Moore LB, Wilson JG, Lewis MC, Jones SA, Willson TM. (2000). Identification of a chemical tool for the orphan nuclear receptor FXR. J Med Chem 43: 2971-297

Maran RR, Thomas A, Roth M, Sheng Z, Esterly N, Pinson D, Gao X, Zhang Y, Ganapathy V, Gonzalez FJ, Guo GL. (2009). Farnesoid X receptor deficiency in mice leads to increased intestinal epithelial cell proliferation and tumor development. J Pharmacol Exp Ther 2: 469-77.

Meng S, Tripathy D, Shete S, Ashfaq R, Haley B, Perkins S, Beitsch P, Khan A, Euhus D, Osborne C, Frenkel E, Hoover S, Leitch M, Clifford E, Vitetta E, Morrison L, Herlyn D, Terstappen LW, Fleming T, Fehm T, Tucker T, Lane N, Wang J, Uhr J. (2004). HER-2 gene amplification can be acquired as breast cancer progresses. Proc Natl Acad Sci USA 101: 9393-9398.

Modica S, Murzilli S, Salvatore L, Schmidt D R, Moschetta A. (2008). Nuclear bile acid receptor FXR protects against intestinal tumorigenesis. Cancer Res 68: 9589-9594.

Nicholson RI, Staka C, Boyns F, Hutcheson IR, Gee JM. (2004). Growth factor-driven mechanisms associated with resistance to estrogen deprivation in breast cancer: new opportunities for therapy. Endocr Relat Cancer 11: 623-641.

Oren M, Damalas A, Gottlieb T, Michael D, Taplick J, Leal JF, Maya R, Moas M, Seger R, Taya Y, Ben-Ze'ev A. (2002). Regulation of p53: intricate loops and delicate balances. Biochem Pharmacol 5-6: 865-71.

Osborne CK, Bardou V, Hopp TA, Chamness GC, Hilsenbeck SG, Fuqua SA, Wong J, Allred DC, Clark GM, Schiff R. (2003). Role of the estrogen receptor coactivator AIB1 (SRC-3) and HER-2/neu in tamoxifen resistance in breast cancer. J Natl Cancer Inst 95: 353-361.

Otte K, Kranz H, Kober I, Thompson P, Hoefer M, Haubold B, Remmel B, Voss H, Kaiser C, Albers M, Cheruvallath Z, Jackson D, Casari G, Koegl M, Pääbo S, Mous J, Kremoser C, Deuschle U. (2003). Identification of farnesoid X receptor β as a novel mammalian nuclear receptor sensing lanosterol. Mol Cell Biol 23: 864-872.

Pellicciari R, Costantino G, Fiorucci S. (2005). Farnesoid X Receptor: from structure to potential clinical applications. J Med Chem 48: 5383-5403

Qin C, Nguyen T, Stewart J, Samudio I, Burghardt R, Safe. (2002). Estrogen up-regulatio of p53 gene expression in MCF-7 breast cancer cells is mediated by calmodulin kinase IV-dependent activation of a nuclear factor kB/CCAAT-bindig transcription factor-1 complex. Mol Endocrinol 16: 1793-1809.

Rizzo G, Renga B, Antonelli E, Passeri D, Pellicciari R, Fiorucci S. (2005). The methyl transferase PRMT1 functions as co-activator of farnesoid X receptor (FXR)/9-cis retinoid X receptor and regulates transcription of FXR responsive genes. Mol Pharmacol 2: 551-8.

Sabnis GJ, Jelovac D, Long B, Brodie A. (2005). The role of growth factor receptor pathways in human breast cancer cells adapted to long-term estrogen deprivation. Cancer Res 65: 3903-3910.

Schiff R, Massarweh SA, Shou J, Bharwani L, Mohsin SK, Osborne CK. (2004). Cross-talk between estrogen receptor and growth factor pathways as a molecular target for overcoming endocrine resistance. Clin Cancer Res 10: 331S-336S.

Schuler M, Green DR. Mechanisms of p53-dependent apoptosis. (2001). Biochem Soc Trans 29(Pt 6): 684-8.

Seidman AD, Fornier MN, Esteva FJ, Tan L, Kaptain S, Bach A, Panageas KS, Arroyo C, Valero V, Currie V, Gilewski T, Theodoulou M, Moynahan ME, Moasser M, Sklarin N, Dickler M, D'Andrea G, Cristofanilli M, Rivera E, Hortobagyi GN, Norton L, Hudis CA. (2001). Weekly trastuzumab and paclitaxel therapy for metastatic breast cancer with analysis of efficacy by HER2 immunophenotype and gene amplification. J Clin Oncol 10: 2587-95.

Sengupta S, Wasylyk B. (2004). Physiological and pathological consequences of the interactions of the p53 tumor suppressor with the glucocorticoid, androgen, and estrogen receptors. Ann N Y Acad Sci 1024: 54-71.

Seol W, Choi HS, Moore DD. (1996). An orphan nuclear hormone receptor that lacks a DNA binding domain and heterodimerizes with other receptors. Science 272: 1336-1339

Shibata M, Morizane T, Uchida T, Yamagami T, Onozuka Y, Nakano M, Mitamura K, Ueno Y. (1998). Irregular regeneration of hepatocytes and risk of hepatocellular carcinoma in chronic hepatitis and cirrhosis with hepatitis-C-virus infection. Lancet 351: 1773-1777

Shou J, Massarweh S, Osborne CK, Wakeling AE, Ali S, Weiss H, Schiff R. (2004). Mechanisms of tamoxifen resistance: increased estrogen receptor-HER2/neu cross-talk in ER/HER2-positive breast cancer. J Natl Cancer Inst 12: 926-35.

Sinal CJ, Tohkin M, Miyata M, Ward JM, Lambert G, Gonzalez FJ. (2000). Targeted disruption of the nuclear receptor FXR/BAR impairs bile acid and lipid homeostasis. Cell 102: 731-744

Slamon DJ, Godolphin W, Jones LA, Holt JA, Wong SG, Keith DE, Levin WJ, Stuart SG, Udove J, Ullrich A. (1989). Studies of the HER-2/neu proto-oncogene in human breast and ovarian cancer. Science 244: 707-712.

Slamon DJ, Leyland-Jones B, Shak S, Fuchs H, Paton V, Bajamonde A, Fleming T, Eiermann W, Wolter J, Pegram M, Baselga J, Norton L. (2001). Use of chemotherapy plus a monoclonal antibody against HER2 for metastatic breast cancer that overexpresses HER2. N Engl J Med 344: 783–792.

Song CS, Echchgadda I, Baek BS, Ahn SC, Oh T, Roy AK, Chatterjee B. (2001). Dehydroepiandrosterone sulfotransferase gene induction by bile acid activated farnesoid X receptor. J Biol Chem 276: 42549-42556

Staka CM, Nicholson RI, Gee JM. (2005). Acquired resistance to estrogen deprivation: role for growth factor signalling kinases/oestrogen receptor cross-talk revealed in new MCF-7X model. Endocr Relat Cancer 12(Suppl 1): S85-S97.

Swales KE, Korbonits M, Carpenter R, Walsh DT, Warner TD, Bishop-Bailey D. (2006). The farnesoid X receptor is expressed in breast cancer and regulates apoptosis and aromatase expression. Cancer Res 66: 10120-10126

Urizar NL, Dowhan DH, Moore DD. (2000). The farnesoid X-activated receptor mediates bile acid activation of phospholipid transfer protein gene expression. J Biol Chem 275: 39313-39317.

Vavassori P, Mencarelli A, Renga B, Distrutti E, Fiorucci S. (2009). The bile acid receptor FXR is a modulator of intestinal innate immunity. J Immunol 183: 6251-6261.

Wang H, Chen J, Hollister K, Sowers LC, Forman BM. (1999). Endogenous bile acids are ligands for the nuclear receptor FXR/BAR. Mol Cell 5: 543-53.

Wang YD, Chen WD, Moore DD, Huang, WD. (2008). FXR: a metabolic regulator and cell protector. Cell Research 11: 1087-1095

Yarden Y. (2001). Biology of HER2 and its importance in breast cancer. Oncology 61(Suppl 2): 1-13.

Yu J, Zhang L. (2005). The transcriptional targets of p53 in apoptosis control. Biochem Biophys Res Commun. 3: 851-8.

Zhang Y, Kast-Woelbern HR, Edwards PA. (2003). Natural structural variants of the nuclear receptor farnesoid X receptor affect transcriptional activation. J Biol Chem 1: 104-110

Leptin as a novel mediator of tumor/stroma interaction promotes the invasive growth of breast cancer cells

Ines Barone[1,2*], Stefania Catalano[1,3*], Luca Gelsomino[3], Stefania Marsico[1,3], Cinzia Giordano[1], Salvatore Panza[3], Daniela Bonofiglio[1,3], Gianluca Bossi[4], Kyle R. Covington[5], Suzanne A.W. Fuqua[5] and Sebastiano Andò[1,2].

*These authors contributed equally to this work

Author Affiliations:
[1]Centro Sanitario and [2]Department of Cellular Biology, [3]Department of Pharmaco-Biology, University of Calabria, Rende, Italy, [4]Regina Elena Cancer Institute, Rome, Italy, [5]Lester and Sue Smith Breast Center and Department of Molecular and Cellular Biology, Baylor College of Medicine, Houston, Texas

Running Title: Bidirectional CAFs-Breast Cancer Cells Interaction

Key Words: Breast Cancer/Estrogen Receptor/K303R mutant ERα/CAFs/Leptin Signaling Pathway

Corresponding Author:
Sebastiano Andò, MD
Full Professor General Pathology
Department of Cellular Biology
Faculty of Pharmacy, Nutritional and Health Sciences
University of Calabria, Via P. Bucci, Arcavacata di Rende (CS) 87036, Italy
Phone: +390984496201
Fax: +390984496203
e-mail: sebastiano.ando@unical.it

Disclosure of Potential Conflict of Interest: The authors declare they have no conflict of interest.

Word Count: 5000

Number of Figures and Tables: 6 Figs, 4 Supplementary Figs, 1 Table, 3 Supplementary Tables

Resubmission to: Cancer Research, December 1, 2011

Abstract

Tumor phenotype is a result of the complex interactions between malignant cells and sorrounding stroma. However, the mechanisms by which cancer cells and fibroblasts, the most abundant and active part of the tumor stroma, interact remain to be elucidated. The K303R mutation of estrogen-receptor (ERα) was identified in 50% of invasive breast tumors and associated with poorer survival outcomes. Here, we show that human cancer-associated fibroblasts (CAFs) stimulated proliferation and migration of wild-type (WT) ERα stably transfected breast cancer cells and to a higher extent in cells expressing the K303R ERα hyperactive receptor. We identified, for the first time, leptin, a known cytokine involved in breast cancer development, as a determinant for CAFs tumor-promoting activities in both WT and K303R ERα-expressing cells. Indeed, we found an increase in leptin receptor isoforms expression, and in its signalling activation in K303R-expressing cells compared to WT ERα clones. These data correlated well with the amplified effects of leptin on cell growth, motility and invasiveness in mutant cells. Mutant expression generated a leptin hypersensitive phenotype also *in vivo*. Lastly, K303R ERα cell-secreted factors stimulated CAFs proliferation and migration and their ability to secrete leptin. We demonstrated that the epidermal growth factor is the paracrine factor by which breast cancer cells affect CAFs phenotype. Thus, our work uncovers a bidirectional cross-talk between breast cancer cells and 'educated' CAFs, which leads via leptin signaling to increased tumor progression. The blockade of these intercellular communications might represent an effective strategy for molecular targeted therapies in breast cancer.

Introduction

For the past three decades, cancer research focused predominantly on the characteristics of breast cancer cells. Recently, clinical and experimental studies revealed that both tumor initiation and progression are related to the complex interactions that transpire within the tumor microenvironment. The stromal compartment is composed of mesenchymal cells (fibroblasts/adipocytes/blood cells), extracellular matrix-ECM (lamin/fibronectin/collagen/proteoglicans/etc), and signals from these cells come as soluble secreted factors, ECM-components or direct cell-cell contacts. Growth factors, cytokines, adipokines, proteases, and vascular-stimulating factors are involved in stroma-mediated procancerous activities (1-4). The chemokines CXCL12, CXCL14, and CCL7 stimulated tumor cell proliferation and invasion *in vitro* and *in vivo*, increased tumor angiogenesis and macrophage presence at tumor sites (5-7). The interleukin-1 and -8 induced cancer progression by enhancing metastasis and cachexia (8,9). As important adipocyte-derived endocrine and paracrine mediator, the adipokine leptin has been correlated with breast cancer occurrence. Indeed, leptin synthesis and plasma levels increase with obesity, a pandemic condition that influences both risk and prognosis of breast cancers (10).

The processes of heterotypic signalling involve a constant bidirectional cross-talk between stromal cells, and malignant cells. Stromal cells influence tumor invasiveness and malignancy, whereas at the onset and during breast cancer progression, the microenvironment is reorganized by cancer cells (11). Tumors recruit stromal fibroblasts in a process referred to as the desmoplasmic reaction, and these carcinoma-associated fibroblasts (CAFs) are reprogrammed to produce growth factors, cytokines, and ECM-remodeling proteins, that acting in autocrine and paracrine fashion support tumor proliferation and invasion into surrounding tissues (4). Moreover, a variety of these factors may activate estrogen receptor alpha (ERα) (12).

Estrogens and its receptor play a crucial role in regulating breast cancer growth and differentiation. Variant forms of ERα due to alternative splicing or gene mutation have been reported, but their clinical significance is still unresolved (13,14). A naturally-occurring mutation at nucleotide 908, introducing a lysine to arginine transition at residue 303 within the hinge domain of the receptor (K303R ERα), was identified in a third of premalignant breast hyperplasias, and one-half of invasive breast tumors. This mutation correlated with poor outcomes, older age, larger tumor size, and lymph node-positive disease

(15,16). Other studies did not detect the mutation in invasive cancers (17-20), but our studies suggest that the detection method used might be insensitive. However, K303R expression was found at low frequency in invasive breast tumors by Conway and colleagues (21). K303R mutation allows ERα to be more highly phosphorylated by different kinases, and it alters the dynamic recruitment of coactivators and corepressors (22-24). Mutant overexpression in MCF-7 breast cancer cells increased sensitivity to subphysiological levels of estrogen, and decreased tamoxifen responsiveness when elevated growth factors signaling was present (15,25). K303R ERα mutation also conferred resistance to the aromatase inhibitor anastrozole (23,26), suggesting a pivotal role for this mutation in more aggressive breast cancers.

The aim of this study was to elucidate the mechanisms underlying tumor/stroma interaction in ERα–positive breast cancer cells. First, we investigated how tumoral microenvironment pressure, exerted by CAFs, impacts breast cancer cell proliferation, migration and invasiveness in relation to the expression of wild-type or the K303R ERα. We then defined the effect that a single factor-leptin has on stroma-mediated breast cancer progression. Finally, we examined the bidirectional interactions between CAFs and breast cancer cells, leading to increased malignancy.

Materials and Methods

Reagents and antibodies

Leptin/17β-estradiol/EGF from Sigma. ICI182,780 by Tocris Bioscience. AG490/AG1478/PD98059/LY294002 by Calbiochem. ERα/ERβ/GAPDH/ObRl/ObRs/Ob/Akt/pAkt^{Ser437} antibodies from Santa Cruz Biotechnology. MAPK/JAK2/STAT3/pMAPK$^{Thr202/Tyr204}$/pJAK2$^{Tyr1007/1008}$/ pSTAT3^{Tyr705}/pERα^{Ser118}/pERα^{Ser167} from Cell Signaling Technology.

Plasmids

Generation of yellow-fluorescent protein (YFP)-tagged expression constructs, YFP-WT and YFP-K303R-ERα, as described (22). XETL plasmid, containing an estrogen-responsive-element, by Dr Picard, University Geneva/Switzerland.

Cell culture

MCF-7 and SKBR3 cells were acquired in 2010 from American-Type-Culture-Collection where they were authenticated. Cells were stored according to supplier's instructions, and used within four months after frozen aliquots resuscitations. YFP-WT and YFP-K303R ERα-stable expressing MCF-7 cells, MCF-7 and SKBR3 pools stably transfected with YFP-WT and YFP-K303R ERα generated as described (23,26). Immortalized normal human foreskin fibroblasts BJ1-hTERT by Dr Lisanti, Jefferson University/Philadelphia/USA. Cell phenotype was ensured by morphology, doubling-times and ERα-transactivation assays.

CAFs-isolation

Human breast cancer specimens were collected from primary tumors of patients who signed informed consent. Following tumor excision, small pieces were digested (500IUcollagenase in Hank's-Balanced-salt-solution, Sigma; 37°C/2h). After differential centrifugation (90g/2min), the surnatant containing cancer-associated fibroblasts (CAFs) was centrifugated (500g/8min), resuspended and cultured in RPMI-1640 medium supplemented with 15% Fetal-Bovine-Serum/FBS, and antibiotics. CAFs between 4-10passages were used and authenticated by morphology and FAP expression.

Conditioned medium systems

CAFs were incubated with regular-full media (48-72h). Conditioned media were collected, centrifugated to remove cellular debris and used in respective experiments. Alternatively, conditioned media were collected from WT and K303R ERα-expressing MCF-7 cells incubated in 5% charcoal-stripped-FBS (72h).

Expression microarray analysis

Expression profiles were determined with Affymetrix GeneChip human genome U133plus2.0 arrays. Data quality and statistical analysis evaluated as described (23).

Immunoblot analysis

Protein extracts were subjected to SDS-PAGE as described (27). Immunoblots show a single representative of three separate experiments.

Immunofluorescence

Cells were fixed with 4% paraformaldehyde, permeabilized with PBS+0.2%TritonX-100 followed by blocking with 5%BSA (1h/room temperature), incubated with anti-ObR antibody (4°C/overnight) and with FITC-conjugated secondary antibody (30min/room temperature). IgG primary antibody as negative control. 4′,6-Diamidino-2-phenylindole (DAPI, Sigma) staining for nuclei detection. Fluorescence was photographed using OLYMPUS BX51 microscope,100Xobjective.

RT-PCR and Real-time RT-PCR assays

FAP/Ob/CyclinD1/pS2/CathepsinD/36B4 gene expression were evaluated by reverse transcription(RT)-PCR method as decribed (27). ObRl/ObRs/CXCR4/IR/IL2RB/IL6R/EGFR/IGF1R/FGFR3/ERα/EGF/IL6/ Insulin gene expression were assessed by Real-time RT-PCR, using SYBR Green Universal PCR Master Mix (Biorad). Each sample was normalized on 18s mRNA content. Relative gene expression levels were calculated as described (28). Primers in Supplementary Table 1.

ERα-transactivation assays

ERα-transactivation as described (29).

Cell proliferation assays

MTT assays. After 4 days of treatments, cell proliferation was assessed using 3-[4,5-Dimethylthiazol-2-yl]-2,5-diphenyltetrazolium bromide reagent/MTT (Sigma) and expressed as fold change relative to vehicle-treated cells.

Tripan-blue cell-count assays. After 4 days of treatment, cell numbers were evaluated by trypsin suspension of samples followed by microscopic evaluation using a hemacytometer.

Soft agar growth assays. Anchorage-independent growth as described (26).

Data represent three independent experiments, performed in triplicate.

Wound-healing scratch assays

Cell monolayers were scraped and treated as indicated. Wound closure was monitored over 24h, cells were fixed and stained with Comassie-Brillant-Blue. Pictures represent one of three independent experiments (10Xmagnifications, phase-contrast microscopy).

Transmigration assays

Cells treated with/without leptin were placed in Boyden-chamber upper compartments (8micron membranes/Corning Costar). Bottom well contained regular-full media. After 24h, migrated cells were fixed and stained with Comassie-Brillant-Blue. Migration was quantified by viewing five separate fields per membrane at 20Xmagnification and expressed as the mean number of migrated cells. Data represent three independent experiments, assayed in triplicate.

Invasion assays

Matrigel-based invasion assay was performed by invasion chambers (8micron membranes) coated with Matrigel (BD Bioscences,0.4μg/ml). Cells treated with/without leptin were seeded into top transwell chambers, while regular-full medium was used as chemoattractant in lower chambers. After 24h, invaded cells were evaluated as described for transmigration assays. Data represent three independent experiments, assayed in triplicate.

Tumor Xenografts

In vivo studies performed as described (30).

Leptin measurement by RIA

Leptin was measured by a competitive in-house immunoassay (Chematil) following manufacturer's protocol. Results are presented as ng/cells.

Leptin-immunodepleted conditioned media

Protein G-agarose beads were incubated with anti-leptin or IgG antibodies (4°C/3h). Antibody-beads complexes were incubated with CAFs-conditioned media (4°C/overnight) and centrifugated (three times/15000g/10min). Leptin-immunodepletion was verified by RIA.

Statistical analysis

Data were analyzed for statistical significance using two-tailed student's Test, Graph Pad Prism4. Standard deviations/S.D. are shown. Survival curves were computed by the Kaplan–Meier method and compared using two-sided log-rank tests.

Results

Tumor/stroma interactions stimulate cell proliferation and motility

Epithelial-stromal interactions support tumor cell proliferation and invasion. Thus, we first investigated the role of tumoral microenvironment in influencing breast cancer phenotype in relation to the expression of wild-type (WT) or K303R ERα mutant receptor.

We used as experimental models for breast cancer ERα-positive MCF-7 cells stably transfected with YFP-WT or YFP-K303R ERα expression vectors. We chose this approach because WT receptor was present along with K303R ERα in invasive breast tumors (16). Stable clones were screened for ERα expression using immunoblot analysis (Fig. 1A). Two clones stably expressing YFP-WT (WT1-2) or YFP-K303R ERα (K303R1-2) are shown along with WT or mutant receptor stable pools (WT P and K303R P). As stromal cells, we employed cancer-associated fibroblasts (CAFs), isolated from biopsies of primary breast tumors. CAFs possessed the basic fibroblast characteristics of long and spindle-shaped morphology, and highly expressed the fibroblast activation protein-FAP (Fig. 1B). To create *in vitro* conditions that can mimic the complex *in vivo* microenvironment, we used coculture experiments. Breast cancer cells were incubated with regular-full media (FM), CAFs-derived conditioned media (CM) or normal fibroblasts (NFs)-CM and growth was evaluated by soft agar assays (Fig. 1C). As previously demonstrated (23,26), control basal growth of mutant-expressing cells was elevated compared to WT-expressing cells. CAFs-CM significantly increased colony numbers in both WT and K303R ERα-expressing cells; however, CAFs-CM

enhanced K303R-expressing cell growth at a higher extent compared to WT-expressing cells. We then examined the ability of CAFs-CM to promote WT- and K303R-expressing cell movement in wound-healing scratch assays (Fig. 1C). The mutant cells moved the farthest in either direction to close the gap compared to WT-expressing cells. CAFs-CM promoted net movement of WT-expressing cells compared to FM; but, K303R-expressing cells exposed to CAFs-CM moved at higher rate to close the gap in the cell bed. As expected, CAFs possessed a higher ability to enhance both proliferation and motility of breast cancer cells than NFs (Fig. 1C). CAFs-CM-induced cell growth and migratory potential was blocked by inhibition of the classic cytokine JAK2/STAT3 signaling cascade (AG490) and the ERα signaling inhibitor (ICI182,780), although to a higher extent in K303R clones (Fig. 1D). All functional effects described so far are the results of exposure to the total complement of CAFs-secreted proteins. However, it is desirable albeit experimentally difficult to define the contribution of a single factor. Thus, we addressed which CAFs-secreted factor may promote breast cancer cell growth and motility.

Gene transcription patterns of WT and K303R ERα-overexpressing cells

Diffusible growth factors, interleukins, chemokines and adipokines implicated as mediators of stromal-epithelial interactions are involved in breast carcinoma initiation and progression. To determine changes in gene expression for the different receptors of CAFs-secreted factors, that may be responsible of the different sensitivity of WT and mutant clones to CAFs-CM exposure, we performed microarray analysis. Gene expression profile comparing RNA isolated from K303R-expressing with WT-expressing cells are shown in Table 1 and Supplementary Table 2. K303R ERα expression induced several genes potentially involved into tumor/stroma interactions; however, the leptin receptor (ObR) gene was the most highly induced (2.4fold, Table 1). We also observed increased expression of different leptin signaling downstream effectors such as JAK2, the transcription factors fos, STAT, as well as the suppressor of cytokine signaling 3 (Supplementary Table 3). To validate the microarray study, YFP-WT and YFP-K303R ERα-expressing cells were evaluated for a panel of genes using real-time PCR (Fig. 2A). K303R-associated induction could be confirmed for all of them, and, again, the gene encoding the long and short leptin receptor isoforms (ObRl/ObRs) was the most highly upregulated in mutant-expressing cells. However, we did not detect any differences in IGF1R

mRNA expression levels between the two cells, although microarray analysis showed a significant decrease of IGF1R. ERα RNA levels were similar between K303R and WT ERα-expressing cells.

The increase in both ObRl and ObRs was then confirmed by evaluating protein levels using immunoblotting analysis (Fig. 2B) and immunofluorescence staining of WT and K303R ERα-expressing cells (red, Fig. 2C).

K303R ERα-overexpressing cells exhibit increased leptin signaling activation

Given the gene expression profile identified in the microarray study, we defined the impact that a single factor-leptin may have on K303R ERα breast cancer cell progression. First, time-course response studies were performed to analyze phosphorylation of leptin downstream effectors using immunoblot analysis (Fig. 2D). WT-expressing cells exhibited low basal levels of phosphorylated JAK2, STAT3, Akt and MAPK that were increased in a time-dependent manner after leptin treatment. In contrast, K303R-expressing cells showed elevated constitutive phosphorylation of these signaling molecules in control-vehicle conditions that was slightly increased after leptin treatment. Thus, the mutant ERα expression was associated with increased leptin signaling activation.

Leptin directly activates ERα in the absence of its own ligand in MCF-7 breast cancer cells (29). As a consequence of the enhanced leptin signaling, we found increased ERα-transcriptional activity and upregulated mRNA levels of the classical ERα-target genes Cyclin D1, pS2 and Cathepsin D in both control and leptin-treated conditions in K303R ERα-expressing cells. In addition, the mutant exhibited elevated pS118 and pS167 YFP-ERα levels (Supplementary Fig. 1).

K303R ERα mutation and leptin hypersensitivity

We next used these stably transfected clones as model systems to study leptin sensitivity, in relation to mutant receptor expression. First, we evaluated leptin effects on growth using anchorage-dependent growth assays (Supplementary Fig. 2). As expected, in both WT and K303R-expressing cells treatment with leptin 100ng/ml increased cell proliferation. However, low leptin treatment (10ng/ml) significantly enhanced cell viability only in K303R-expressing clones. We also evaluated leptin-mediated proliferative effects in

anchorage-independent growth assays (Fig. 3A). Leptin treatments at 100 and 1000ng/ml concentrations enhanced colony numbers in all four clones tested, even though to a higher extent in mutant-expressing cells. Again, leptin at 10ng/ml increased anchorage-independent growth only in K303R cells. The increase in colony numbers induced by leptin was reversed by the JAK2/STAT3 inhibitor AG490 (Fig. 3B). We also used the antiestrogen ICI182,780 and found that this treatment suppressed anchorage-independent growth of both cell lines, indicating that ER expression remains important in growth regulation of these cells (Fig. 3B).

We next evaluated the ability of increasing doses of leptin to influence cell migration in wound-healing scratch assays (Fig. 3C). Again, the mutant cells moved farthest in either direction to close the gap compared to WT-expressing cells. Leptin treatments at 100 and 1000ng/ml promoted cell motility in both WT and K303R-expressing cells, although to a higher extent in mutant cells. Interestingly, leptin at 10ng/ml stimulated migration only in K303R-expressing cells. Then, the capacity of cells to migrate across uncoated membrane in transmigration assays or to invade an artificial basement membrane-Matrigel in invasion assays was tested in the presence of leptin (Fig. 3D). While WT cells exhibited little motile and no invasive behaviour *in vitro*, our data clearly demonstrated that mutant receptor expression increased both motility and invasion of cells. High doses of leptin increased the number of migrated and invaded cells in both clones and again low doses of leptin stimulated motility and invasion only of cells expressing the K303R receptor. As expected, treatment with AG490 and ICI182,780 resulted in a clear reduction of both control-untreated and leptin-induced cell motility in wound-healing scratch assays, especially in K303R-expressing cells (Fig. 3E). We recently published that K303R ERα MCF-7 xenograft tumors grew faster than WT ERα tumors (26). In addition, MCF-7 xenograft tumors doubled control value after 13 weeks of leptin exposure (30). Thus, we determined if the mutant receptor-expressing breast cancer cells might exhibit an increased sensitivity to leptin stimulation also *in vivo*. We found that in mice treated with leptin, all xenografts derived from cells with K303R ERα expression doubled in size within 6 weeks of treatment, while none of xenografts from WT ERα-expressing cells doubled in size during this experiment (Fig. 3F). Thus, expression of the mutant generated a leptin hypersensitive phenotype *in vitro* and *in vivo*.

Leptin is responsible for CAFs-induced cell growth and motility

We next assessed the role of leptin in the context of heterotypic signalings working in tumor/stroma interactions. First, RIA measurement in CAFs-CM showed that leptin secretion varied from 10±4.5ng/200.000cells. RT-PCR evidenced Ob mRNA expression in CAFs; CAFs also expressed ObR long isoform, but they did not express ObR short isoform, ERα, or ERβ (Supplementary Fig. 3). Leptin was then immunodepleted from CAFs-CM by leptin specific antibodies and resulting media were tested for the ability to induce anchorage-independent growth and migration of breast cancer cells. Leptin-depletion (CM+LepAb) significantly decreased growth and migration-promoting activities of CAFs-CM, particularly in K303R-expressing cells (Fig. 4A). CM treated with a non specific mouse IgG had not effects, suggesting that the neutralizing effects of leptin antibodies were specific. Our results identify leptin as a main molecular player that mediates CAFs effects on tumor cell growth and migration.

Leptin activates via JAK2 the MAPK and PI3K/Akt pathways (31). Thus, we investigated the specific signaling involved in the CAFs/breast cancer cells interaction, and found that the PI3K/Akt inhibitor LY294002 was more effective in inhibiting CAFs-induced proliferation and migration than the MEK1 inhibitor PD98059 (Fig. 4B).

Tumor/stroma interactions in SKBR3 breast cancer cells

To extend the results obtained, we generated pools of YFP-WT and YFP-K303R ERα stable transfectants in ERα-negative SKBR3 breast cancer cells (Supplementary Fig. 4). As previously shown for MCF-7 cells, we found a significant increase in both long and short leptin receptor isoforms mRNA in mutant-expressing cells. Again, treatment with leptin at 100 and 1000ng/ml significantly increased colony numbers of WT clones, and to a higher extent of K303R-expressing cells; however 10ng/ml of leptin enhanced anchorage-independent growth only in K303R-expressing clones. Similarly, low leptin promoted migration only in mutant cells. Finally, we tested CAFs-CM for its effects on cell growth and migration. We found a great induction of anchorage-independent growth and motility after treatment with CM, especially in K303R-expressing SKBR3 pools. Leptin-immunodepleted CM strongly reduced CM-proliferative and migratory-promoting activities on K303R cells, confirming that leptin hypersensitive phenotype was associated with K303R ERα expression in different cellular backgrounds.

Effects of breast cancer cell-secreted factors on CAFs phenotype

CAFs and tumor cells cross-talk via different soluble factors, whose effects on both subpopulations determine the final outcome of the tumorogenic process. Thus, as a final step of this study we defined the effects of CM from WT and K303R ERα-expressing breast cancer cells on CAFs phenotype. Treatment with K303R-CM elicited a dramatic alteration in the shape of CAFs *in vitro*, accompanied by an increased FAP mRNA expression (Fig. 5A). K303R-CM also stimulated CAFs viability and motility compared to WT-CM effects (Fig. 5B), suggesting how soluble K303R ERα cell-secreted factors may generate a more activated CAFs phenotype. Since leptin synthesis is influenced by different humoral factors (32-34), we evaluated the effects of breast cancer-derived CM in modulating leptin secretion from CAFs. Incubation of CAFs with K303R-CM increased leptin mRNA expression and leptin release compared with WT-CM, while no differences were detected in leptin levels among WT and K303R-CM (Fig. 5C). Finally, to investigate the paracrine factor by which breast cancer cells may affect CAFs phenotype, we used microarray analyses to measure the expression of different genes known to be associated with CAFs and/or leptin secretion (11,32-35). Our results showed that the genes encoding for EGF (2,8 fold), IL6 (1,2 fold) and Insulin (1,2 fold) were induced in mutant cells, and realtime PCR confirmed that the EGF gene was the most highly upregulated (Fig. 5D). Thus, we evaluated the role of EGF. First, addition of EGF in WT-CM mimicked the induction of K303R-CM on CAF motility, and the EGFR signaling inhibitor (AG1478) reduced K303R-CM effects (Fig. 5E). Second, treatment with AG1478 reversed K303R-CM stimulated FAP mRNA expression (Fig. 5F). Third, Ob mRNA expression and leptin secretion from CAFs cocultured with K303R-CM was significantly decreased in the presence of AG1478 (Fig. 5F).

Our data show that K303R ERα-expressing breast cancer cells through their soluble secreted factors may take advantage of the plastic nature of reactive surrounding cell populations, as CAFs, to generate a tumor enhancing microenvironment.

Discussion

ERα expression has important implications for breast cancer biology and therapy. Fuqua *et al.* identified a lysine to arginine transition at residue 303 of ERα (K303R ERα) in 30% of breast hyperplasias, and in 50%

of invasive breast cancers (15,16), although using another detection method the mutation was identified in only 6% of tumors (21); thus the frequency is still unresolved. This mutation was associated with older age, larger tumor size, lymph-node positivity, and shorter time to recurrence, all features related with a more aggressive breast cancer phenotype. Because of the recently-recognized importance of tumor/stroma cross-talk in promoting breast cancer progression and metastasis, it is imperative to elucidate the molecular events occurring between cancer cells and adjacent stroma at the site of primary tumors to provide new treatment options for breast cancer.

Here, we elucidated the complex interactions between peritumoral tissue, locally-derived factors and neoplastic cells in dependency of ERα status, with a special focus on leptin effects in influencing the behavior of breast cancer cells bearing the naturally-occurring K303R ERα mutation. We proposed a model in which leptin, secreted from CAFs, binds to its receptor, activates K303R ERα and promotes proliferation, migration and invasiveness of K303R ERα-expressing breast cancer cells. In turn, K303R cells release factors as EGF that 'educate' CAFs to enhance secretion of leptin, which, acting back on malignant cells, may establish a positive feedback loop between cancer and stromal cells to further support breast tumor progression (Fig. 6).

CAFs promote breast cancer cell malignancy through leptin signaling

The phenotype of malignant cells appears regulated not only by cell autonomous signals, but also is dependent on heterotypic signals coming from surrounding stromal cells, able to create a specific local microenvironment to tightly control breast cancer proliferation and differentiation (36-38).

We defined the molecular interactions between stromal fibroblasts isolated from biopsies of primary breast tumors (CAFs), WT and K303R ERα-expressing MCF-7 breast cancer cells. The initial conditioned media experiments demonstrated that the entire complement of secretory proteins released by CAFs have more profound effects on K303R ERα-expressing cell proliferation and migration than on WT ERα cells. We evidenced an important role for JAK2/STAT3 and ERα signaling pathways in CM-mediated effects. Our microarray study pointed to the regulation of several important transcriptional programs of growth factors and cytokines receptors that, acting as mediators of stromal-epithelial interactions, are potentially involved in

carcinoma progression. Among them, the gene encoding for leptin receptor was the most highly induced in K303R-expressing breast cancer cells.

Leptin is primarily synthesized from adipocytes, but is also produced by other cells, including fibroblasts (39-41). We demonstrated, for the first time, Ob mRNA expression and leptin secretion in CAFs. CAFs expressed ObR long isoforms, implying that an autocrine feedback loop may exist. Leptin-immunodepletion from CAFs-CM substantially reduced the growth and migration-promoting activities of CAFs. As one of the leptin downstream effectors (31), we found that the PI3K/Akt inhibitor LY294002 was effective in inhibiting CAFs-induced effects.

Since fibroblasts are the principal cellular component of the stroma, our results suggest that in the breast microenvironment CAFs through leptin signaling may become the main actor in influencing tumor cell behavior, especially in K303R ERα-expressing breast cancer cells.

Crosstalk between leptin and K303R ERα signaling pathways in breast cancer

Leptin, a pleiotropic molecule that regulates food intake, haematopoiesis, inflammation, cell differentiation and proliferation, is also required for mammary gland development and tumorigenesis. Indeed, leptin and its receptor isoforms (ObRs) have been detected in mammary epithelium and breast cancer cell lines, and are overexpressed in cancer tissue compared with healthy epithelium, with a positive correlation between ObR and ERα expression (42,43). Realtime PCR, immunoblotting and immunofluorescence experiments revealed an increase in mRNA and protein expressions of ObR long and short isoforms in K303R ERα-expressing cells. We also demonstrated that the mutant expression was associated with enhanced leptin signaling activation, and increased sensitivity to leptin stimulation on growth, motility, and invasiveness. Moreover, a significant increase in the growth of leptin-treated mutant tumors was observed *in vivo*.

Leptin is a potent modulator of the estrogen signaling pathway (29,44). On the other hand, estradiol modulates ObR expression in rat brain, through a putative estrogen-responsive-element in its promoter (45,46), and others demonstrated that estradiol induces leptin and ObR expression in MCF-7 breast cancer cells (43). Thus, leptin and estrogen might cooperate in sustaining estrogen-dependent breast carcinoma growth. We showed an increased S167 and S118 phosphorylation of the K303R receptor, an enhanced

K303R ERα transactivation, and a more pronounced up-regulation of classical estrogen-regulated genes in K303R-expressing cells. Indeed, the pure antiestrogens ICI182,760 drastically suppressed leptin-stimulated anchorage-independent growth and motility of mutant cells.

These results suggest that the mutation may potentiate ERα's role as an effector of leptin intracellular signal transduction, which may enhance cell proliferation, migration and invasiveness, contributing to the more aggressive phenotype of K303R-associated breast cancers.

K303R ERα cell-derived factors contribute to CAFs tumor-promoting activities

In the same way as tumor microenvironment plays active roles in shaping the fate of a tumor, cancer cells actively recruit fibroblasts into the tumor mass, in particular, the subpopulation named cancer-associated fibroblasts (CAFs). This cell-type is defined based on morphological characteristics or expression of markers as the fibroblast activating protein-FAP (1-4).

Studies addressing these issues are heterogeneous in terms of cell systems used, tumor cell types, and fibroblast sources. Experimental systems have used different tumor-derived conditioned media to stimulate CAFs, and others have cocultured tumor cells with normal fibroblasts or mesenchymal stem cells and measured chemokines levels in the resulting CM. For instance, fibroblasts growth with tumor cells resulted in increased production of chemokines whose source is in CAFs themselves. Chemokines produced under these "mixed" conditions promoted tumor promalignancy activities (6,9,47). We showed increased leptin mRNA expression and secretion by CAFs in response to soluble K303R ERα cell-secreted factors compared to WT-CM, suggesting that K303R cells have the ability to instruct their surrounding fibroblasts to augment leptin production, thereby enhancing tumor growth. This further indicates that interactions between the two subpopulations are actually bidirectional.

These interactions become more productive when tumor cells have a higher aggressiveness phenotype (47-49). CAFs exposed to K303R cell-derived CM acquired a more activated phenotypic characteristic, as revealed by an altered morphology, an increased FAP mRNA expression, and enhanced proliferative and migratory capabilities. We identified the epidermal growth factor, known to affect CAFs phenotype and leptin secretion (11,32-35), as the factor responsible of the paracrine activation of the surrounding stroma.

Thus, a positive feedback loop is established which leads to the development and growth of the tumor.

Conclusions

Our study highlights the functional importance of tumor-host cross-talk in impacting malignant cell behavior, and implies several clinical implications. First, since K303R mutation was identified in breast premalignant hyperplasia, it is tempting to speculate that this specific mutation hypersensitive to leptin signaling may promote or accelerate the development of cancers from premalignant breast lesions, further increasing risk in obese women. Second, understanding the key genes involved differently in relation to ERα status in tumor/stroma interactions may help to identify novel biomarkers for breast cancer. Finally, our findings support the development of new therapeutics targeting stroma signaling components (e.g. leptin) to be implemented in the adjuvant therapy for improving clinical care and reducing mortality from breast cancer.

Acknowledgements

We are grateful to Dr F. Romeo for providing the breast cancer specimens.

Grant Support

This work was supported by Reintegration AIRC/Marie Curie International Fellowship in Cancer Research to IB, Lilli Funaro Foundation to IB and LG, European Commission/FSE/Regione Calabria to LG, AIRC Grant (IG11595) to SC, DB, CG and SA, and NCI RO1 CA72038 to SF.

References

1. Bhowmick NA, Neilson EG, Moses HL. Stromal fibroblasts in cancer initiation and progression. Nature 2004; 432:332-37.
2. Hanahan D, Weinberg RA. The hallmarks of cancer. Cell 2000; 100:57-70.
3. Mueller MM, Fusenig NE. Friends or foes - bipolar effects of the tumour stroma in cancer. Nat Rev Cancer 2004; 4:839-49.
4. Orimo A, Weinberg RA. Stromal fibroblasts in cancer: a novel tumor-promoting cell type. Cell Cycle 2006; 5:1597-601.
5. Augsten M., Hagglof C, Olsson E, Stolz C, Tsagozis P, Levchenko T, et al. CXCL14 is an autocrine growth factor for fibroblasts and acts as a multimodal stimulator of prostate tumor growth. Proc Natl Acad Sci 2009; 106:3414-19.
6. Jung DW, Che ZM, Kim J, Kim K, Kim KY, Williams D. Tumor-stromal crosstalk in invasion of oral squamous cell carcinoma: a pivotal role of CCL7. Int J Cancer 2009; 127:332-44.
7. Matsuo Y, Ochi N, Sawai H, Yasuda A, Takahashi H, Funahashi H, et al. CXCL8/IL-8 and CXCL12/SDF-1 co-operatively promote invasiveness and angiogenesis in pancreatic cancer. Int J Cancer 2009; 124:853-61.
8. Wolf JS, Chen Z, Dong G, Sunwoo JB, Bancroft CC, Capo DE, et al. IL (interleukin)-1 alpha promotes nuclear factor-kappaB and AP-1-induced IL-8 expression, cell survival, and proliferation in head and neck squamous cell carcinomas. Clin Cancer Res 2001; 7:1812-20.
9. Kumar S, Kishimoto H, Chua HL, Badve S, Miller KD, Bigsby RM, et al. Interleukin-1 alpha promotes tumor growth and cachexia in MCF-7 xenograft model of breast cancer. Am J Pathol 2003; 163:2531-41.
10. Wu MH, Chou YC, Chou WY, Hsu GC, Chu CH, Yu CP, et al. Circulating levels of leptin, adiposity and breast cancer risk. Br J Cancer 2009; 100:578-82.
11. Schäffler A, Schölmerich J, Buechler C. Mechanisms of disease: adipokines and breast cancer-endocrine and paracrine mechanisms that connect adiposity and breast cancer. Nat Clin Pract Endocrinol Metab 2007; 3:345-54.
12. Osborne CK, Schiff R. Estrogen-receptor biology: continuing progress and therapeutic implications. J Clin Oncol 2005; 23:1616-22.
13. Herynk MH, Fuqua SA. Estrogen receptor mutations in human disease. Endocr Rev 2004; 25:869-98.
14. Barone I, Brusco L, Fuqua SA. Estrogen receptor mutations and changes in downstream gene expression and signaling. Clin Cancer Res 2010; 16:2702-08.
15. Fuqua SA, Wiltschke C, Zhang QX, Borg A, Castles CG, Friedrichs WE, et al. A hypersensitive estrogen receptor-alpha mutation in premalignant breast lesions. Cancer Res 2000; 60:4026-29.
16. Herynk MH, Parra I, Cui Y, Beyer A, Wu MF, Hilsenbeck SG, et al. Association between the estrogen receptor alpha A908G mutation and outcomes in invasive breast cancer. Clin Cancer Res 2007; 13:3235-43.
17. Tebbit CL, Bentley RC, Olson JA, Marks JR. Estrogen receptor a (ESR1) mutant A908G is not a common feature in benign and malignant proliferations of the breast. Genes Chromosomes Cancer 2004; 40:51-4.
18. Tokunaga E, Kimura Y, Maehara Y. No hypersensitive estrogen receptor-a mutation (K303R) in Japanese breast carcinomas. Breast Cancer Res Treat 2004; 84:289-92.
19. Davies MP, O'Neill PA, Innes H, Sibson DR. Hypersensitive K303R oestrogen receptor-a variant not found in invasive carcinomas. Breast Cancer Res 2005; 7:R113-18.
20. Zhang Z, Yamashita H, Toyama T, Omoto Y, Sugiura H, Hara Y, et al. Estrogen receptor a mutation (A-to-G transition at nucleotide 908) is not found in different types of breast lesions fromJapanese women. Breast Cancer 2003; 10:70–3.
21. Conway K, Parrish E, Edmiston SN, Tolbert D, Tse CK, Geradts J, et al. The estrogen receptor-a A908G (K303R) mutation occurs at a low frequency in invasive breast tumors: results from a population-based study. Breast Cancer Res 2005; 7:R871-80.
22. Cui Y, Zhang M, Pestell R, Curran EM, Welshons WV, Fuqua SA. Phosphorylation of estrogen receptor alpha blocks its acetylation and regulates estrogen sensitivity. Cancer Res 2004; 64:9199-208.

23. Barone I, Iacopetta D, Covington KR, Cui Y, Tsimelzon A, Beyer A, et al. Phosphorylation of the mutant K303R estrogen receptor alpha at serine 305 affects aromatase inhibitor sensitivity. Oncogene 2010; 29:2404-14.
24. Herynk MH, Hopp T, Cui Y, Niu A, Corona-Rodriguez A, Fuqua SA. A hypersensitive estrogen receptor alpha mutation that alters dynamic protein interactions. Breast Cancer Res Treat 2010; 122:381-93.
25. Giordano C, Cui Y, Barone I, Andò S, Mancini M, Berno V, et al. Growth factor-induced resistance to tamoxifen is associated with a mutation of estrogen receptor and its phosphorylation at serine 305. Breast Cancer Res Treat 2010; 119:71-81.
26. Barone I, Cui Y, Herynk MH, Corona-Rodriguez A, Giordano C, Selever J, et al. Expression of the K303R estrogen receptor breast cancer mutation induces resistance to an aromatase inhibitor via addiction to the PI-3K/Akt kinase pathway. Cancer Res 2009; 69:4724-32.
27. Catalano S, Malivindi R, Giordano C, Gu G, Panza S, Bonofiglio D, et al. Farnesoid X receptor, through the binding with steroidogenic factor 1-responsive element, inhibits aromatase expression in tumor Leydig cells. J Biol Chem 2010; 285:5581-93.
28. Sirianni R, Chimento A, Malivindi R, Mazzitelli I, Andò S, Pezzi V. Insulin-like growth factor-I, regulating aromatase expression through steroidogenic factor 1, supports estrogen-dependent tumor Leydig cell proliferation. Cancer Res 2007; 67:8368-77.
29. Catalano S, Mauro L, Marsico S, Giordano C, Rizza P, Rago V, et al. Leptin induces, via ERK1/ERK2 signal, functional activation of estrogen receptor alpha in MCF-7 cells. J Biol Chem 2004; 279:19908-15.
30. Mauro L, Catalano S, Bossi G, Pellegrino M, Barone I, Morales S, et al. Evidences that leptin up-regulates E-cadherin expression in breast cancer: effects on tumor growth and progression. Cancer Res 2007; 67:3412-21.
31. Cirillo D, Rachiglio AM, la Montagna R, Giordano A, Normanno N. Leptin signaling in breast cancer: an overview. J Cell Biochem 2008; 105:956-64.
32. Leroy P, Dessolin S, Villageois P, Moon BC, Friedman JM, Ailhaud G, et al. Expression of ob gene in adipose cells Regulation by insulin. J Biol Chem 1996; 271:2365-68.
33. Cascio S, Ferla R, D'Andrea A, Gerbino A, Bazan V, Surmacz E et al. Expression of angiogenic regulators, VEGF and leptin, is regulated by the EGF/PI3K/STAT3 pathway in colorectal cancer cells. J Cell Physiol 2009; 221:189-94.
34. Trujillo ME, Sullivan S, Harten I, Schneider SH, Greenberg AS, Fried SK. Interleukin-6 regulates human adipose tissue lipid metabolism and leptin production in vitro. J Clin Endocrinol Metab 2004; 89:5577–82.
35. Iwabu A, Smith K, Allen FD, Lauffenburger DA, Wells A. Epidermal growth factor induces fibroblast contractility and motility via a protein kinase C delta-dependent pathway. J Biol Chem 2004; 279:14551-60.
36. Fidler IJ. The pathogenesis of cancer metastasis: the "seed and soil" hypothesis revisited. Nat Rev Cancer 2003; 3:453-58.
37. Witz IP. Yin-yang activities and vicious cycles in the tumor microenvironment. Cancer Res 2008; 68:9-13.
38. Wiseman BS, Werb Z. Stromal effects on mammary gland development and breast cancer. Science 2002; 296:1046-49.
39. Glasow A, Kiess W, Anderegg U, Berthold A, Bottner A, Kratzsch J. Expression of Leptin (Ob) and Leptin Receptor (Ob-R) in Human Fibroblasts: Regulation of Leptin Secretion by Insulin. J Clin Endocrinol Metab 2001; 86:4472-79.
40. Torday JS, Sun H, Wang L, Torres E. Leptin mediates the parathyroid hormone-related protein paracrine stimulation of fetal lung maturation. Am J Physiol Lung Cell Mol Physiol 2002; 282:L405-10.
41. Lin TC, Lee TC, Hsu SL, Yang CS. The Molecular Mechanism of Leptin Secretion and Expression Induced by Aristolochic Acid in Kidney Fibroblast. Plos one 2011; 6:e16654.
42. Ishikawa M, Kitayama J, Nagawa H. Enhanced expression of leptin and leptin receptor (OB-R) in human breast cancer. Clin Cancer Res 2004; 10:4325-31.
43. Garofalo C, Koda M, Cascio S, Sulkowska M, Kanczuga-Koda L, Golaszewska J, et al. Increased expression of leptin and the leptin receptor as a marker of breast cancer progression: possible role of obesity-related stimuli. Clin Cancer Res 2006; 12:1447-53.

44. Catalano S, Marsico S, Giordano C, Mauro L, Rizza P, Panno ML, et al. Leptin enhances, via AP-1, expression of aromatase in the MCF-7 cell line. J Biol Chem 2003; 278:28668-76.
45. Bennett PA, Lindell K, Karlsson C, Robinson IC, Carlsson LM, Carlsson B. Differential expression and regulation of leptin receptor isoforms in the rat brain: effects of fasting and oestrogen. Neuroendocrinology 1998; 67:29-36.
46. Lindell K, Bennett PA, Itoh Y, Robinson IC, Carlsson LM, Carlsson B. Leptin receptor 5'untranslated regions in the rat: relative abundance, genomic organization and relation to putative response elements. Mol Cell Endocrinol 2001; 172:37-45.
47. Li L, Dragulev B, Zigrino P, Mauch C, Fox JW. The invasive potential of human melanoma cell lines correlates with their ability to alter fibroblast gene expression in vitro and the stromal microenvironment in vivo. Int. J. Cancer 2009; 125:1796-804.
48. Tsujino T, Seshimo I, Yamamoto H, Ngan CY, Ezumi K, Takemasa I, et al. Stromal myofibroblasts predict disease recurrence for colorectal cancer. Clin Cancer Res 2007; 13:2082-90.
49. Infante JR, Matsubayashi H, Sato N, Tonascia J, Klein AP, Riall TA, et al. Peritumoral fibroblast SPARC expression and patient outcome with resectable pancreatic adenocarcinoma. J Clin Oncol 2007; 25:319-25.

Figures Legends

Figure 1. CAFs-induced breast cancer cell growth and motility. **A**, Immunoblotting for ERα expression in YFP-WT and YFP-K303R ERα stable-expressing MCF-7 cells and WT P and K303R P stable pools. GAPDH, loading control. **B**, CAFs morphology in monolayer growth using phase-contrast microscopy. RT-PCR for fibroblast activation protein-FAP and 36B4 (internal standard). *NC*, negative-control. **C**, Soft agar and scratch assays in cells treated with regular full media (FM), CAFs- or normal fibroblasts (NFs)-derived conditioned media (CM). **D**, Soft agar and scratch assays in cells treated with FM, CAFs-CM with/without AG490 (AG,10μM) or ICI182,760 (ICI,1μM). *P<0.05, **P<0.005. *Small squares*, time 0.

Figure 2. Leptin signaling activation in mutant cells. **A**, Real-time RT-PCR for different receptors of CAFs-secreted factors. n.s.=nonsignificant, **P<0.01, ***P<0.005. **B**, Immunoblotting showing leptin receptor long and short isoforms (ObRl/ObRs). GAPDH, loading control. Numbers represent the average fold change in ObRl/GAPDH and ObRs/GAPDH levels. **C**, Immunofluorescence of ObR (a,c) and DAPI (b,d). *Small squares*, negative-controls. **D**, Immunoblotting of phosphorylated pJAK2/pSTAT3/pAKT/pMAPK, and total proteins from cells treated with vehicle(-) or leptin (Lep100ng/ml, 5 and 10min). GAPDH, loading control. Numbers represent the average fold change between phospho/total/GAPDH levels.

Figure 3. The K303R ERα mutation generates a leptin hypersensitive phenotype. **A**, Soft agar assay in cells treated with vehicle(-), or Lep10/100/1000ng/ml. **B**, Soft agar assay in cells treated with vehicle(-) or Lep100ng/ml, with/without ICI182,760 (ICI,1μM) or AG490 (AG,10μM). **C**, scratch, and **D**, transmigration and invasion assays in cells treated as indicated. n.s.=nonsignificant, *P<0.05, **P<0.005, ***P<0.001. **E**, Scratch assay in cells treated with vehicle(-) or Lep100ng/ml, with/without ICI182,760 or AG490. *Small squares*, time 0. **F**, WT and K303R ERα-expressing cells were injected into mice (n=6/group) supplemented with E_2 (0.72mg/pellet/90-day-release) and 230μg/kg leptin or vehicle (Control). Survival curves (shown as % of mice in which tumors had not doubled in size) are graphed as the time in weeks from treatment to a twofold increase in total tumor volume over baseline (time to tumor doubling).

Figure 4. Leptin-immunodepletion reduces CAFs-induced cell growth and migration. **A**, Soft agar and scratch assays in cells treated with FM, CAFs-CM, or leptin-depleted CM (CM+LepAb). CM treated with a non specific IgG as a control (CM+IgG). **B**, Soft agar and scratch assays in cells treated with FM, CAFs-CM with/without PD98059 (PD,10μM) or LY294002 (LY,10μM). n.s.=nonsignificant, **P*<0.05, ***P*<0.005. *Small squares*, time 0.

Figure 5. CAFs activated phenotype after K303R ERα cell-CM exposure. **A**, Phase-contrast microscopy for CAFs morphology and RT-PCR for FAP and 36B4 (internal standard) after treatment with CM from WT or K303R ERα-expressing cells. *NC*, negative-control. **B,** MTT growth and scratch assays in CAFs treated with WT-CM and K303R-CM. **C**, RT-PCR for leptin/Ob and 36B4, and leptin release by RIA. **D**, Real-time RT-PCR for EGF, IL6 and Insulin. **E,** Scratch assays in CAFs treated with WT-CM with/without EGF100ng/ml or K303R-CM with/without AG1478 10μM. **F**, RT-PCR for FAP, leptin/Ob and 36B4, and leptin release from CAFs by RIA. Numbers represent the average fold change of FAP/36B4 and Ob/36B4 levels. n.s.=nonsignificant, **P*<0.05, ***P*<0.005, ****P*<0.0001. *Small squares*, time 0.

Figure 6. Schematic illustration of tumor/stroma interactions in K303R ERα breast cancer microenvironment. CAFs secrete leptin, which, acting in a paracrine fashion, binds to its cognate receptors (ObR), overexpressed on the surface of K303R ERα breast cancer cells and activates K303R ERα. This results in increased cell proliferation, motility, and invasion. K303R ERα-expressing cells, in turn, secrete factors that stimulate leptin production by adjacent CAFs, thus creating a positive feedback loop between cancer and stromal cells to further promote breast tumor progression.

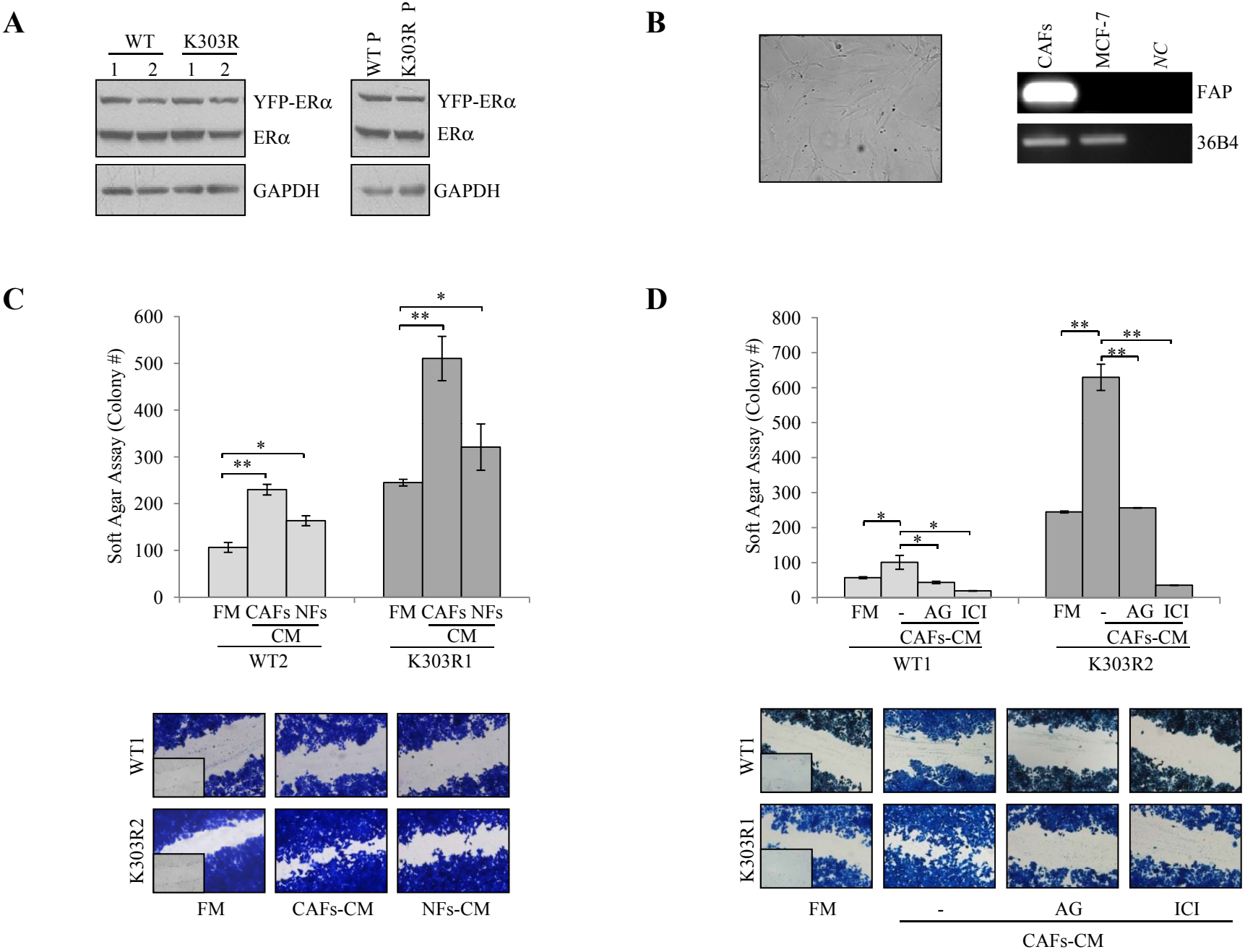
A
WT
K303R
1
2
1
2
YFP-ERα
ERα
GAPDH
WT P
K303R P
YFP-ERα
ERα
GAPDH
B
CAFs
MCF-7
NC
FAP
36B4
C
Soft Agar Assay (Colony #)
600
500
400
300
200
100
0
*
**
*
**
FM CAFs NFs
CM
WT2
FM CAFs NFs
CM
K303R1
WT1
K303R2
FM
CAFs-CM
NFs-CM
D
Soft Agar Assay (Colony #)
800
700
600
500
400
300
200
100
0
**
**
**
*
*
*
FM - AG ICI
CAFs-CM
WT1
FM - AG ICI
CAFs-CM
K303R2
WT1
K303R1
FM
-
AG
ICI
CAFs-CM

Figure 1

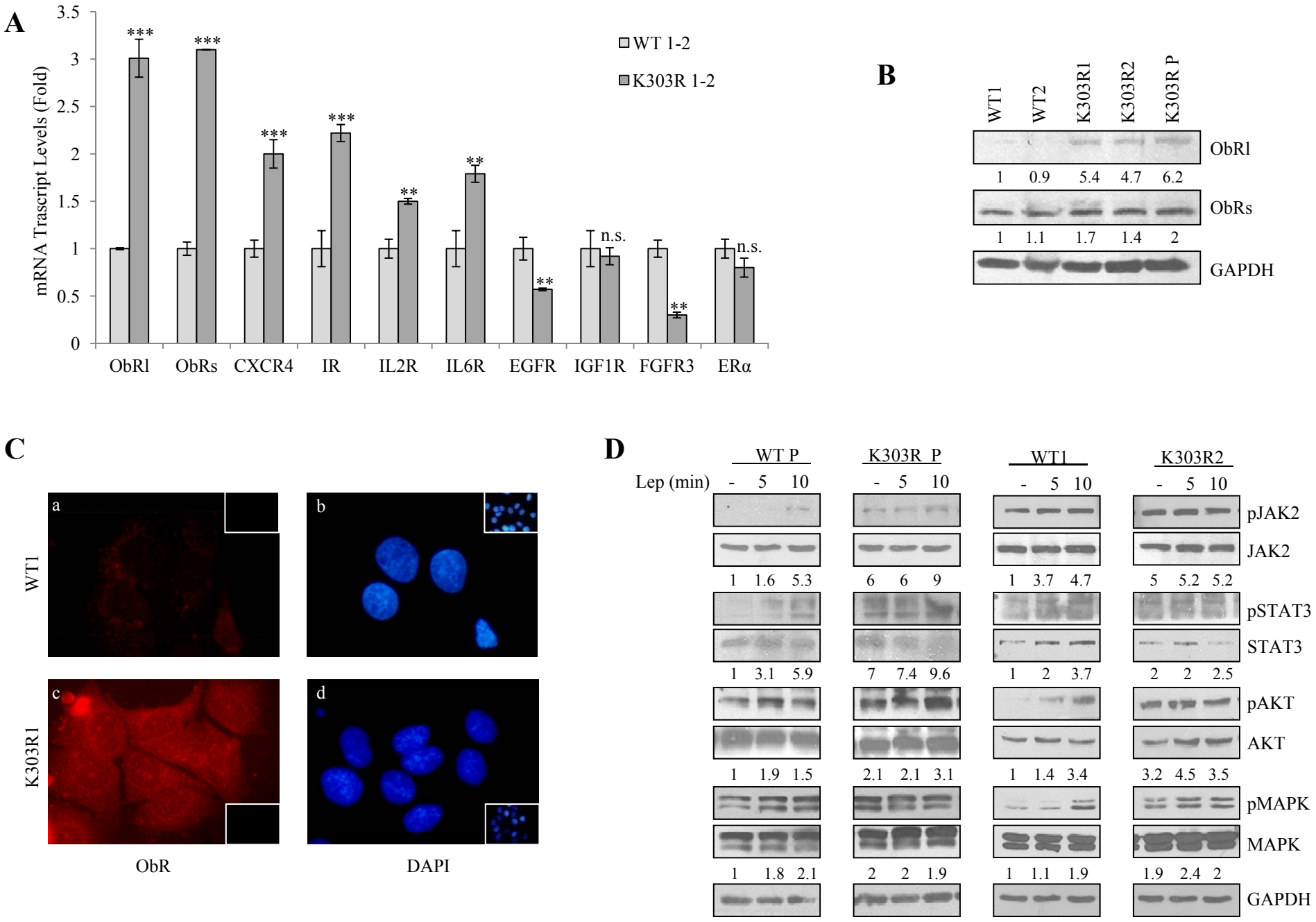
A
mRNA Trascript Levels (Fold)
WT 1-2
K303R 1-2
ObRl
ObRs
CXCR4
IR
IL2R
IL6R
EGFR
IGF1R
FGFR3
ERα
n.s.
B
WT1
WT2
K303R1
K303R2
K303R P
ObRl
1 0.9 5.4 4.7 6.2
ObRs
1 1.1 1.7 1.4 2
GAPDH
C
WT1
K303R1
a
b
c
d
ObR
DAPI
D
WT P
K303R P
WT1
K303R2
Lep (min) - 5 10
pJAK2
JAK2
1 1.6 5.3
6 6 9
1 3.7 4.7
5 5.2 5.2
pSTAT3
STAT3
1 3.1 5.9
7 7.4 9.6
1 2 3.7
2 2 2.5
pAKT
AKT
1 1.9 1.5
2.1 2.1 3.1
1 1.4 3.4
3.2 4.5 3.5
pMAPK
MAPK
1 1.8 2.1
2 2 1.9
1 1.1 1.9
1.9 2.4 2
GAPDH

Figure 2

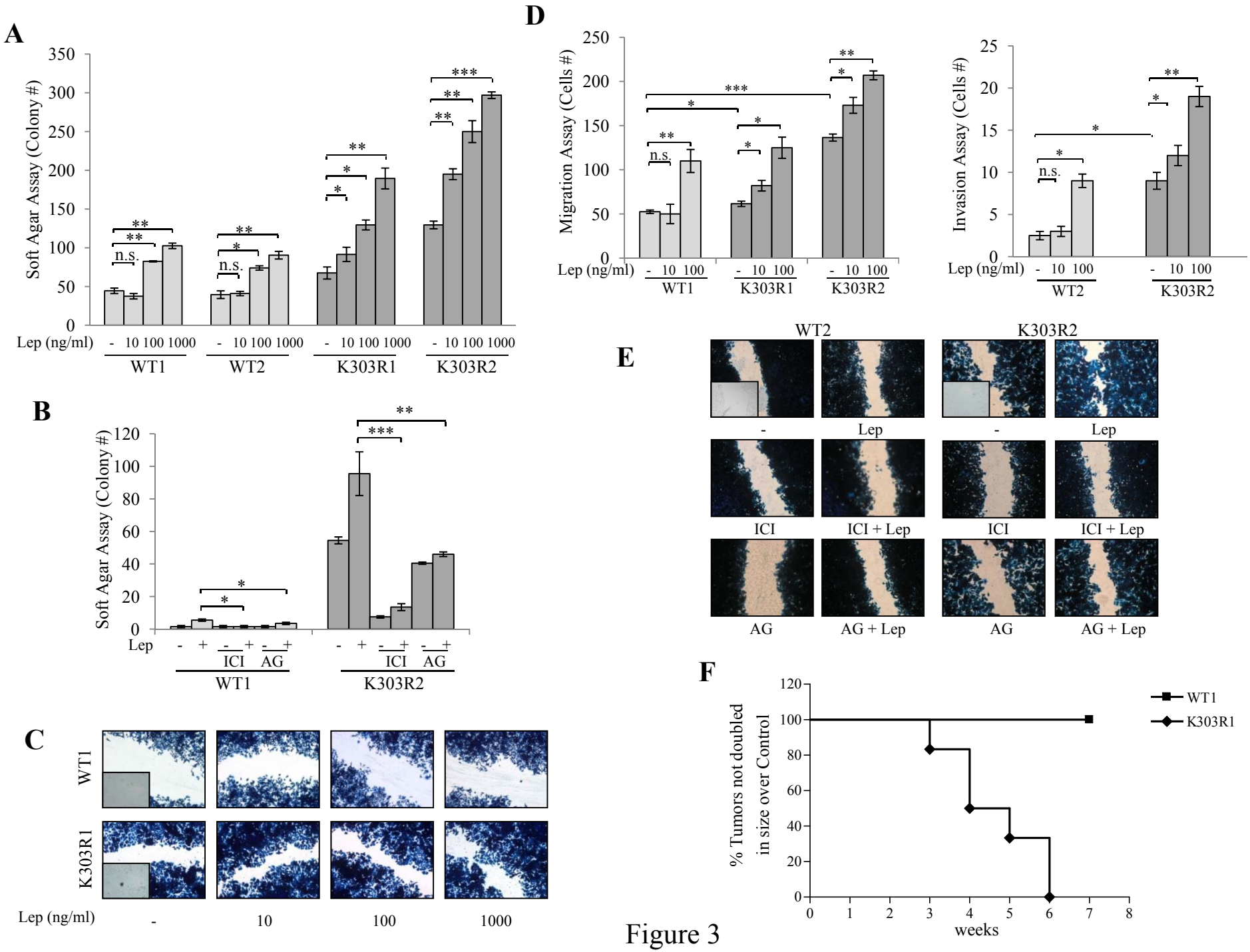
A
Soft Agar Assay (Colony #)
Lep (ng/ml) - 10 100 1000
WT1
WT2
K303R1
K303R2
n.s.
B
Soft Agar Assay (Colony #)
Lep
ICI
AG
WT1
K303R2
C
WT1
K303R1
Lep (ng/ml)
-
10
100
1000
D
Migration Assay (Cells #)
Lep (ng/ml) - 10 100
WT1
K303R1
K303R2
Invasion Assay (Cells #)
WT2
K303R2
E
WT2
K303R2
-
Lep
ICI
ICI + Lep
AG
AG + Lep
F
% Tumors not doubled in size over Control
weeks
WT1
K303R1

Figure 3

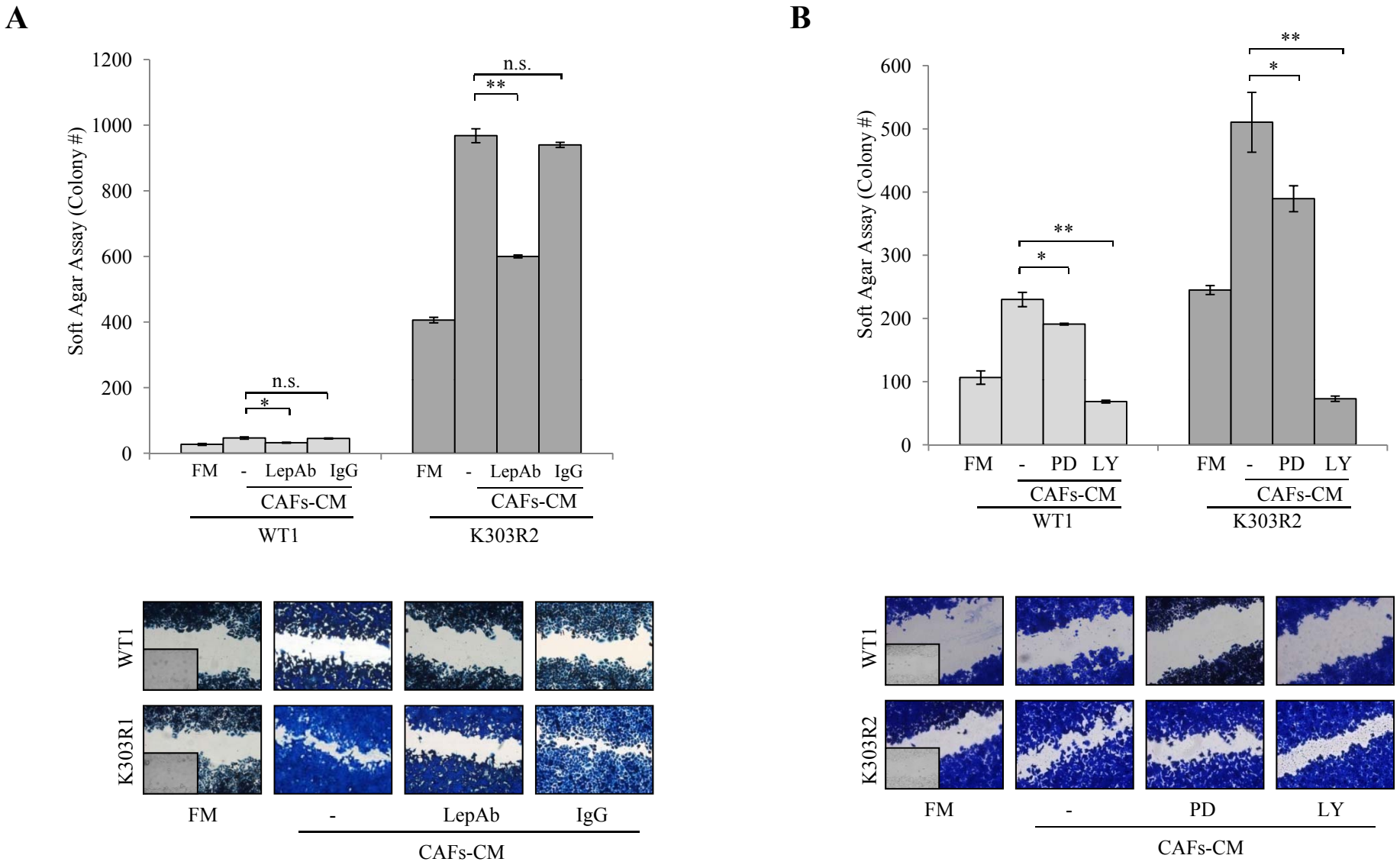
A
Soft Agar Assay (Colony #)
1200
1000
800
600
400
200
0
n.s.
**
n.s.
*
FM
-
LepAb
IgG
CAFs-CM
WT1
K303R2
WT1
K303R1
FM
-
LepAb
IgG
CAFs-CM
B
Soft Agar Assay (Colony #)
600
500
400
300
200
100
0
**
*
**
*
FM
-
PD
LY
CAFs-CM
WT1
K303R2
WT1
K303R2
FM
-
PD
LY
CAFs-CM

Figure 4

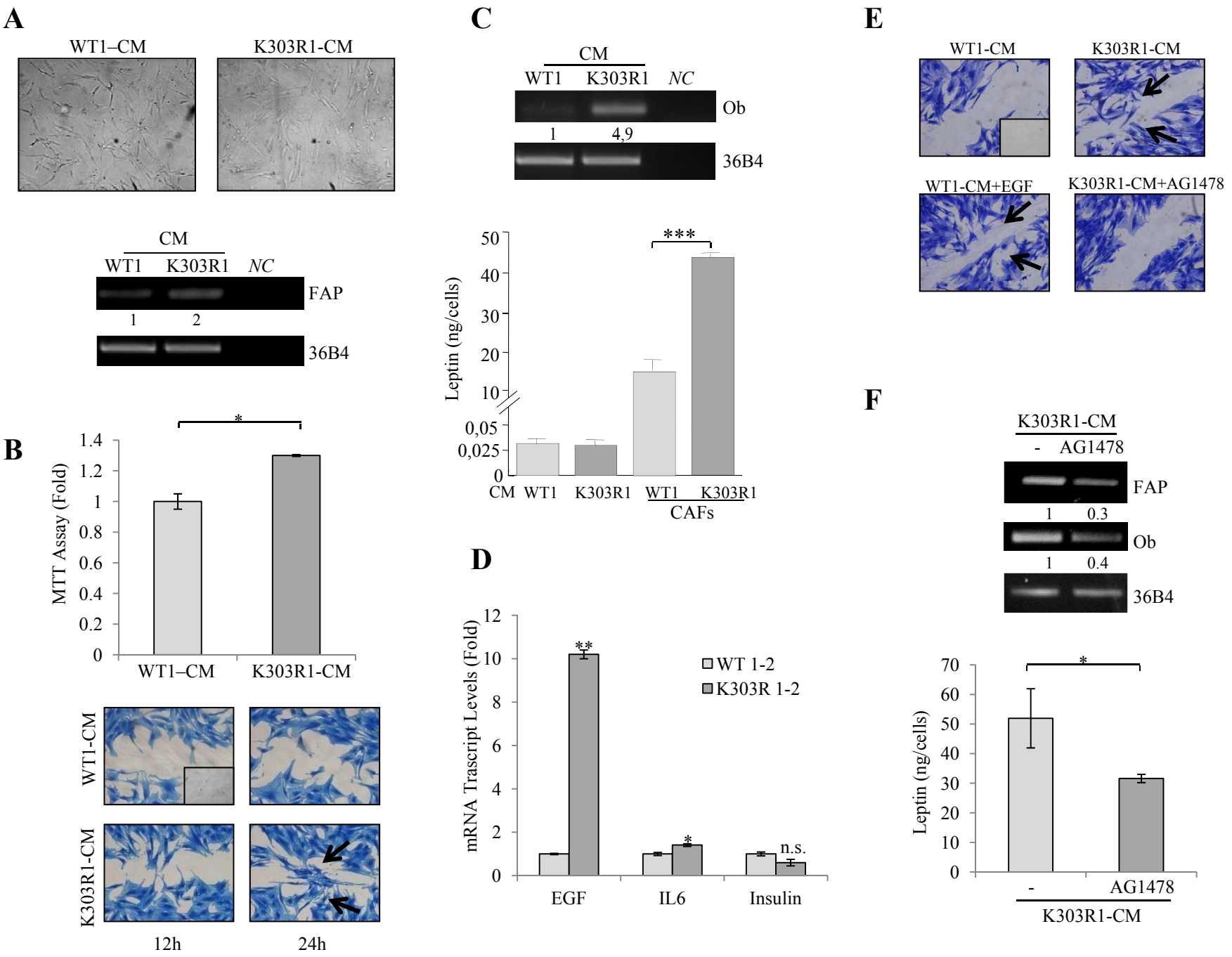
A
WT1–CM
K303R1-CM
CM
WT1
K303R1
NC
FAP
1
2
36B4
B
MTT Assay (Fold)
1.4
1.2
1
0.8
0.6
0.4
0.2
0
*
WT1–CM
K303R1-CM
WT1-CM
K303R1-CM
12h
24h
C
CM
WT1
K303R1
NC
Ob
1
4,9
36B4
Leptin (ng/cells)
50
40
30
20
10
0,05
0,025
0
***
CM
WT1
K303R1
WT1
K303R1
CAFs
D
mRNA Trascript Levels (Fold)
12
10
8
6
4
2
0
**
*
n.s.
WT 1-2
K303R 1-2
EGF
IL6
Insulin
E
WT1-CM
K303R1-CM
WT1-CM+EGF
K303R1-CM+AG1478
F
K303R1-CM
-
AG1478
FAP
1
0.3
Ob
1
0.4
36B4
Leptin (ng/cells)
70
60
50
40
30
20
10
0
*
-
AG1478
K303R1-CM

Figure 5

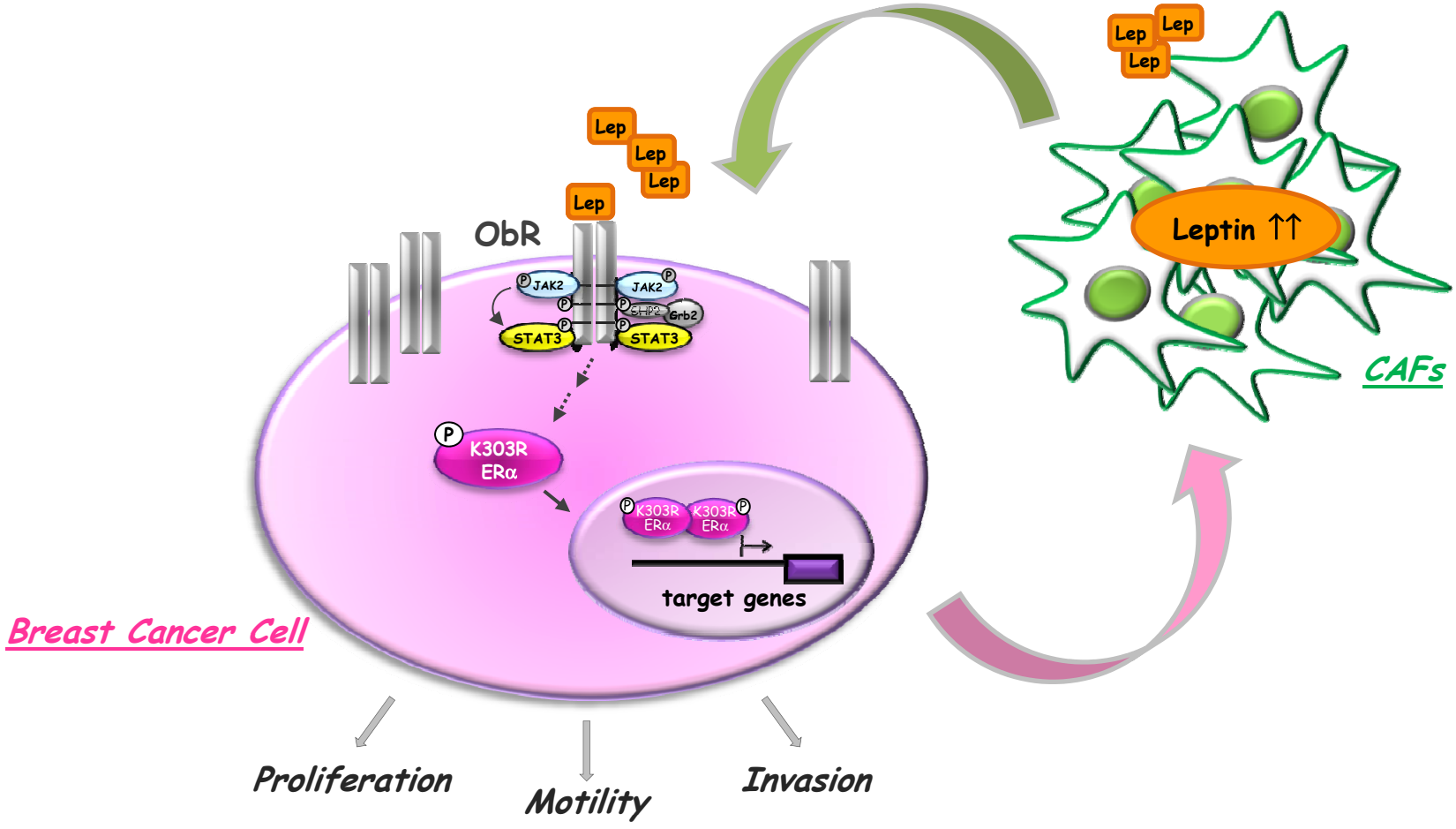
Lep
Lep
Lep
Lep
ObR
JAK2
JAK2
SHP2
Grb2
STAT3
STAT3
P
K303R
ERα
K303R
ERα
K303R
ERα
target genes
Breast Cancer Cell
Proliferation
Motility
Invasion
Lep
Lep
Lep
Leptin ↑↑
CAFs

Table 1 Gene expression profile of the different receptors of CAFs-secreted factors among WT and K303R ERα expressing MCF-7 breast cancer cells.

Gene Name	*Gene Symbol*	*Parametric P-value*	*Fold Change in K303R Clones*
Leptin receptor	*ObR/LepR*	<1e-07	**2.4**
Interleukin 28 receptor α	*IL28RA*	<1e-07	1.9
Chemokine (C-X-C motif) receptor 4	*CXCR4*	<1e-07	1.9
Insulin receptor	*IR*	1.7e-06	1.68
Interleukin 17 receptor C	*IL17RC*	7e-07	1.6
Insulin-like growth factor 2 receptor	*IGF2R*	1e-07	1.57
Interleukin 15 receptor α	*IL15RA*	3e-07	1.5
Macrophage stimulating receptor 1	*MSR1*	9.2e-06	1.44
Hepatocyte growth factor receptor	*MET*	1.69e-05	1.39
Interleukin 1 receptor, type I	*IL1R1*	0.0004	1.38
Chemokine (C-C motif) receptor 7	*CCR7*	0.0001	1.3
Chemokine (C-X3-C motif) receptor 1	*CX3CR1*	7.9e-05	1.32 1.27
Interleukin 2 receptor β	*IL2RB*	3.57e-05	1.25
Interleukin 9 receptor	*IL9R*	0.0002	1.23
Interleukin 10 receptor β	*IL10RB*	0.0003	1.21
Interleukin 6 receptor	*IL6R*	0.01	1.2
Interleukin 21 receptor	*IL21R*	0.0006	0.8
Interleukin 4 receptor	*IL4R*	0.0007	0.7
Epidermal growth factor receptor	*EGFR*	7.6e-06	0.7
Insulin-like growth factor 1 receptor	*IGF1R*	0.0006	0.7
Fibroblast growth factor receptor 3	*FGFR3*	0.0005	0.7

Representative probesets from pathway analysis showing gene expression changes in the receptor family of CAFs-secreted factors along with the p-value and the fold change of K303R-expressing cells compared to WT cells studied by microarray analysis. In cases where the same genes were deemed significant across multiple probesets, only one is shown.

Oncogene (2011) 1–12

www.nature.com/onc

ORIGINAL ARTICLE

Farnesoid X receptor inhibits tamoxifen-resistant MCF-7 breast cancer cell growth through downregulation of HER2 expression

C Giordano[1,5], S Catalano[1,2,5], S Panza[2], D Vizza[2], I Barone[1,3], D Bonofiglio[1,2], L Gelsomino[2], P Rizza[3], SAW Fuqua[4] and S Andò[1,3]

[1]*Centro Sanitario, University of Calabria, Arcavacata di Rende, Italy;* [2]*Department of Pharmaco-Biology, University of Calabria, Arcavacata di Rende, Italy;* [3]*Department of Cellular Biology, University of Calabria, Arcavacata di Rende, Italy and* [4]*Lester and Sue Smith Breast Center and Department of Molecular and Cellular Biology, Baylor College of Medicine, One Baylor Plaza, Houston, TX, USA*

Tamoxifen (Tam) treatment is a first-line endocrine therapy for estrogen receptor-α-positive breast cancer patients. Unfortunately, resistance frequently occurs and is often related with overexpression of the membrane tyrosine kinase receptor HER2. This is the rationale behind combined treatments with endocrine therapy and novel inhibitors that reduce HER2 expression and signaling and thus inhibit Tam-resistant breast cancer cell growth. In this study, we show that activation of farnesoid X receptor (FXR), by the primary bile acid chenodeoxycholic acid (CDCA) or the synthetic agonist GW4064, inhibited growth of Tam-resistant breast cancer cells (termed MCF-7 TR1), which was used as an *in vitro* model of acquired Tam resistance. Our results demonstrate that CDCA treatment significantly reduced both anchorage-dependent and anchorage-independent epidermal growth factor (EGF)-induced growth in MCF-7 TR1 cells. Furthermore, results from western blot analysis and real-time reverse transcription–PCR revealed that CDCA treatment reduced HER2 expression and inhibited EGF-mediated HER2 and p42/44 mitogen-activated protein kinase (MAPK) phosphorylation in these Tam-resistant breast cancer cells. Transient transfection experiments, using a vector containing the human HER2 promoter region, showed that CDCA treatment downregulated basal HER2 promoter activity. This occurred through an inhibition of nuclear factor-κB transcription factor binding to its specific responsive element located in the HER2 promoter region as revealed by mutagenesis studies, electrophoretic mobility shift assay and chromatin immunoprecipitation analysis. Collectively, these data suggest that FXR ligand-dependent activity, blocking HER2/MAPK signaling, may overcome anti-estrogen resistance in human breast cancer cells and could represent a new therapeutic tool to treat breast cancer patients that develop resistance.

Correspondence: Professor S Andò, Department of Cell Biology and Faculty of Pharmacy, Nutritional and Health Sciences, University of Calabria, Via P. Bucci, Arcavacata di Rende (CS) 87036, Italy.
E-mail: sebastiano.ando@unical.it
[5]These authors contributed equally to this work.
Received 15 November 2010; revised 8 March 2011; accepted 15 March 2011

Oncogene advance online publication, 18 April 2011; doi:10.1038/onc.2011.124

Keywords: FXR; breast cancer; tamoxifen resistance; HER2; NF-κB

Introduction

Administration of the selective estrogen receptor (ER) modulator tamoxifen (Tam), to block ERα activity, is still a first-line endocrine therapy for the management of all stages of ERα-positive breast cancer (Fisher *et al.*, 1998; Gradishar, 2004). Unfortunately, not all patients who have ERα-positive tumors respond to Tam (*de novo* resistance), and a large number of patients who do respond will eventually develop disease progression or recurrence while on therapy (acquired resistance), limiting the efficacy of the treatment.

Multiple mechanisms are responsible for the development of endocrine resistance. Among these are the loss of ERα expression or function (Encarnacion *et al.*, 1993), alterations in the balance of regulatory cofactors, increased oncogenic kinase signaling (Blume-Jensen and Hunter, 2001), and altered expression of growth factor signaling pathways (Arpino *et al.*, 2004; Schiff *et al.*, 2004; Sabnis *et al.*, 2005; Staka *et al.*, 2005). For instance, several preclinical and clinical studies suggest that both *de novo* and acquired resistance to Tam in breast cancers can be associated with elevated levels of the membrane tyrosine kinase HER2 (c-ErbB2, Her2/neu) (Chung *et al.*, 2002; Meng *et al.*, 2004; Shou *et al.*, 2004; Gutierrez *et al.*, 2005).

The *HER2* gene codes for a 185 kDa receptor, a member of the epidermal growth factor receptor (EGFR) family of transmembrane tyrosine kinases, which also includes HER3 and HER4, mainly involved in signal transduction pathways that regulate cell growth and differentiation. This receptor has no ligand of its own, but is activated by hetero-oligomerization with other ligand-activated receptors (Yarden, 2001). The *HER2* gene is amplified and/or overexpressed in 20–25% of ERα-positive breast cancers (Slamon *et al.*, 1989), and

clinical observations indicate that tumors with high levels of HER2 have poor outcome when treated with Tam (Osborne *et al*., 2003; Kirkegaard *et al*., 2007).

The mechanisms by which HER2 overexpression mediates Tam resistance result from an intimate cross-talk between ERα and growth factor receptors kinase cascades, such as Ras/mitogen-activated protein kinase (MAPK) signaling, that in turn can promote growth and progression in breast cancer cells, negating the inhibitory effects of Tam on nuclear ERα activity (Arpino *et al*., 2008). HER2 overexpression is not attributed solely to amplification of the *HER2* gene copy number, but can also occur from a single-copy gene due to deregulation events at the transcriptional level (Hurst, 2001).

Thus, an analysis of new mechanisms controlling HER2/neu receptor gene expression could be important to enhance strategies to reverse Tam resistance in breast cancer patients.

Farnesoid X receptor (FXR), a member of the nuclear receptor superfamily of ligand-dependent transcription factors, is mainly expressed in the liver and the gastrointestinal tract, where it regulates expression of genes involved in bile acids, cholesterol and triglyceride metabolism (Forman *et al*., 1995; Makishima *et al*., 1999; Parks *et al*., 1999). Recently, this receptor was also detected in different non-enterohepatic compartments, including breast cancer tissue and breast cancer cell lines (Bishop-Bailey, 2004; Swales *et al*., 2006; Journe *et al*., 2008; Catalano *et al*., 2010). For instance, FXR activation inhibits breast cancer cell proliferation and negatively regulates aromatase activity reducing local estrogen production (Swales *et al*., 2006), whereas other authors have reported that FXR activation stimulates MCF-7 cell proliferation but only in steroid-free medium (Journe *et al*., 2008). However, the functions of FXR in breast cancer tissue are still not completely understood, and there are no data regarding its role in the endocrine-resistant breast cancer phenotype. Thus, we have investigated whether activated FXR may modulate the growth of human MCF-7 Tam-resistant breast cancer cells, a model that was developed to mimic *in vitro* the occurrence of acquired Tam resistance.

Here, we demonstrate that a specific FXR ligand chenodeoxycholic acid (CDCA) or its synthetic agonist GW4064 inhibited Tam-resistant breast cancer cell proliferation and EGF-induced growth, by reducing expression of the HER2 receptor. This occurs through an FXR-mediated inhibition of nuclear factor (NF)-κB binding on the human HER2 promoter region.

Results

FXR expression in Tam-resistant breast cancer cells

Acquired resistance to Tam has been associated with elevated levels of the membrane tyrosine kinase HER2 (Knowlden *et al*., 2003; Nicholson *et al*., 2004; Gutierrez *et al*., 2005). In agreement with these reports, we found a marked increase in the levels of total HER2 protein content in Tam-resistant MCF-7 TR1 compared with MCF-7 cells, whereas no differences were seen in the expression of EGFR and ERα (Figure 1a). We therefore evaluated anchorage-independent growth of MCF-7 and MCF-7 TR1 cells after treatment with herceptin, a humanized monoclonal antibody directed against the extracellular domain of HER2, in the presence or not of EGF. Herceptin had no effect on MCF-7 growth, whereas significantly inhibited anchorage-independent growth of MCF-7 TR1 cells in basal conditions as well as upon EGF treatment (Figure 1b). These data confirm that the HER2 overexpression found in the MCF-7 TR1 cells renders them more sensitive to the inhibitory effect of this selective HER2-targeted agent.

Next, we evaluated the expression of FXR in MCF-7 and MCF-7 TR1 cells. Our results revealed the presence of FXR mRNA (Figure 1c, upper panel) and protein (Figure 1c, lower panel) in both MCF-7 and MCF-7 TR1 cells. To assess the ability of FXR to be transactivated by CDCA, we transiently transfected cells with an FXR-responsive reporter gene (*FXRE-IR1*) followed by treatment with increasing doses of CDCA. The specificity of the system was tested by co-transfecting the cells with a dominant negative FXR (FXR-DN) plasmid. As shown in Figure 1d, CDCA treatment induced a dose-dependent FXR activation in both cell lines and expression of the FXR-DN completely abrogated the CDCA-induced transactivation.

FXR activation inhibits Tam-resistant breast cancer cell growth

We examined, by MTT growth assays, the effects of increasing doses of CDCA and GW4064. Treatment with both ligands reduced cell proliferation in a dose-dependent manner in MCF-7 and MCF-7 TR1 cells, whereas had no effects on normal breast epithelial cells MCF-10A (Figures 2a and b). Similar results in growth inhibition were also obtained in another Tam-resistant breast cancer cell line termed MCF-7 TR2 (Supplementary Figures 2a and b). It is worth noting that the inhibitory effects exerted by FXR ligands on cell proliferation were significant at lower dose in MCF-7 TR1 cells compared with MCF-7 cells, as evidenced by half-maximal inhibitory concentration (IC_{50}) values (Table 1). The antiproliferative effects exerted by CDCA were completely reversed in the presence of a FXR-DN plasmid, supporting the specific involvement of the FXR (Figure 2c).

Next, we tested the effects of CDCA in the presence of Tam on cell growth (Figure 2d). As expected, with anti-estrogen treatment, cell viability was significantly reduced in MCF-7 cells, whereas MCF-7 TR1 cells growth was unaffected, confirming the Tam-resistant phenotype. Interestingly, combined treatment with CDCA and Tam reduced growth of MCF-7 TR1 cells compared with treatment with Tam alone, but showed no additive effects in MCF-7 cells (Figure 2d). The ability of CDCA and Tam to inhibit Tam-resistant growth was also confirmed using anchorage-independent growth assays (Figure 2e). These results suggest that FXR activation can interfere with the cellular

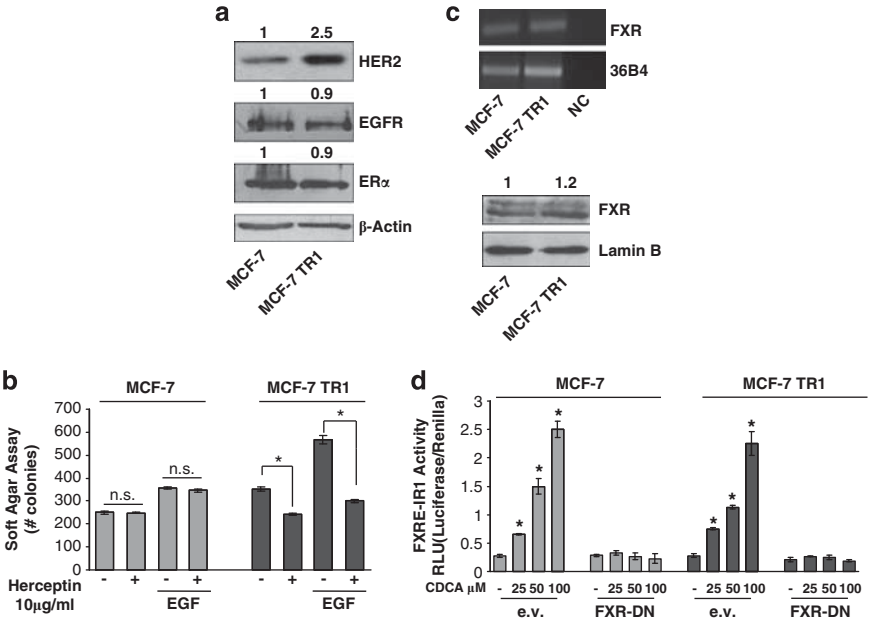

Figure 1 FXR expression and activation in MCF-7 and MCF-7 TR1 cells. (**a**) Western blot analysis of HER2, EGFR, ERα in total protein extracts from MCF-7 and MCF-7 TR1 cells; β-Actin was used as loading control. (**b**) Soft-agar growth assay in MCF-7 and MCF-7 TR1 cells plated in 0.35% agarose and treated with EGF 100 ng/ml in the presence or absence of herceptin (10 μg/ml). After 14 days of growth, colonies >50 μm diameter were counted. n.s., nonsignificant; $*P<0.05$ compared with vehicle or EGF. (**c**) Total RNA was extracted from MCF-7 and MCF-7 TR1 cells, reverse transcribed and cDNA was subjected to PCR using primers specific for FXR or 36B4 (upper panel). NC: negative control, RNA sample without the addition of reverse transcriptase. Nuclear proteins were extracted from MCF-7 and MCF-7 TR1 and then western blotting analysis was performed using anti-FXR antibody. Lamin B was used as loading control (lower panel). (**d**) MCF-7 and MCF-7 TR1 cells were transiently transfected with a FXR-responsive reporter gene (*FXRE-IR1*), with either empty vector (e.v.) or FXR-DN expression plasmid. After transfection, cells were treated for 24 h with vehicle (−) or increasing doses of CDCA (25–50–100 μM) and then luciferase activity was measured. Results represent the mean ± s.d. of three different experiments each performed in triplicate. $*P<0.05$ compared with vehicle. Numbers on top of the blots represent the average fold change versus control of MCF-7 cells normalized for β-Actin or Lamin B.

mechanisms by which MCF-7 TR1 cells escape antihormonal treatments.

CDCA reduces HER2 expression and signaling in MCF-7 TR1 cells

To understand the mechanisms associated with CDCA-mediated inhibition of Tam-resistant growth in breast cancer cells, we evaluated the possible role of FXR ligands in modulating HER2 expression. As shown in Figure 3a, treatment with CDCA downregulated HER2 protein expression in both cell lines, but with higher reduction seen in MCF-7 TR1 cells. Similar results were also observed after treatment with GW4064 (data not shown). A reduction in HER2 levels was also found upon CDCA treatment in MCF-7 TR2 cells (Supplementary Figure 2c). No differences were found in EGFR expression upon CDCA treatment (Supplementary Figure 3), confirming that activated FXR specifically target HER2 expression in breast cancer cells. In the presence of an FXR-DN the HER2 downregulation was completely abrogated, confirming FXR involvement in CDCA-induced effects on HER2 (Figure 3b). Next, we questioned whether these HER2-decreased levels could modify the responsiveness of breast cancer cells after growth factor stimulation. Thus, we investigated the effects of short-term stimulation with EGF, in the presence of CDCA treatment, on phosphorylation levels of HER2 and MAPK, the main downstream effectors of the growth factor signaling. EGF treatment increased phosphorylation of both HER2 and MAPK, even though in higher extent in MCF-7 TR1 cells. However, pretreatment with CDCA reduced EGF-induced phosphorylation of HER2 in both cell lines and drastically prevented MAPK activation in MCF-7 TR1 cells (Figure 3c). In addition, data obtained from MTT (Figure 3d upper panel) as well as soft-agar (Figure 3d lower panel) growth assays revealed that CDCA treatment inhibited EGF-induced growth by 70% in anchorage-dependent and 50% in anchorage-independent assays in MCF-7 TR1 cells. CDCA was less effective in MCF-7 cells. These results well correlated with the downregulatory effect of CDCA on EGF-induced cyclin D1 expression, particularly in MCF-7 TR1 cells (Figure 3e).

Activated FXR inhibits the binding of NF-kB to HER2 promoter region

To explore whether HER2 downregulation relies on transcriptional mechanisms, we evaluated, using real-time reverse transcription (RT)–PCR, HER2 mRNA levels after treatment with CDCA for different times. Exposure to CDCA exhibited a time-dependent reduction in HER2 mRNA levels in both MCF-7 and MCF-7 TR1 cells (Figure 4a). Also, transcriptional activity of a

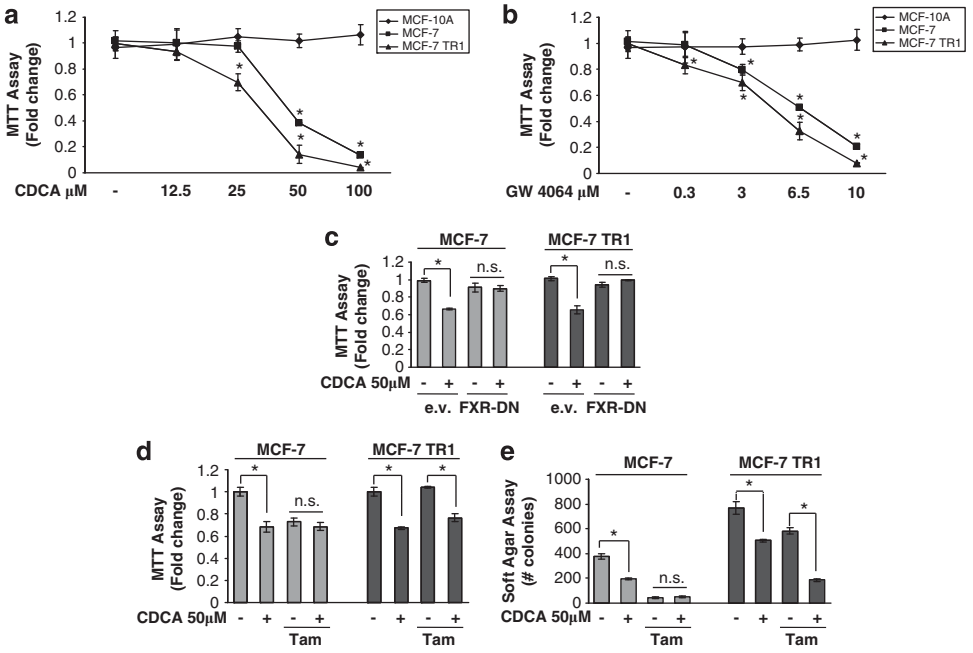

Figure 2 FXR ligands effects on breast cancer cells proliferation. MTT growth assays in MCF-10A, MCF-7 and MCF-7 TR1 cells treated with vehicle (−) or increasing doses of CDCA (12.5–25–50–100 μM) (**a**) or GW4064 (0.3–3–6.5–10 μM) (**b**) for 7 days. Cell proliferation is expressed as fold change ± s.d. relative to vehicle-treated cells and is representative of three different experiments each performed in triplicate. (**c**) MCF-7 and MCF-7 TR1 cells, transiently transfected with either empty vector (e.v.) or FXR-DN vector plasmids, were treated with vehicle (−) or CDCA 50 μM for 4 days before testing cell viability using MTT assay. Results are expressed as fold change ± s.d. relative to vehicle-treated cells and are representative of three different experiments each performed in triplicate. (**d**) MTT growth assay in MCF-7 and MCF-7 TR1 cells treated with vehicle (−) or CDCA 50 μM in the presence or not of Tam 1 μM for 4 days. Results are expressed as fold change ± s.d. relative to vehicle-treated cells and are representative of three different experiments each performed in triplicate. (**e**) Soft-agar growth assay in MCF-7 and MCF-7 TR1 cells plated in 0.35% agarose and treated as indicated above. After 14 days of growth, colonies >50 μm diameter were counted. n.s. (nonsignificant); $*P<0.05$ compared with vehicle or Tam.

Table 1 IC_{50} of CDCA and GW4064 for MCF-7 and MCF-7 TR1 cells on anchorage-dependent growth

Cell lines	*IC_{50} (μmol/l) CDCA*	*95% confidence interval*	P	*IC_{50} (μmol/l) GW4064*	*95% confidence interval*	P
MCF-7	46	42.2–50.1		6.04	5.44–6.70	
MCF-7 TR1	31	28.6–33.9	0.0001	4.47	3.6–5.49	0.008

Abbreviations: CDCA, chenodeoxycholic acid; IC_{50}, half-maximal inhibitory concentration.

reporter plasmid containing the human HER2 promoter region (pNeuLite) was significantly reduced with CDCA treatment in both cell lines (Figures 4c and d).

The human HER2 promoter contains multiple consensus sites for several transcription factors, including Sp1, as well as activator protein (AP)-1 and NF-κB, the well known effectors of FXR transrepression (He *et al*., 2006; Vavassori *et al*., 2009) (Figure 4b). To identify the region within the HER2 promoter responsible for CDCA inhibitory effects, HER2 promoter-deleted construct (−232 pNeuLite) activity was tested (Figure 4b). We observed that the responsiveness to CDCA was still maintained, suggesting that the region from −232 to +1 containing the NF-κB motif might be involved in transrepression mechanisms exerted by activated FXR (Figures 4c and d). Thus, we performed site-directed mutagenesis on the NF-κB domain (NF-κB Mut) within the HER2 promoter (Figure 4b). Mutation of this domain abrogated CDCA effects (Figures 4c and d). These latter results demonstrate that the integrity of NF-κB-binding site is necessary for FXR modulation of HER2 promoter activity in breast cancer cells.

The specific role of the NF-κB motif in the transcriptional regulation of HER2 by CDCA was investigated using electrophoretic mobility shift assays. We observed the formation of a complex in nuclear extracts from MCF-7 and MCF-7 TR1 cells using synthetic oligodeoxyribonucleotides corresponding to the NF-κB motif (Figure 5a, lanes 1 and 5), which was abrogated by incubation with 100-fold molar excess of unlabeled probe (Figure 5a, lanes 2 and 6), demonstrating the specificity of the DNA-binding complex. This inhibition was no longer observed when mutated oligodeoxyribonucleotide was used as competitor (Figure 5a, lanes 3 and 7). Interestingly, treatment with CDCA strongly decreased the DNA-binding protein complex compared with

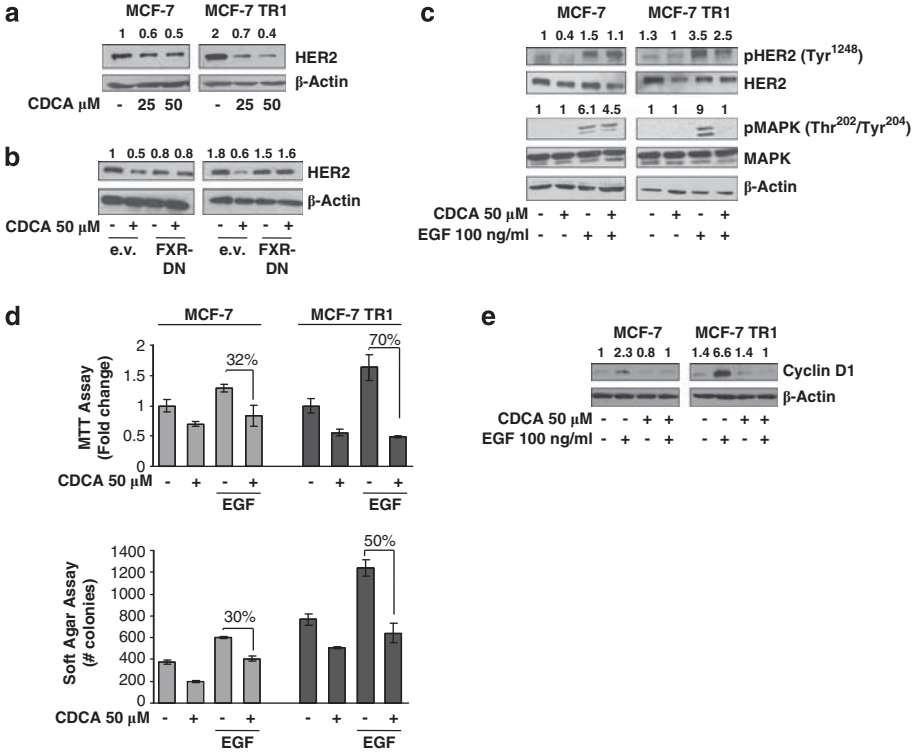

Figure 3 Effects of CDCA on HER2 expression and its transduction pathways in MCF-7 and MCF-7 TR1 cells. (**a**) MCF-7 and MCF-7 TR1 cells were treated for 24 h with vehicle (−) or CDCA 25 and 50 μM before lysis. Equal amounts of total cellular extract were analyzed for HER2 levels by western blotting. β-Actin was used as loading control. (**b**) Cells were transiently transfected with either empty vector (e.v.) or FXR-DN plasmids and then treated with vehicle (−) or CDCA 50 μM for 24 h and HER2 levels were evaluated by western blotting. β-Actin was used as loading control. (**c**) Immunoblot analysis showing phosphorylated HER2 (pHER2 Tyr^{1248}) and MAPK (pMAPK Thr^{202}/Tyr^{204}), total HER2, total MAPK in MCF-7 and MCF-7 TR1 cells pretreated for 24 h with CDCA 50 μM and then treated for 10 min with EGF 100 ng/ml. β-Actin was used as loading control. (**d**) MTT growth assay (upper panel) and soft-agar assay (lower panel) in cells treated with CDCA 50 μM with or without EGF 100 ng/ml for 4 days and 14 days, respectively. The MTT assay results are expressed as fold change ± s.d. relative to vehicle-treated cells and are representative of three different experiments each performed in triplicate. The soft-agar assay values are represented as a mean of colonies number >50 μm diameter counted at the end of assay. Percentages of inhibition induced by CDCA versus EGF treatment alone are shown. (**e**) Cells were treated for 24 h with vehicle (−) or EGF 100 ng/ml in the presence or not of CDCA 50 μM before lysis and then cellular extracts were analyzed for cyclin D1 levels by western blot analysis. β-Actin was used as loading control. Numbers on top of the blots represent the average fold change versus control of MCF-7 cells normalized for β-Actin.

control samples (Figure 5a, lanes 4 and 8). The inclusion of an anti-NF-κB antibody in the reaction immunodepleted the specific band, confirming the presence of NF-κB in the complex (Figure 5b, lanes 3 and 9). Nonspecific IgG did not affect NF-κB complex formation (Figure 5b, lanes 4 and 10). Recombinant NF-κB protein revealed a complex migrating at the same level as that of nuclear extracts from cells (Figure 5a, lane 9; Figure 5b, lanes 5 and 11). Of note, the CDCA-induced reduction in the DNA-binding complex was no longer observed utilizing as probe synthetic oligodeoxyribonucleotides corresponding to the AP-1 and Sp1 motifs (Supplementary Figures 1a and b). To better define the role of FXR in the inhibition of NF-κB binding on HER2 promoter, a competition assay using recombinant NF-κB protein and increasing amounts of *in vitro*-translated FXR protein (1, 3 and 5 μl) was carried out. A dose-dependent reduction in the NF-κB complex was seen (Figure 5c, lanes 1–4), suggesting that physical interaction between these two transcription factors may inhibit the binding of NF-κB to human HER2 promoter region. To further test this possibility, we performed coimmunoprecipitation studies using nuclear protein fractions from MCF-7 and MCF-7TR1 cells treated with CDCA. As shown in Figure 6a, the formation of an FXR and NF-κB complex was detected in untreated cells, and this association was enhanced with FXR ligand treatment.

Moreover, to confirm the involvement of NF-κB in CDCA-mediated HER2-downregulation at the promoter level, ChIP assays were performed. Using specific antibodies against NF-κB and RNA-polymerase II, protein–chromatin complexes were immunoprecipitated from cells cultured with or without CDCA for 1 h. The resulting precipitated DNA was then quantified using real-time PCR with primers spanning the NF-κB-binding element in the HER2 promoter region. NF-κB recruitment was significantly decreased upon CDCA treatment in both cell lines (Figure 6b). This result was well correlated with a lower association of RNA-polymerase II to the HER2 regulatory region (Figure 6c).

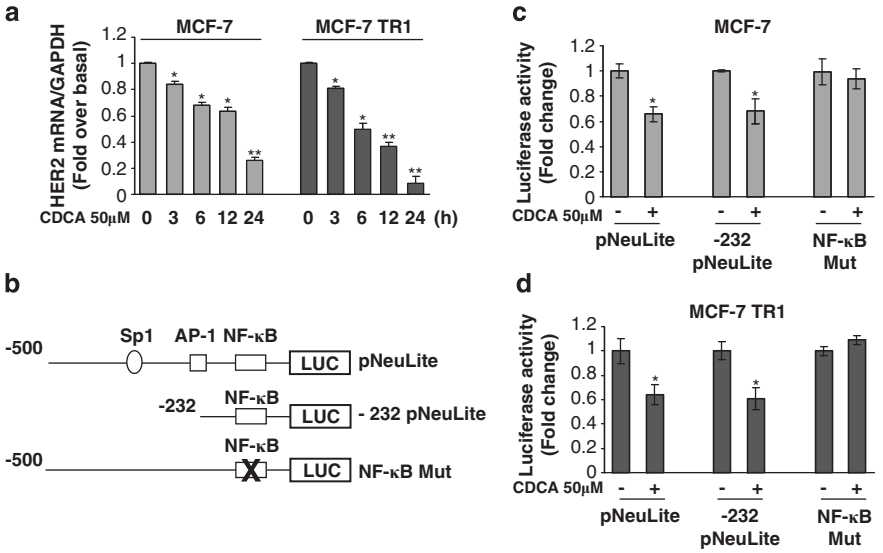

Figure 4 Effects of CDCA on human HER2 promoter activity. (**a**) mRNA HER2 content, evaluated by real-time RT–PCR, after treatment with vehicle or CDCA 50 μM, as indicated. Each sample was normalized to its GAPDH mRNA content. $*P<0.05$ and $**P<0.001$ compared with vehicle. (**b**) Schematic map of the human HER2/neu promoter region constructs used in this study. All of the promoter constructs contain the same 3′ boundary. The 5′ boundaries of the promoter fragments varied from −500 (pNeuLite) to −232 (−232 pNeuLite). A mutated NF-κB-binding site is present in NF-κB mut construct. HER2 transcriptional activity in MCF-7 (**c**) and MCF-7 TR1 (**d**) cells transfected with promoter constructs are shown. After transfection, cells were treated in the presence of vehicle (−) or CDCA 50 μM for 6 h. The values represent the means ± s.d. of three different experiments each performed in triplicate. $*P<0.05$ compared with vehicle.

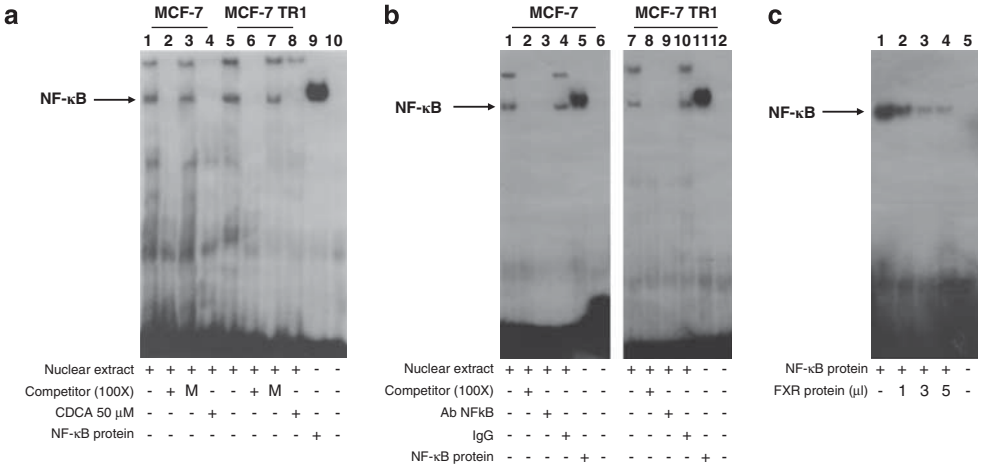

Figure 5 Electrophoretic mobility shift assay of the NF-κB-binding site in the HER2 promoter region. (**a**) Nuclear extracts from MCF-7 and MCF-7 TR1 cells were incubated with a double-stranded NF-κB specific sequence probe labeled with [γ^{32}P]ATP and subjected to electrophoresis in a 6% polyacrylamide gel (lanes 1 and 5). Competition experiments were performed adding as competitor a 100-fold molar excess of unlabeled probe (lanes 2 and 6) or a 100-fold molar excess of unlabeled oligonucleotide containing a mutated NF-κB RE (lanes 3 and 7). Lanes 4 and 8, nuclear extracts from CDCA (50 μM) -treated MCF-7 and MCF-7 TR1 cells, respectively, incubated with probe. Lane 9, NF-κB protein. Lane 10, probe alone. (**b**) Nuclear extracts from MCF-7 and MCF-7 TR1 cells were incubated with a double-stranded NF-κB specific sequence probe labeled with [γ^{32}P]ATP (lanes 1 and 7) or with a 100-fold molar excess of unlabeled probe (lanes 2 and 8). Nuclear extracts incubated with anti-NF-κB (lanes 3 and 9) or IgG (lanes 4 and 10). Lanes 5 and 11, NF-κB protein. Lanes 6 and 12, probe alone. (**c**) Lane 1, NF-κB protein. Lanes 2, 3 and 4, NF-κB protein incubated with increasing doses (1, 3 and 5 μl) of transcribed and translated *in vitro* FXR protein. Lane 5, probe alone.

To further confirm the transcriptional repression mediated by activated FXR, we also evaluated the histone deacetylase 3 association on the NF-κB-responsive sequence within the HER2 promoter. CDCA stimulation enhanced the recruitment of histone deacetylase 3 to this NF-κB promoter site (Figure 6d).

HER2 downregulation underlies the ability of FRX ligands to inhibit breast cancer cell growth

We evaluated the effects of CDCA on cell growth in the ERα-negative and HER2-overexpressing breast cancer cells SKBR3. Treatment with CDCA inhibited SKBR3 anchorage-dependent growth in a dose-dependent

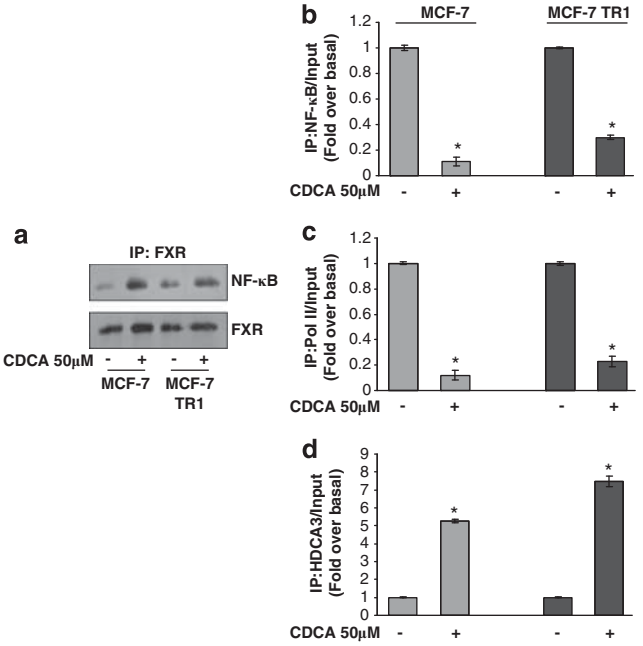

Figure 6 FXR inhibits NF-κB recruitment to HER2 promoter. (**a**) MCF-7 and MCF-7 TR1 cells were treated with vehicle (−) or CDCA 50 μM for 1 h before lysis. FXR protein was immunoprecipitated using an anti-FXR polyclonal antibody (IP:FXR) and resolved in SDS–polyacrylamide gel electrophoresis. Immunoblotting was performed using an anti-NF-κB (p65 subunit) monoclonal antibody and anti-FXR antibody. MCF-7 and MCF-7 TR1 cells were treated in the presence of vehicle (−) or CDCA 50 μM for 1 h, then crosslinked with formaldehyde, and lysed. The precleared chromatin was immunoprecipitated with anti-NF-κB (**b**), anti-RNA polymerase II (**c**) and anti-HDCA3 (**d**) antibodies. A 5 μl volume of each sample and input was analyzed by real-time PCR using specific primers to amplify HER2 promoter sequence, including the NF-κB site. Similar results were obtained in multiple independent experiments. $*P<0.01$ compared with vehicle.

manner (Figure 7a) and reduced colony growth in anchorage-independent assay (Figure 7b). Indeed, we found, after 48 h of treatment with CDCA, a marked decrease in both HER2 protein and mRNA levels (Figures 7c and d). In these cells, HER2 promoter activity was similarly reduced with CDCA treatment (Figure 7e).

Finally, we explored the ability of FXR ligands to inhibit proliferation using as additional model Tam-resistant derivative cell line engineered to stably overexpress HER2 (MCF-7/HER2-18). As expected, Tam-resistant growth in these cells was not affected by both CDCA and GW4064 treatments (Figure 7f). Altogether, these results well evidence how FXR-mediated downregulation of HER2 at transcriptional level is fully responsible for inhibiting breast cancer cell proliferation.

Discussion

In this study, we show for the first time that the activated FXR downregulates HER2 expression in ERα-positive breast cancer cells resistant to Tam. This occurs through the inhibition of NF-κB binding to its responsive element located in the human HER2 promoter region and results in a significant reduction of Tam-resistant growth.

The HER2/neu transmembrane kinase receptor is a signaling amplifier of the HER family network, as activation of membrane tyrosine receptors (EGFR, HER3 and HER4) by their respective ligands determines the formation of homodimeric and heterodimeric kinase complexes into which this receptor is recruited as a preferred partner (Yarden, 2001). Multiple lines of evidences suggest a role of HER2 in the pathogenesis of breast carcinoma (Allred *et al*., 1992; Glockner *et al*., 2001), and clinical data suggest that breast tumors expressing elevated levels of HER2 show a more aggressive phenotype and worse outcome when treated with Tam (Arpino *et al*., 2004; De Laurentiis *et al*., 2005). Thus, inhibitory agents targeting HER2, such as the monoclonal antibody trastuzumab (herceptin), have been explored to improve hormonal treatment or delay emergence of endocrine resistance in estrogen-dependent breast tumors (Johnston, 2009). However, even though an increased response rate is obtained when trastuzumab is used in combination with chemotherapeutic agents (Seidman *et al*., 2001; Slamon *et al*., 2001), patients can still develop resistance (Slamon *et al*., 2001). These observations highlight the importance of discovering new therapeutic tools interfering with HER2-driven signaling to overcome therapy resistance.

We have demonstrated that treatment of breast cancer cells resistant to Tam with the FXR natural ligand CDCA resulted in a reduction of HER2 protein expression. Similar results were also obtained in the ERα-negative and HER2-overexpressing SKBR3 breast cancer cells, suggesting that it may represent a general mechanism not related to cell specificity. Moreover, it assumes more relevance in Tam-resistant breast cancer cells, which are strongly dependent on HER2 activity for their growth. The complete abrogation of FXR-mediated HER2 downregulation with expression of an FXR-DN vector, along with the effects exerted by the synthetic FXR agonist GW4064, clearly demonstrated that activated FXR is involved in the regulation of HER2 expression. Furthermore, quantitative RT–PCR analysis demonstrated that HER2 mRNA levels were significantly decreased in both MCF-7 and MCF-7 TR1 cells treated with CDCA, suggesting that the FXR-induced HER2 downregulation arises via transcriptional mechanisms. Therefore, we focused on the molecular mechanisms by which FXR mediates repression of *HER2* gene expression and on the biological consequences of FXR activation on anti-estrogen-resistant growth of breast cancer cells.

FXR acts mainly by regulating the expression of target genes by binding either as a monomer or heterodimer with the retinoid X receptor to FXR response elements (Laffitte *et al*., 2000; Ananthanarayanan *et al*., 2001; Claudel *et al*., 2002; Kalaany and Mangelsdorf, 2006). Human HER2 promoter did not display any FXR response elements, thus it is reasonable to hypothesize that FXR-induced downregulation of HER2 promoter activity may occur through its interaction with other transcriptional factors. For instance, it

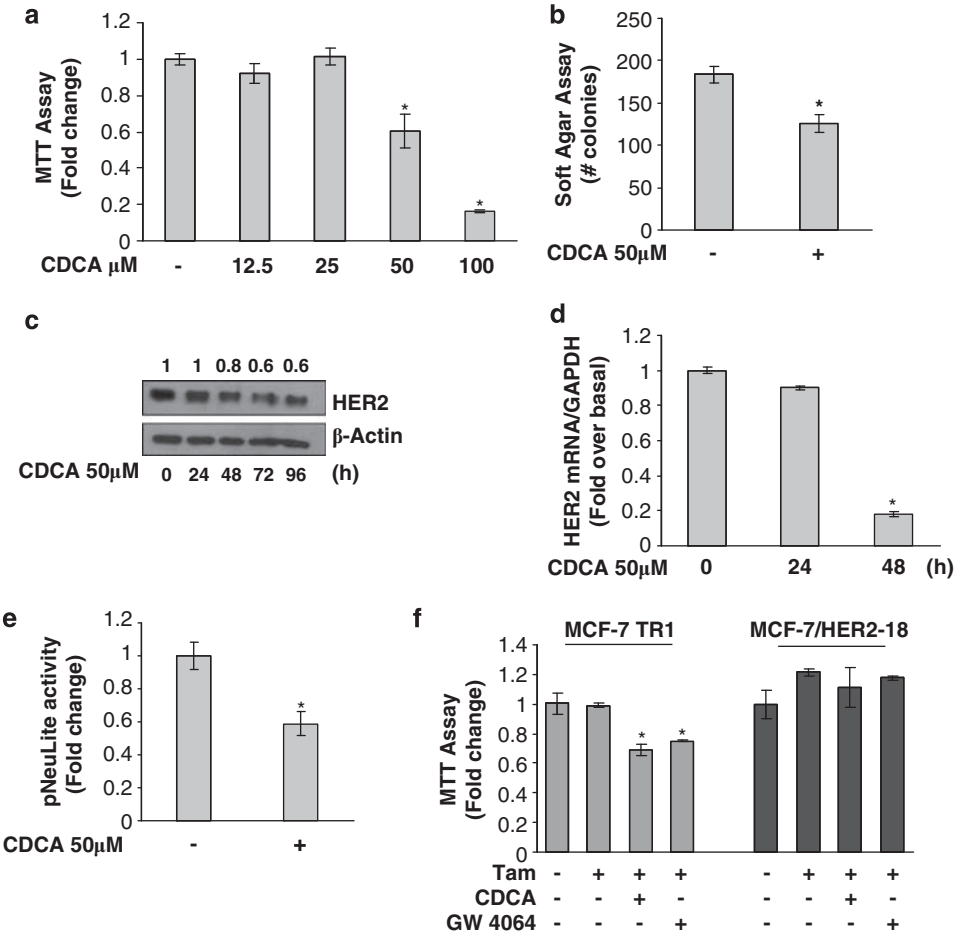

Figure 7 Effects of FXR ligand on SKBR3 breast cancer cells. (**a**) MTT proliferation assay of SKBR3 cells treated with vehicle (−) or increasing doses of CDCA (12,5–25–50–100 μM) for 7 days. Results are expressed as fold change ± s.d. relative to vehicle-treated cells and are representative of three different experiments each performed in triplicate. (**b**) Soft-agar growth assay in SKBR3 cells plated in 0.35% agarose and treated with vehicle (−) or CDCA 50 μM. After 14 days of growth, colonies >50 μm diameter were counted. (**c**) SKBR3 cells were treated with CDCA 50 μM as indicated before lysis. Equal amounts of total cellular extract were analyzed for HER2 levels by western blotting. β-Actin was used as loading control. Numbers on top of the blots represent the average fold change relative to control normalized for β-Actin. (**d**) mRNA HER2 content, evaluated by real-time RT–PCR, after treatment with CDCA 50 μM as indicated. Each sample was normalized to its GAPDH mRNA content. (**e**) SKBR3 cells were transiently transfected with pNeuLite construct. After transfection, cells were treated in the presence of vehicle (−) or CDCA 50 μM for 24 h and the promoter activity was evaluated. The values represent the means ± s.d. of three different experiments each performed in triplicate. $*P<0.05$ compared with vehicle. (**f**) MTT growth assay in MCF-7 TR1 and MCF-7/HER2-18 cells treated with vehicle (−), CDCA 50 μM and GW4064 3 μM in the presence or not of Tam 1 μM for 4 days. Results are expressed as fold change ± s.d. relative to vehicle-treated cells and are representative of three different experiments each performed in triplicate. $*P<0.05$ compared with Tam alone.

has been described the transrepression mechanisms for FXR-mediated inhibition of endothelin-1 expression in vascular endothelial cells (He *et al*., 2006). In addition, it has also been demonstrated that FXR negatively regulates IL-1β expression by stabilizing the nuclear corepressor NCoR on the NF-κB sequence within the IL-1β promoter (Vavassori *et al*., 2009). Several recognition elements are present within the HER2 proximal promoter (Ishii *et al*., 1987; Hurst, 2001) and among these functional motifs we have identified both AP-1 and NF-κB response elements as potential targets of FXR. We have demonstrated by functional studies and site-specific mutagenesis analysis that the integrity of the NF-κB sequence is a prerequisite for the downregulatory effects of the FXR ligand on HER2 promoter activity. These results were supported by electrophoretic mobility shift assays, which revealed a marked decrease in a specific DNA-binding complex in nuclear extracts from MCF-7 and MCF-7 TR1 cells treated with CDCA. *In vitro* competition studies showed that FXR protein was able to inhibit the binding of NF-κB to its consensus site on the HER2 promoter. Furthermore, we observed a reduced recruitment of both NF-κB and RNA polymerase II in CDCA-treated cells, concomitant with an enhanced recruitment of histone deacetylase 3 supporting a negative transcriptional role for FXR in modulating HER2 expression.

The physiological relevance of these effects is pointed out by proliferation studies showing that FXR activation reduced breast cancer cell growth, but did not affect

the proliferation of the non-tumorogenic breast epithelial MCF-10A cell line. MCF-7 TR1 cells exhibited lower IC_{50} values for both ligands compared with parental MCF-7 cells, suggesting a higher sensitivity of the Tam-resistant cells to the effects of FXR ligands. This suggestion is also well supported by the results obtained from growth assays, showing that combined treatment with CDCA and Tam significantly reduced Tam-resistant growth in MCF-7 TR1 cells, compared with Tam alone, but had no additive effects in MCF-7 parental cells. Moreover, FXR ligands failed to inhibit Tam-resistant growth in MCF-7/HER2-18 cells, in which HER2 expression is not driven by its own gene promoter activity. These latter results provided evidences that the downregulation of HER2 expression at transcriptional level underlies the ability of activated FXR to inhibit Tam-resistant growth in breast cancer cells.

Previous *in vitro* studies showed that enhanced EGFR/HER2 expression together with activation of downstream signaling pathways such as p42/44 MAPK are involved in acquired Tam resistance (Knowlden *et al*., 2003; Nicholson *et al*., 2004). Our studies showed that CDCA treatment significantly reduced the ability of EGF to activate its signal transduction cascade in MCF-7 TR1 cells, inhibiting both HER2 and MAPK phosphorylation. In addition, FXR activation was associated with a marked inhibition in EGF-induced growth, concomitant with a reduction in cyclin D1 expression in Tam-resistant breast cancer cells. All together these data demonstrate, as represented in Figure 8, that activated FXR, by preventing the binding of NF-κB to its response element located in the HER2 promoter sequence, abrogates HER2 expression and signaling, resulting in an inhibition of Tam-resistant growth in breast cancer cells.

Deciphering the molecular mechanisms responsible for the development of hormonal resistance is essential for establishing the most appropriate hormone agent according to tumor characteristics and for defining the optimal sequence of endocrine therapies. Moreover, this knowledge is critical for development of new therapeutic approaches able to either overcome or prevent endocrine resistance in breast cancer patients. Over the last years, significant survival benefits for breast cancer were derived from the use of combined treatment of endocrine therapies with new targeted therapies in endocrine responsive breast cancer (Johnston, 2009). In this scenario, the sequencing or the combination of Tam with FXR ligands may represent an important research issue to explore as an alternative therapeutic strategy to treat breast cancer patients whose tumors exploit HER2 signaling to escape Tam treatment.

Materials and methods

Reagents and antibodies

The following components were obtained from the given respective companies, with their addresses in brackets. DMEM, L-glutamine, penicillin, streptomycin, fetal bovine serum, MTT, 4-hydroxytamoxifen, CDCA and EGF from Sigma (Milan, Italy). TRIzol by Invitrogen (Carlsbad, CA, USA). FuGENE 6 by Roche (Indianapolis, IN, USA). TaqDNA polymerase, RETROscript kit, Dual Luciferase kit, TNT master mix and NF-κB protein from Promega (Madison, WI, USA). SYBR Green Universal PCR Master Mix by Biorad (Hercules, CA, USA). Antibodies against FXR, β-actin, Cyclin D1, p65, ERα, EGFR and Lamin B by Santa Cruz

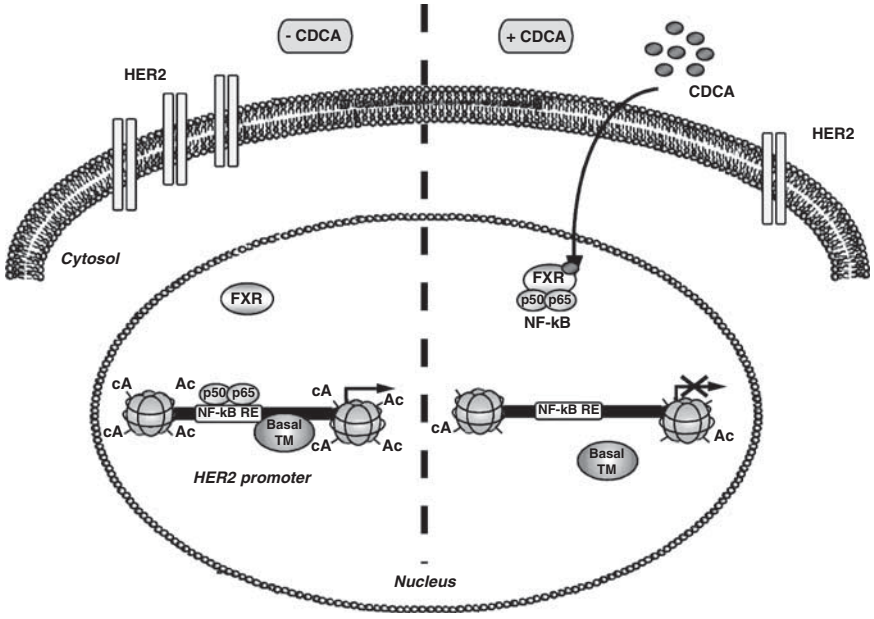

Figure 8 Proposed working model of the FXR-mediated regulation of HER2 expression in Tam-resistant breast cancer cells. In the absence of CDCA, HER2 expression is regulated by several serum factors, including NF-κB, acting through a regulatory region in HER2 promoter and enabling gene transcription. Upon CDCA treatment, FXR binds NF-κB, inhibiting its recruitment on the response element located in the proximal HER2 promoter, causing displacement of RNA polymerase II with consequent repression of HER2 expression.

Biotechnology (Santa Cruz, CA, USA). MAPK, phosphorylated p42/44 MAPK (Thr^{202}/Tyr^{204}), phosphorylated HER2 (Tyr^{1248}) from Cell Signaling Technology (Beverly, MA, USA). HER2 from NeoMarker (Fremont, CA, USA). ECL system and Sephadex G-50 spin columns from Amersham Biosciences (Buckinghamshire, UK). [γ^{32}P]ATP from PerkinElmer (Wellesley, MA, USA). Herceptin from Genentech (San Francisco, CA, USA).

Plasmids
The plasmid pNeuLite containing human HER2/neu promoter region was kindly provided by Dr Mien-Chie Hung (University of Texas, M.D. Anderson Cancer Center, Houston, TX, USA) (Xing *et al*., 2000). The FXR-responsive reporter gene (*FXRE-IR1*) and FXR-DN expression plasmids were provided from Dr T.A. Kocarek (Institute of Environmental Health Sciences, Wayne State University, USA) (Kocarek *et al*., 2002).

The −232 pNeuLite construct was generated by PCR using as template the pNeuLite plasmid with the following primers: forward 5′-GATAAGTGTGAGAACGGCTGCAGGC-3′ and reverse 5′-GGGCAGATCTGGTTTTCCGGTCCCAAT GGA-3′. The amplified DNA fragment was digested with *Bgl*II and *Kpn*I and ligated into pGL2-basic vector. Deletion was confirmed by DNA sequencing.

Site-directed mutagenesis
The pNeuLite promoter plasmid-bearing NF-κB-responsive element-mutated site (NF-κB mut) was created by site-directed mutagenesis using Quick Change kit (Stratagene, La Jolla, CA, USA), according to manufacturer's method. We used as template the pNeuLite plasmid and the following primers (mutations are shown as lowercase letters): 5′-AGAGAGGG AGAAAGTGAAGCTaatcGTTGCCGACTCCCAGACTTC G-3′ and 5′-CGAAGTCTGGGAGTCGGCAACgattAGC TTCACTTTCTCCCTCTCT-3′. Mutation was confirmed by DNA sequencing.

Cell culture
MCF-7 cells were cultured in DMEM containing 10% fetal bovine serum. MCF-7 TR1 and MCF-7 TR2 cells were generated in the laboratory of Dr Fuqua as previously described (Barone *et al*., 2011) and maintained with 10^{-6} M (MCF-7 TR1) and 10^{-7} M (MCF-7 TR2) of 4-hydroxytamoxifen. SKBR3 cells were cultured in phenol red-free RPMI medium containing 10% fetal bovine serum. MCF-10A normal breast epithelial cells were grown in DMEM–F12 medium containing 5% horse serum. MCF-7/HER2-18 were kindly provided by Dr Schiff (Baylor College of Medicine, Houston, TX, USA) and maintained as described (Shou *et al*., 2004). Before each experiment, cells were grown in phenol red-free medium, containing 5% charcoal-stripped fetal bovine serum for 2 days and treated as described.

Cell proliferation assays
Cell proliferation was assessed using MTT and soft-agar anchorage-independent growth assays as described (Barone *et al*., 2009; Giordano *et al*., 2010). The IC_{50} values were calculated using GraphPad Prism 4 (GraphPad Software Inc., San Diego, CA) as described (Herynk *et al*., 2006).

Immunoprecipitation and immunoblot analysis
Cells were treated as indicated before lysis for total protein extraction (Catalano *et al*., 2010). Nuclear extracts were prepared as described (Morelli *et al*., 2004). For coimmunoprecipitation experiments, we used 1 mg of nuclear protein extract and 2 μg of FXR antibody, followed by protein A/G precipitation. Equal amounts of cell extracts and coimmunoprecipitated protein were subjected to SDS–polyacrylamide gel electrophoresis, as described (Catalano *et al*., 2010).

RT–PCR and Real-time RT–PCR assays
FXR gene expression was evaluated by the RT–PCR method using a RETROscript kit. The cDNAs obtained were amplified using the following primers: forward 5′-CGAGCCTGAAG AGTGGTACTGTC-3′ and reverse 5′-CATTCAGCCAACA TTCCCATCTC-3′ (FXR); forward 5′-CTCAACATCTCCC CCTTCTC-3′ and reverse 5′-CAAATCCCATATCCTCGT-3′ (36B4).

The PCR was performed for 35 cycles for hFXR (94 °C 1 min, 65 °C 1 min, 72 °C 1 min) and 18 cycles for 36B4 (94 °C for 1 min, 58 °C for 1 min and 72 °C for 1 min), as described (Catalano *et al*., 2010).

HER2 gene expression was evaluated by real-time RT–PCR. Total RNA was reverse transcribed with the RETROscript kit; 5 μl of diluted (1:3) cDNA was analyzed in triplicates by real-time PCR in an iCycler iQ Detection System (Bio-Rad) using SYBR Green Universal PCR Master Mix, following the manufacturer's recommendations. Each sample was normalized on its GAPDH mRNA content. Primers used for the amplification were: forward 5′-CACCTACAACACAGACAC GTTTGA-3′ and reverse 5′-GCAGACGAGGGTGCAGGA T-3′ (HER2); forward 5′-CCCACTCCTCCACCTTTGAC-3′ and reverse 5′-TGTTGCTGTAGCCAAATTCGTT-3′ (GAPDH). The relative gene expression levels were calculated as described (Sirianni *et al*., 2007).

Transient transfection assays
MCF-7 and MCF-7 TR1 cells were transiently transfected using the FuGENE 6 reagent with FXR reporter gene (*FXRE-IR1*) in the presence or absence of FXR-DN plasmid. In a set of experiments, MCF-7, MCF-7 TR1 and SKBR3 cells were transfected with different HER2 promoter constructs. Luciferase activity was assayed as described (Catalano *et al*., 2010).

Electrophoretic mobility shift assays
Nuclear extracts from cells, treated or not for 3 h with CDCA, were prepared as described (Andrews and Faller, 1991). The DNA sequences used as probe or as cold competitors are the following (nucleotide motifs of interest are underlined and mutations are shown as lowercase letters): NF-κB, 5′-AA GTGAAGCTGGGAGTTGCCGACTCCCAGA-3′; mutated NF-κB, 5′-AAGTGAAGCTaatcGTTGCCGACTCCCAGA-3′; AP-1, 5′-AGGGGGCAGAGTCAC CAGCCTCTG-3′; mutated AP-1, 5′-AGGGGGCAtcaTCACCAGCCTCTG-3′; Sp1 5′-ATCCCGGACTCCGGGGGAGGGGGC-3′; mutated Sp1, 5′-ATCCCGGACCTCattG GGAGGGGGC-3′. *In vitro*-transcribed and -translated FXR protein was synthesized using the T7 polymerase in the rabbit reticulocyte lysate system. Probe generation and the protein-binding reactions were carried out as described (Catalano *et al*., 2010). For experiments involving anti-NF-κB (p65) antibody, the reaction mixture was incubated with this antibody at 4 °C for 12 h before addition of labeled probe.

Chromatin immunoprecipitation assays
Cells were treated with CDCA or left untreated for 1 h and then DNA/protein complexes were extracted as described (Catalano *et al*., 2010). The precleared chromatin was immunoprecipitated with anti-NF-κB (p65), anti-histone

deacetylase 3 or anti-polymerase II antibodies. A normal mouse serum IgG was used as negative control. A 5 µl volume of each sample and input DNA was used for real-time PCR using the primers flanking NF-κB sequence in the human HER2 promoter region: 5′-TGAGAACGGCTGCAGGCA AC-3′ and 5′-CCCACCAACTGCATTCCAA-3′. Real-time PCR was performed as described above. Final results were calculated using the ΔΔCt method, using input Ct values instead of the GAPDH mRNA. The basal sample was used as calibrator.

Statistical analyses

Each datum point represents the mean ± s.d. of three different experiments. Data were analyzed by Student's *t*-test using the GraphPad Prism 4 software program. $P<0.05$ was considered as statistically significant.

Conflict of interest

The authors declare no conflict of interest.

Acknowledgements

This work was supported by AIRC grants, MIUR Ex 60% 2009, PRIN 2009 and Lilli Funaro Foundation. NIH/NCI R01 CA72038 and RP101251 from the Cancer Prevention and Research Institute of Texas (SAWF). We thank Dr Mien-Chie Hung for providing the pNeuLite plasmid and Dr T.A. Kocarek for providing the FXR-responsive reporter gene and FXR-DN expression plasmids. We also thank Dr Rachel Schiff for providing the MCF-7/HER2-18 cells.

References

Allred DC, Clark GM, Molina R, Tandon AK, Schnitt SJ, Gilchrist KW *et al*. (1992). Overexpression of HER-2/neu and its relationship with other prognostic factors change during the progression of *in situ* to invasive breast cancer. *Hum Pathol* **23**: 974–979.

Ananthanarayanan M, Balasubramanian N, Makishima M, Mangelsdorf DJ, Suchy FJ. (2001). Human bile salt export pump promoter is transactivated by the farnesoid X receptor/bile acid receptor. *J Biol Chem* **276**: 28857–28865.

Andrews NC, Faller DV. (1991). A rapid micropreparation technique for extraction of DNA-binding proteins from limiting numbers of mammalian cells. *Nucleic Acids Res* **19**: 2499.

Arpino G, Green SJ, Allred DC, Lew D, Martino S, Osborne CK *et al*. (2004). HER-2 amplification, HER-1 expression, and tamoxifen response in estrogen receptor-positive metastatic breast cancer: a southwest oncology group study. *Clin Cancer Res* **10**: 5670–5676.

Arpino G, Wiechmann L, Osborne CK, Schiff R. (2008). Crosstalk between the estrogen receptor and the HER tyrosine kinase receptor family: molecular mechanism and clinical implications for endocrine therapy resistance. *Endocr Rev* **29**: 217–233.

Barone I, Brusco L, Gu G, Selever J, Beyer A, Covington KR *et al*. (2011). Loss of Rho GDI α and resistance to tamoxifen via effects on estrogen receptor α. *Journal Natl Cancer Inst* (in press).

Barone I, Cui Y, Herynk MH, Corona-Rodriguez A, Giordano C, Selever J *et al*. (2009). Expression of the K303R estrogen receptor-alpha breast cancer mutation induces resistance to an aromatase inhibitor via addiction to the PI3K/Akt kinase pathway. *Cancer Res* **69**: 4724–4732.

Bishop-Bailey D. (2004). FXR as a novel therapeutic target for vascular disease. *Drug News Perspect* **17**: 499–504.

Blume-Jensen P, Hunter T. (2001). Oncogenic kinase signalling. *Nature* **411**: 355–365.

Catalano S, Malivindi R, Giordano C, Gu G, Panza S, Bonofiglio D *et al*. (2010). Farnesoid X receptor, through the binding with steroidogenic factor 1-responsive element, inhibits aromatase expression in tumor Leydig cells. *J Biol Chem* **285**: 5581–5593.

Chung YL, Sheu ML, Yang SC, Lin CH, Yen SH. (2002). Resistance to tamoxifen-induced apoptosis is associated with direct interaction between Her2/neu and cell membrane estrogen receptor in breast cancer. *Int J Cancer* **97**: 306–312.

Claudel T, Sturm E, Duez H, Torra IP, Sirvent A, Kosykh V *et al*. (2002). Bile acid-activated nuclear receptor FXR suppresses apolipoprotein A-I transcription via a negative FXR response element. *J Clin Invest* **109**: 961–971.

De Laurentiis M, Arpino G, Massarelli E, Ruggiero A, Carlomagno C, Ciardiello F *et al*. (2005). A meta-analysis on the interaction between HER-2 expression and response to endocrine treatment in advanced breast cancer. *Clin Cancer Res* **11**: 4741–4748.

Encarnacion CA, Ciocca DR, McGuire WL, Clark GM, Fuqua SA, Osborne CK. (1993). Measurement of steroid hormone receptors in breast cancer patients on tamoxifen. *Breast Cancer Res Treat* **26**: 237–246.

Fisher B, Costantino JP, Wickerham DL, Redmond CK, Kavanah M, Cronin WM *et al*. (1998). Tamoxifen for prevention of breast cancer: report of the National Surgical Adjuvant Breast and Bowel Project P-1 Study. *J Natl Cancer Inst* **90**: 1371–1388.

Forman BM, Goode E, Chen J, Oro AE, Bradley DJ, Perlmann T *et al*. (1995). Identification of a nuclear receptor that is activated by farnesol metabolites. *Cell* **81**: 687–693.

Giordano C, Cui Y, Barone I, Andò S, Mancini MA, Berno V *et al*. (2010). Growth factor-induced resistance to tamoxifen is associated with a mutation of estrogen receptor alpha and its phosphorylation at serine 305. *Breast Cancer Res Treat* **119**: 71–85.

Glockner S, Lehmann U, Wilke N, Kleeberger W, Langer F, Kreipe H. (2001). Amplification of growth regulatory genes in intraductal breast cancer is associated with higher nuclear grade but not with the progression to invasiveness. *Lab Invest* **81**: 565–571.

Gradishar WJ. (2004). Tamoxifen—what next? *Oncologist* **9**: 378–384.

Gutierrez MC, Detre S, Johnston S, Mohsin SK, Shou J, Allred DC *et al*. (2005). Molecular changes in tamoxifen-resistant breast cancer: relationship between estrogen receptor, HER-2, and p38 mitogen-activated protein kinase. *J Clin Oncol* **23**: 2469–2476.

He F, Li J, Mu Y, Kuruba R, Ma Z, Wilson A *et al*. (2006). Downregulation of endothelin-1 by farnesoid X receptor in vascular endothelial cells. *Circ Res* **98**: 192–199.

Herynk MH, Beyer AR, Cui Y, Weiss H, Anderson E, Green TP *et al*. (2006). Cooperative action of tamoxifen and c-Src inhibition in preventing the growth of estrogen receptor-positive human breast cancer cells. *Mol Cancer Ther* **5**: 3023–3031.

Hurst HC. (2001). Update on HER-2 as a target for cancer therapy: the ERBB2 promoter and its exploitation for cancer treatment. *Breast Cancer Res* **3**: 395–398.

Ishii S, Imamoto F, Yamanashi Y, Toyoshima K, Yamamoto T. (1987). Characterization of the promoter region of the human c-erbB-2 protooncogene. *Proc Natl Acad Sci USA* **84**: 4374–4378.

Johnston SR. (2009). Enhancing the efficacy of hormonal agents with selected targeted agents. *Clin Breast Cancer* **9**(Suppl 1): S28–S36.

Journe F, Laurent G, Chaboteaux C, Nonclercq D, Durbecq V, Larsimont D *et al*. (2008). Farnesol, a mevalonate pathway intermediate, stimulates MCF-7 breast cancer cell growth through farnesoid-X-receptor-mediated estrogen receptor activation. *Breast Cancer Res Treat* **107**: 49–61.

Kalaany NY, Mangelsdorf DJ. (2006). LXRS and FXR: the yin and yang of cholesterol and fat metabolism. *Annu Rev Physiol* **68**: 159–191.

Kirkegaard T, McGlynn LM, Campbell FM, Muller S, Tovey SM, Dunne B *et al*. (2007). Amplified in breast cancer 1 in human epidermal growth factor receptor—positive tumors of tamoxifen-treated breast cancer patients. *Clin Cancer Res* **13**: 1405–1411.

Knowlden JM, Hutcheson IR, Jones HE, Madden T, Gee JM, Harper ME *et al*. (2003). Elevated levels of epidermal growth factor receptor/c-erbB2 heterodimers mediate an autocrine growth regulatory pathway in tamoxifen-resistant MCF-7 cells. *Endocrinology* **144**: 1032–1044.

Kocarek TA, Shenoy SD, Mercer-Haines NA, Runge-Morris M. (2002). Use of dominant negative nuclear receptors to study xenobiotic-inducible gene expression in primary cultured hepatocytes. *J Pharmacol Toxicol Methods* **47**: 177–187.

Laffitte BA, Kast HR, Nguyen CM, Zavacki AM, Moore DD, Edwards PA. (2000). Identification of the DNA binding specificity and potential target genes for the farnesoid X-activated receptor. *J Biol Chem* **275**: 10638–10647.

Makishima M, Okamoto AY, Repa JJ, Tu H, Learned RM, Luk A *et al*. (1999). Identification of a nuclear receptor for bile acids. *Science* **284**: 1362–1365.

Meng S, Tripathy D, Shete S, Ashfaq R, Haley B, Perkins S *et al*. (2004). HER-2 gene amplification can be acquired as breast cancer progresses. *Proc Natl Acad Sci USA* **101**: 9393–9398.

Morelli C, Garofalo C, Sisci D, del Rincon S, Cascio S, Tu X *et al*. (2004). Nuclear insulin receptor substrate 1 interacts with estrogen receptor alpha at ERE promoters. *Oncogene* **23**: 7517–7526.

Nicholson RI, Staka C, Boyns F, Hutcheson IR, Gee JM. (2004). Growth factor-driven mechanisms associated with resistance to estrogen deprivation in breast cancer: new opportunities for therapy. *Endocr Relat Cancer* **11**: 623–641.

Osborne CK, Bardou V, Hopp TA, Chamness GC, Hilsenbeck SG, Fuqua SA *et al*. (2003). Role of the estrogen receptor coactivator AIB1 (SRC-3) and HER-2/neu in tamoxifen resistance in breast cancer. *J Natl Cancer Inst* **95**: 353–361.

Parks DJ, Blanchard SG, Bledsoe RK, Chandra G, Consler TG, Kliewer SA *et al*. (1999). Bile acids: natural ligands for an orphan nuclear receptor. *Science* **284**: 1365–1368.

Sabnis GJ, Jelovac D, Long B, Brodie A. (2005). The role of growth factor receptor pathways in human breast cancer cells adapted to long-term estrogen deprivation. *Cancer Res* **65**: 3903–3910.

Schiff R, Massarweh SA, Shou J, Bharwani L, Mohsin SK, Osborne CK. (2004). Cross-talk between estrogen receptor and growth factor pathways as a molecular target for overcoming endocrine resistance. *Clin Cancer Res* **10**: 331S–336S.

Seidman AD, Fornier MN, Esteva FJ, Tan L, Kaptain S, Bach A *et al*. (2001). Weekly trastuzumab and paclitaxel therapy for metastatic breast cancer with analysis of efficacy by HER2 immunophenotype and gene amplification. *J Clin Oncol* **19**: 2587–2595.

Shou J, Massarweh S, Osborne CK, Wakeling AE, Ali S, Weiss H *et al*. (2004). Mechanisms of tamoxifen resistance: increased estrogen receptor-HER2/neu cross-talk in ER/HER2-positive breast cancer. *J Natl Cancer Inst* **96**: 926–935.

Sirianni R, Chimento A, Malivindi R, Mazzitelli I, Ando S, Pezzi V. (2007). Insulin-like growth factor-I, regulating aromatase expression through steroidogenic factor 1, supports estrogen-dependent tumor Leydig cell proliferation. *Cancer Res* **67**: 8368–8377.

Slamon DJ, Godolphin W, Jones LA, Holt JA, Wong SG, Keith DE *et al*. (1989). Studies of the HER-2/neu proto-oncogene in human breast and ovarian cancer. *Science* **244**: 707–712.

Slamon DJ, Leyland-Jones B, Shak S, Fuchs H, Paton V, Bajamonde A *et al*. (2001). Use of chemotherapy plus a monoclonal antibody against HER2 for metastatic breast cancer that overexpresses HER2. *N Engl J Med* **344**: 783–792.

Staka CM, Nicholson RI, Gee JM. (2005). Acquired resistance to oestrogen deprivation: role for growth factor signalling kinases/oestrogen receptor cross-talk revealed in new MCF-7X model. *Endocr Relat Cancer* **12**(Suppl 1): S85–S97.

Swales KE, Korbonits M, Carpenter R, Walsh DT, Warner TD, Bishop-Bailey D. (2006). The farnesoid X receptor is expressed in breast cancer and regulates apoptosis and aromatase expression. *Cancer Res* **66**: 10120–10126.

Vavassori P, Mencarelli A, Renga B, Distrutti E, Fiorucci S. (2009). The bile acid receptor FXR is a modulator of intestinal innate immunity. *J Immunol* **183**: 6251–6261.

Xing X, Wang SC, Xia W, Zou Y, Shao R, Kwong KY *et al*. (2000). The ets protein PEA3 suppresses HER-2/neu overexpression and inhibits tumorigenesis. *Nat Med* **6**: 189–195.

Yarden Y. (2001). Biology of HER2 and its importance in breast cancer. *Oncology* **61**(Suppl 2): 1–13.

Supplementary Information accompanies the paper on the Oncogene website (http://www.nature.com/onc)

International Journal of Andrology
international journal of andrology ISSN 0105-6263

ORIGINAL ARTICLE

Conventional progesterone receptors (PR) B and PRA are expressed in human spermatozoa and may be involved in the pathophysiology of varicocoele: a role for progesterone in metabolism

F. De Amicis,*†[1] C. Guido,*†[1] T. Perrotta,‡ P. Avena,*† S. Panza,*† S. Andò*§[2] and S. Aquila*†[2]

*Centro Sanitario, †Department of Pharmaco-Biology, ‡Department of Ecology, and §Department of Cellular Biology, University of Calabria, Arcavacata di Rende (CS), Italy

Keywords:
human ejaculated spermatozoa, male reproduction, PR

Correspondence:
Saveria Aquila, Centro Sanitario, University of Calabria, Arcavacata di Rende (CS) 87036, Italy. E-mail: aquisav@libero.it

[1]These authors contributed equally to the study
[2]These authors are joint senior authors

Received 7 May 2010; revised 20 July 2010; accepted 8 August 2010

doi:10.1111/j.1365-2605.2010.01111.x

Summary

The physiological roles of intracellular progesterone (PRG) receptors (PRs) have been studied intensively in female mammals, while their functions in male are scarce. Conventional PRs were evidenced in our study by Western blotting, concomitantly in healthy spermatozoa and in oligoasthenoteratozoospermic samples without and with varicocoele. Transmission electron microscopy revealed the presence of the PRs on the membrane as well as in the nucleus, mitochondria and flagellum. A reduced expression of the PRs was observed only in varicocoele spermatozoa. Responses to PRG treatment on cholesterol efflux, tyrosine phosphorylation, src and Akt activities, acrosin activity and acrosome reaction in varicocoele spermatozoa were reduced or absent. To further investigate PRG significance in human male gamete, we focused its action on lipid and glucose metabolism. The evaluation of the triglycerides content, lipase and acyl-CoA dehydrogenase activities suggests that PRG through the PRs exerts a lipolytic effect on human spermatozoa. An increase in glucose-6-phosphate dehydrogenase activity was also obtained, evidencing a role for PRG on glucose metabolism. In 'varicocoele' spermatozoa, the PRG did not induce energy consumption. The action of PRs on sperm metabolism is a novel finding that renews the importance of PRG in male fertility. Our results showed that varicocoele may lead to male factor infertility by a mechanism involving a decreased PR expression in human spermatozoa that evidences a detrimental effect on spermatozoa at the molecular level, going beyond the abnormal sperm morphology described to date.

Introduction

The enigma of the varicocoele has always attracted the researchers' attention as attested by the substantial body of literature on the topic. Varicocoeles, defined as abnormally dilated scrotal veins, are present in 15% of the normal male population and in approximately 40% of men presenting infertility [World Health Organization (WHO) 1992; Koksal *et al.*, 2007]. Although it is widely accepted that varicocoele is the most common cause of male infertility (Romeo & Santoro, 2009), scientific support for this contention is almost lacking. The preponderance of experimental data from clinical and animal models demonstrates an adverse effect of varicocoeles on spermatogenesis, as venous reflux and testicular temperature elevation cause impaired spermatogenesis (Zorgniotti & Macleod, 1973; Gorelick & Goldstein, 1993). Studies using light microscopy have shown in ejaculated spermatozoa from men with varicocoele an increased number of elongated tapered sperm heads (Portuondo *et al.*, 1983), although the pathophysiology of the spermatogenesis underlying the relationship between sperm cell quality and varicocoele is still poorly understood.

It is well known that progesterone (PRG) is an essential regulator of several female reproductive events such as ovulation, regulation of the menstrual cycle, implanta-

tion and maintenance of pregnancy (Rothchild, 1983; Graham & Clarke, 1997). In contrast to the established unequivocal roles of PRG in female reproductive physiology, there are limited data on the role of PRG in male reproductive events. The actions of PRG are generally mediated via conventional intracellular PRG receptors (PRs) that belong to the superfamily of transcription factors (Horwitz & Alexander, 1983; Kastner *et al.*, 1990) expressed in a variety of female foetal and adult tissues (Jensen, 1996; Lau *et al.*, 1996). Gene targeting strategies showed pleiotropic reproductive abnormalities in PR null female mice (Lydon *et al.*, 1995; Conneely & Lydon, 2000). Deletion of both PR isoforms, PRB and the N terminally truncated PRA renders female mice infertile with ovarian deficits that prevent ovulation (Pinter *et al.*, 1996; Conneely *et al.*, 2001). Far less is known of the reproductive consequences of PR disruption or blockade in male animals. Although the reproductive phenotype of PR knockout male mice has not been reported in detail, mice null for steroid receptor coactivator-1 (SRC-1; an intracellular PR coactivator) show reduced testicular growth and fertility compared with their wild-type littermates (Xu *et al.*, 1998).

Ejaculated mammalian spermatozoa are highly differentiated attractive cells showing intriguing features: extreme polarization of cellular architecture and functions; a little amount of cytoplasm; they seem to be transcriptionally inactive; they go through two different physiological conditions comprising a steady state in the male genital tract and a functional maturation, known as capacitation, in the female genital tract (Yanagimachi, 1994; Rathi *et al.*, 2001; Suarez, 2008). Capacitation is a multifaceted process occurring in the female genital tract by which spermatozoa acquires the ability to fertilize an oocyte. PRG has been shown to activate several signalling pathways involved in the regulation of sperm functions. It was reported that PRG induces hyperactive motility and acrosome reaction (AR) of mammalian spermatozoa during the transit along the female reproductive tract (Kay *et al.*, 1994; Gadkar-Sable *et al.*, 2005). Cheng *et al.* (1998a,b) were the first to report the existence of a sperm plasma membrane PR in stallion spermatozoa. Later, a non-genomic plasma membrane PR (Contreras & Llanos, 2001) was found in the acrosomal region (Wu *et al.*, 2005, 2006). Specific PRG sperm-binding sites are located on the plasma membrane of the spermatozoon (Blackmore *et al.*, 1994). Binding studies also revealed the presence of two classes of PRs in the human spermatozoon: one class has an elevated affinity constant (nanomolar) and it is specific for PRG, whereas the other class has an affinity constant in the micromolar range. The blocking of these surface receptors inhibits PRG-induced AR (Sabeur *et al.*, 1996; Cheng *et al.*, 1998b). Besides, PRG has been shown to activate several signalling pathways, such as generation of cAMP, increase of intracellular calcium (Ca^{2+}), promotion of tyrosine phosphorylation of proteins, activation of phospholipases and many others, all involved in the regulation of human spermatozoa physiology (Thomas & Meizel, 1989; Blackmore *et al.*, 1990). However, the mechanism/s through which PRG exerts its effects in this context and the role of PRG in male reproductive events are still complex to define.

In this study, we investigated the expression of the classical PRs and their ultrastructural location in human spermatozoa and interestingly, 'varicocoele' spermatozoa showed a reduced expression of the receptors. The functional role of PRG/PRs was tested on capacitation, Akt and p60c-src (src) activities and AR. To define further the significance of PRG in human male gamete, we evaluated its action on lipid and glucose metabolism as it has never been investigated.

Materials and methods

Chemicals

Percoll (colloidal PVP-coated silica for cell separation), sodium bicarbonate, sodium lactate, sodium pyruvate, dimethyl sulphoxide (DMSO), Earle's balanced salt solution, PRG, fluorescein isothiocyanate-conjugated peanut agglutinin (FITC-PNA) and all other chemicals were purchased from Sigma Chemical (Milan, Italy). The anti-progestin RU486 {RU38486, mifepristone, 17(-hydroxy-11(8-[4-(dimethylamino)phenyl]-17a-propynylestra-4,9-dien-3-one} binds with high affinity to the intracellular PR receptor in most vertebrate species (Schatz *et al.*, 2003). Acrylamide bisacrylamide was from Labtek Eurobio (Milan, Italy). Triton X-100 and Eosin Y were from Farmitalia Carlo Erba (Milan, Italy). ECL Plus Western blotting detection system, Hybond ECL, Hepes Sodium Salt were from Amersham Pharmacia Biotech (Buckinghamshire, UK). Colloidal gold-conjugated goat anti-mouse immunoglobulin G (IgG) secondary antibody (Ab) was from Sigma-Aldrich. Rabbit polyclonal anti-human PR (C-19) Ab, anti-phosphotyrosine Ab (PY99), goat polyclonal actin Ab (1-19), peroxidase-coupled anti-mouse, anti-rabbit and anti-goat IgG secondary Abs were from Santa Cruz Biotechnology (Heidelberg, Germany). Cholesterol-oxidase (CHOD)–peroxidase (POD) enzymatic colorimetric kit, triglycerides assay kit, lipase activity kit, glucose-6-phosphate dehydrogenase (G6PDH) activity assay kit and insulin radioimmunoassay (RIA) kit were from Inter-Medical (Biogemina Italia Srl, Catania, Italy). PRG and RU486 were dissolved in ethanol (0.02% final concentration in culture) and used, as solvent controls did not induce any positive result in all in vitro assays (data not shown).

Semen samples and spermatozoa preparations

Human semen sample was collected, according to the WHO-recommended procedure, by masturbation from healthy volunteer donors of proven fertility. Spermatozoa preparations were performed as described previously (Aquila *et al.*, 2005a). Briefly, semen samples with normal parameters of volume, sperm count, motility, morphology and vitality, according to the WHO's (1992) *Laboratory Manual*, were included in this study. Varicocoele samples of patients who consulted us for fertility investigation were also included in our study. Reflux of blood in the pampiniform plexus was determined by palpation employing the Valsalva manoeuvre. Physical examination is the reference standard to diagnose varicocoeles in subfertile men. Additional radiological imaging is not necessary to diagnose subclinical varicocoele because only a varicocoele detected by physical examination should be considered potentially significant (Pryor & Howards, 1987). Varicocoele samples used in this study were from oligoasthenoteratozoospermic (OAT) patients with diagnosed varicocoele of grade III (visible without palpation) on the left testis and their ejaculates were found to have total sperm count of 17×10^6 sperm cells per ejaculate, percentage of motility a + b of 30%, percentage of normally formed features of 30% and viability percentage of 67%. Samples of OAT patients without varicocoele, but with similar semen characteristics with respect to those with varicocoele, were considered as control in our study to isolate a specific effect of varicocoele. Mean ± SD age of men with normal semen parameters, OAT samples without and with varicocoele was 30.8 ± 4.5, 31.4 ± 3.8 and 29.7 ± 4.1 years, respectively. Testicular volume, measured with an ellipsoid Prader orchidometer comparing the sizes of both testes, was 15.8 ± 2.5 mL right testis (Rt) and 15.4 ± 2.5 mL left testis (Lt) in men with normal semen parameters; 15.2 ± 3.5 mL Rt and 15.0 ± 2.2 mL Lt in OAT patients without varicocoele; 14.9 ± 3.5 mL Rt and 14.3 ± 3.5 mL Lt in varicocoele patients. Despite statistically significant differences in the hormones of some varicocoele patients that were reported by many investigators (Andò *et al.*, 1984), the actual values were within normal limits (Al-Ali *et al.*, 2010). In our study, all subjects were also evaluated by reproductive plasma hormone determinations, including follicle-stimulating hormone (FSH), luteinizing hormone (LH) and testosterone. Mean plasma levels for FSH were 6.6 ± 0.5 mlU/mL in men with normal semen parameters, 6.9 ± 0.7 mlU/mL in OAT patients without varicocoele and 7.2 ± 0.5 mlU/mL in varicocoele patients. Mean plasma levels for LH were 10.2 ± 0.4 mlU/mL in men with normal semen parameters, 10.0 ± 0.7 in OAT patients without varicocoele and 10.8 ± 0.5 mlU/mL in varicocoele patients. Mean plasma levels for testosterone were 487 ± 19.9 ng/100 mL in men with normal semen parameters, 478 ± 10.9 ng/100 mL in OAT patients without varicocoele and 446 ± 16.9 ng/100 mL in varicocoele patients. There have also been some controversial studies on this latter issue (Mohammed & Chinegwundoh, 2009).

The study was approved by the local medical-ethical committee and all participants gave their informed consent.

Processing and treatments of ejaculated spermatozoa

For each experiment (many times repeated as reported in the 'Statistical analysis' section), three normozoospermic samples or four OAT or four varicocoele samples were pooled. In fact, after liquefaction, semen samples were first pooled and then subjected to centrifugation (800 ***g***) on a discontinuous Percoll density gradient (80% : 40% v : v; Aquila *et al.*, 2002). The 80% Percoll fraction was examined using an optical microscope equipped with a 100× oil objective to ensure that a pure sample containing only spermatozoa was obtained. These spermatozoa had a motility of about 65% (grades a + b, WHO, 1999) and a viability of 80% for both normal or pathological samples. An independent observer inspected several fields for each slide. Particularly, the same number for both normal and pathological samples of Percoll-purified spermatozoa was washed with unsupplemented Earle's medium (uncapacitating medium) and the samples were incubated for 30 min at 37 °C and 5% CO_2, without (control, NC) or with the following treatments: increasing PRG concentrations (3, 30 and 60 μM) or with RU486 (10 μM) alone or combined with 30 μM PRG. When the cells were treated with RU486, a pre-treatment of 15 min was performed. It deserves to be mentioned that in humans, PRG is present in low concentrations in blood, but it can be extraordinarily high in periovulatory follicular fluid (up to 20 μg/mL; Saaranen *et al.*, 1993); therefore, high levels of PRG may become available to spermatozoa at the time of fertilization.

Immunogold labelling for PR

Spermatozoa fixed overnight in 4% paraformaldehyde were washed in phosphate-buffered saline (PBS) to remove excess fixative, dehydrated in graded alcohol, infiltrated in LR white resin, polymerized in a vacuum oven at 45 °C for 48 h, while 60 nm ultra-thin sections were cut and placed on coated nickel grids for post-embedding immunogold labelling with the rabbit polyclonal Ab to human PR. Potential non-specific labelling was blocked by incubating the sections in PBS containing 5% normal goat serum, 5% bovine serum albumin and

0.1% cold water fish gelatin at room temperature for 1 h. Sections were then incubated overnight at 4 °C with rabbit polyclonal PR Ab at a dilution of 1 : 500 in PBS buffer. They were then incubated in 10-nm colloidal gold-conjugated anti-mouse or anti-rabbit IgG secondary Abs at 1 : 50 dilution for 2 h at room temperature. The sections were then subsequently washed in PBS, later fixed in gluteraldehyde, counterstained in uranyl acetate and lead acetate and examined under a Zeiss EM 900 (Zeiss, Oberkochen, Germany) transmission electron microscope (TEM). To assess the specificity of the immunolabelling, negative controls were carried out in corresponding sections of spermatozoa that were labelled with colloidal gold-conjugated secondary Ab with normal rabbit serum instead of primary Ab.

Western blot analysis of sperm proteins

Percoll-purified sperm samples, washed twice with uncapacitating medium, were incubated as mentioned before and then centrifuged for 5 min at 5000 ***g***. The pellet was resuspended in lysis buffer as previously described (Aquila *et al.*, 2002). An equal amount of protein (80 μg) was boiled for 5 min, separated on a 11% polyacrylamide gel electrophoresis, transferred to nitrocellulose membranes and probed with an appropriate dilution of the indicated primary Ab. The binding of the secondary Ab was observed with the ECL Plus Western blotting detection system, according to the manufacturer's instructions. As internal control, all membranes were subsequently stripped (glycine 0.2 M, pH 2.6 for 30 min at room temperature) and re-probed with anti β-actin Ab or with total Akt or src. The protein bands were quantified by scanning densitometry (Imaging Densitometer GS-700; Bio-Rad, Hercules, CA, USA). Western blot analysis was performed in at least four independent experiments and more representative results are shown.

Measurement of cholesterol in the sperm culture medium

Cholesterol was measured in duplicate by a CHOD–POD enzymatic colorimetric method according to the manufacturer's instructions in the incubation medium from human spermatozoa, as described previously (Aquila *et al.*, 2006, 2009). Percoll-purified sperm samples, washed twice with uncapacitating medium, were incubated in the same medium (control) or in capacitating medium for 30 min at 37 °C and 5% CO_2. Some samples were incubated in the presence of increasing PRG concentrations (3–60 μM). Other samples were incubated in the presence of 10 μM RU486 alone or combined with 30 μM PRG. At the end of sperm incubation, the culture media were recovered by centrifugation, lyophilized and subsequently dissolved in 1 mL of buffer reaction. The samples were incubated for 10 min at room temperature and then the cholesterol content was measured spectrophotometrically at 505 nm. Cholesterol standard used was 200 mg/dL. The limit of sensitivity for the assay was 0.05 mg/dL. Inter- and intra-assay variations were 0.04% and 0.03%, respectively. Cholesterol results are presented as mg per 10×10^6 number of spermatozoa.

Acrosin activity assay

Acrosin activity was assessed by the method of Kennedy *et al.* (1989) and as described previously (Aquila *et al.*, 2003). Spermatozoa were washed in Earle's medium and centrifuged at 800 ***g*** for 20 min, then resuspended in different tubes (final concentration of 10×10^6 sperm/mL) in the presence and absence of treatments. One millilitre of substrate–detergent mixture (23 mmol/L of BAPNA in DMSO and 0.01% Triton X-100 in 0.055 mol/L of NaCl, 0.055 mol/L of HEPES at pH 8.0, respectively) was added for 3 h at room temperature. Aliquots (20 μL) were removed at 0 and 3 h and the percentage of viable cells was determined for each treatment. After incubation, a final concentration of 0.5 mol/L of benzamidine was added to each tube and then centrifuged at 1000 ***g*** for 30 min. Supernatants were collected and the acrosin activity was measured using a spectrophotometer at 410 nm. In this assay, the total acrosin activity was defined as the amount of active (non-zymogen) acrosin associated with spermatozoa plus the amount of active acrosin that is obtained by proacrosin activable. The acrosin activity was expressed as μIU/10^6 spermatozoa. Quantification of acrosin activity was performed as described previously (Aquila *et al.*, 2003).

Acrosome reaction

The evaluation of AR was performed by utilizing FITC-PNA. At the end of incubation, sperm cells were washed thrice with 0.5 mmol/L of Tris-HCl buffer, pH 7.5, and were allowed to settle onto slides. Smears, dried in air, were dipped in absolute methanol for 15 min and left at room temperature. The samples were then incubated with a solution of FITC-PNA in a humid chamber at room temperature. After 30 min, the slides were washed with PBS to remove the excess label. Scoring was completed within 24 h of staining that was assessed according to a published scoring system (Mendoza *et al.*, 1992). A minimum of 200 live spermatozoa were examined for each treatment and they were classified into two main categories based on the FITC-PNA staining as follows: (i) acrosome-reacted cells with uniform green FITC-PNA

fluorescence of the acrosome cap; (ii) acrosome-intact cells without any fluorescence. Values were expressed as percentage of acrosome-reacted cells.

Triglycerides assay

Triglycerides were measured in duplicate by a GPO-POD enzymatic colorimetric method according to the manufacturer's instructions in sperm lysates and as described previously (Aquila *et al.*, 2006). Percoll-purified sperm samples, washed twice by centrifugation with uncapacitating medium, were incubated in the same medium (control) for 30 min at 37 °C and 5% CO_2. Other samples were incubated in the presence of the indicated treatments. At the end of sperm incubation, 10 μL of the lysate was added to 1 mL of the buffer reaction and incubated for 10 min at room temperature. Then, the triglycerides content was measured at 505 nm using a spectrophotometer. Data are presented as μg/10^6 spermatozoa.

Lipase activity assay

Lipase activity was evaluated by the method of Panteghini *et al.* (2001) based on the use of 1,2-*o*-dilauryl-rac-glycero-3-glutaric acid-(6′-methylresorufin) ester (DGGR) as substrate; 50 μg of sperm extracts was loaded into individual cuvettes containing buffer for spectrophotometric determination. DGGR is cleaved by lipase, resulting in an unstable dicarbonic acid ester, which is spontaneously hydrolysed to yield glutaric acid and methylresorufin, a bluish-purple chromophore with peak absorption at 580 nm. The absorbance of samples was read every 20 s for 1.5 min. The rate of methylresorufin formation is directly proportional to the lipase activity in the sample. Analysis of total imprecision gave a coefficient of variation between 0.02% and 0.032%. The estimated reference interval was 6–38 U/L (μmol/min/mg protein). The enzymatic activity was determined with three control media: one without the substrate, another without the co-enzyme (colipase) and the third without either substrate or co-enzyme (data not shown).

Assay of acyl-CoA dehydrogenase activity

Acyl-CoA dehydrogenases are a class of enzymes, which function to catalyse the initial step in each cycle of fatty acid β-oxidation in the mitochondria of cells. Assay of acyl-CoA dehydrogenase was performed on spermatozoa, using a modification of the method described by Lehman *et al.* (1990). In brief, after protein lysis, 70 μg of sperm proteins was added to the buffer containing 20 mM Mops, 0.5 mM EDTA and 100 μM FAD^+ at pH 7.2. Reduction of FAD^+ to FADH was read at 340 nm upon addition of octanoyl-CoA (100 μM) every 20 s for 1.5 min. Data are expressed as nmol/min/mg protein. The enzymatic activity was determined with three control media: one without octanoyl-CoA as substrate, another without the coenzyme (FAD^+) and the third without either substrate or coenzyme (data not shown).

Assay of the G6PDH activity

The conversion of $NADP^+$ to NADPH, catalysed by G6PDH, was measured by the increase in absorbance at 340 nm (Aquila *et al.*, 2009). Spermatozoa samples, washed twice with uncapacitating medium, were incubated in the same medium (control) for 30 min at 37 °C and 5% CO_2. Other samples were incubated in the presence of the indicated treatments. After incubation, 50 μL of sperm extracts was loaded into individual cuvettes containing buffer (100 mM triethanolamine, 100 mM $MgCl_2$, 10 mg/mL glucose-6-phosphate, 10 mg/mL $NADP^+$, pH 7.6) for spectrophotometric determination. The absorbance of samples was read at 340 nm every 20 s for 1.5 min. Data are expressed as nmol/min/10^6 spermatozoa. The enzymatic activity was determined with three control media: one without glucose-6-phosphate as substrate, another without the coenzyme ($NADP^+$) and the third without either substrate or coenzyme (data not shown).

Statistical analysis

The experiments for TEM and AR were performed in at least three independent experiments. The experiments for the Western blotting analysis were performed in at least eight independent experiments. The data obtained from cholesterol assay, acrosin activity, triglycerides assay, lipase activity, acyl-CoA dehydrogenase activity, G6PDH activity (10 replicate experiments using duplicate determinations) were presented as the mean ± SEM. The differences in mean values were calculated using analysis of variance (ANOVA) with a significance level of $p \leq 0.05$.

Results

Western blotting analysis of PRs

The presence of PR protein in human ejaculated spermatozoa was investigated by Western blot (Fig. 1A) using a rabbit polyclonal Ab raised against the c-terminal region of the human PR. Two immunoreactive bands, corresponding to the molecular mass values of 116 and 94 kDa were observed. As positive controls, T47D and MCF7 breast cancer cells, which expressed both isoforms as previously reported (Sartorius *et al.*, 1994), were used. Interestingly, it appears that varicocoele samples exhibit a

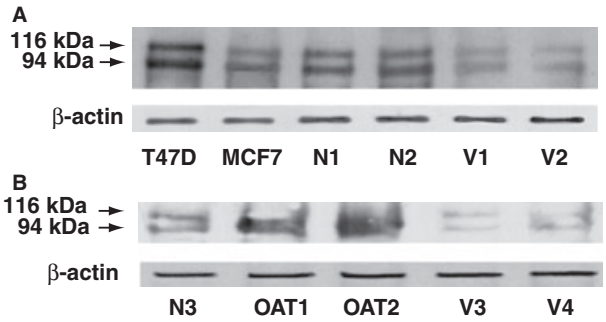

Figure 1 Western blot analysis of human sperm proteins showed expression of the conventional progesterone receptors (PRs). Extracts of pooled purified ejaculated spermatozoa were subjected to electrophoresis on 11% sodium dodecyl sulphate (SDS)-polyacrylamide gels, blotted onto nitrocellulose membranes and probed with rabbit polyclonal antibody to human PR. (A) N1 and N2 expression of PRs in two samples of ejaculated spermatozoa from normal men. V1 and V2 expression of PRs in two samples of ejaculated spermatozoa from varicocoele men. T47D and MCF-7 extracts were used as controls. (B) N3, expression of PRs in samples of ejaculated spermatozoa from normal men (lane 1). OAT1 and OAT2 expression of PRs in samples of ejaculated spermatozoa from oligoasthenoteratozoospermic patients. V3 and V4 expression of PRs in two samples of ejaculated sperm from varicocoele men. The number on the left corresponds to molecular masses (kilodaltons) of the marker proteins. The experiments were repeated at least eight times, and the autoradiographs of the figure show the results of one representative experiment.

reduced expression of PRs. When we compared PR expression among normal, OAT and varicocoele spermatozoa, only the latter showed a drastic decrement addressing a role for PRs in varicocoele pathophysiology (Fig. 1B).

Immunogold localization of PRs in human spermatozoa

Ultrastructural analysis of spermatozoa by TEM revealed that it is immunoreactive to the conventional PRs (Fig. 2). Interestingly, the label decorated mostly the head (at both the membrane and nucleus levels; Fig. 2, part a). The midpiece with the mitochondria also showed an appreciable presence of gold particles (Fig. 2, part d). PR expression was progressively reduced from the principal piece of the flagellum up to the end piece (Fig. 2, part g). Intriguingly, receptors were present not only on the sperm membrane but also as components of the flagellum, between the ribs of the fibrous sheath, outer dense fibres and axoneme. Simultaneous negative control experiments with the normal rabbit serum did not show any label in the corresponding regions (Fig. 2, parts c, f and i). In 'varicocoele' spermatozoa, a strong reduction in the gold particles was detected in the head (Fig. 3, parts a and b), along the midpiece and the tail of all the spermatozoa observed (Fig. 3, parts e and h), in agreement with the Western blotting data. Negative control experiments with the normal rabbit serum did not show signal in the corresponding sperm regions (Fig. 3, parts c, f and i).

PRG induces cholesterol efflux and protein tyrosine phosphorylation in human spermatozoa

To further investigate the PRG significance in male fertility, we evaluated its effects on two hallmarks of capacitation process, sperm membrane cholesterol efflux and protein tyrosine phosphorylation, considering both normozoospermic and varicocoele samples. Capacitation encompasses different features and sperm membrane cholesterol efflux contributes to one signalling mechanism that controls the process (Visconti *et al.*, 1995; Aquila *et al.*, 2006). Cholesterol efflux initiates signalling events leading to tyrosine phosphorylation of sperm proteins (Visconti *et al.*, 1995). Our results showed a dose-dependent increase in the cholesterol efflux upon PRG treatments (Fig. 4A). This effect was attenuated by using the PR antagonist RU486. In varicocoele samples, a slight, not significant, dose-dependent increase upon PRG was observed.

We then tested the effects of hormone on protein tyrosine phosphorylations; the treatments under our experimental conditions particularly affected the 95 ± 97 kDa tyrosine-phosphorylated proteins as previously reported (Aquila *et al.*, 2003). The densitometric evaluation of the double 95 ± 97 kDa band revealed a significant increase in the tyrosine phosphorylation in normal samples from 3 μM to 60 μM concentrations (Fig. 4B, and panel on the right side), whereas in varicocoele spermatozoa, although to a lesser extent, an increment from 30 μM to 60 μM PRG was obtained (Fig. 4C, and panel on the right side). In both cases, the RU486 abolished the PRG-induced effects. A significant increase in both serine and threonine phosphorylations upon increasing PRG was obtained as reported in supplementary data (Fig. S1).

PRG activates src and Akt in human spermatozoa

The mechanisms involved in the control of sperm functions are not well known yet; strong evidence indicates that they are associated with or controlled by different signal transduction elements. It appears that the tyrosine kinase src is a key player in the signal transduction cascade involved in the regulation of tyrosine phosphorylation occurring during sperm capacitation. To evaluate the impact of PRG on src activity, we used an Ab that specifically recognizes the active form of this kinase, by targeting an activating tyrosine phosphorylation at position 139. The results of this study clearly showed that PRG significantly induced src activity in a dose-dependent

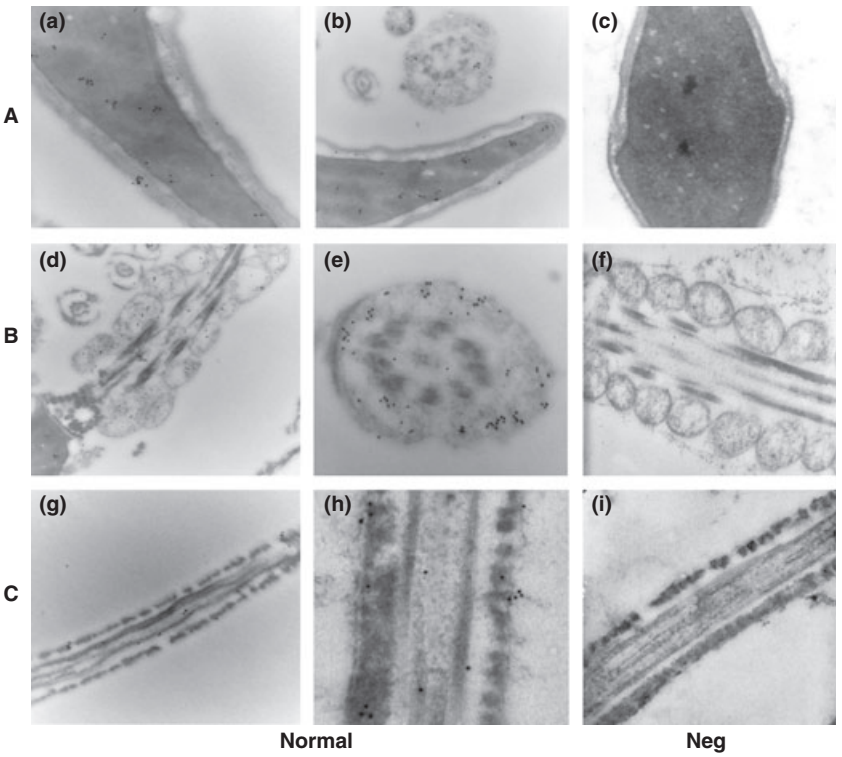

Figure 2 Immunoelectron localization of progesterone receptors (PRs) in spermatozoa of normozoospermic patients. Spermatozoa were collected and prepared as described in 'Materials and methods'. Micrographs of sections from ejaculated spermatozoa of normozoospermic patients were probed with rabbit polyclonal antibody (Ab) to human PR: panels a, b, d, e, g and h, original magnification, a, ×80 000; b, ×50 000; d, ×40 000; e, ×63 000; g, ×50 000; h, ×83 000. Panels c, f and i are the negative controls (Neg) carried out in corresponding sections of spermatozoa that were labelled with colloidal gold-conjugated secondary Ab with normal rabbit serum instead of primary Ab, original magnification, c, ×63 000; f, ×50 000; i, ×63 000. In all cases, a secondary anti-rabbit antibody conjugated to 10-nm colloidal gold particles was used for labelling. (A) Longitudinal sections through the head; (B) longitudinal and cross-sections of the midpiece of the flagellum; (C) longitudinal sections of the principal piece of the flagellum. Representative of three similar experiments.

manner and the combination with RU486 lightly attenuated the PRG-induced effects (Fig. 5A, upper panel). These data suggested that PRG is capable of inducing capacitation via mechanisms that lie upstream of src activation and that it does not act through the PRs alone. In varicocoele spermatozoa, no significant effects were observed (Fig. 5A, lower panel) upon PRG treatment.

In somatic cells, downstream signalling proteins potentially involved in mediating PRG activity include Akt, a key kinase involved in the metabolism and survival of the cells and also identified in spermatozoa (Aquila *et al.*, 2004, 2007). Increasing doses of the PRG resulted in an induction of the Akt phosphorylation on both Ser473 and Thr308 residues, indicating a full activation of the kinase (Fig. 5B, upper panel). The PRG-induced actions were not completely reversed by RU486. Similar to the src activity, the varicocoele spermatozoa did not show being responsive to PRG action on Akt phosphorylations.

Acrosin activity and AR are lower in varicocoele spermatozoa

PRG, which is secreted by cumulus cells, has been indicated as a physiological stimulus or co-stimulus for initiating the AR in spermatozoa. To give a biological evidence of this observation and with the aim to strengthen our data at the molecular level, we examined the role of PRG/PRs on acrosin activity in both healthy and varicocoele spermatozoa. The enzymatic activity highly increased upon PRG in normal samples (Fig. 6A), whereas a weak enhancement was obtained in pathological spermatozoa. The RU486 did not completely reverse the PRG-induced effect, suggesting that factors other than PRs are involved in mediating PRG action in this sperm activity. It deserves to be mentioned that in humans, PRG is present in low concentrations in blood, but it can be extraordinarily high in periovulatory follicular fluid (up to 20 μg/mL; Saaranen *et al.*, 1993); therefore, high levels of PRG may become available to spermatozoa at the time of fertilization.

Moreover, the AR increased in a dose-dependent manner upon PRG (Fig. 6B). In varicocoele samples, the percentage of reacted spermatozoa significantly increased from 30 μM to 60 μM PRG, albeit by a lower extent with respect to normal spermatozoa.

PRG influences both lipid and glucose metabolism in human spermatozoa

A role of PRG in lipid metabolism was reported in brown adipose tissue (Monjo *et al.*, 2003; Caprio *et al.*, 2008); however, in spermatozoa, a similar action of the hormone was never tested. We first investigated triglyceride intracellular content upon increasing PRG levels. As shown in

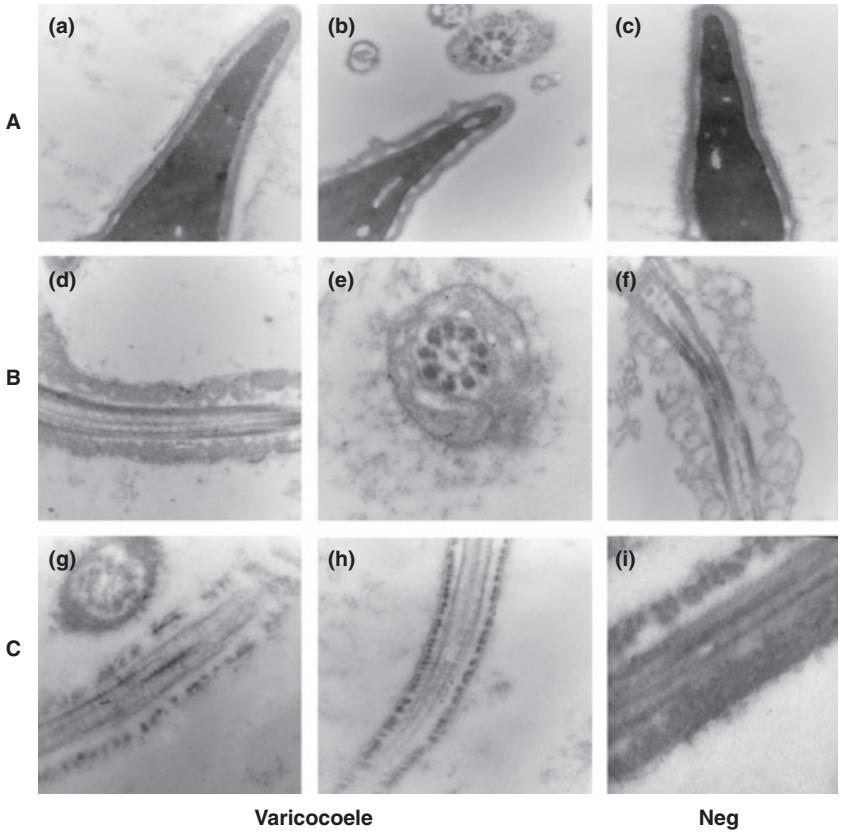

Figure 3 Immunoelectron microscopic localization of progesterone receptors (PRs) in varicocoele spermatozoa. Spermatozoa were collected and prepared as described in 'Materials and methods'. Micrographs of sections from ejaculated spermatozoa of varicocoele patients probed with rabbit polyclonal antibody (Ab) to human PR: panels a, b, d, e, g and h, original magnification, a, ×50 000; b, ×40 000; d, ×40 000; e, ×63 000; g, ×62 000; h, ×50 000. Panels c, f and i are the negative controls (Neg) carried out in the corresponding sections of spermatozoa that were labelled with colloidal gold-conjugated secondary Ab with normal rabbit serum instead of the primary Ab, original magnification, c, ×40 000; f, ×40 000; i, ×70 000. In all cases, a secondary anti-rabbit antibody conjugated to 10-nm colloidal gold particles was used for labelling. (A) Longitudinal sections through the head; (B) longitudinal and cross-sections of the midpiece of the flagellum; (C) longitudinal sections of the principal piece of the flagellum. Representative of three similar experiments.

Fig. 7A, PRG was able to decrease significantly the triglycerides, and 30 μM PRG plus 10 μM RU reversed the effect. These data suggest that PRG may induce a lipolytic effect in human spermatozoa. On the contrary, in varicocoele, a decrease in triglycerides content was not obtained. Therefore, to investigate the mechanism through which this hormone may influence sperm lipid metabolism, we evaluated its action on lipase and acyl-CoA dehydrogenase activities. Interestingly, lipase activity was enhanced by PRG in a dose-dependent manner and 30 μM PRG combined with 10 μM RU reduced the PRG-induced action (Fig. 7B). Strong activation of the acyl-CoA dehydrogenase activity was concomitantly obtained, indicating also a role for PRG/PRs in the β-oxidation of the fatty acids in human spermatozoa (Fig. 7C). The combination of 10 μM RU plus 30 μM PRG reversed the PRG-induced effect. In varicocoele samples, the hormone did not increase the enzymatic activities.

To gain a greater insight into sperm energy management, we evaluated the PRG action on glucose metabolism. The effect of glucose on the fertilizing ability of spermatozoa appears to be mediated by its metabolism through the pentose phosphate pathway (PPP); therefore, we investigated whether PRG was able to modulate the G6PDH activity, the key rate-limiting enzyme in the PPP. As shown in Fig. 7D, PRG greatly and unequivocally induced the enzymatic activity; 30 μM PRG combined with 10 μM RU reversed PRG action. Similar to the other enzymatic activities, the varicocoele spermatozoa did not seem to be responsive to PRG.

Discussion

Varicocoele is one of the most common causes of male infertility; however, the mechanisms through which it negatively affects male reproduction are not still fully clarified. Similarly, despite the demonstration that responsiveness to PRG is related to fertilization, the role of this female hormone in male reproduction is yet to be defined. Besides, levels of PR expression are only slightly lower in males than in females (Gadkar-Sable *et al.*, 2005), and their distributions throughout target tissues such as the brain and pituitary gland are similar in the two genders (Shannon *et al.*, 1982; Scarpin *et al.*, 2009). The presence of both ligand and receptor strongly suggests a physiological role for PRG and PRs in male reproductive physiology and/or behaviour; yet, few studies have directly assessed this possibility. The present study was designed to identify and localize clearly the conventional PR isoforms in human 'healthy' spermatozoa and to examine a possible molecular

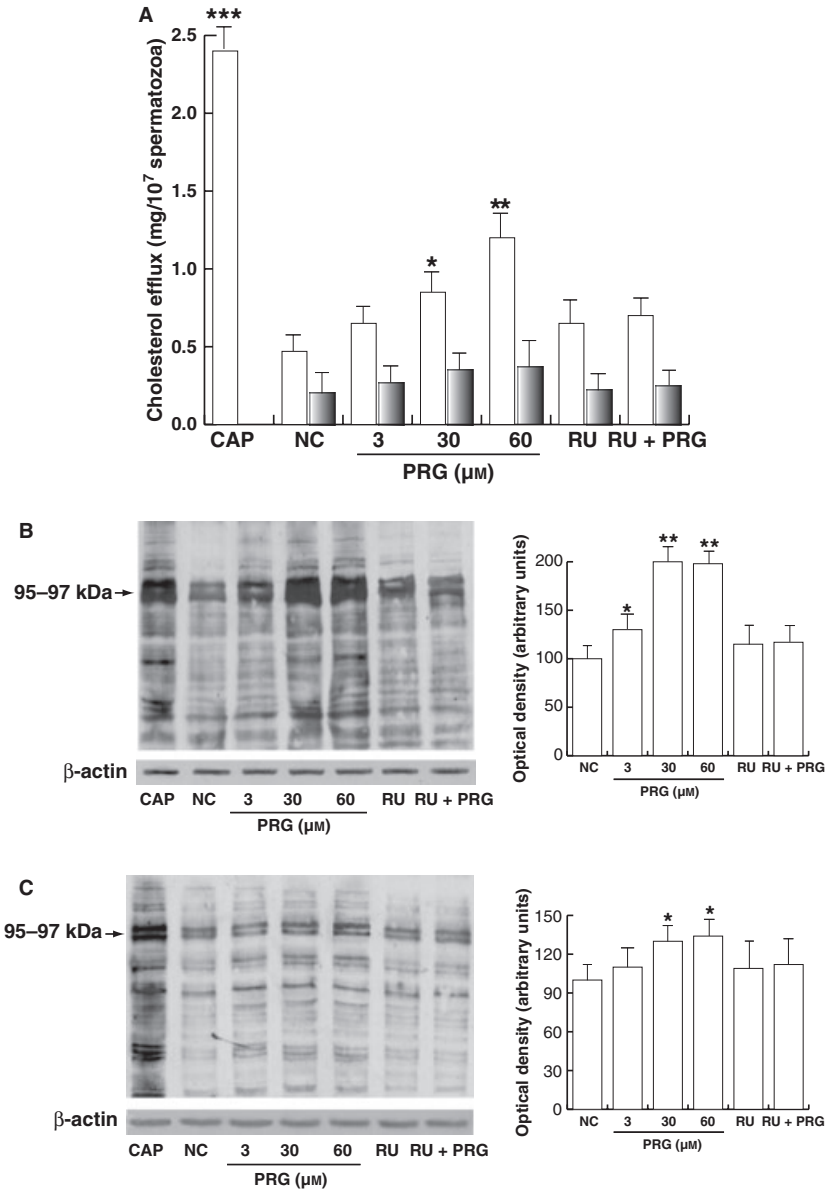

Figure 4 Effects of progesterone on capacitation. Purified spermatozoa were incubated in the unsupplemented Earle's medium for 30 min at 37 °C and 5% CO_2, in the absence (NC) or in the presence of indicated treatments. (A) Cholesterol in culture medium from human ejaculated spermatozoa was measured by enzymatic colorimetric assay. Columns are mean ± SEM of 10 independent experiments performed in duplicate. Data are expressed in mg/10^7 spermatozoa. *$p \leq 0.05$ vs. control ; **$p < 0.02$ vs. control : □, normal; ■, varicocoele. (B) Exactly 70 μg of sperm lysates was used for Western blot analysis of protein tyrosine phosphorylations in normal samples. Actin was used as loading control. On the right, quantitative representation after densitometry of the double 95 ± 97-kDa band, representative of protein tyrosine phosphorylations in human spermatozoa. (C) Protein tyrosine phosphorylation in varicocoele samples. On the right, quantitative representation after densitometry of the double 95 ± 97-kDa band. The autoradiographs presented are representative examples of experiments that were performed at least eight times with repetitive results. *$p < 0.05$ vs. control; **$p < 0.01$ vs. control; ***$p < 0.001$ vs. control.

difference in 'varicocoele' spermatozoa to highlight the pathophysiology of this condition. By assessing a more profound approach on the role of PRG in sperm physiology, we evaluated different events of capacitation and we tested for the first time its action in the modulation of lipid and glucose metabolism.

In spermatozoa, a large number of studies have attempted to define the molecular mechanisms underlying PRG action as well as to identify the receptors mediating its effects. Despite many efforts, the identity of the sperm receptor for the hormone remains uncertain and contradictory. Most of the studies on the PR subtypes in spermatozoa have supported the original hypothesis that they function as specific membrane receptors through which progestins induce rapid, non-genomic responses in target cells (Thomas *et al.*, 2009). In fact, there is universal agreement that the effects of PRG on spermatozoa occur only via membrane-bound PRs and this reflects the accepted description that spermatozoa are highly differentiated, specialized cells of minimal cytoplasm and compacted nucleus that is transcriptionally inactive. However, in the recent years, a new picture of this cell is emerging: it expresses various receptor types, including nuclear receptors (Travis & Kopf, 2002; Aquila *et al.*, 2005a,b, 2007), and it also produces their ligands, suggesting that through an autocrine short loop, it may modulate its

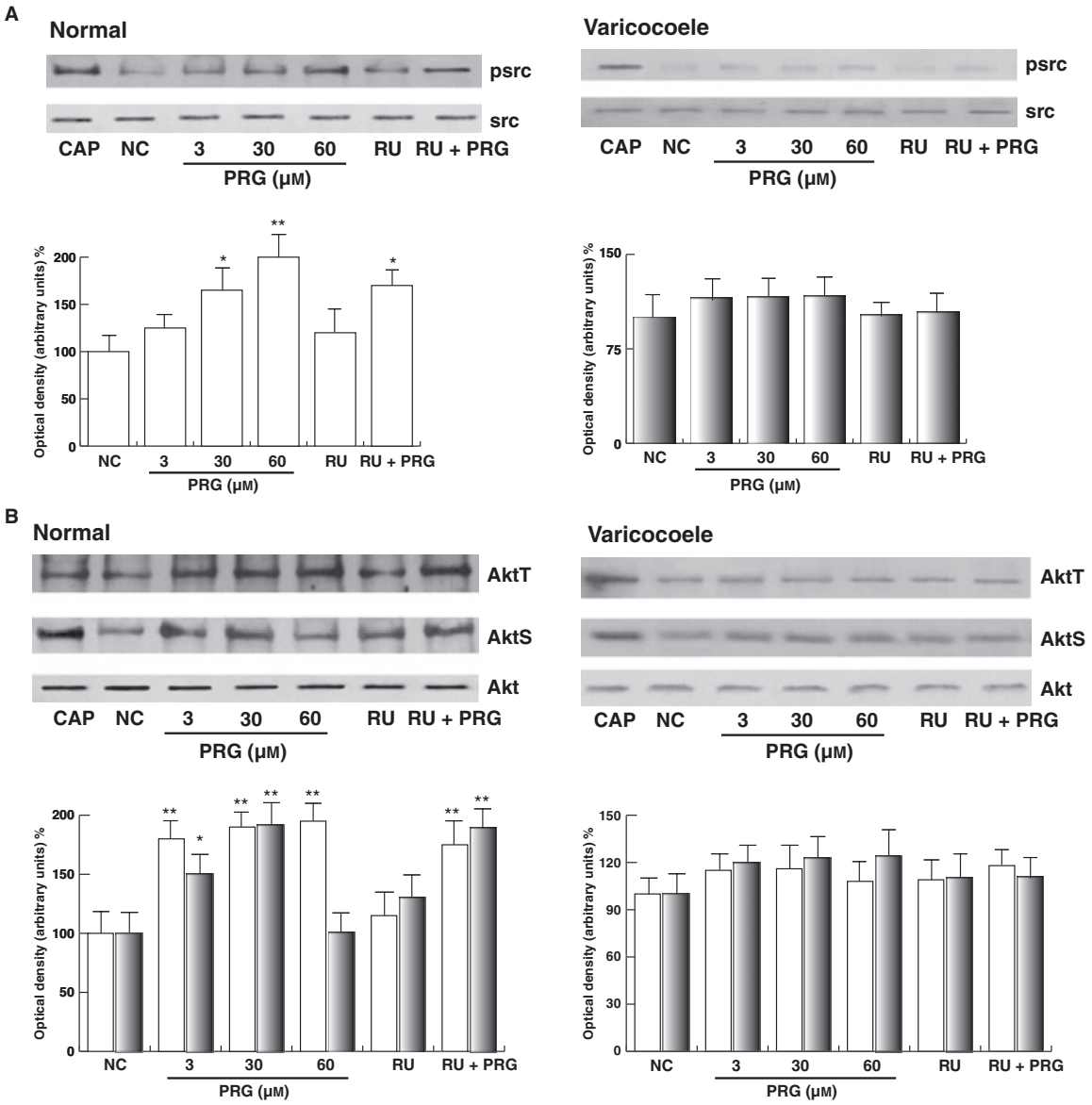

Figure 5 Progesterone (PRG) increases src, AktS and AktT phosphorylations. Washed spermatozoa were incubated in the unsupplemented Earle's medium for 30 min at 37 °C and 5% CO_2, in the absence (NC) or in the presence of increasing PRG concentrations (3, 30 and 60 μm). Some samples were treated with 10 μm RU486 (RU) alone or combined with 30 μm PRG. Exactly 70 μg of sperm lysates were used for Western blot analysis of src (A), AktS and AktT (B) phosphorylations. (A) Upper panel represents p-src evaluated in normal samples, while the lower panel in varicocoele samples. Total src was used as loading control. (B) Upper panel represents AktS and AktT phosphorylations evaluated in normal samples, while the lower panel in varicocoele samples. Total Akt was used as loading control. On the right, quantitative representation after densitometry. *$p < 0.05$ vs. control; **$p < 0.01$ vs. control: □, normal; ■, varicocoele.

own functions independently by the systemic regulation. Intriguingly, it has been demonstrated that spermatozoa is able to translate de novo by mitochondrial-type ribosomes (Gur & Breitbart, 2006). Despite this, while questions linger, different intriguing avenues remain to be extended on the biology of this cell. However, it is well established that post-translational modifications are the major means by which spermatozoa acquire full functionality (Ross *et al.*, 1990; Baker *et al.*, 2004).

It has been reported that the membrane fraction analysis shows the existence of PRG-binding proteins (Luconi *et al.*, 1998) and that spermatozoa lack genomic PRs (Castilla *et al.*, 1995). Several attempts have been made to identify the sperm membrane PR protein (Buddhikot

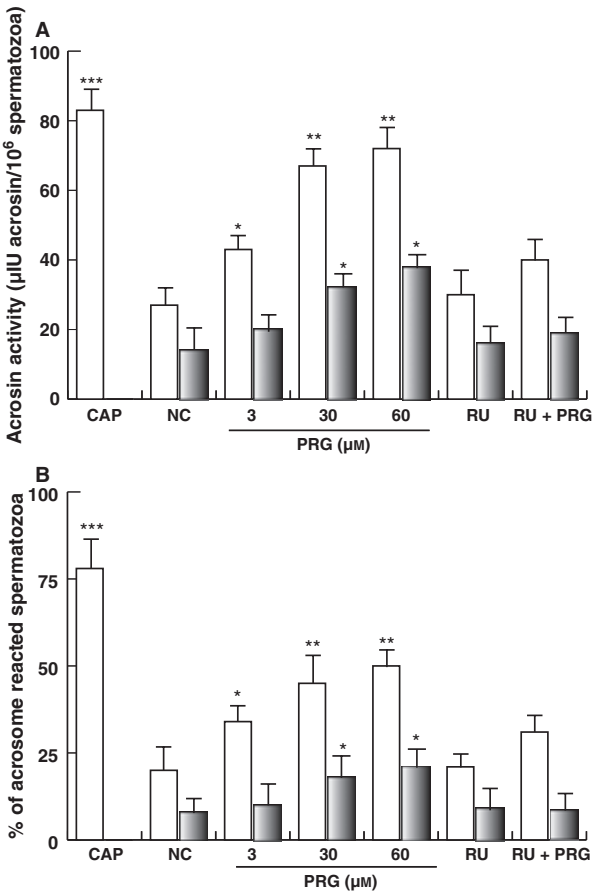

Figure 6 Progesterone (PRG) induces acrosin activity and acrosome reaction in human spermatozoa. Washed spermatozoa were incubated in unsupplemented Earle's medium for 30 min at 37 °C and 5% CO_2, in the absence (NC) or in the presence of PRG (from 3 μm to 60 μm) and 1 μm RU486 alone or in combination with 30 μm PRG. (A) Acrosin activity was determined as described in 'Materials and methods'. Columns represent mean ± SEM of 10 independent experiments each performed in duplicate. $*p < 0.05$ and $**p < 0.01$ vs. control: CAP, capacitated spermatozoa; □, normal; ■, varicocoele. (B) Acrosome reaction was determined as described in 'Materials and methods' and the values are expressed as percentage of acrosome-reacted cells. Columns represent mean ± SEM of three independent experiments each performed in duplicate. $*p < 0.05$ and $**p < 0.02$ vs. control; $***p < 0.001$ vs. control; CAP, capacitated spermatozoa; □, normal; ■, varicocoele.

et al., 1999; Luconi *et al.*, 2002; Zhu *et al.*, 2003; Thomas *et al.*, 2004) and specific PRs have been discovered in the plasma membrane of human spermatozoa by Western blotting analysis and ligand blot analysis (Luconi *et al.*, 1998). The classic PRs are not seen with antibodies to the DNA-binding domain (DBD) or the amino-terminal domains. Using antibodies directed against the C-terminal region of the conventional PR, proteins of 5l–57 kDa in sperm lysate have been revealed by Western blot analysis (Blackmore & Lattanzio, 1991; Sabeur *et al.*, 1996; Luconi *et al.*, 1998), a 52-kDa antigen has been found on the spermatozoa head (Thomas *et al.*, 2004); the same Ab detected four bands of molecular masses of 28, 54, 57 and 66 kDa in human spermatozoa preparations (Luconi *et al.*, 1998). The presence of a 55-kDa protein in testicular and sperm lysates using another Ab that recognized the epitopes encompassing the DBD and the hormone binding domain (HBD) regions of conventional PR was also reported (Shah *et al.*, 2005a).

In our study, an Ab produced against the C-terminal region of the human PR revealed the expression of the conventional PRB and PRA. Classically, PRB (116 kD) and PRA (94 kD) have been considered nuclear receptors controlling gene transcription. PRA is a truncated version of B, lacking the first 164 amino acids. It is now clear that there are two main kinds of cellular effects mediated by nuclear receptors. One involves the alteration in gene expression (De Amicis *et al.*, 2009) and the other is associated with a rapid onset of cellular effects. This latter model of action appears to be the more appropriate modality of PRG in spermatozoa as it happens too quickly because of gene regulation. The apparent contradiction among previous studies and our study probably originates from the real presence of different types of PRs in the spermatozoa and/or from different methods of sperm processing.

Intriguingly, the expression of conventional PRs was evidenced concomitantly in semen samples from healthy volunteer donors of proven fertility, semen samples of OAT patients with or without varicocoele, but both with similar semen parameters. A decreased expression of PRs seems to be related only to varicocoele as it distinguishes healthy and OAT spermatozoa from those with varicocoele, suggesting that the stress caused by this pathology impairs spermatogenesis bringing a reduced PR expression. It was reported that glucocorticoid receptor is rapidly degraded in heat-shocked cells (Vedeckis *et al.*, 1989); therefore, it may also be possible that the increased testicular temperature in varicocoele subjects determines this effect.

An nPR-like form A of 55 kDa has been localized to the posterior head and the acrosome region of spermatozoa (Blackmore & Lattanzio, 1991); this observation is consistent with three other studies: the first reporting that only 30% of spermatozoa have detectable PRs on their heads (Sabeur *et al.*, 1996; Benoff, 1998), the second localizing PRs at the equatorial region of the sperm head (Luconi *et al.*, 1998) and the third in the mid-head region (Buddhikot *et al.*, 1999). In the present study, TEM with immunogold analysis improved understanding of the human spermatozoa anatomical regions containing the PRs and confirmed the abated expression of the receptors in the varicocoele spermatozoa. In fact, in 'healthy' spermatozoa, numerous gold particles decorated the head

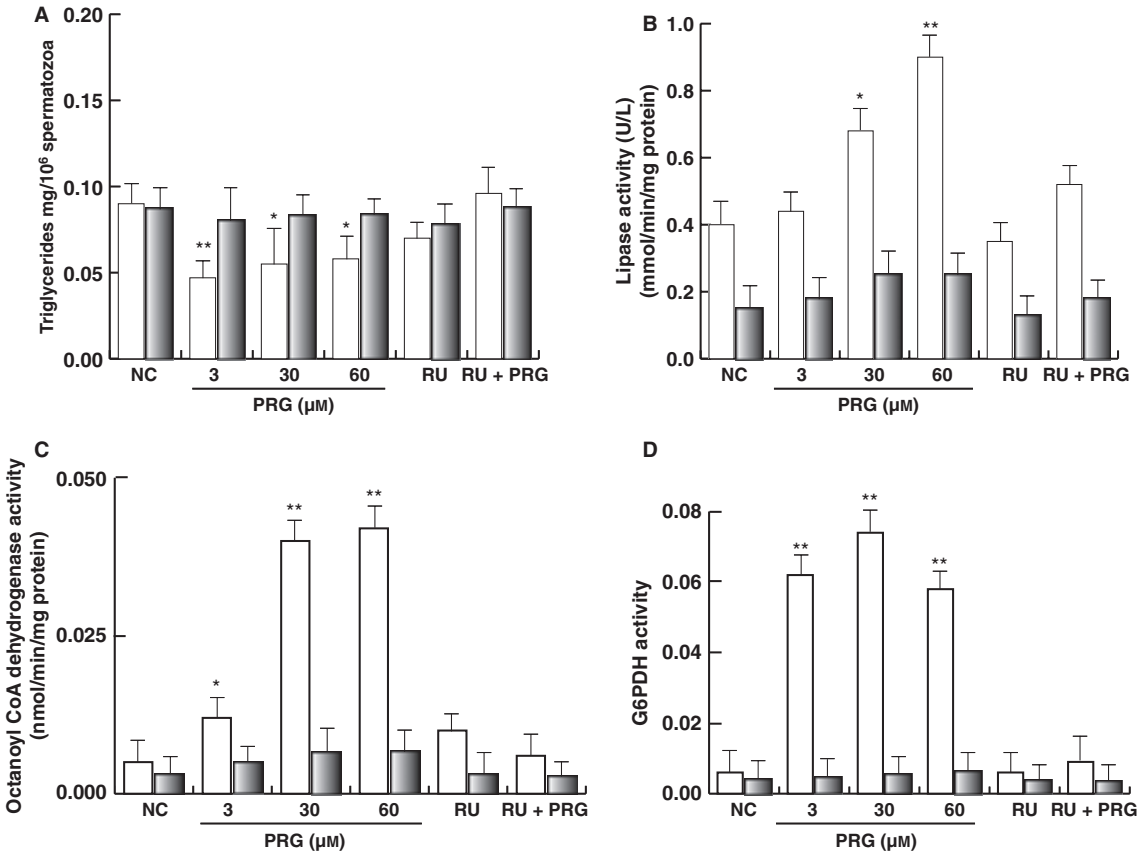

Figure 7 Effects of progesterone (PRG) on lipid and glucose metabolism in human spermatozoa. Washed spermatozoa were incubated in the unsupplemented Earle's medium for 30 min at 37 °C and 5% CO_2, in the absence (NC) or in the presence of increasing PRG concentrations (3, 30 and 60 μm). Some samples were treated with 10 μm RU486 (RU) alone or combined with 30 μm PRG. (A) Triglycerides assay was performed as reported in 'Materials and methods'. Columns represent mean ± SEM. *$p < 0.05$ vs. control; **$p < 0.01$ vs. control. (B) Lipase activity was performed as reported in 'Materials and methods'. Columns represent mean ± SEM. *$p < 0.05$ vs. control; **$p < 0.01$ vs. control. (C) Octanoyl-CoA dehydrogenase activity was performed as reported in 'Materials and methods'. Columns represent mean ± SEM. *$p \leq 0.05$ vs. control; **$p < 0.001$ vs. control. (D) G6PDH activity was performed as reported in 'Materials and methods'. Columns represent mean ± SEM. **$p < 0.001$ vs. control: □, normal; ■, varicocoele.

both at the membrane and at the nucleus. Interestingly, PR expression was progressively reduced from the principal piece of the flagellum up to the end piece. Particularly, the midpiece comprising mitochondria contains PRs. Therefore, the receptors were present not only on the sperm membrane but also inside the body spermatozoa as component of the nucleus and the flagellum, between the mitochondria, the ribs of the fibrous sheath, outer dense fibres and axoneme. The high polarization in the structure and function of spermatozoa requires a compartmentalization of metabolic and signalling pathways in the regions where they are needed. Altogether, based on these observations, the PRs could be implicated in different sperm activities according to their specific cellular localization. Interestingly, in 'varicocoele' spermatozoa, a reduction in the PR expression was noticed, confirming Western blotting data and suggesting that the PRs could be involved in the diminished functionality of the male gamete under this pathological condition.

The presence of PRs in all the spermatozoa body supports earlier evidence that the responses to progestins in mammals involve different signalling pathways many of which result in the capacitation and the AR (Kay *et al.*, 1994; Cheng *et al.*, 1998a; Shah *et al.*, 2005b). During its life, spermatozoa goes through two different physiological conditions: uncapacitated condition during which spermatozoa remain in a resting state accumulating and/or economizing energy substrates, which are going to be successively spent, and the capacitated condition, which allows spermatozoa to achieve the final competence to fertilize the oocyte. Capacitation implies striking changes in all the sperm activities and many of these were tested upon different PRG concentrations (Harper *et al.*, 2004). In this study, we evidenced PRG action on known hall-

marks of capacitation by evaluating its effects on cholesterol efflux and tyrosine phosphorylations as well as on two key kinases such as src and Akt. During capacitation, an increase in the cholesterol efflux and tyrosine phosphorylation of sperm proteins occurs. From our results, it could be observed that PRG was able to induce these activities considered priming events of the process, therefore confirming a role of the hormone in capacitation.

Following capacitation-associated cholesterol efflux and its consequent increase in membrane fluidity, spermatozoa show a rise in cyclic AMP, which precedes an upregulation of sperm motion parameters and tyrosine phosphorylation (Luconi *et al.*, 2005). It was speculated that the sperm dysfunction associated with varicocoele may be related to an alteration in plasma membrane dynamic, which causes tyrosine phosphorylation insufficiency and the consequent alteration in sperm function (Buffone *et al.*, 2006). Therefore, our data reporting a decreased cholesterol efflux, which in turn decreases sperm membrane fluidity and reduces protein tyrosine phosphorylation, are consistent with the study of Buffone *et al.* (2006) in considering these hallmarks of capacitation as two pathophysiological defects associated with grade II/III infertile varicocoele. Interestingly, in addition in our research, we demonstrated that the mechanism through which this effect occurs may be related to a diminished expression of the PRs in varicocoele.

In somatic cells, activation of src is an extranuclear function of the PR (Boonyaratanakornkit *et al.*, 2007) and PRG potentiates IP3-mediated calcium signalling through Akt/PKB (Koulen *et al.*, 2008). Therefore, these two kinases are involved in the PRG signalling and in spermatozoa src was found to play an important role in capacitation (Pujianto *et al.*, 2010), whereas Akt in survival (Aquila *et al.*, 2004, 2007). From our data, given the activation of src and Akt by PRG, it may be supposed that the hormone concurs in these activities during spermatozoa life. The negligible or absence of action of PRG on src and Akt activities in varicocoele samples may be explained by the reduced expression of the PRs.

When we performed the acrosin activity and AR to give biological evidence of the data obtained at the molecular level, a reduced enzymatic activity and percentage of reacted spermatozoa, both in the basal levels and in PRG-treated varicocoele sperm were observed. Few reports in the literature showed the relationship between acrosin activity and varicocoele. Although the acrosin activity previously described in varicocoele was measured by a different method, it was significantly lower in the varicocoele group than in the normal samples (El Mulla *et al.*, 1995), in agreement with our data. Besides, the RU486 did not completely reverse the PRG-induced effect in normal spermatozoa, suggesting that different factors other than PRs are involved in mediating PRG action in this sperm activity.

The sperm energy management is an intriguing issue and it appears that this cell is able to regulate its own metabolism independently by the systemic regulation. A role of PRG in lipid metabolism was observed in somatic cells (Correia *et al.*, 2007; Wada *et al.*, 2010); however, this action was not investigated in spermatozoa cells. From our data, it could be observed that PRG was able to reduce the triglycerides content, whereas it induced lipase and acyl-CoA dehydrogenase activities, suggesting a lipolytic effect on human spermatozoa metabolism. During capacitation, energy demand increases and capacitated spermatozoa shows an increased metabolism and overall energy expenditure, and therefore it may be assumed of the possibility of PRG co-working with other factors to stimulate such enzymatic activities providing additional metabolic fuel to sustain capacitation process. Nature has endowed spermatozoa with striking cellular peculiarities given its essential role in the propagation of life, but with a single, irreversible chance to fertilize an egg; therefore, its metabolism needs to be fine-tuned and probably independent of the systemic regulation. Interestingly, PRG strongly increased G6PDH activity and this is in agreement with its reported insulinotropic effect (Landau & Poulos, 1971; Beck, 1977). Previous data from our laboratory lead us to speculate that insulin might be considered an endogenous factor involved in the autocrine induction of the capacitation (Aquila *et al.*, 2005a) and that the insulin secretion by spermatozoa may provide an autocrine regulation of glucose metabolism as proved on G6PDH activity. The induced G6PDH activity, as we found in this study, confirms the importance of PRG/PRs in human spermatozoa functional maturation.

Our results of PRG action on metabolism in varicocoele spermatozoa renew the role of PR expression in the human male gamete, also indicating that a metabolic dysfunction is present in these cells.

To strengthen the idea that the PRG effects are 'extranuclear' and 'non-genomic' and happen through a membrane receptor in spermatozoa, there is general consensus that the effects of the hormone are not counteracted by classical PRG antagonists such as mifepristone, RU486 (Schatz *et al.*, 2003). From our data, it emerges that RU486 was not able to abolish all the PRG-induced effects tested, and this may be imputable to different mechanisms in the hormone action and/or that different proteins responding to PRG exist. Particularly, the PRG-induced action was reversed by RU486 on metabolic studies, suggesting that in this context, the conventional PRs mediate PRG action in spermatozoa.

In conclusion, varicocoele affects testicular function in a variety of ways, in spermatogenesis, in semen quality, in

sperm functions and in morphology. From our data, it emerges that this pathology may induce damage in the gamete at molecular level, opening a new chapter in the already multifactorial pathophysiology of the varicocoele and complicating this issue. By the time of ovulation, PRG is almost everywhere in the egg microenvironment affecting ability of the spermatozoa to fertilize. Therefore, the reduced expression of PRs in varicocoele spermatozoa, as we evidenced, may negatively affect different sperm activities. Undoubtedly, there is a need for more molecular and genetic studies to clarify the pathophysiology of this condition.

Acknowledgements

The authors offer their special thanks to Dr. Vincenzo Cunsolo (Biogemina Italia Srl, Catania, Italy) for technical and scientific assistance. They also thank Perrotta Enrico for the excellent technical assistance and Serena and Maria Clelia Gervasi for the English language review of the manuscript. This work was supported by MIUR Ex 60% – 2010.

References

Al-Ali BM, Marszalek M, Shamloul R, Pummer K & Trummer H. (2010) Clinical parameters and semen analysis in 716 Austrian patients with varicocoele. *Urology* 75, 1069–1073.

Andò S, Giacchetto C, Colpi G, Beraldi E, Panno ML, Lombardi A & Sposato G. (1984) Physiopathologic aspects of Leydig cell function in varicocoele patients. *J Androl* 5, 163–170.

Aquila S, Sisci D, Gentile M, Middea E, Siciliano L & Andò S. (2002) Human ejaculated spermatozoa contain active P450 aromatase. *J Clin Endocrinol Metab* 87, 3385–3390.

Aquila S, Sisci D, Gentile M, Carpino A, Middea E, Catalano S, Rago V & Andò S. (2003) Towards a physiological role for cytochrome P450 aromatase in ejaculated human sperm. *Hum Reprod* 18, 1650–1659.

Aquila S, Sisci D, Gentile M, Middea E, Catalano S, Carpino A, Rago V & Andò S. (2004) Estrogen receptor (ER) alpha and ER beta are both expressed in human ejaculated spermatozoa: evidence of their direct interaction with phosphatidylinositol-3-OH kinase/Akt pathway. *J Clin Endocrinol Metab* 89, 1443–1455.

Aquila S, Gentile M, Middea E, Catalano S & Andò S. (2005a) Autocrine regulation of insulin secretion in human ejaculated spermatozoa. *Endocrinology* 146, 552–557.

Aquila S, Gentile M, Middea E, Catalano S, Morelli C, Pezzi V & Andò S. (2005b) Leptin secretion by human ejaculated spermatozoa. *J Clin Endocrinol Metab* 90, 4753–4761.

Aquila S, Bonofiglio D, Gentile M, Middea E, Gabriele S, Belmonte M, Catalano S, Pellegrino M & Ando S. (2006) Peroxisome proliferator-activated receptor (PPAR) gamma is expressed by human spermatozoa: its potential role on the sperm physiology. *J Cell Physiol* 20, 977–986.

Aquila S, Middea E, Catalano S, Marsico S, Lanzino M, Casaburi I, Barone I, Bruno R, Zupo S & Andò S. (2007) Human sperm express a functional androgen receptor: effects on PI3K/AKT pathway. *Hum Reprod* 22, 2594–2605.

Aquila S, Guido C, Laezza C, Santoro A, Pezzi V, Panza S, Andò S & Bifulco M. (2009) A new role of anandamide in human sperm: focus on metabolism. *J Cell Physiol* 221, 147–153.

Baker MA, Hetherington L, Ecroyd H, Roman SD & Aitken RJ. (2004) Analysis of the mechanism by which calcium negatively regulates the tyrosine phosphorylation cascade associated with sperm capacitation. *J Cell Sci* 117, 211–222.

Beck P. (1977) Effect of progestins on glucose and lipid metabolism. *Ann N Y Acad Sci* 286, 434–445.

Benoff S. (1998) Modelling human sperm–egg interactions *in vitro*: signal transduction pathways regulating the acrosome reaction. *Mol Hum Reprod* 4, 453–471.

Blackmore PF & Lattanzio FA. (1991) Cell surface localization of a novel non-genomic progesterone receptor on the head of human sperm. *Biochem Biophys Res Commun* 181, 331–336.

Blackmore PF, Beebe SJ, Danforth DR & Alexander N. (1990) Progesterone and 17α-hydroxyprogesterone: novel stimulators of calcium influx in human sperm. *J Biol Chem* 265, 1376–1380.

Blackmore PF, Im WB & Bleasdale JE. (1994) The cell surface progesterone receptor which simulates influx in human sperm is unlike the A ring reduced steroid site on the $GABA_A$ receptor/chloride channel. *Mol Cell Endocrinol* 104, 237–243.

Boonyaratanakornkit V, McGowan E, Sherman L, Mancini M, Cheskis B J & Edwards Dean P. (2007) The role of extranuclear signaling actions of progesterone receptor in mediating progesterone regulation of gene expression and the cell cycle. *Mol Endocrinol* 21, 359–375.

Buddhikot M, Falkenstein E, Wehling M & Meizel S. (1999) Recognition of a human sperm surface protein involved in the progesterone-initiated acrosome reaction by antisera against an endomembrane progesterone binding protein from porcine liver. *Mol Cell Endocrinol* 158, 187–193.

Buffone MG, Brugo-Olmedo S, Calamera JC, Verstraeten SV, Urrutia F, Grippo L, Corbetta JP & Doncel GF. (2006) Decreased protein tyrosine phosphorylation and membrane fluidity in spermatozoa from infertile men with varicocoele. *Mol Reprod Dev* 73, 1591–1599.

Caprio M, Zennaro MC, Fève B, Mammi C, Fabbri A & Rosano G. (2008) Potential role of progestogens in the control of adipose tissue and salt sensitivity via interaction with the mineralocorticoid receptor. *Climateric* 11, 258–266.

Castilla JA, Gil T, Molina J, Hortas ML, Rodriguez F, Torres-Muñoz J, Vergara F & Herruzo AJ. (1995) Undetectable expression of genomic progesterone receptor in human spermatozoa. *Hum Reprod* 10, 1757–1760.

Cheng FP, Fazeli AR, Voorhout WF, Tremoleda JL, Bevers MM & Colenbrander B. (1998a) Progesterone in mare follicular fluid induces the acrosome reaction in stallion spermatozoa and enhances *in vitro* binding to the zona pellucida. *Int J Androl* 21, 57–66.

Cheng FP, Gadella BM, Voorhout WF, Fazeli A, Bevers MM & Colenbrander B. (1998b) Progesterone-induced acrosome reaction in stallion spermatozoa is mediated by a plasma membrane progesterone receptor. *Biol Reprod* 59, 733–742.

Conneely OM & Lydon JP. (2000) Progesterone receptors in reproduction: functional impact of the A and B isoforms. *Steroids* 65, 571–577.

Conneely OM, Mulac-Jericevic B, Lydon JP & De Mayo FJ. (2001) Reproductive functions of the progesterone receptor isoforms: lessons from knock-out mice. *Mol Cell Endocrinol* 179, 97–103.

Contreras HR & Llanos MN. (2001) Detection of progesterone receptors in human spermatozoa and their correlation with morphological and functional properties. *Int J Androl* 4, 246–252.

Correia JN, Conner SJ & Kirkman-Brown JC. (2007) Non-genomic steroid actions in human spermatozoa. ''Persistent tickling from a laden environment''. *Semin Reprod Med* 25, 208–219.

De Amicis F, Zupo S, Panno ML, Malivindi R, Giordano F, Barone I, Mauro L, Fuqua SA & Andò S. (2009) Progesterone receptor B recruits a repressor complex to a half-PRE site of the estrogen receptor alpha gene promoter. *Mol Endocrinol* 23, 454–465.

El Mulla KF, Köhn FM, El Beheiry AH & Schill WB. (1995) The effect of smoking and varicocoele on human sperm acrosin activity and acrosome reaction. *Hum Reprod* 10, 3190–3194.

Gadkar-Sable S, Shah C, Rosario G, Sachdeva G & Puri C. (2005) Progesterone receptors: various forms and functions in reproductive tissues. *Front Biosci* 10, 2118–2130.

Gorelick JI & Goldstein M. (1993) Loss of fertility in men with varicocoele. *Fertil Steril* 59, 613–616.

Graham JD & Clarke CL. (1997) Physiological action of progesterone in target tissues. *Endocr Rev* 18, 502–519.

Gur Y & Breitbart H. (2006) Mammalian sperm translate nuclear-encoded proteins by mitochondrial-type ribosomes. *Genes Dev* 20, 411–416.

Harper CV, Barratt CL & Publicover RSJ. (2004) Stimulation of human spermatozoa with progesterone gradients to simulate approach to the oocyte. *J Biol Chem* 279, 46315–46325.

Horwitz KB & Alexander PS. (1983) *In situ* photolinked nuclear progesterone receptors of human breast cancer cells: subunit molecular weights after transformation and translocation. *Endocrinology* 113, 2195–2201.

Jensen EV. (1996) Steroid hormones, receptors, and antagonists. *Ann N Y Acad Sci* 784, 1–17.

Kastner P, Krust A, Turcotte B, Stropp U, Tora L, Gronemeyer H & Chambon P. (1990) Two distinct estrogen-regulated promoters generate transcripts encoding the two functionally different human progesterone receptor forms A and B. *EMBO J* 9, 1603–1610.

Kay VJ, Coutts JR & Robertson L. (1994) Effects of pentoxifylline and progesterone on human sperm capacitation and acrosome reaction. *Hum Reprod* 9, 2318–2313.

Kennedy WP, Kamisky JM, Van der Ven HH, Jeyendran RS, Reid DS, Blackwell J, Biefeld P & Zaneveld LJD. (1989) A simple, classical assay to evaluate the acrosin activity of human spermatozoa. *J Androl* 10, 221–231.

Koksal IT, Ishak Y, Usta M, Danisman A, Guntekin E, Bassorgun IC & Ciftcioglu A. (2007) Varicocoele-induced testicular dysfunction may be associated with disruption of blood-testis barrier. *Arch Androl* 53, 43–48.

Koulen P, Madry C, Duncan RS, Hwang JY, Nixon E, McClung N, Gregg EV & Singh M. (2008) Progesterone potentiates IP(3)-mediated calcium signaling through Akt/PKB. *Cell Physiol Biochem* 21, 161–172.

Landau RL & Poulos JT. (1971) The metabolic influence of progestins. *Adv Metab Disord* 5, 119–147.

Lau TM, Witjaksono J & Rogers PA. (1996) Progesterone receptor in Norplant endometrium. *Hum Reprod* 2, 90–94.

Lehman TC, Hale DE, Bhala A & Thorpe C. (1990) An acyl-coenzyme A dehydrogenase assay utilizing the ferricenium ion. *Anal Biochem* 186, 280–284.

Luconi M, Bonaccorsi L, Maggi M, Pecchioli P, Krausz C, Forti G & Baldi E. (1998) Identification and characterization of functional nongenomic progesterone receptors on human sperm membrane. *J Clin Endocrinol Metab* 83, 877–885.

Luconi M, Bonaccorsi L, Bini L, Liberatori S, Pallini V, Forti G & Baldi E. (2002) Characterization of membrane nongenomic receptors for progesterone in human spermatozoa. *Steroids* 67, 505–509.

Luconi M, Porazzi I, Ferruzzi P, Marchiani S, Forti G & Baldi E. (2005) Tyrosine phosphorylation of the A kinase anchoring protein 3 (AKAP3) and soluble adenylate cyclase are involved in the increase of human sperm motility by bicarbonate. *Biol Reprod* 72, 22–32.

Lydon JP, DeMayo FJ, Funk CR, Mani SK, Hughes AR, Montgomery CA Jr, Shyamala G, Conneely OM & O'Malley BW. (1995) Mice lacking progesterone receptor exhibit pleiotropic reproductive abnormalities. *Genes Dev* 9, 2266–2278.

Mendoza C, Carreras A, Moos J & Tesarik J. (1992) Distinction between true acrosome reaction and degenerative acrosome loss by a one-step staining method using *Pisum sativum* agglutinin. *J Reprod Fertil* 95, 755–763.

Mohammed A & Chinegwundoh F. (2009) Testicular varicocoele: an overview. *Urol Int* 82, 373–379.

Monjo M, Rodríguez AM, Palou A & Roca P. (2003) Direct effects of testosterone, 17 beta-estradiol, and progesterone on adrenergic regulation in cultured brown adipocytes: potential mechanism for gender-dependent thermogenesis. *Endocrinology* 144, 4923–4930.

Osheroff JE, Visconti PE, Valenzuela JP, Travis AJ, Alvarez J & Kopf GS. (1999) Regulation of human sperm capacitation by a cholesterol efflux-stimulated signal transduction pathway leading to protein kinase A-mediated up-regulation of protein tyrosine phosphorylation. *Mol Hum Reprod* 5, 1017–1026.

Panteghini M, Bonora R & Pagani F. (2001) Measurement of pancreatic lipase activity in serum by a kinetic colorimetric assay using a new chromogenic substrate. *Ann Clin Biochem* 38, 365–370.

Pinter JH, Deep C & Park-Sarge OK. (1996) Progesterone receptors: expression and regulation in the mammalian ovary. *Clin Obstet Gynecol* 39, 424–435.

Portuondo JA, Calabozo M & Echanojauregui AD. (1983) Morphology of spermatozoa in infertile men with and without varicocoele. *J Androl* 4, 312–315.

Pryor JL & Howards SS. (1987) Varicocele. *Urol Clin N Am* 14, 499–513.

Pujianto DA, Curry BJ & Aitken RJ. (2010) Prolactin exerts a prosurvival effect on human spermatozoa via mechanisms that involve the stimulation of Akt phosphorylation and suppression of caspase activation and capacitation. *Endocrinology* 151, 1269–1279.

Rathi R, Colenbrander B, Bevers MM & Gadella BM. (2001) Evaluation of *in vitro* capacitation of stallion spermatozoa. *Biol Reprod* 65, 462–470.

Romeo C & Santoro GJ. (2009) Varicocele and infertility: why a prevention? *J Endocrinol Invest* 32, 559–561.

Ross P, Kan FW, Antaki P, Vigneault N, Chapdelaine A & Roberts KD. (1990) Protein synthesis and secretion in the human epididymis and immunoreactivity with sperm antibodies. *Mol Reprod Dev* 26, 12–23.

Rothchild I. (1983) Role of progesterone in initiating and maintaining pregnancy. In: Progesterone and Progestins (eds Bardin CW, Milgrom E & Mauvais-Jarvis P), pp. 219–229. Raven Press, New York.

Saaranen MJ, Calvo L, Dennison L, Banks S, Bustillo M, Dorfmann AD, Goldstein M, Thorsell L, Schulman JD & Sherins RJ. (1993) Acrosome reaction inducing activity in follicular fluid correlates

with progesterone concentration but not with oocyte maturity or fertilizability. *Hum Reprod* 8, 1448–1454.

Sabeur K, Edwards DP & Meizel S. (1996) Human sperm plasma membrane progesterone receptor(s) and the acrosome reaction. *Biol Reprod* 54, 993–1001.

Sartorius CA, Groshong SD, Miller LA, Powell RL, Tung L, Takimoto GS & Horwitz KB. (1994) New T47D breast cancer cell lines for the independent study of progesterone B- and A-receptors: only anti-progestin-occupied B-receptors are switched to transcriptional agonists by cAMP. *Cancer Res* 54, 3868–3877.

Scarpin KM, Graham JD, Mote PA & Clarke CL. (2009) Progesterone action in human tissues: regulation by progesterone receptor (PR) isoform expression, nuclear positioning and coregulator expression. *Nucl Recept Signal* 7, e009.

Schatz F, Krikun G, Caze R, Rahman M & Lockwood CJ. (2003) Progestin-regulated expression of tissue factor in decidual cells: implications in endometrial hemostasis, menstruation and angiogenesis. *Steroids* 68, 849–860.

Shah C, Modi D, Sachdeva G, Gadkar S, D'Souza S & Puri C. (2005a) N-terminal region of progesterone receptor B isoform in human spermatozoa. *Int J Androl* 28, 360–371.

Shah C, Modi D, Sachdeva G, Gadkar S & Puri C. (2005b) Coexistence of intracellular and membrane-bound progesterone receptors in human testis. *J Clin Endocrinol Metab* 90, 474–483.

Shannon JM, Cunha GR, Taguchi O, Vanderslice KD & Gould SF. (1982) Autoradiographic localization of steroid binding in human tissue labeled *in vitro*. *J Histochem Cytochem* 30, 1059–1065.

Suarez SS. (2008) Regulation of sperm storage and movement in the mammalian oviduct. *Int J Dev Biol* 52, 455–462.

Thomas P & Meizel S. (1989) Phosphatidylinositol 4,5-biphosphate hydrolysis in human stimulated with follicular fluid or progesterone is dependent upon Ca^{2+} influx. *Biochem J* 264, 539–546.

Thomas P, Pang Y, Zhu Y, Detweiler C & Doughty K. (2004) Multiple rapid progestin actions and progestin membrane receptor subtypes in fish. *Steroids* 69, 567–573.

Thomas P, Tubbs C & Garry VF. (2009) Progestin functions in vertebrate gametes mediated by membrane progestin receptors (mPRs): identification of mPRalpha on human sperm and its association with sperm motility. *Steroids* 74, 614–621.

Travis AJ & Kopf GS. (2002) The role of cholesterol efflux in regulating the fertilization potential of mammalian spermatozoa. *J Clin Invest* 110, 731–736.

Vedeckis WV, Ali M & Allen HR. (1989) Regulation of glucocorticoid receptor protein and mRNA levels. *Cancer Res* 49, 2295s–2302s.

Visconti PE, Baley JL, Moore GD, Pan D, Olds-Clarke P & Kopf GS. (1995) Capacitation in mouse spermatozoa I. Correlation between the capacitation state and protein phosphorylation. *Development* 121, 1129–1137.

Wada T, Hori S, Sugiyama M, Fujisawa E, Nakano T, Tsuneki H, Nagira K, Saito S & Sasaoka T. (2010) Progesterone inhibits glucose uptake by affecting diverse steps of insulin signaling in 3T3-L1 adipocytes. *Am J Physiol Endocrinol Metab* 298, E881–E888.

World Health Organization. (1992) The influence of varicocoele on parameters of fertility in a large group of men presenting to infertility clinics. *Fertil Steril* 57, 1289–1293.

Wu JT, Tsai PS, Lee SL & Cheng FP. (2005) Characterisation of the progesterone receptor on canine spermatozoa. *Reprod Fertil Dev* 17, 733–741.

Wu JT, Chiang KC & Cheng FP. (2006) Expression of progesterone receptor(s) during capacitation and incidence of acrosome reaction induced by progesterone and zona proteins in boar spermatozoa. *Anim Reprod Sci* 93, 34–45.

Xu J, Qiu Y, DeMayo FJ, Tsai SY, Tsai MJ & O'Malley BW. (1998) Partial hormone resistance in mice with disruption of the steroidal receptor coactivator-1 (SRC-1) gene. *Science* 279, 1922–1925.

Yanagimachi R. (1994) Fertility of mammalian spermatozoa: its development and relativity. *Zygote* 2, 371–382.

Zhu Y, Bond J & Thomas P. (2003) Identification, classification, and partial characterization of genes in humans and other vertebrates homologous to a fish membrane progestin receptor. *Proc Natl Acad Sci USA* 100, 2237–2242.

Zorgniotti AW & Macleod J. (1973) Studies in temperature, human semen quality, and varicocoele. *Fertil Steril* 24, 854–863.

Supporting Information

Additional Supporting Information may be found in the online version of this article:

Figure S1. Progesterone induces phosphorylation of the proteins on serine and threonine residues in human spermatozoa.

Please note: Wiley-Blackwell is not responsible for the content or functionality of any supporting materials supplied by the authors. Any queries (other than missing material) should be directed to the corresponding author for the article.

Original Article

"Human sperm physiology: estrogen receptor alpha (ERα) and estrogen receptor beta (ERβ) influence sperm metabolism and may be involved in the pathophysiology of varicocele-associated male infertility."

Guido Carmela[1,2], Perrotta Ida[3], Panza Salvatore[1,2], Middea Emilia[1,2], Avena Paola[1,2], Santoro Marta[1,2], Marsico Stefania[1,2], Imbrogno Pietro[5], Andò Sebastiano[1,4§] and Aquila Saveria[1,2§*].

[1] *Centro Sanitario,* [2]*Department of Pharmaco-Biologic,* [3]*Department of Ecology,* [4]*Department of Cellular Biology, University of Calabria 87030 Arcavacata di Rende (Cosenza) Italy.* [5] *LILT – Via Montegrappa, 45(Cosenza) – Italy.* [§]Joint senior authors.

Short title: ERs and human sperm metabolism

Corresponding address: Prof. Aquila Saveria, Dept. Pharmaco-Biologic - Faculty of Pharmacy-University of Calabria - Arcavacata di Rende (Cosenza) 87036 - ITALY
TEL: +39 0984 496210 - FAX: +39 0984 496203 - E-mail: aquisav@libero.it

Disclosure of Potential Conflict of Interest: The authors declare that there is no conflict of interest that would prejudice the impartiality of this scientific work.

This work was supported by MIUR Ex 60 % -2010.

Additional Supporting information may be found in the online version of this article.

Received 28 April 2010; Revised 27 January 2011; Accepted 11 February 2011
Journal of Cellular Physiology

DOI 10.1002/jcp.22703

ABSTRACT

The mechanisms by which varicocele affects fertility remain undetermined. Estrogens play a key role in the human male reproduction and human sperm expresses the estrogen receptors (ERs) and aromatase. In this study, by western blotting we evidenced the ERs content concomitantly in healthy sperm and in oligoastenoteratozoospermic (OAT) samples without and with varicocele. In varicocele a strong reduction of the ERβ was observed, while the ERα was almost absent. Besides, transmission electron microscopy (TEM) confirmed the reduction of ERs expression in 'varicocele' sperm, indicating that varicocele has a detrimental effect on sperm structure at molecular level. To further define the estrogen significance in male gamete and the pathophysiology of varicocele we investigated both the expression of ERα and ERβ in normal and pathologic sperm samples as well as we evaluated estradiol (E2) action on lipid and glucose sperm metabolism. Responses to E2 treatments on cholesterol efflux, protein tyrosine phosphorylations, motility and acrosin activity in varicocele sperm were reduced or absent. The evaluation of the triglycerides content, lipase and acyl-CoA dehydrogenase activities, suggest that E2 exerts a lipolytic effect on human sperm metabolism. Concerning glucose metabolism, it appears that E2 induces G6PDH activity concomitantly to the insulin secretion. In 'varicocele' sperm, the E2 did not induce energy expenditure. OAT sperm had E2-responsiveness but in a lesser extent with respect healthy sperm. This study discovered a novel role for E2/ERs in human sperm physiology, since they modulate sperm metabolism and new detrimental effects related to the pathophysiology of the varicocele condition.

Key words: ERβ, Estradiol, ERα, human ejaculated spermatozoa, male reproduction.

INTRODUCTION

Varicocele, a pathologic dilatation of the venous pampiniform plexus of the spermatic cord, accounts for about a third of all cases of male factor infertility (Koksal et al., 2007). The detrimental role of varicocele in fertility is supported by the presence of a higher frequency of affected men among the infertile population (World Health Organization, 1992; Practice Committee of American Society for Reproductive Medicine, 2008). The precise mechanism by which the pathology impairs male fertility remains uncertain (Mohammed et al., 2009). Many efforts have been made to find semen indicators of varicocele, nonetheless, its management continues to stimulate controversy among reproductive experts. The ambiguity of the results may be due to lack of uniformity in patient selection since varicocele may be associated with different spermatogenic conditions. Studies using light microscopy have shown that ejaculated spermatozoa from men with varicocele show an altered morphology (Portuondo et al., 1983), however the relation between sperm cell quality and varicocele is poorly understood.

The development of male transgenic mice lacking estrogen receptors (ERs) (Eddy et al., 1996) or aromatase enzyme (Robertson et al., 1999) as well as the discovery of mutations in both the human estrogen receptor (ER) α (Smith et al., 1994) and aromatase (Carani et al., 1997) genes have reinforced the idea that estrogens play a key role in the human male reproductive system. ERα and β are detected in germ cells from spermatogonia to spermatozoa (Hess et al., 1995; Aquila et al., 2004). In human sperm, ERs were found differently located being both receptors in the midpiece, while ERβ continues to be expressed in the flagellum.

Sperm are able to synthesize estrogen (Aquila et al., 2002) raising the possibility that they not only will be exposed to estrogens in female genital tract but provide themselves a persisting local source of estrogen. This autocrine loop E2/ERs may modulate the extra-ejaculation sperm acquisition of fertilizing ability. In ejaculated sperm**,** E2 stimulates various sperm functions including motility,

longevity, capacitation and acrosome reaction (Idaomar et al., 1987; Adeoya-Osiguwa SA et al., 2003; Aquila et al., 2003). The biochemical changes during capacitation induced by estrogens occur rapidly, addressing the nongenomic action of ERs as demonstrated in other cell types and in sperm (Aquila et al., 2004). On the other hand, the fast ERs responses, instead to their classic genomic action, may represent the exclusive modality of ERs action in spermatozoa because they are considered transcriptionally inactive. During its life, sperm goes across two different physiological conditions: uncapacitated, during which it remains in a quiescent state accumulating and / or economizing energy substrates; capacitated, that allows the sperm to achieve the final competence to fertilize the oocyte. Capacitation involves physiological changes including an increased metabolic rate and overall energy expenditure (Visconti et al., 1998; Baldi et al., 2000; Aquila et al., 2005a; Andò et al., 2005), however, sperm energy management is only beginning to be understood. Estrogens have been reported to affect adiposity by modulating lipogenesis, lipolysis or adipogenesis (Pallottini et al., 2008) and also play an important role in glucose homeostasis and modulate insulin sensitivity (Bryzgalova et al., 2006). The mechanisms involved in ER-actions on these issues are only now being unveiled and they had never been studied in human sperm .

In this study we evidenced a different ERs expression between normal and varicocele sperm and showed the ultrastructural location of the two receptors in these cells. To further define estrogen significance in sperm we evidenced its action on lipid and glucose metabolism. Interestingly, ‘varicocele’ sperm showed a reduced expression of both ERs and a different response to E2 with respect ‘healthy’ sperm on capacitation, acrosin activity, motility and metabolism.

MATERIALS AND METHODS

Chemicals

Percoll (colloidal PVP coated silica for cell separation), Estradiol (oestra-1,3,5,(10)-triene-3,17β-diol) (E2), Earle's balanced salt solution and all other chemicals were purchased from Sigma Chemical (Milan, Italy). Acrylamide bisacrylamide was from Labtek Eurobio (Milan, Italy). Eosin Y was from Farmitalia Carlo Erba. ICI 182, 780 (ICI) was purchased from Zeneca Pharmaceuticals (Cheshire, UK). Monoclonal mouse antibody (Ab) to human ER α (F-10), rabbit polyclonal Abs to human ER β (H-150), to β-actin (AC-15), to phosphotyrosine proteins (PY99), peroxidase-coupled anti-rabbit, anti-mouse IgG, normal rabbit serum (NRS) and normal mouse serum (NRS) were from Santa Cruz Biotechnology (Heidelberg, Germany). Colloidal gold conjugated goat anti-mouse and anti-rabbit IgG secondary Abs were from Sigma Aldrich (Milan, Italy). Cholesterol-oxidase (CHOD) - peroxidase (POD) enzymatic colorimetric assay, triglycerides assay, lipase activity, glucose-6-phosphate dehydrogenase (G6PDH) activity and insulin RIA assay kits were from Inter-Medical (Biogemina Italia Srl, Catania, Italy). E2 and ICI were dissolved in ethanol (0.02% final concentration) and used as solvent controls did not induce any positive result in all in vitro assays (data not shown). Detailed methods for each assay are reported as supplementary data.

Semen samples and spermatozoa preparations

Human semen was collected, according to the World Health Organization (WHO) Laboratory Manual (World Health Organization, 2010), from healthy volunteer donors of proven fertility. Varicocele samples of patients who consulted us for fertility investigation were also placed in the study. Reflux of blood in the pampiniform plexus was determined by palpation employing the Valsalva manoeuver. Additional radiologic imaging is not necessary to diagnose subclinical

varicocele, because only a varicocele detected by physical examination should be considered potentially significant (Pryor et al., 1987). Varicocele samples used in this study were from oligoastenoteratozoospermic (OAT) patients with diagnosed varicocele of grade III (visible without palpation) on the left testis and their ejaculates were found to have total sperm count of $18x10^6$ sperm cells per ejaculate, percentage of motility a+b of 32%, percentage of normally formed features of 30% and viability percentage of 70%. Samples of OAT patients without varicocele but with similar semen parameters with respect to that with varicocele, were also considered in this report to evaluate if eventual differences observed between normal and varicocele samples are related to other infertility problems. The study has been approved by the local medical-ethical committee and all participants gave their informed consent.

Processing of ejaculated sperm

For each experiment three normozoospermic samples or four OAT or four varicocele samples were pooled. After liquefaction, semen samples were pooled and then subjected to centrifugation (800 *g*) on a discontinuous Percoll density gradient (80:40 % v:v) (Aquila et al., 2002). The 80 % Percoll fraction was examined using an optical microscope equipped with a x100 oil objective to ensure that a pure sample containing only spermatozoa was obtained. These sperms had a motility of about 65% (World Health Organization, 2010) and a viability of 80% both for normal or pathologic samples. Particularly, the same number for both normal, OAT and varicocele samples of Percoll-purified sperm were washed with unsupplemented Earle's medium (uncapacitating medium) and were incubated in unsupplemented Earle's balanced salt solution for 30 minutes (min) at 37 °C and 5 % CO_2, without (NC) or with the following treatments: increasing E2 concentrations (1 nM, 10 nM, 100 nM and 1 μM) and ICI (1 μM) alone or combined with 10 nM or 100 nM E2 (i.e. the concentration at which we evidenced the E2 effect on the considered activity). When the cells were treated with ICI, a pre-treatment of 15 min was performed. From 0.1

nM to 1 nM E2 levels are in a range of previously reported physiological E2 concentrations in human male serum and in spermatic vein respectively (Pentikainen et al., 2000; Nakazumi et al., 1996). The other concentrations we used are supraphysiologic. It deserves to be mentioned that in males, the E2 can be extraordinarily high in the spermatic vein (about 1 nM), similar to that observed in the female during the onset of ovulation (Nakazumi et al., 1996).

Evaluation of sperm viability

Viability was assessed by using Eosin Y method. Spermatozoa were washed in uncapacitating medium and centrifuged at 800g for 20 min. To test androgen effects on sperm viability, spermatozoa 10 ml of Eosin Y [0.5% in phosphate-buffered saline (PBS)] were mixed with an equal volume of sperm sample on a microscope slide. The stained dead cells and live cells that excluded the dye, were scored among a total of 200 cells and by an independent observer. Sperm viability was calculated as percentage of total motile sperm, to exclude some toxic effects of the treatments.

Western blot analysis of sperm proteins

Percoll-purified sperm samples, washed twice with uncapacitating medium, were incubated as mentioned above and then centrifuged for 5 min at 5000 g. The pellet was resuspended in lysis buffer and western blotting analysis was performed as previously described (Aquila et al., 2004; Aquila et al., 2002). As internal control, all membranes were subsequently stripped (glycine 0.2 M, pH 2.6 for 30 min at room temperature) and reprobed with anti β-actin Ab. The protein bands were quantified by scanning densitometry (Imaging Densitometer GS-700 BIO–RAD USA).

Immunogold labeling for ERα and ERβ.

Immunogold assay by TEM was performed as previously described (Aquila et al., 2008; Aquila et al., 2010a). The mouse anti-human ERα Ab or the rabbit polyclonal to human ERβ Ab and 10 nm

colloidal gold conjugated anti-mouse or anti-rabbit IgG secondary Abs were used. To assess the specificity of the immunolabeling, negative controls were carried out in corresponding sections of sperm from fertile men that were labelled with colloidal gold conjugated secondary Ab without the primary Ab.

Measurement of cholesterol efflux

Cholesterol was measured in duplicate by a CHOD - POD enzymatic colorimetric method according to manufacturer's instructions in the incubation medium from human spermatozoa, as previously described (Aquila et al 2006; Aquila et al 2009a). Percoll-purified sperm samples, washed twice with uncapacitating medium, were incubated in the absence (NC, control) or in the presence of increasing concentrations of E2 (from 1 nM to 1 μM) or with 1 μM ICI alone or combined with 10 nM E2, for 30 min at 37 °C and 5 % CO_2. At the end of the sperm incubation the culture media were recovered by centrifugation, lyophilized and subsequently dissolved in 1 ml of buffer reaction. The samples were incubated for 10 min at room temperature, then the cholesterol content was measured spectrophotometrically at 505 nm. Cholesterol standard used was 200 mg/dl. The limit of sensitivity for the assay was 0.05 mg/dl. Inter- and intraassay variations were 0,04 % and 0,03 % respectively. Cholesterol results are presented as mg per 10 x 10^6 number of spermatozoa.

Evaluation of sperm motility

Sperm motility was assessed by means of light microscopy examining an aliquot of each sperm sample in absence or in the presence of increasing E2 (from 1 nM to 1 μM) or with 1 μM ICI alone or combined with 10 nM E2. Sperm motility was expressed as percentage of total motile sperm. An independent observer scored at least 200 cells.

Acrosin activity assay

Acrosin activity was assessed by the method of Kennedy et al. (1989) and as previously described (Aquila et al., 2003). Sperm were washed in Earle's medium and centrifuged at 800 *g* for 20 min, then were resuspended (final concentration of 10 x 10^6 sperm/ml) in different tubes containing no treatment (NC, control) or in the presence of increasing E2 concentrations (from 1 nM to 1 μM) or with 1 μM ICI alone or combined with 10 nM E2 incubated for 30 min under uncapacitating conditions. 1 ml of substrate-detergent mixture (23 mmol/l BAPNA in DMSO and 0.01% Triton X-100 in 0.055 mol/l NaCl, 0.055 mol/l HEPES at pH 8.0 respectively) was added and incubated for 3 hours at room temperature. Aliquots (20 μl) were removed at 0 and 3 hours and the percentages of viable cells were determined. After incubation, 0.5 mol/l benzamidine was added (0.1 ml) to each of the tubes and then centrifuged at 1000 *g* for 30 min. The supernatants were collected and the acrosin activity measured with the spectrophotometer at 410 nm. In this assay, the total acrosin activity is defined as the amount of the active (nonzymogen) acrosin associated with sperm plus the amount of active acrosin that is obtained by proacrosin activable. The acrosin activity was expressed as μIU/10^6 sperms. Quantification of acrosin activity was performed as previously described (Aquila et al., 2003).

Triglycerides Assay

Triglycerides were measured in duplicate by a GPO-POD enzymatic colorimetric method according to manufacturer's instructions in sperm lysates and as previously described (Aquila et al., 2006; Aquila et al., 2009a; Aquila et al., 2009b). Data are presented as μg/10^6 sperms.

Assay of acyl-CoA dehydrogenase activity

Acyl-CoA dehydrogenases are a class of enzymes which function to catalyze the initial step in each cycle of fatty acid β-oxidation. Assay of acyl-CoA dehydrogenase was performed on sperm,

using a modification of the method described by Lehman et al. (Lehman et al., 1990) as previously described (Aquila et al., 2006).

Lipase activity assay

Lipase activity was evaluated, by the method of Panteghini et al.(Panteghini et al., 2001) based on the use of 1,2-o-dilauryl-rac-glycero-3-glutaric acid-(6'-methylresorufin) ester (DGGR) as substrate, as previously described (Aquila et al., 2006; Aquila et al., 2009).

Assay of the G6PDH activity

The conversion of $NADP^+$ to NADPH, catalyzed by G6PDH, was measured by the increase of absorbance at 340 nm as previously described (Aquila et al., 2005b).

Measurement of insulin secreted by human spermatozoa

A competitive RIA was applied to measure insulin in the sperm culture medium as previously described (Aquila et al., 2005b). The limit of sensitivity for the assay was 0.02 μIU/ml. Inter- and intra-assay variations were 3.2 % and 3.4 %, respectively. Insulin results are presented as the original concentrations of the supernatants and are expressed as micro international units per millilitre.

STATISTICAL ANALYSIS

The experiments for TEM assay were performed in at least three independent experiments. The experiments for Western blotting analysis were performed in at least six independent experiments. The data obtained from cholesterol efflux, motility, acrosin activity, triglycerides assay, lipase activity, acyl-CoA dehydrogenase activity, G6PDH activity, insulin assay (six replicate experiments using duplicate determinations), were presented as the mean ± SEM. The differences

in mean values were calculated using analysis of variance (ANOVA) with a significance level of $P \leq 0.05$.

RESULTS

ERβ and ERα expression in normal, OAT and varicocele sperm samples

First we investigated the ERs expression in normal, OAT and varicocele sperm. Interestingly, ERβ content appears strongly reduced only in varicocele samples (Fig. 1A), while ERα was almost undetectable (Fig. 1B). Therefore, the ERs content might distinguish men with normozoospermia and OAT from those with varicocele. The bands were not detected by non-immune rabbit serum (panel A1) or by non-immune mouse serum (panel B1) indicating that these proteins are specific for ERβ and ERα respectively.

Immunogold localization of ERβ in human sperm

By TEM, ultrastructural analysis revealed well preserved outer dense fibers, axoneme and mitochondria. The sperm head showed no ERβ label (Fig. 2a), while the midpiece with the mitochondria was decorated with gold particles (Fig. 2d). Strong label was seen throughout the principal piece of the flagellum, including fibrous sheath and the outer dense fibers (Fig. 2g). ERβ appears to be also present in sperm membranes. Simultaneous negative control experiments performed with sperm from fertile men did not show any label in the corresponding regions (Figs. 2c, 2f and 2i). In 'varicocele' sperm, the ERβ was absent in the head (Fig. 2b) and a strong reduction of the labelling was noticed along the midpiece and the tail (Fig. 2e and Fig. 2h).

Immunogold localization of ERα

Low levels of ERα labelling were confined to the midpiece (mitochondria, between outer dense fibers and axoneme) (Fig. 3d and 3g). Labelling was completely absent from the head (Fig 3a) and no gold particles were seen lower down the midpiece, in all the sperm observed. Immunogold labelling was not observed in negative control experiments in the corresponding sperm regions (Fig. 3c, 3f and 3i). Consistent with western blot experiments, in the 'varicocele' sperm the ERα was almost absent in the majority of the sperm observed (3b, 3e and 3h).

E2 induces capacitation in human normal sperm

Then we evaluated E2 effects on two hallmarks of capacitation process, sperm membrane cholesterol efflux and protein tyrosine phosphorylation in normozoospermic, OAT and varicocele samples. Capacitation encompasses different features and sperm membrane cholesterol efflux contributes to one signalling mechanism that controls the process (Aquila et al 2006; Visconti et al 1998; Travis et al 2002). Our results showed a dose-dependent increase in the cholesterol efflux from 1nM to 100 nM E2 (Fig. 4A), while 1 μM did not give further increase. This effect was abrogated by using ICI combined with 100 nM E2. It deserved to be mentioned that ICI is a potent steroidal antiestrogen, which can bind to both ER subtypes (Vladusic et al., 2000; Roger et al., 2005). The OAT sperm showed a similar pattern of E2-response although in a lesser extent. In varicocele samples, no increase upon E2 treatment was observed.

Cholesterol efflux initiates signalling events leading to tyrosine phosphorylation of sperm proteins (Visconti et al 1995; Osheroff et al 1999). In our study, it appears that an increase in the protein tyrosine phosphorylation was obtained from 1 nM to 100 nM E2 (Fig 4B). A similar response to E2 was observed in OAT samples, however in a lesser extent. The combination of ICI with 100 nM E2 reduced this action. In varicocele samples, no significant increase upon E2 was observed.

E2 induces sperm motility and acrosin activity

The sperm cell uses its flagellum to move itself through the female reproductive tract. In our experiments, E2 induced sperm motility at 1 nM and 10 nM, after then it significantly decreased at 1 μM (Fig. 5A), showing a biphasic effect. OAT showed an increase at 1 nM and 10 nM E2 as it occurs in healthy sperm, albeit in a lesser extent. In varicocele samples, an increase upon 10 nM E2 was observed. The acrosin activity significantly increased upon E2 in normal samples (Fig. 5B), while a weak not significant enhancement was obtained in varicocele sperm. OAT sperm had a similar response to that of healthy sperm. Besides, in normal samples, the ICI didn't completely reverse the E2-induced effect in both motility and acrosin activity, suggesting that other factors other than ERs are involved in mediating these sperm activities.

E2 modulates the triglycerides content, lipase and acyl-CoA dehydrogenase activities in human sperm

An action of estrogen on lipid and glucose metabolism was demonstrated in adipocyte cells. In sperm, we first investigated triglycerides intracellular content upon increasing E2 levels. As shown in Fig. 6A, E2 was able to significantly decrease the triglycerides content in a dose-dependent fashion and the combination of 100 nM E2 with 1 μM ICI reduced the E2-induced action. OAT samples displayed a significantly decrease at 100 nM and 1 μM E2. In varicocele, on the contrary an increase of triglycerides was obtained at 100 nM and 1 μM E2.

To further investigate the mechanism through which E2 may influence sperm lipid metabolism, we evaluated its role on lipase and acyl-CoA dehydrogenase activities. The E2-induced increase in lipolysis was recently suggested in somatic cells, however an E2 regulation of lipase activity in sperm was never studied. Interestingly, lipase activity was enhanced by E2 in a dose-dependent manner and 100 nM E2 plus 1 μM ICI reduced the E2-induced effect (Fig. 6B). The E2-induced

action in OAT samples was evidenced at 100 nM. The effect was not observed in 'varicocele' sperm.

In aromatase-deficient mouse which lacks intrinsic estrogen production, an altered expression of acyl-CoA dehydrogenase was observed (Nemoto et al., 2000). In sperm, it appears that E2 induces β-oxidation of the fatty acids from 1 nM to 100 nM (Fig. 6C), while 1 μM E2 didn't give further effect. The combined treatment of 100 nM E2 with 1 μM ICI attenuated the effect. OAT samples had similar results although in a minor order of magnitude. In varicocele samples, E2 didn't induce the enzymatic activity.

E2 regulates G6PDH activity in human sperm

A role of E2 in glucose metabolism was investigated in somatic cells, however this possible E2-action in sperm was not studied yet (Puah et al., 1985). The effect of glucose on the sperm fertilizing ability appears to be mediated by its metabolism through the Pentose Phosphate Pathway, therefore we evaluated whether E2 is able to modulate the G6PDH activity, as it is the key factor of this pathway. As shown in Fig. 7A, E2-induced this activity. When 100 nM E2 were combined with 1 μM ICI a reversion was obtained. OAT sperm mirror the E2-induced effect in normal sperm, but in a lesser extent. Similarly to the other enzymatic activities, the 'varicocele' sperm did not respond to E2.

E2 affects insulin secretion by sperm

The ER plays an important role in the regulation of insulin biosynthesis, secretion and β-cell survival (Nadal et al., 2009). We previously demonstrated that insulin is expressed in and secreted from human spermatozoa (Aquila et al., 2005b). In this study, from 1 nM to 100 nM E2 induced a dose-dependent increase in insulin secretion, reaching levels that were similar to that elicited upon glucose stimulation in human sperm (Aquila et al., 2005b), while 1 μM E2 didn't give further

increase (Fig. 7B). 100 nM E2 combined with 1 μM ICI attenuated the effect. OAT samples resemble the E2-induced effect in normal sperm, but in a lesser extent. Interestingly, the 'varicocele' sperm seems to be sensitive to E2 on insulin secretion in a similar behaviour to that of normal sperm, however with a different order of magnitude that is similar to that observed in uncapacitated sperm (Aquila et al., 2005b).

DISCUSSION

Despite current knowledge in the pathophysiology of varicocele-associated male infertility, the exact mechanism/s by which it impairs fertility remains elusive. In the male reproductive tract, a key action of estrogens was observed in the regulation of the spermatogenesis, spermiogenesis and gamete functional maturation (Robertson et al., 1999; Sharpe, 1998; O'Donnel et al., 2001). In the present study, we evidenced the sperm ultrastructural compartmentalization of the ERα and ERβ. Interestingly, we discovered a new role of E2 in the regulation of lipid and glucose metabolism in human male gamete. Intriguingly, comparing 'healthy' and 'varicocele' sperm at molecular and functional levels, differences in the amount of the two receptors and in the response to the hormone were observed.

First, we examined the expression of ERs simultaneously in semen samples from healthy donors and from OAT patients with or without varicocele. Worthy, a reduced expression of the ERs appears to be related only to varicocele since it discriminates healthy and OAT sperm from those with varicocele. Therefore, this pattern of ERs expression in varicocele may be considered a molecular marker of the damaging effects of the pathology on spermatogenesis and/or sperm maturation. It was reported that glucocorticoid receptor is rapidly degraded in heat-shocked cells (Vedeckis et al., 1989), therefore it may also be possible that the increased testicular temperature in varicocele subjects determinates this effect.

We previously demonstrated that ERα is prevalently expressed in the mid-piece, while ERβ is distributed along the tail with an overlap of the two proteins in the proximal region of the tail (Aquila et al., 2004). In the present finding, to gain an improved understanding of the human sperm anatomical region containing the ERs we employed TEM with immunogold analysis. Ultrastructural analysis revealed ERβ label in the midpiece with the mitochondria and a strong label throughout the principal piece of the flagellum, including fibrous sheath and the outer dense fibers. Low levels of ERα labelling were confined to the midpiece (mitochondria, between outer dense fibers and axoneme). From an overview of the ERs localization and abundance in the male genital tract, ERβ seems to be the predominant ER subtype in male reproductive system, conversely ERα appears to be very weakly expressed, as we found in our study. Intriguingly, in 'varicocele' sperm, a strong reduction of the ERβ labelling was noticed while the ERα was almost absent. These data are consistent with western blotting results, and may suggest, at least in part, a link between the expression of ERs, the reduced motility and survival of the gametes in subjects suffering of varicocele, taking also into account our previously reported roles of ERs on human sperm (Aquila et al., 2004). The reduced expression of both proteins in 'varicocele' sperm, may be brought back to the spermatogenesis during which some factor related to the varicocele condition interferes with a production of the ERs correct amount, or during the spermiogenesis when the formation of the flagellum occurs. This varicocele-induced damage may also happen during the transit of the sperm along the male reproductive tract (epididymus and sex accessory glands), where it undergoes modifications in the macromolecules composition. It was previously demonstrated that E2 stimulates various sperm functions including motility, longevity, capacitation and acrosome reaction (Idaomar et al., 1987; Adeoya-Osiguwa SA et al., 2003; Aquila et al., 2003). Our report confirmed some of these data, such as the capacitation and ascrosin activity, besides evidenced that the varicocele sperm did not seem to be responsive to E2 and this may be due to the reduced expression of both the ERs.

The highly polarization in the structure and function of spermatozoa compartmentalize specific signalling pathways to the regions were they are needed. The massive presence of ERβ in the flagellum may indicate an important role in the sperm motility. In this regards, it was previously reported that estrogens affect sperm motility (Aquila et al., 2003), however in the present study we highlight that the ERs may be involved. In sperm, flagellum serves dual functions: in addition to being a basic engine for locomotion it is involved in physiological functions such as capacitation and acrosome reaction (Breitbart et al., 2005). Besides, most of the glycolytic enzymes have been localized to the flagellum and the central role of mitochondria in energy production is well known. The concomitant location of the two ERs in the flagellum and midpiece, where mitochondria are present, led us to hypothesize that these receptors could be involved in sperm metabolism. Estrogens have been reported to affect adiposity either directly, by modulating lipogenesis, lipolysis or adipogenesis, or indirectly, by modulating energy expenditure. Capacitation involves numerous physiological changes including an increased metabolic rate and overall energy expenditure to accomplish all the necessary changes. Our recent data suggest that sperm has the ability to modulate itself the energetic substrate availability on the basis of its energy needs independently of the systemic regulation (Aquila et al., 2005a; Aquila et al., 2005b). Besides, our previous studies demonstrated that the substances which induced capacitation had the effect to reduce the triglycerides content while concomitantly some enzymatic activities related to the energy expenditure increased (Aquila et al., 2006; Aquila et al., 2009a; Aquila et al., 2009b; Aquila et al., 2010b). These data also implicate that the uncapacitated sperm is involved in the accumulation of energy substrates, which will be spent during capacitation when the energy is used to accomplish sperm's mission to fertilize the oocyte. Although the relationship between the signalling events associated with capacitation and the changes in sperm metabolism energy is only beginning to be understood, it may be generalized that uncapacitated sperm is associable with an anabolic metabolism while capacitation with a catabolic metabolism. Particularly, from this new

manuscript it appears that E2 is able to induce both capacitation and acrosin activity in normal sperm in agreement with other studies, therefore the increased lipid and carbohydrate metabolism upon E2 well fit with the role of estrogens in the sperm acquisition of fertilizing ability.

We would like to point out that in our study, the E2 induces G6PDH activity concomitantly to the insulin secretion. From our previous data, insulin can be considered an endogenous factor involved in the autocrine induction of the capacitation and the high insulin secretion by sperm may be considered another feature of this process (Aquila et al., 2005a); here we found that E2 is able to modulate insulin secretion, confirming the importance of E2/ER in sperm functional maturation. In 'varicocele' sperm, the E2 did not induce energy expenditure thereby signifying a metabolic dysfunction. It may be also deduced that the 'varicocele' sperm did not respond to estrogen since it doesn't have enough ERs. Particularly, it appears that E2 was able to induce insulin secretion also in varicocele sperm, however the levels were comprised in the typical range of the uncapacitated status (0.1– 0.73 μIU/ml) (Aquila et al., 2005a). Altogether, it may be presumed that 'varicocele' sperm has difficulty to switch into capacitation.

Undoubtedly, there is a need for more molecular and genetic studies to clarify the pathophysiology of varicocele. Besides, from our data, ICI was not able to completely revert all the sperm activities studied, suggesting that different factors induced by E2 other than ERs are involved. To strengthen the idea that the steroid hormones effects are "extranuclear" and "nongenomic" and happen through a membrane receptor in sperm, there is a general consensus that their effects are not counteracted by the classical antagonists (Schatz et al 2003). However, from our previous data, by using antagonists or inhibitors for some nuclear receptors including ICI for the ERs (Aquila et al., 2004), GW9662 for the Peroxisome proliferator-activated receptor (PPAR) gamma (Aquila et al., 2006), Casodex and hydroxy-flutamide for androgen receptors (Aquila et al., 2007), it emerges that these substances were able to abolish or to attenuate different sperm actions induced activating the receptor by its specific ligand. Mechanistic studies have shown that ICI, possesses high ER-

binding affinity and has multiple effects on ER signalling: it blocks dimerisation and nuclear localisation of the ER, reduces cellular levels of ER and blocks ER-mediated gene transcription (Anthony Howell, 2006). In different cell types fulvestrant has also been shown to abolish rapid, 'nongenomic' estrogen signaling (Fatehi et al., 2006). For example, the activation of the MAPK pathway and a mobilization of intracellular calcium stores via estrogen stimulation of ER is abolished by ICI in vitro (Improta-Brears et al. 1999). All these observations, corroborated by the identification of the classical ERs in sperm, indicate that the receptor action may be blocked by ICI also when some rapid effects were taken into account, both in somatic cells and in the sperm.

The steroid hormone estrogen has been long known to exert both genomic and nongenomic effects. Although the identity of all the receptors that might mediate the latter effects remains unclear, substantial evidence now indicates that both types of the effects can be mediated through the classical estrogen receptors, ERα and ERβ. Because many of these estrogen-stimulated pathways are typically initiated at the plasma membrane, many investigators have sought to determine the existence of a membrane-associated ER. In many instances, rapid signalling are stimulated by the classical steroid/nuclear receptor (Hammes and Levin, 2007), but may be also mediated by membrane-associated ER (Hanstein et al. 2004) or by structurally unrelated receptors of the 7-transmembrane G protein-coupled receptor family such as GPR30 that has also been shown to be capable to mediate signaling following E2 stimulation (Prossnitz et al., 2008). In CHO cells, expression of a single cDNA for either ERα or ERβ produces both membrane and nuclear receptor populations and results in E2 activation of signal transduction from the membrane (Razandi *et al*., 1999). Another proposed mechanism for membrane-initiated signaling by ER involves receptor association with membrane caveolae favoring the idea that the membrane and nuclear ER are the same protein. However, there is still substantial evidence arguing for the existence of novel membrane estrogen receptors (mER) that mediate the rapid effects of estrogen. It is likely that both populations of receptors play a role in rapid signaling. It is generally accepted that the sperm

nucleus is transcriptional inactive due to the highly condensed architecture of its chromatin, therefore the rapid actions appears to be more appropriate in sperm as the hormone's effects happen too quickly to be due to gene regulation. Anyway, it is well established that the conventional estrogen receptors induce rapid effects both in somatic and in sperm cells.

Going along our previous studies, the presence of both ERs and aromatase in sperm, create the conditions for an autocrine estradiol short loop. It may be hypothesised that the E2 produced by sperm may act on its own receptors triggering or modulating various sperm activities, comprising the metabolism. Intriguingly, in almost all the performed assays, the OAT cases not associated with varicocele are sensitive to E2, although in a lesser extent with respect to the healthy sperm. The OAT samples seem to contain a major ERs amount with respect normal sperm, anyway they exhibited a reduced sensibility to E2. This may be due to the fact that in the cells a fine regulation and a balanced content of the various proteins is needed, even more in a cell with peculiar features like sperm. OAT with varicocele greatly lose the responsiveness to E2. This supports that varicocele is an additional factor to decrease the acquisition of sperm fertilizing ability and denotes that the ERs may be involved in this detrimental action.

Concluding, varicocele has a negative effect on sperm structure at molecular level and this go beyond the abnormal sperm morphology described to date, complicating this issue.

ACKNOWLEDGMENTS

Our special thanks to Dr. Vincenzo Cunsolo (Biogemina Italia Srl, Catania – Italy) for the technical and scientific assistance. We would like also to thank Perrotta Enrico for the excellent technical and scientific assistance and Serena Gervasi for the English language review of the manuscript.

FIGURE & LEGENDS

FIG. 1 ERβ **and** ERα **expression is reduced in varicocele sperm**

Extracts of pooled purified ejaculated spermatozoa were subjected to electrophoresis on 11% SDS-polyacrylamide gels,blotted onto nitrocellulose membranes, and probed with rabbit polyclonal antibody to human ERβ (A) or with mouse monoclonal antibody to human ERα (B). **A**: Norm, expression of ERβ in ejaculated sperm from normal men. OAT1 and OAT2 expression of ERβ in ejaculated sperm from two oligoastenoteratozoospermic patients. V1 and V2 expression of ERβ in two samples of ejaculated sperm from varicocele men. **A1**: Immunoblot of the negative control membrane incubated with normal rabbit serum). **B:** Norm, expression of ERα in ejaculated sperm from normal men. OAT1 and OAT2 expression of ERα in ejaculated sperm from two oligoastenoteratozoospermic patients. V1 and V2 expression of ERα in two samples of ejaculated sperm from varicocele men. The number on the left corresponds to molecular masses (kilodaltons) of the marker proteins. **B1**: Immunoblot of the negative control membrane incubated with normal mouse serum).The experiments were repeated at least six times, and the autoradiographs of the figure show the results of one representative experiment.

FIG. 2 Immunoelectron localization of ERβ in human spermatozoa

Sperm were collected and prepared as described in *Materials and Methods*. **Panels a, d and g** are micrographs of sections from ejaculated sperm of normozoospermic patients probed with rabbit polyclonal Ab to human ERβ: original magnification, **a** x30000; **d** x40000; **g** x50000. **Panels b, e and h** are micrographs of sections of the corresponding regions from sperm of varicocele patients probed with rabbit polyclonal Ab to human ERβ, original magnification**, b** x20000; **e** x40000; **h** x50000. **Panels c, f and i**, samples from fertile men, are the negative controls (N) of the corresponding regions obtained without the incubation with the primary Ab, original

magnification**, c** x30000; **f** x40000; **i** x20000. In all cases, a secondary anti-rabbit antibody conjugated to 10-nm colloidal gold particles was used for labelling. **A**: Longitudinal sections through the head; **B**: Cross-sections of the midpiece of the flagellum; **C:** Longitudinal sections of the principal piece of the flagellum. Representative of 3 similar experiments.

FIG. 3 Immunoelectron microscopic localization of ERα in human spermatozoa

Sperm were collected and prepared as described in *Materials and Methods*. **Panels a, d and g** are micrographs of sections from ejaculated sperm of normozoospermic patients probed with mouse monoclonal Ab to human ERα, original magnification**, a** x30000; **d** x80000; **g** x50000. **Panels b, e and h** are micrographs of sections of the corresponding regions from sperm of varicocele patients probed with mouse monoclonal Ab to human ERα, original magnification**, b** x30000; **e** x50000; **h** x60000. **Panels c, f and i**, are the negative controls (N) of the corresponding regions obtained without the incubation with the primary Ab, original magnification**, c** x30000; **f** x60000; **i** x70000. In all cases, a secondary anti-mouse antibody conjugated to 10-nm colloidal gold particles was used for labelling. **A**: Longitudinal sections through the head; **B**: Longitudinal sections of the midpiece of the flagellum; **C:** Cross-sections of the midpiece of the flagellum. Representative of 3 similar experiments.

FIG. 4 Effects of E2 on capacitation

Purified spermatozoa were incubated in the unsupplemented Earle's medium for 30 min at 37 °C and 5% CO2, in the absence (NC) or in the presence of indicated treatments. **A:** Cholesterol in culture medium from human ejaculated spermatozoa was measured by enzymatic colorimetric assay. Columns are mean ± SEM of six independent experiments performed in duplicate. Data are expressed in mg/107 spermatozoa. *$p<0.05$ vs. control ; **$p < 0.02$ vs. control. **B:** 70 μg of sperm lysates were used for western blot analysis of protein tyrosine phosphorylations in normal samples.

Actin was used as loading control. **C:** protein tyrosine phosphorylation in OAT samples without varicocele. **D:** protein tyrosine phosphorylation in varicocele samples. The autoradiographs presented are representative examples of experiments that were performed at least six times with repetitive results. On the right, quantitative representations after densitometry of the double 95±97 kDa band, representative of the protein tyrosine phosphorylations in human sperm. *P = 0.05 versus control, **P = 0.01 versus control.

Fig. 5 E2 effects on sperm motility and acrosin activity in human sperm

Purified spermatozoa were incubated in the unsupplemented Earle's medium for 30 min at 37 °C and 5% CO_2, in the absence (NC) or in the presence of increasing E2 concentrations (1 nM, 10 nM, 100 nM and 1 μM). Some samples were treated with 1 μM ICI alone or combined with 10 nM E2. Sperm motility and acrosin activity were assessed as reported in *Materials and methods*. **A:** Data are expressed as % of sperm motility. *P < 0.05 versus control; ** P=0.02, versus control. **B:** The acrosin activity was expressed as μIU/10^6 sperms;*P < 0.05 and **P = 0.01 versus control. Columns represent mean ± SEM of six independent experiments each done in duplicate.

Fig. 6 E2 affects triglycerides content, lipase and acyl-CoA dehydrogenase activities in human sperm

Purified spermatozoa were incubated in the unsupplemented Earle's medium for 30 min at 37 C and 5% CO_2, in the absence (NC) or in the presence of increasing E2 concentrations (1 nM, 10 nM, 100 nM and 1 μM). Some samples were treated with 1 μM ICI alone or combined with 100 nM E2. **A:** Triglycerides content was measured as reported in *Materials and Methods*. Columns represent mean ± SEM of six independent experiments each done in duplicate. *P < 0.05 versus control, **P < 0.02 versus control. Lipase (**B**) and octanoyl-CoA dehydrogenase (**C**) activities were performed as reported in *Materials and Methods*. Columns represent mean ± SEM of six

independent experiments each done in duplicate. **B**: *$P < 0.05$ versus control; **$P < 0.01$ versus control. **C:** *$P < 0.05$ versus control; **$P < 0.01$ versus control.

Fig. 7 E2 effects on sperm glucose metabolism

Purified sperm were incubated in the uncapacitating medium (control) for 30 min at 37 C and 5 % CO_2. Sperm were treated with 1 nM, 10 nM, 100 nM and 1 μM E2. Some samples were treated with 1 μM ICI alone or combined with 100 nM E2. **A:** G6PDH activity was performed as reported in *Materials and Methods*. **B:** Insulin secretion by sperm was evaluated as reported in *Materials and Methods*. Columns represent mean ± SEM of six independent experiments each done in duplicate, *$P < 0.01$ versus control, **$P < 0.001$ versus control.

REFERENCES

Adeoya-Osiguwa SA, Markoulaki S, Pocock V, Milligan SR, Fraser LR. 2003. 17beta-Estradiol and environmental estrogens significantly affect mammalian sperm function. Hum Reprod 18:100-7.

Andò S, Aquila S. 2005. Arguments raised by the recent discovery that insulin and leptin are expressed in and secreted by human ejaculated spermatozoa. Mol Cell Endocrinol 245:1-6.

Aquila S, Bonofiglio D, Gentile M, Middea E, Gabriele S, Belmonte M, Catalano S, Pellegrino M, Ando S. 2006. Peroxisome proliferator-activated receptor (PPAR)gamma is expressed by human spermatozoa: its potential role on the sperm physiology. J Cell Physiol 209:977-986.

Aquila S, Gentile M, Middea E, Catalano S, Andò S. 2005b. Autocrine regulation of insulin secretion in human ejaculated spermatozoa. Endocrinology 146:552-7.

Aquila S, Gentile M, Middea E, Catalano S, Morelli C, Pezzi V, Andò S. 2005a. Leptin secretion by human ejaculated spermatozoa. J Clin Endocrinol Metab 90:4753-61.

Aquila S, Guido C, Laezza C, Santoro A, Pezzi V, Panza S, Andò S, Bifulco M. 2009a. A new role of anandamide in human sperm: focus on metabolism. J Cell Physiol 221:147-53.

Aquila S, Guido C, Middea E, Perrotta I, Bruno R, Pellegrino M, Andò S. 2009b. Human male gamete endocrinology: 1alpha, 25-dihydroxyvitamin D3 (1,25(OH)2D3) regulates different aspects of human sperm biology and metabolism. Reprod Biol Endocrinol. 7:140-152.

Aquila S, Guido C, Perrotta I, Santoro A, Laezza C, Bifulco M, Andò S. 2010a. Human sperm anatomy: ultrastructural localization of the cannabinoid1 receptor (CB1-R) and a potential role of anandamide in sperm survival and acrosome reaction. Anat Rec (Hoboken) 93:298-309.

Aquila S, Guido C, Perrotta I, Tripepi S, Nastro A, Andò S. 2008. Human sperm anatomy: ultrastructural localization of 1alpha,25-dihydroxyvitamin D receptor and its possible role in the human male gamete. J Anat 213:555-564.

Aquila S, Guido C, Santoro A, Gazzerro P, Laezza C, Baffa MF, Andò S.2010b. Rimonabant (SR141716) induces metabolism and acquisition of fertilizing ability in human sperm. Br J Pharmacol. 159:831-41.

Aquila S, Middea E, Catalano S, Marsico S, Lanzino M, Casaburi I, Barone I, Bruno R, Zupo S, Andò S. 2007. Human sperm express a functional androgen receptor: effects on PI3K/AKT pathway. Human Reproduction 22: 2594-2605.

Aquila S, Sisci D, Gentile M, Carpino A, Middea E, Catalano S, Rago V, Andò S. 2003. Towards a physiological role for cytochrome P450 aromatase in ejaculated human sperm. Hum Reprod 18:1650-9.

Aquila S, Sisci D, Gentile M, Middea E, Catalano S, Carpino A, Rago V, Andò S. 2004. Estrogen receptor (ER)alpha and ER beta are both expressed in human ejaculated spermatozoa: evidence of their direct interaction with phosphatidylinositol-3-OH kinase/Akt pathway. J Clin Endocrinol Metab 89:1443-51.

Aquila S, Sisci D, Gentile M, Middea E, Siciliano L, Andò S. 2002. Human ejaculated spermatozoa contain active P450 aromatase. J Clin Endocrinol Metab 87:3385-90.

Baldi E, Luconi M, Bonaccorsi L, Muratori M, and Forti G. 2000. Intracellular events and signalling pathways involved in sperm acquisition of fertilizing capacity and acrosome reaction. Frontiers in Bioscience 5:110-123.

Breitbart H, Cohen G, Rubinstein S. 2005. Role of actin cytoskeleton in mammalian sperm capacitation and the acrosome reaction. Reproduction 129:263-8.

Bryzgalova G, Gao H, Ahren B, Zierath JR, Galuska D, Steiler TL, Dahlman-Wright K, Nilsson S, Gustafsson JA, Efendic S, Khan A. 2006. Evidence that oestrogen receptor-alpha plays an important role in the regulation of glucose homeostasis in mice: insulin sensitivity in the liver. Diabetologia 49:588-97.

Carani C, Qin K, Simoni M, Faustini-Faustini M, Serpente S, Boyd J, Korach KS, Simpson ER. 1997. Effect of testosterone and estradiol in a man with aromatase deficiency. N Engl J Med 337:91–95.

Eddy EM, Washburn TF, Bunch DO, Goulding EH, Gladen BC, Lubahn DB, Korach KS. 1996. Targeted disruption of the estrogen receptor gene in male mice causes alteration of spermatogenesis and infertility. Endocrinology 137:4796–4805.

Fatehi M, Zidichouski JA, Kombian SB, Saleh TM. 2006. 17beta-estradiol attenuates excitatory neurotransmission and enhances the excitability of rat parabrachial neurons in vitro. J Neurosci Res. 84:666-74.

Flötotto T, Niederacher D, Hohmann D, Heimerzheim T, Dall P, Djahansouzi S, Bender HG, Hanstein B. 2004 Molecular mechanism of estrogen receptor (ER)alpha-specific, estradiol-dependent expression of the progesterone receptor (PR) B-isoform. J Steroid Biochem Mol Biol. 88:131-42.

Hammes SR, Levin ER. 2007 Extranuclear steroid receptors: nature and actions. Endocr Rev. 7:726-41.

Hess RA, Bunik D, Bahr JM. 1995. Sperm, a source of estrogen. Environ Healt Perspect 10: 59-62.
Howell A 2006. Pure oestrogen antagonists for thetreatment of advanced breast cancer. Endocrine-Related Cancer 13:689–706.

Idaomar M, Guerin JF, Lorange J, Monchamont P, Cziba JC. 1987. Effects of estradiol and its antagonist-tamoxifen on motility and metabolism of human spermatozoa. Adv contracept 3: 337-41.

Improta-Brears T, Whorton AR, Codazzi F, York JD, Meyer T, McDonnell DP. 1999. Estrogen-induced activation of mitogen-activated protein kinase requires mobilization of intracellular calcium. Proc Natl Acad Sci U S A. 96:4686-91.

Kennedy WP, Kaminski JM, Van der Ven HH, Jeyendran RS, Reid DS, Blackwell J, Bielfeld P, Zaneveld LJ. 1989. A simple, clinical assay to evaluate the acrosin activity of human spermatozoa. J Androl 10:221-231.

Koksal IT, Ishak Y, Usta M, Danisman A, Guntekin E, Bassorgun IC, Ciftcioglu A. 2007. Varicocele-induced testicular dysfunction may be associated with disruption of blood-testis barrier. Arch Androl 53:43-8.

Mohammed A, Chinegwundoh F. 2009. Testicular varicocele: an overview. Urol Int 82:373-9.

Nadal A, Alonso-Magdalena P, Soriano S, Quesada I, Ropero AB. 2009. The pancreatic beta-cell as a target of estrogens and xenoestrogens: Implications for blood glucose homeostasis and diabetes. Mol Cell Endocrinol. 304:63-8.

Nakazumi H, Sasano H, Maehara I, Ozaki M, Tezuka F, Orikasa S. 1996. Estrogen metabolism and impaired spermatogenesis in germ cell tumors of the testis. J Clin Endocrinol Metab 81:1289-95.

Nemoto Y, Toda K, Ono M, Fujikawa-Adachi K, Saibara T, Onishi S, Enzan H, Okada T, Shizuta Y. 2000. Altered expression of fatty acid-metabolizing enzymes in aromatase-deficient mice. J Clin Invest 105:1819-25.

O'Donnel L, Robertson KM, Jones ME, Simpson ER. 2001. Estrogen and spermatogenesis. Endocr rev 22: 289-318.

Osheroff JE, Visconti PE, Valenzuela JP, Travis AJ, Alvarez J, Kopf GS. 1999 Regulation of human sperm capacitation by a cholesterol efflux-stimulated signal transduction pathway leading

to protein kinase A-mediated up-regulation of protein tyrosine phosphorylation. Molecular Human Reproduction 5:1017-1026.

Pallottini V, Bulzomi P, Galluzzo P, Martini C, Marino M. 2008. Estrogen regulation of adipose tissue functions: involvement of estrogen receptor isoforms. Infect Disord Drug Targets 8:52-60.

Panteghini M, Bonora R, Pagani F. 2001. Measurement of pancreatic lipase activity in serum by a kinetic colorimetric assay using a new chromogenic substrate. Ann Clin Biochem 38: 365-370.

Pentikainen V, Erkkila K, Suomalainen L, Parvinen M and Dunkel L.2000 Estradiol Acts as a Germ Cell Survival Factor in the Human Testis *in Vitro*. Journal of Clinical Endocrinology & Metabolism 85:2057-67.

Portuondo JA, Calabozo M, Echanojauregui AD. 1983. Morphology of spermatozoa in infertile men with and without varicocele. J Androl 4:312-5.

Practice Committee of American Society for Reproductive Medicine. 2008. Report on varicocele and infertility. Fertil Steril 90: S247-9.

Prossnitz ER, Arterburn JB, Smith HO, Oprea TI, Sklar LA, Hathaway HJ. 2008. Estrogen signaling through the transmembrane G protein-coupled receptor GPR30. Annu Rev Physiol.70:165-90.

Pryor JL, Howards SS. 1987. Varicocele. Urol Clin North Am 14:499-513.

Puah JA, Bailey CJ. 1985. Effect of ovarian hormones on glucose metabolism in mouse soleus muscle. Endocrinology 117:1336-40.

Razandi M, Pedram A, Greene GL, Levin ER.1999.Cell membrane and nuclear estrogen receptors (ERs) originate from a single transcript: studies of ERalpha and ERbeta expressed in Chinese hamster ovary cells. Mol Endocrinol 2:307-19.

Robertson KM, O'Donnell L, Jones ME, Meachem SJ, Boon WC, Fisher CR, Graves KH, McLachlan RI, Simpson ER. 1999. Impairment of spermatogenesis in mice lacking a functional aromatase (*cyp 19*) gene. Proc Natl Acad Sci USA 96:7986–7991.

Schatz F, Krikun G, Caze R, Rahman M, Lockwood CJ. 2003. Progestin-regulated expression of tissue factor in decidual cells: implications in endometrial hemostasis, menstruation and angiogenesis. Steroids 68:849-860.

Sharpe RM. 1998.The roles of oestrogen in the male. Trends Endocrinol Metab 9:371–376.

Smith EP, Boyd J, Frank GR, Takahashi H, Cohen RM, Specker B, Williams TC, Lubahn DB, Korach KS. 1994. Estrogen resistance caused by a mutation in the estrogen-receptor gene in a man. N Engl J Med 331: 1056–1061.

Travis AJ, Kopf GS. 2002 The role of cholesterol efflux in regulating the fertilization potential of mammalian spermatozoa. Journal Clinical Investigation 110,731–736.

Vedeckis WV, Ali M, Allen HR. 1989. Regulation of glucocorticoid receptor protein and mRNA level. Cancer Res 15:4, 2295s-2302s.

Visconti PE, Galantino-Homer H, Moore GD, Baley JL, Ning X, Fornes M, Kopf GS. 1998. The molecular basis of sperm capacitation. J. Androl 19:242-248.

Vladusic EA, Hornby AE, Guerra-Vladusic FK, Lakins J, Lupu R. 2000. Expression and regulation of estrogen receptor beta in human breast tumors and cell lines. Oncol Rep 7:157-67.

World Health Organization. 1992. The influence of varicocele on parameters of fertility in a large group of men presenting to infertility clinics. Fertil Steril 57:1289-93.

World Health Organization. 2010. WHO laboratory manual for the Examination and processing of human semen. FIFTH EDITION ed. Cambridge University Press: Cambridge, UK.

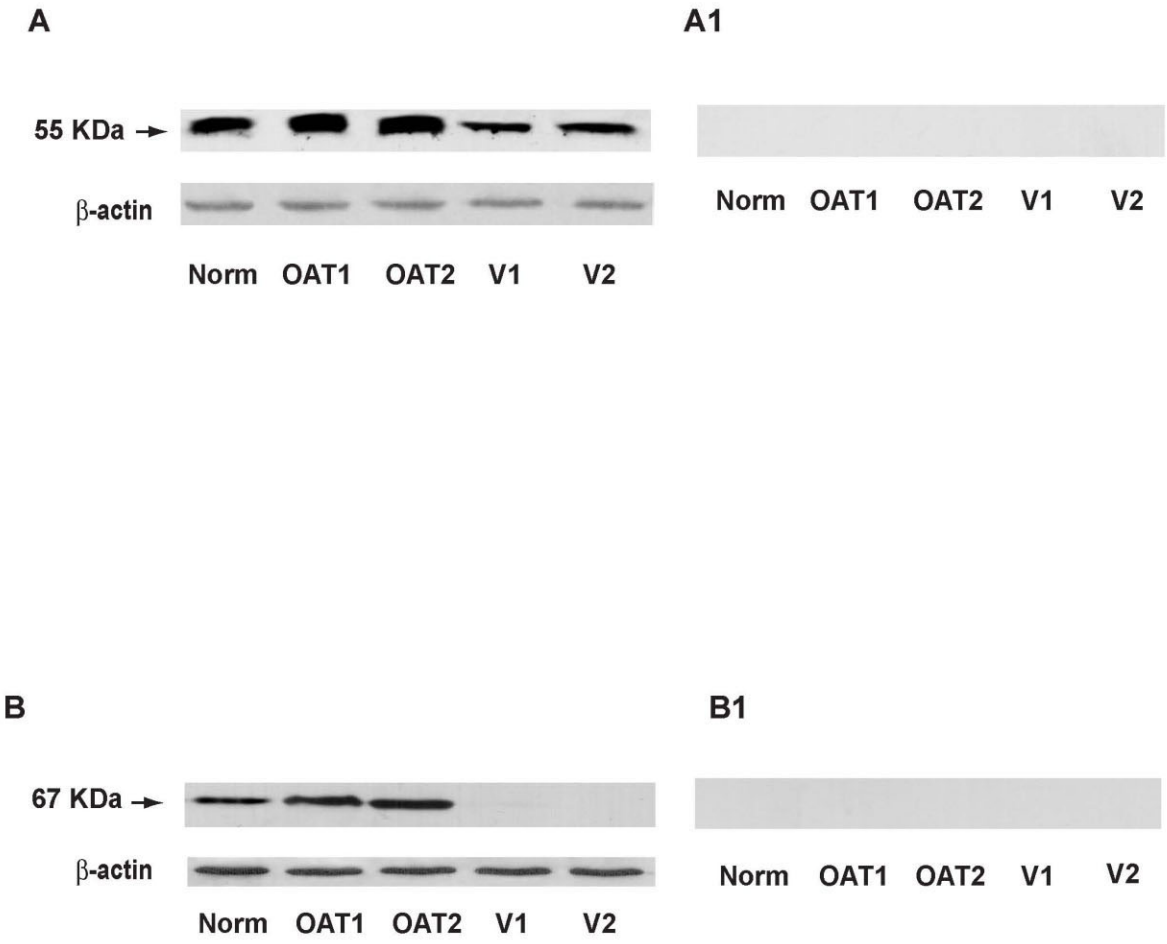

Fig. 1

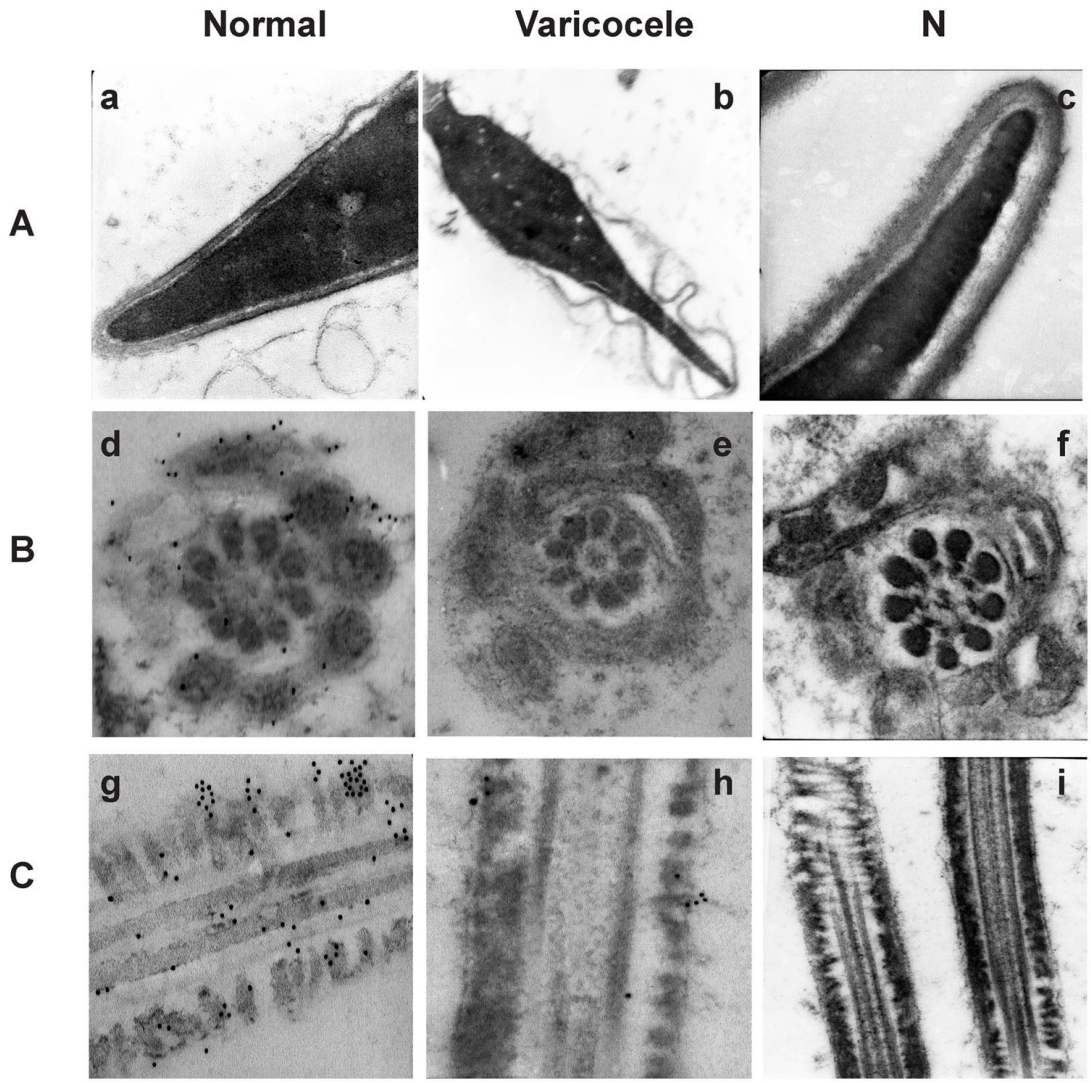

Fig. 2

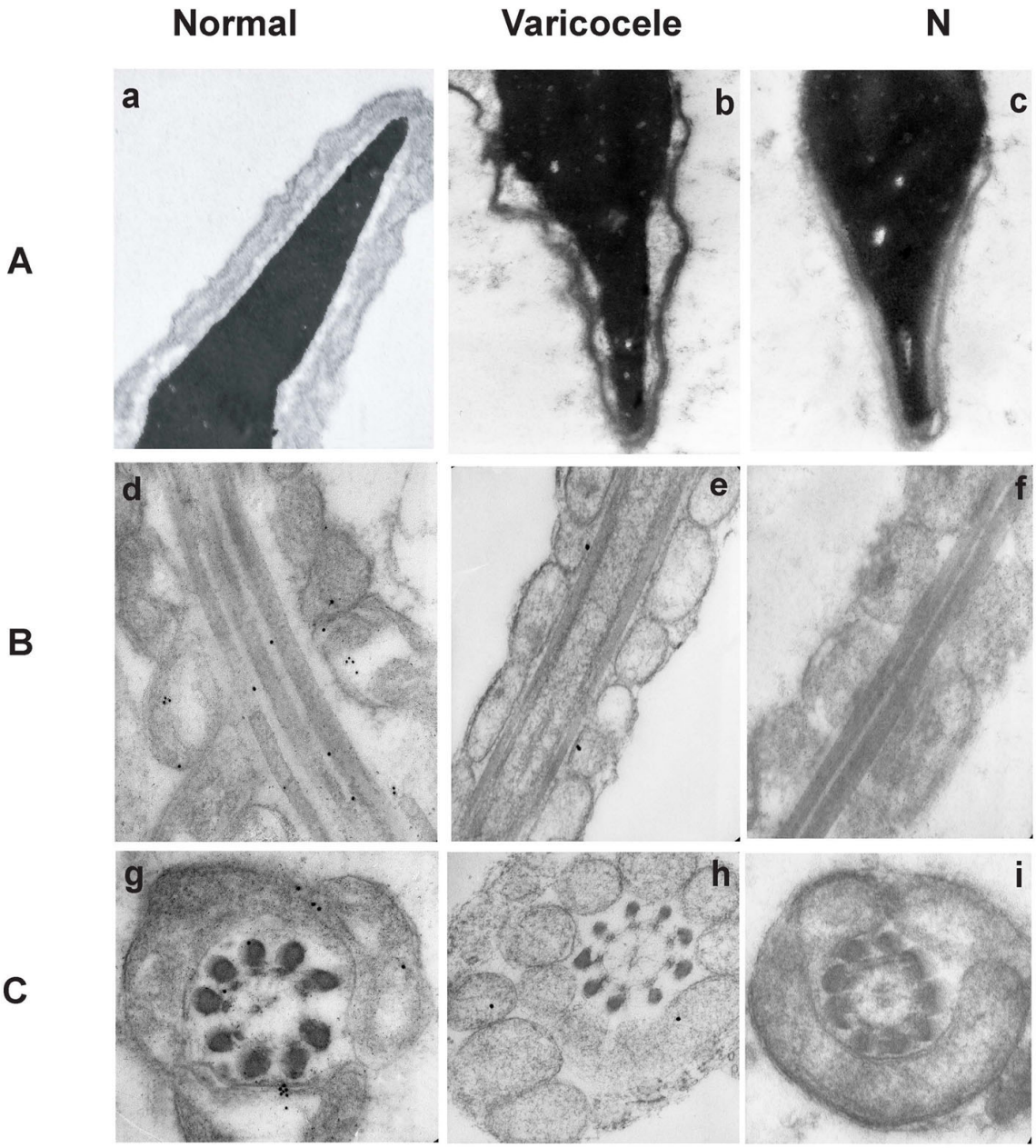

Fig. 3

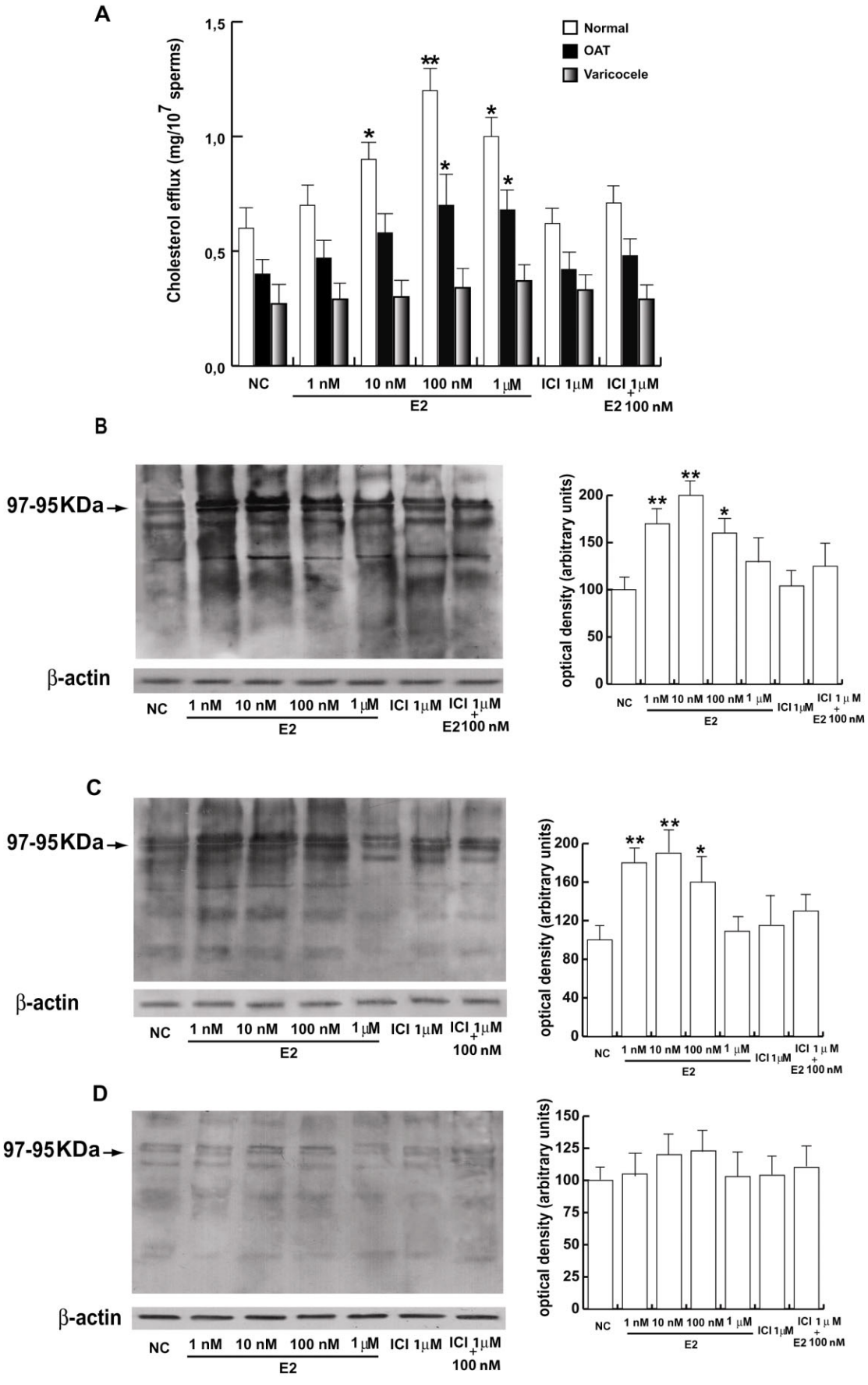

Fig. 4

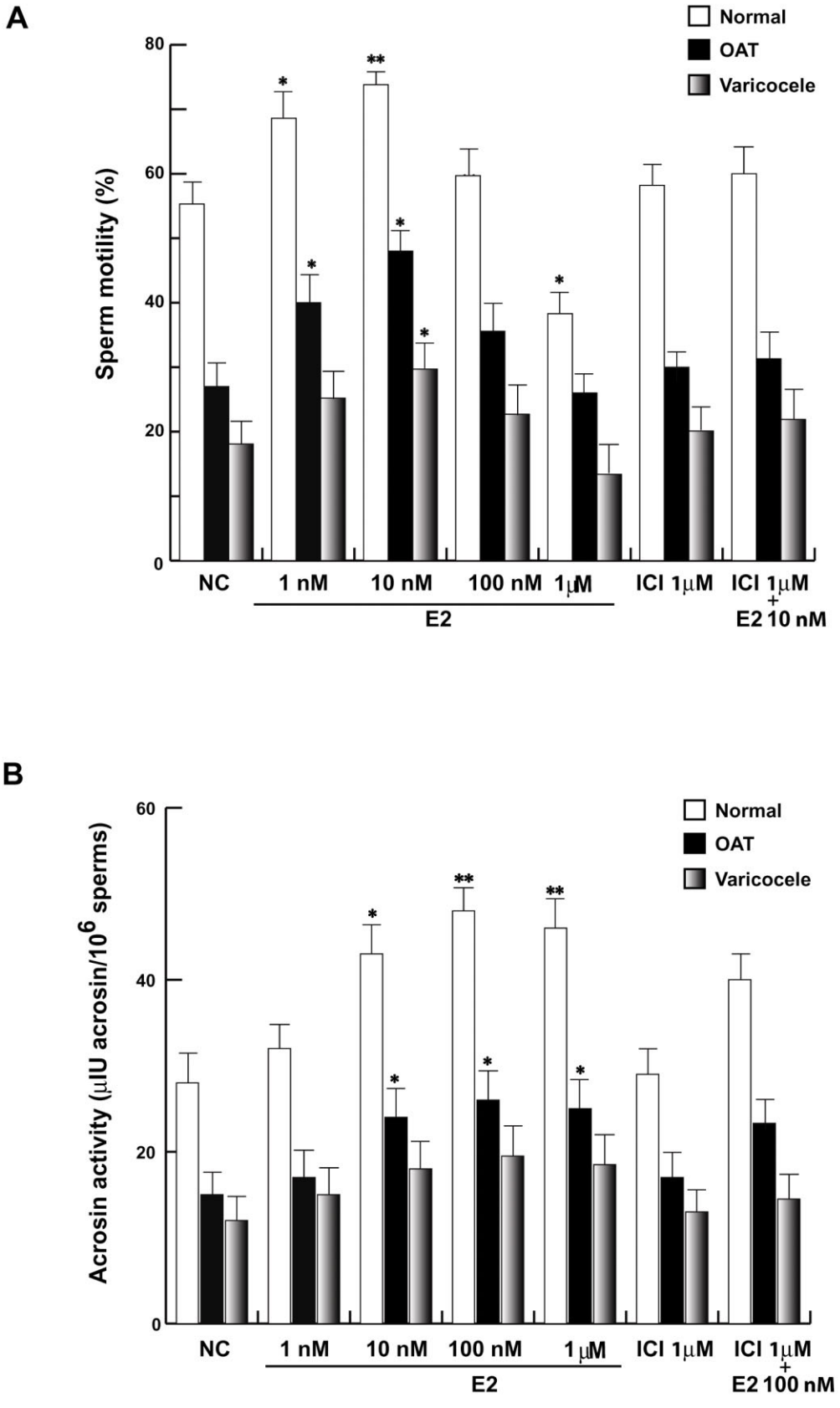

Fig. 5

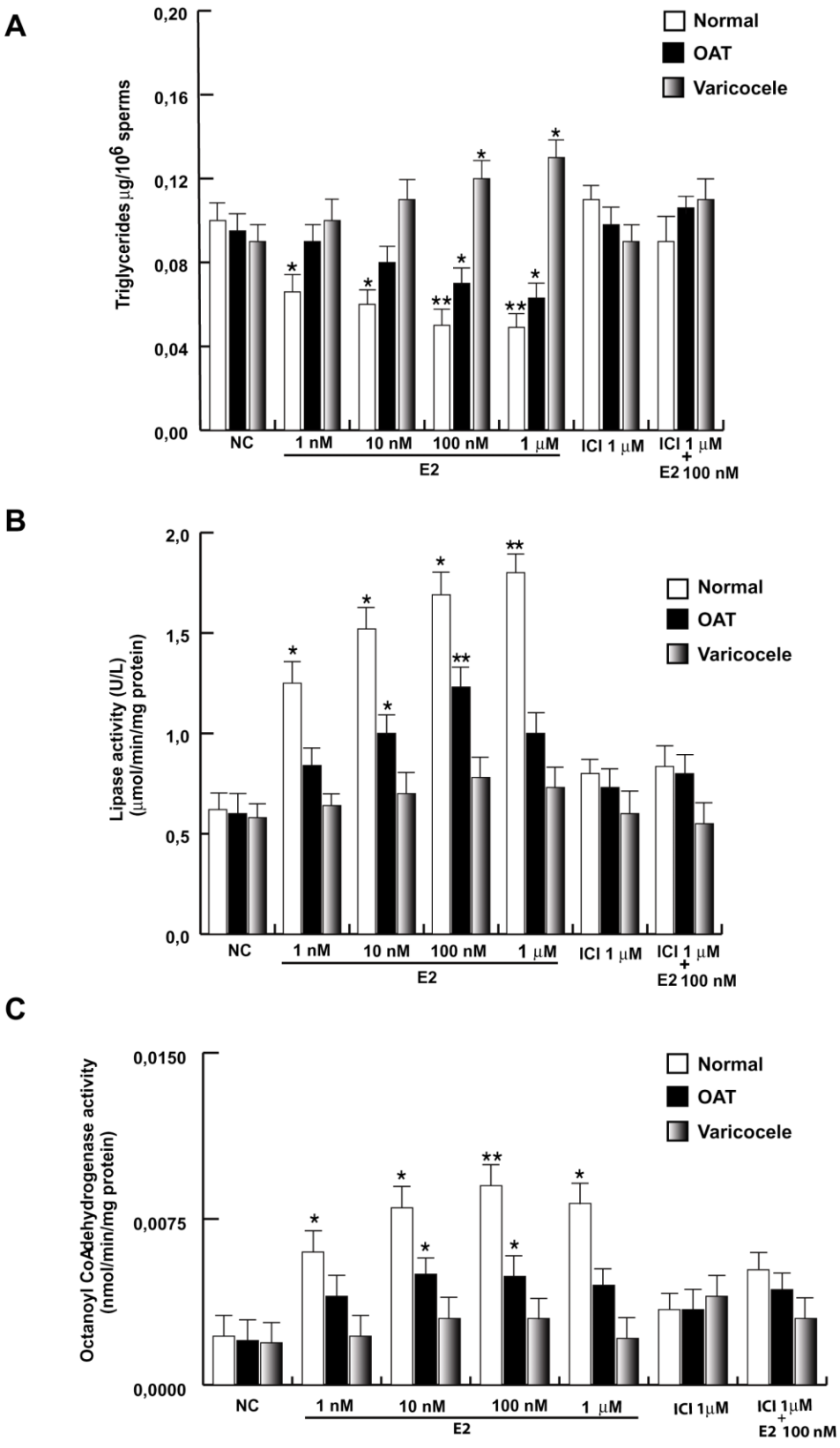

Fig. 6

A

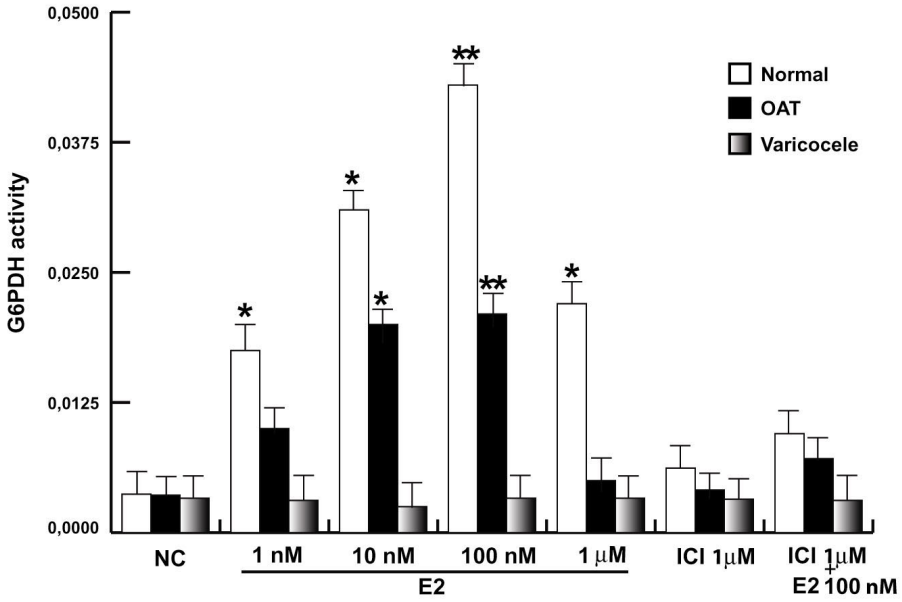

B

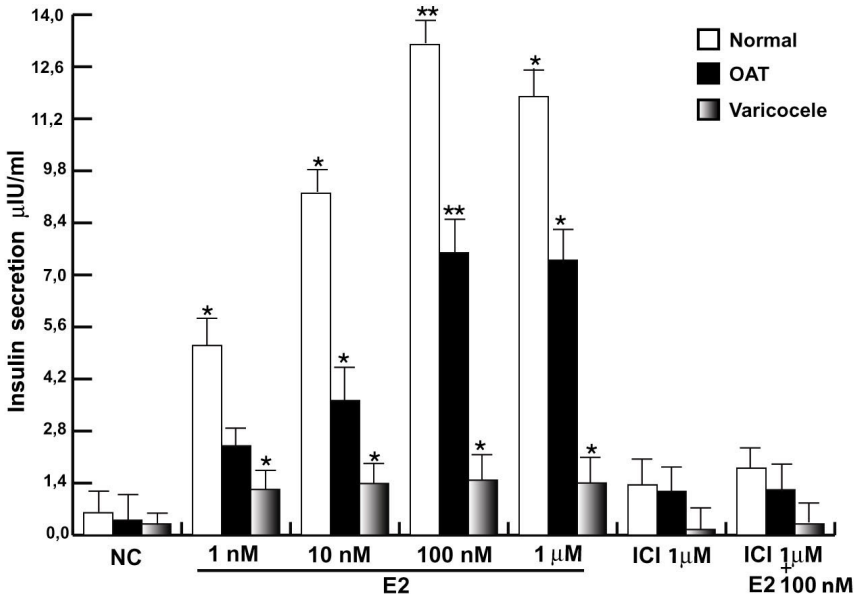

Fig. 7

THE JOURNAL OF BIOLOGICAL CHEMISTRY VOL. 285, NO. 8, pp. 5581–5593, February 19, 2010

Farnesoid X Receptor, through the Binding with Steroidogenic Factor 1-responsive Element, Inhibits Aromatase Expression in Tumor Leydig Cells*[S]

Received for publication, August 5, 2009, and in revised form, December 17, 2009 Published, JBC Papers in Press, December 21, 2009, DOI 10.1074/jbc.M109.052670

Stefania Catalano[‡1], Rocco Malivindi[‡1], Cinzia Giordano[‡§], Guowei Gu[‡], Salvatore Panza[‡], Daniela Bonofiglio[‡], Marilena Lanzino[‡], Diego Sisci[‡], Maria Luisa Panno[¶], and Sebastiano Andò[§¶2]

From the Departments of [‡]Pharmaco-Biology and [¶]Cell Biology and [§]Centro Sanitario, University of Calabria, 87030 Arcavacata di Rende (CS), Italy

The farnesoid X receptor (FXR) is a member of the nuclear receptor superfamily that regulates bile acid homeostasis. It is expressed in the liver and the gastrointestinal tract, but also in several non-enterohepatic tissues including testis. Recently, FXR was identified as a negative modulator of the androgen-estrogen-converting aromatase enzyme in human breast cancer cells. In the present study we detected the expression of FXR in Leydig normal and tumor cell lines and in rat testes tissue. We found, in rat Leydig tumor cells, R2C, that FXR activation by the primary bile acid chenodeoxycholic acid (CDCA) or a synthetic agonist GW4064, through a SHP-independent mechanism, down-regulates aromatase expression in terms of mRNA, protein levels, and its enzymatic activity. Transient transfection experiments, using vector containing rat aromatase promoter PII, evidenced that CDCA reduces basal aromatase promoter activity. Mutagenesis studies, electrophoretic mobility shift, and chromatin immunoprecipitation analysis reveal that FXR is able to compete with steroidogenic factor 1 in binding to a common sequence present in the aromatase promoter region interfering negatively with its activity. Finally, the FXR-mediated anti-proliferative effects exerted by CDCA on tumor Leydig cells are at least in part due to an inhibition of estrogen-dependent cell growth. In conclusion our findings identify for the first time the activators of FXR as negative modulators of the aromatase enzyme in Leydig tumor cell lines.

The farnesoid X receptor (FXR)[3] (NR1H4) is a member of the nuclear receptor superfamily of ligand-dependent transcription factors, normally produced in the liver and the gastrointestinal tract, where it acts as a bile acid sensor (1–3). FXR regulates the expression of a wide variety of target genes involved in bile acid, lipid, and glucose metabolism by binding either as monomer or as a heterodimer with the retinoid X receptor (RXR) to FXR response element (FXREs) (4–7). FXR induces the up-regulation of nuclear receptor SHP (small heterodimer partner), which interacts with other nuclear receptors preventing their activation (8–10).

Recently, new functions of FXR beyond its roles in metabolism were discovered in several nonenterohepatic tissues, including its control in regulating cell growth and carcinogenesis (11–14). For instance, it has been demonstrated that FXR activation inhibits breast cancer cell proliferation and negatively regulates aromatase activity reducing local estrogen production, which sustains tumor growth and progression (13).

Estrogen dependence is also a feature of testicular tumor, which is the most frequent solid malignant tumor diagnosed in young men (20–40 years old) accounting for up to 20% of all malignancies diagnosed at this age. Ninety-five percent of all human testicular neoplasms arise from germinal cells, whereas Leydig cell tumors are the most common tumors of the gonadal stroma (15). The molecular basis of testicular cell malignant transformation is poorly defined. It has been reported that estrogen serum levels are elevated in patients with testicular germ cell cancer as a consequence of increased local estrogen production reflecting an higher aromatase activity present in Sertoli and Leydig cells (16). Several studies on both rodents and humans indicate that prenatal, early postnatal, and adult exposure to an excess of estrogens might have a central role in the mechanism leading to male reproductive tract malformations such as testicular and prostatic tumors (17). The biological significance of estrogen-induced testicular tumorogenesis has been suggested by transgenic mice overexpressing aromatase and exhibiting enhancement of 17β-estradiol (E2) circulating levels (18). About half of these male mice were infertile and/or had enlarged testis and showed Leydig cell hyperplasia and Leydig cell tumors (18). Recently, we demonstrated aromatase and ERs expression in testis from patients affected by Leydigioma in which high estradiol levels in the presence of ERα could significantly contribute to tumor cell growth and progression (19). Besides, we also reported that one of the molecular mechanisms determining Leydig cell tumorogenesis is an excessive estrogen produc-

* This work was supported by PRIN-MIUR (Programmi di Ricerca Scientifica di Rilevante Interesse Nazionale-Ministero dell'Istruzione dell'Università della Ricerca) and Associazione Italiana per la Ricerca sul Cancro (AIRC).
[S] The on-line version of this article (available at http://www.jbc.org) contains supplemental Fig. S1.
[1] Both authors contributed equally to this work.
[2] To whom correspondence should be addressed. Tel.: 39-0984-496201; Fax: 39-0984-496203; E-mail: sebastiano.ando@unical.it.
[3] The abbreviations used are: FXR, farnesoid X receptor; RXR, retinoid X receptor; FXRE, FXR response element; SHP, small heterodimer partner; E2, 17β-estradiol; CDCA, chenodeoxycholic acid; FBS, fetal bovine serum; RNAi, RNA interference; FXRE-IR1, FXR-responsive reporter gene; AD, androst-4-ene-3,17-dione; ER, estrogen receptor; LRH-1, liver receptor homolog-1; CRE, cAMP response element; CREB, cAMP response element-binding protein; SF-1, steroidogenic factor 1; GAPDH, glyceraldehyde-3-phosphate dehydrogenase; siRNA, small interfering RNA; ChIP, chromatin immunoprecipitation; PII, promoter II; DN, dominant negative.

tion that stimulates a short autocrine loop determining cell proliferation (20).

Aromatase activity is regulated primarily at the level of gene expression by tissue-specific promoters and is present in testicular somatic cells and along the maturative phases of male germ cells (21, 22). A promoter proximal to the translation start site, called promoter II (PII) regulates aromatase expression in fetal and adult testis, R2C and H540 rat Leydig tumor cells, and in purified preparations of rat Leydig, Sertoli, and germ cells (23, 24). Specific sequences seem to be mainly involved in aromatase expression: cAMP-responsive element (CRE)-like sequences binding CREB/ATF protein families (25, 26) and a sequence containing half-site binding nuclear receptors (AGGTCA) in position −90 binding steroidogenic factor 1 (SF-1) (27), which is essential for sex differentiation and development of gonads (28).

On the basis of all these observations, in this study we investigated in rat tumor Leydig cells R2C whether FXR activation by specific ligand chenodeoxycholic acid (CDCA) or a synthetic agonist GW4064 may modulate aromatase expression and antagonize estrogen signaling, inhibiting testicular tumor growth and progression. We demonstrated that the molecular mechanism by which FXR ligands inhibit aromatase gene expression in R2C cells is mediated by a direct binding of FXR to the SF-1 response element present in the aromatase promoter region.

EXPERIMENTAL PROCEDURES

Reagents—Nutrient mixture Ham's F-10, Dulbecco's modified Eagle's medium/Ham's F-12 nutrient mixture, Dulbecco's modified Eagle's medium, L-glutamine, penicillin, streptomycin, fetal bovine serum (FBS), horse serum, phosphate-buffered saline, aprotinin, leupeptin, phenylmethylsulfonyl fluoride, bovine serum albumin, and sodium orthovanadate were purchased by Sigma. TRIzol and Lipofectamine 2000 were from Invitrogen and FuGENE 6 by Roche Applied Science. *Taq* DNA polymerase, RETROscript kit, 100-bp DNA ladder, Dual Luciferase kit, TnT master mixture, and thymidine kinase *Renilla* luciferase plasmid were provided by Promega (Madison, WI). SYBR Green Universal PCR Master Mix was from Bio-Rad. Antibodies against FXR, β-actin, GAPDH, cyclin D1, cyclin E, and lamin B were from Santa Cruz Biotechnology (Santa Cruz, CA), antibody against Aromatase from Serotec (Raleigh, NC), antibody against SF-1 was kindly provided from Dr. K. Morohashi (National Institute Basic Biology, Myodaiji-cho, Okazaki, Japan), and anti-LRH-1 antibody was kindly provided by Dr. Luc Belanger (Laval University, Quebec, Canada). The ECL system and Sephadex G-50 spin columns were from Amersham Biosciences. [1β-^{3}H]Androst-4-ene-3,17-dione, [γ-^{32}P]ATP, and [^{3}H]thymidine were from PerkinElmer Life Sciences. Salmon sperm DNA/protein A-agarose was from UBI (Chicago, IL).

Plasmids—The plasmids containing different segments of the rat aromatase PII sequence ligated to a luciferase reporter gene (−1037/+94 (p-1037), −688/+94 (p-688), −475/+94 (p-475), −183/+94 (p-183), and −688/+94 mut (p-688m) (SF-1 site mutant)) were previously described (27). The FXR-responsive reporter gene (FXRE-IR1) and FXR-DN (dominant negative) expression plasmids were provided by Dr. T. A. Kocarek (Institute of Environmental Health Sciences, Wayne State University) (29). The FXR expression plasmid was provided by Dr. D. J. Mangelsdorf (Southwestern Medical Center, TX). SF-1 expression plasmid and the *CYP17* gene reporter were obtained from Dr. W. E. Rainey (Medical College of Georgia). XETL plasmid is a construct containing an estrogen-responsive element from the *Xenopus* vitellogenin promoter, driving expression of the luciferase gene.

Cell Cultures and Animals—Rat Leydig tumor cells (R2C) were cultured in Ham's F-10 supplemented with 15% horse serum, 2.5% FBS, and antibiotics. Mouse Leydig cells (TM3) were cultured in Dulbecco's modified Eagle's medium/Ham's F-12 supplemented with 5% horse serum, 2.5% FBS, and antibiotics. Human cervix tumor cells (HeLa) and hepatoma cells (HepG2) were cultured in Dulbecco's modified Eagle's medium supplemented with 10% FBS, 1% L-glutamine and antibiotics. The cells were starved in serum-free medium 24 h before treatments. Male Fisher 344 rats (a generous gift of Sigma-Tau), 6 (FRN) and 24 (FRT) months of age, were used for studies. Twenty-four-month-old animals presented spontaneously developed Leydig cell tumors, which were absent in younger animals. Testes of all animals were surgically removed by qualified, specialized animal care staff in accordance with the Guide for Care and Use of Laboratory Animals (NIH) and used for experiments.

Aromatase Activity Assay—The aromatase activity in subconfluent R2C cells culture medium was measured by the tritiated water release assay using 0.5 μM [1β-^{3}H]androst-4-ene-3,17-dione as substrate (30). The incubations were performed at 37 °C for 2 h under an air/CO_2 (5%) atmosphere. The results obtained were expressed as picomole/h and normalized to mg of protein (pmol/h/mg of protein).

Total RNA Extraction and Reverse Transcription-PCR Assay—Total RNA was extracted from R2C and TM3 cells using TRIzol reagent and evaluation of gene expression was performed by the reverse transcription-PCR method using a RETROscript kit. The cDNAs obtained were amplified by PCR using the following primers: forward 5′-CAGCTATACTGAAGGAATCCACACTGT-3′ and reverse 5′-AATCGTTTCAAAAGTGTAACCAGGA-3′ (P450 aromatase); forward 5′-TTTCTACCCGCAACAACCGGAA-3′ and reverse 5′-GTGACAAAGAAGCCGCGAATGG-3′ (FXR); forward 5′-CAGCCACCAGACCCACCACAA-3′ and reverse 5′-GAGGCACCGGACCCCATTCTA-3′ (rat-SHP); forward 5′-CGTCCGACTATTCTGTATGC-3′ and reverse 5′-CTTCCTCTAGCAGGATCTTC-3′ (mouse-SHP); or forward 5′-GAAATCGCCAATGCCAACTC-3′ and reverse 5′-ACCTTCAGGTACAGGCTGTG-3′ (L19). The PCR was performed for 25 cycles for P450 aromatase (94 °C for 1 min, 58 °C for 1 min, and 72 °C for 2 min), 35 cycles for FXR (94 °C for 1 min, 65 °C for 1 min, and 72 °C for 2 min), 28 cycles for SHP (94 °C for 1 min, 65 °C for 1 min, and 72 °C for 2 min), and 25 cycles for L19 (94 °C for 1 min, 60 °C for 1 min, and 72 °C for 2 min) in the presence of 1 μl of first strand cDNA, 1 μM each of the primers, 0.5 mM dNTP, *Taq* DNA polymerase (2 units/tube), and 2.2 mM magnesium chloride in a final volume of 25 μl. DNA quantity in each lane was analyzed by scanning densitometry.

Immunoblot Analysis—R2C, TM3, HepG2 cells, or total tissue of FRNT and FRTT were lysed in 500 μl of 50 mM Tris-HCl, 150 mM NaCl, 1% Nonidet P-40, 0.5% sodium deoxycholate, 2 mM sodium fluoride, 2 mM EDTA, 0.1% SDS, containing a mixture of protease inhibitors (aprotinin, phenylmethylsulfonyl fluoride, and sodium orthovanadate) for protein extraction. Nuclear extracts were prepared as previously described (31). Equal amounts of proteins were resolved on a 11% SDS-polyacrylamide gel, transferred to a nitrocellulose membrane, and probed with FXR, aromatase, cyclin D1, and cyclin E antibodies. To ensure equal loading all membranes were stripped and incubated with anti-lamin B antibody for nuclear extracts or anti-GADPH and anti-β-actin antibodies for total extracts. The antigen-antibody complex was detected by incubation of the membranes with peroxidase-coupled goat anti-mouse, goat anti-rabbit, or donkey anti-goat IgG and revealed using the ECL system. The bands of interest were quantified by the Scion Image laser densitometry scanning program.

Immunofluorescence—R2C cells seeded on glass coverslips were treated with 50 and 100 μM CDCA for 24 h, washed with PBS, and then fixed with 4% paraformaldehyde in PBS for 20 min at room temperature. Next, cells were permeabilized with 0.2% Triton X-100 in PBS for 5 min, blocked with 5% bovine serum albumin for 30 min, and incubated overnight with anti-aromatase antibody (1:100) in PBS overnight at 4 °C. The day after the cells were washed three times with PBS and incubated with the secondary antibody anti-mouse IgG-fluorescein isothiocyanate (1:200) for 1 h at room temperature. To check the specificity of immunolabeling the primary antibody was replaced by normal mouse serum (negative control). Immunofluorescence analysis was carried out on a OLYMPUS BX51 microscope using a ×40 objective.

Transient Transfection Assay—R2C cells were transiently transfected using FuGENE 6 reagent with the FXR reporter gene (FXRE-IR1) in the presence or absence of FXR-DN or XETL plasmid. A set of experiments was performed transfecting rat aromatase PII constructs *p*-1037, *p*-688, *p*-475, *p*-183, and *p*-688m. HeLa cells were transiently cotransfected with the *CYP17* gene promoter and FXR or SF-1 expression plasmids. After transfection, R2C and HeLa cells were treated with 50 μM CDCA or 3 μM GW4064 for 24 h. Empty vectors were used to ensure that DNA concentrations were constant in each transfection. Thymidine kinase *Renilla* luciferase plasmid was used to normalize the efficiency of the transfection. Firefly and *Renilla* luciferase activities were measured by the Dual Luciferase kit. The firefly luciferase data for each sample were normalized based on transfection efficiency measured by *Renilla* luciferase activity.

RNA Interference (RNAi)—R2C cells were transfected with the RNA duplex of the stealth RNAi targeted rat SHP mRNA sequence, 5′-ACUGAACUGCUUGAAGACAUGCUUU-3′, with RNA duplex of stealth RNAi targeted for the rat FXR mRNA sequence, 5-UCUGCAAGAUCUACCAGCCCGAGAA-3 (Invitrogen), with RNA duplex of the validated RNAi-targeted rat aromatase mRNA sequence, 5-GCUCAUCUUCCAUACCAGGtt-3 (Ambion), or with a stealth RNAi control to a final concentration of 50 nM using Lipofectamine 2000 as recommended by the manufacturer. After 5 h the transfection medium was changed with serum-free medium and then the cells were exposed to treatments.

Electrophoretic Mobility Shift Assay—Nuclear extracts from R2C cells were prepared as previously described (31). The probe was generated by annealing single-stranded oligonucleotides, labeled with [γ-^{32}P]ATP using T4 polynucleotide kinase, and purified using Sephadex G-50 spin columns. The DNA sequences used as probe or as cold competitors were (nucleotide motifs of interest are underlined and mutations are shown as lowercase letters): SF-1, CAGGACCTGAGTCTCCCAAGGTCATCCTTGTTTGACTTGTA; and mutated SF-1, TCTCCCAAtaTCATCCTTGT. *In vitro* transcribed and translated SF-1 and FXR proteins were synthesized using the T7 polymerase in the rabbit reticulocyte lysate system. The protein-binding reactions were carried out in 20 μl of buffer (20 mmol/liter of HEPES (pH 8), 1 mmol/liter of EDTA, 50 mmol/liter of KCl, 10 mmol/liter of dithiothreitol, 10% glycerol, 1 mg/ml of bovine serum albumin, 50 μg/ml of poly(dI-dC)) with 50,000 cpm of labeled probe, 20 μg of R2C nuclear protein, or an appropriate amount of SF-1 or FXR proteins and 5 μg of poly(dI-dC). The mixtures were incubated at room temperature for 20 min in the presence or absence of unlabeled competitor oligonucleotides. For experiments involving anti-SF-1 and anti-FXR antibodies, the reaction mixture was incubated with these antibodies at 4 °C for 12 h before addition of labeled probe. The entire reaction mixture was electrophoresed through a 6% polyacrylamide gel in 0.25 × Tris borate-EDTA for 3 h at 150 V.

Chromatin Immunoprecipitation and Re-ChIP Assays—R2C cells were treated with 50 μM CDCA for 1 h and then cross-linked with 1% formaldehyde and sonicated. Supernatants were immunocleared with salmon sperm DNA/protein A-agarose for 1 h at 4 °C. The precleared chromatin was immunoprecipitated with specific anti-FXR or anti-polymerase II antibodies, and re-immunoprecipitated with anti-SF-1 or anti-LRH-1 antibodies. A normal mouse serum IgG was used as negative control. Pellets were washed as reported, eluted with elution buffer (1% SDS, 0.1 M $NaHCO_3$), and digested with proteinase K. DNA was obtained by phenol/chloroform/isoamyl alcohol extractions and precipitated with ethanol; 3 μl of each sample were used for PCR amplification with the primers flanking the SF-1 sequence present in the P450arom PII promoter region: 5′-ATGCACGTCACTCTACCCACTCAA-3′ and 5′-TAGCACGCAAAGCAGTAGTTTGGC-3′ and 5-CAGAGGAGAACAGGAAGAGTG-3 and 5-TGATAACGACTCCAGCGTCTT-3 upstream of the SF-1 site. The amplification products were analyzed in a 2% agarose gel and visualized by ethidium bromide staining. Moreover, a 5-μl volume of each sample and input were used for real time PCR.

PCR were performed in the iCycler iQ Detection System (Bio-Rad), using 0.1 μM of each primer, in a total volume of 50 μl of reaction mixture following the manufacturer's recommendations. SYBR Green Universal PCR Master Mix with the dissociation protocol was used for gene amplification. Negative controls contained water instead of DNA. Final results were calculated using the DDC_t method as previously reported (20), using input C_t values instead of the 18 S. The basal sample was used as calibrator.

[^{3}H]Thymidine Incorporation—R2C cells were treated with 50 and 100 μM CDCA for 24 and 48 h, respectively. For the last 6 h, [^{3}H]thymidine (1 μCi/ml) was added to the culture medium. After rinsing with PBS, the cells were washed once with 10% and three times with 5% trichloroacetic acid, lysed by adding 0.1 N NaOH, and then incubated for 30 min at 37 °C. Thymidine incorporation was determined by scintillation counting. In other experiments R2C cells were transiently transfected with FXR-DN expression plasmid or transfected with siRNA for FXR or aromatase before starting with the same treatments mentioned above.

Anchorage-independent Soft Agar Growth Assays—R2C cells were plated in 4 ml of Ham's F-10 with 0.5% agarose and 5% charcoal-stripped FBS, in 0.7% agarose base in six-well plates. Two days after plating, medium containing hormonal treatments (androst-4-ene-3,17-dione and CDCA) was added to the top layer, and the appropriate medium was replaced every 2 days. After 14 days, 150 μl of 3-(4,5-dimethylthiazol-2-yl)-2,5-diphenyltetrazolium bromide was added to each well and allowed to incubate at 37 °C for 4 h. Plates were then placed at 4 °C overnight and colonies >50 μm diameter from triplicate assays were counted. Data are the mean colony number of three plates and representative of two independent experiments.

Statistical Analysis—Each data point represents the mean ± S.D. of three different experiments. Statistical analysis was performed using analysis of variance followed by Newman-Keuls testing to determine differences in means. $p < 0.05$ was considered as statistically significant.

RESULTS

FXR Expression in Normal and Tumor Testicular Cells—We first aimed to evaluate, by Western blotting analysis, the expression of FXR receptor in Leydig normal (TM3) and tumor (R2C) cell lines and in testes tissue from younger (FRNT) and older (FRTT) Fisher rats. The latter group have a high incidence of spontaneous Leydig cell neoplasma (32, 33), a phenomenon not observed in younger animals. Immunoblot analysis revealed the presence of a FXR-immunoreactive protein band at ~60 kDa in all samples examined, particularly, the FXR receptor seems to be more expressed in R2C cells with respect to TM3 and in FRTT with respect to its control FRNT (Fig. 1*A*). Human hepatocyte cells (HepG2) were used as a positive control for FXR expression. In R2C cells, incubation for 24 h with 50 and 100 μM CDCA, a natural ligand of FXR, increased the level of the receptor at both mRNA and protein levels (Fig. 1, *B* and *C*). Because CDCA may also exert FXR-independent effects (34), the influence of GW4064, a synthetic FXR agonist, was also investigated. We observed that GW4064 (3 μM) increased FXR mRNA and protein levels to a similar order of magnitude as CDCA (Fig. 1, *B* and *C*). Moreover, to assess the ability of CDCA and GW4064 to transactivate endogenous FXR, we transiently transfected R2C cells with the FXR-responsive reporter gene (FXRE-IR1). As reported in Fig. 1*D*, CDCA and GW4064 induced a significant enhancement in transcriptional activation of the reporter plasmid to a higher extent under GW treatment. In the presence of dominant negative FXR the GW-induced transactivation was completely abrogated.

Inhibitory Effects of FXR Agonists on Aromatase Expression in R2C Cells—Starting from previous findings showing that FXR activation represses aromatase expression in breast cancer cells (13) we investigated the ability of FXR agonists to modulate aromatase enzyme in R2C cells that have been shown to have high aromatase expression and activity (27). Treatment with 50 and 100 μM CDCA for 24 h showed a down-regulation of aromatase mRNA and protein content in a dose related manner (Figs. 2, *A* and *B*). Similar results were observed upon treatment with GW4064 (3 μM) for 24 h (Fig. 2, *A* and *B*). The down-regulatory effects of CDCA on the expression of aromatase was further confirmed by immunofluorescence analysis. The strong P450 aromatase immunoreactivity was detected in the cytoplasm as well as in the perinuclear region of untreated R2C cells and was drastically decreased upon CDCA at the doses of 50 and 100 μM for 24 h (Fig. 2*C*). Next, we evaluated the effects of CDCA on aromatase enzymatic activity by tritiated water release assay. As reported in Fig. 2*D*, exposure to 50 and 100 μM CDCA for 24 h reduced enzymatic activity in a dose-dependent manner in R2C cells.

A direct involvement of FXR in modulating aromatase expression was provided by the evaluation of aromatase mRNA, protein content, and its enzymatic activity after knocking down FXR in R2C cells with a specific siRNA. In preliminary experiments we evaluated, after 24, 48, and 72 h of siRNA transfection, that FXR protein expression was effectively silenced as revealed by Western blotting (Fig. 3*A*). As shown in Fig. 3, *B–D*, silencing the FXR gene reversed the down-regulatory effects induced by CDCA on aromatase expression and its enzymatic activity, whereas no change was observed after transfection of cells with scramble siRNA upon identical experimental conditions.

SHP Is Not Involved in the Down-regulatory Effects Induced by FXR Ligand on Aromatase—Induction of SHP expression is considered one of the canonical features of FXR transactivation. SHP has been shown to be expressed in the interstitial compartment of the adult testis, including steroidogenic Leydig cells (35).

We evidenced that SHP mRNA expression was significantly higher in R2C cells compared with very low levels detected in the TM3 cell line, but administration of CDCA or GW4064 did not induce an increase of SHP mRNA in both cell lines (data not shown). However, to explore the role of SHP in CDCA-mediated repression of the aromatase gene, we knocked SHP by siRNA. SHP mRNA expression was effectively silenced as revealed by reverse transcription-PCR after 24, 48, and 72 h of siRNA transfection (Fig. 4*A*). As shown in Fig. 4, *B* and *C*, silencing of the SHP gene failed to reverse the inhibition of aromatase expression induced by the specific FXR ligand in R2C cells ruling out any SHP involvement in the inhibitory effects of CDCA on aromatase expression.

CDCA Down-regulates Aromatase Promoter Activity through SF-1 Site—The aforementioned observations led us to ascertain if the down-regulatory effects of CDCA on aromatase expression were due to its direct inhibitory influence in regulating aromatase gene transcriptional activity. Thus, we transiently transfected in R2C cells plasmids containing different segments of rat PII aromatase (Fig. 5*A*). A significant reduction of pro-

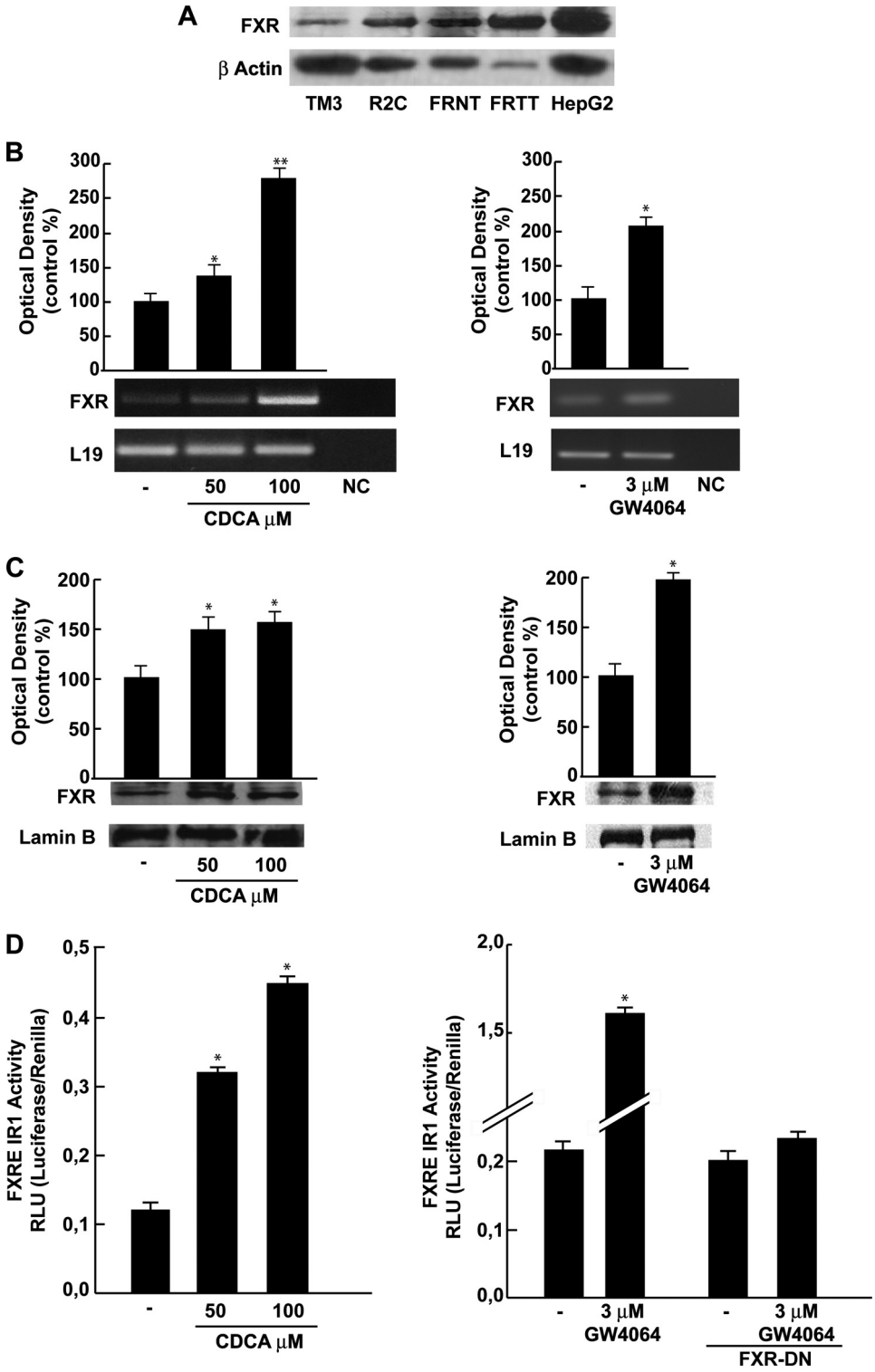

FIGURE 1. **FXR expression and activation in R2C cells.** *A*, Western blot analysis of FXR was done on 50 μg of total proteins extracted from normal (*TM3*), tumor Leydig cells (*R2C*), and human hepatocytes cells (*HepG2*), or from tissues of normal (*FRNT*) and tumor (*FRTT*) Fisher rat testes. β-Actin was used as a loading control. *B*, total RNA was extracted from R2C cells treated with vehicle (−) or 50 and 100 μM CDCA or 3 μM GW4064 for 24 h and reverse transcribed. cDNA was subjected to PCR using primers specific for FXR or L19 (ribosomal protein). *NC*, negative control, RNA sample without the addition of reverse transcriptase. The histograms represent the mean ± S.D. (*error bars*) of three separate experiments in which band intensities were evaluated in terms of optical density arbitrary units and expressed as percentages of the control, which was assumed to be 100%. *, $p < 0.05$; **, $p < 0.01$ compared with vehicle. *C*, nuclear proteins were extracted from R2C cells treated with vehicle (−), 50 and 100 μM CDCA, or 3 μM GW4064 for 24 h and then Western blotting analysis was performed using anti-FXR antibody. Lamin B was used as loading control. The histograms represent the mean ± S.D. of three separate experiments in which band intensities were evaluated in terms of optical density arbitrary units and expressed as percentages of the control, which was assumed to be 100%. *, $p < 0.05$ compared with vehicle. *D*, R2C cells were transiently transfected with the FXR reporter gene (FXRE-IR1) and treated as reported above or co-transfected with FXR-DN and treated with vehicle (−) or 3 μM GW4064. The values represent the mean ± S.D. of three different experiments performed in triplicate. *, $p < 0.01$ compared with vehicle.

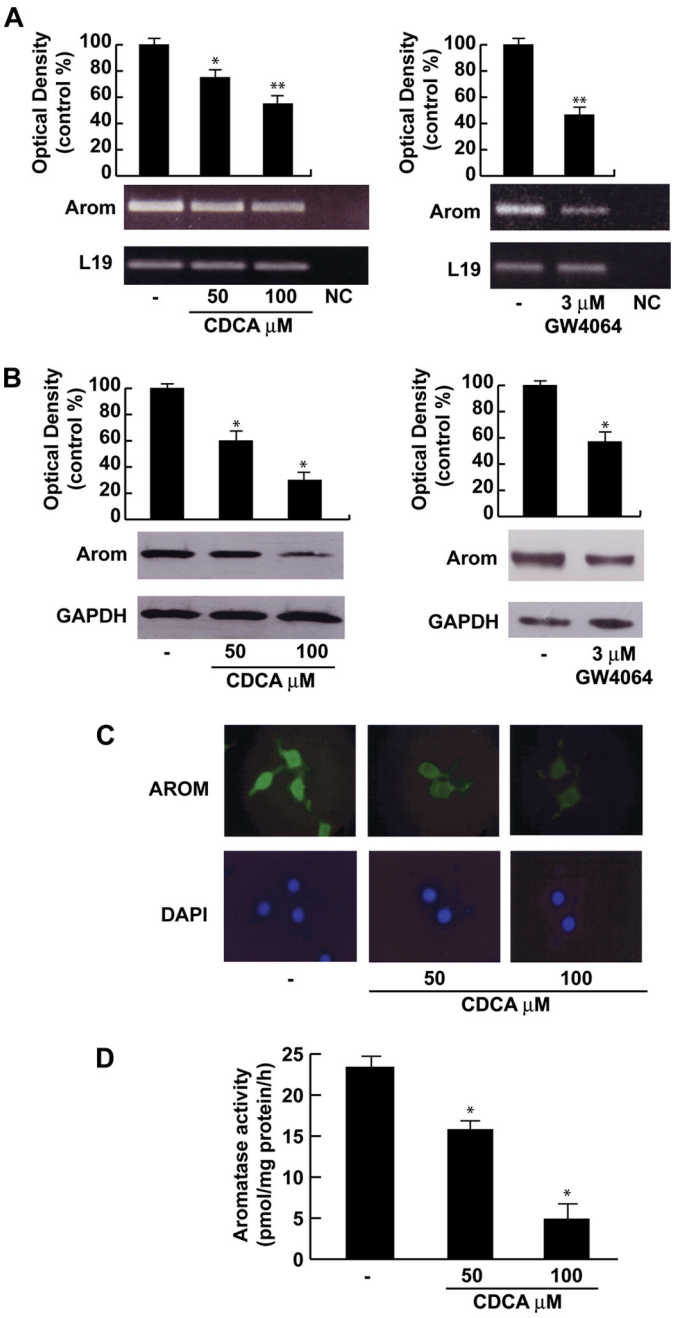

FIGURE 2. **Effects of CDCA on aromatase expression and activity in R2C cells.** *A*, total RNA was extracted from R2C cells treated with vehicle (−), 50 and 100 μM CDCA or 3 μM GW4064 for 24 h and reverse transcribed. cDNA was subjected to PCR using primers specific for P450 aromatase or L19. *NC*, negative control, RNA sample without the addition of reverse transcriptase. The histograms represent the mean ± S.D. (*error bars*) of three separate experiments in which band intensities were evaluated in terms of optical density arbitrary units and expressed as percentages of the control, which was assumed to be 100%. *, $p < 0.05$; **, $p < 0.01$ compared with vehicle. *B*, total proteins extracted from R2C cells treated with vehicle (−), 50 and 100 μM CDCA, or 3 μM GW4064 for 24 h were used for immunoblot analysis of aromatase. GAPDH was used as a loading control. The histograms represent the mean ± S.D. (*error bars*) of three separate experiments in which band intensities were evaluated in terms of optical density arbitrary units and expressed as percentages of the control, which was assumed to be 100%. *, $p < 0.01$ compared with vehicle. *C*, R2C cells were treated with vehicle (−) or 50 and 100 μM CDCA for 24 h and aromatase expression was determined by immunofluorescence analysis. 4′,6-Diamidino-2-phenylindole (*DAPI*) staining was used to visualize the cell nucleus. Each experiment is representative of at least 4. *D*, R2C were cultured in the presence of vehicle (−) or 50 and 100 μM CDCA for 24 h. Aromatase activity was performed as described under "Experimental Procedures." The results obtained were expressed as picomole of $[^3H]H_2O$/h of release and were normalized for milligrams of protein (pmol/mg of proteins/h). The values represent the mean ± S.D. (*error bars*) of three different experiments each performed with triplicate samples. *, $p < 0.01$ compared with vehicle.

moter activity was observed in cells transfected with *p*-1037, *p*-688, *p*-475, and *p*-183 exposed to 50 μM CDCA for 24 h. It is worth noting that the construct *p*-688m bearing the SF-1 mutated site displays significantly lower basal activity compared with the *p*-688 plasmid, whereas no inhibitory effects were noticeable upon CDCA treatment (Fig. 5*B*). This latter result highlights the importance of the SF-1 binding site in regulation of aromatase expression in the R2C cells and suggests that the inhibitory effect of CDCA requires AGGTCA sequence motif.

SF-1 is closely related to liver receptor homologue-1 (LRH-1) and both proteins recognize the same canonical DNA motif (36). However, because LRH-1 is not expressed in R2C cells (supplemental Fig. S1) we focused our attention on the SF-1 transcriptional factor.

To further demonstrate the functional interaction of FXR with SF-1 binding site, we transiently cotransfected HeLa cells, which do not express significant levels of SF-1 (37) with the *CYP17* promoter construct containing multiple SF-1 response elements (38) with or without SF-1 plasmid in the presence of increasing amounts of the FXR expression plasmid. The SF-1 expression vector strongly increased the *CYP17* promoter activity, which was progressively reduced by increasing amounts of FXR (Fig. 5*C*). We observed a similar result also in HeLa cells overexpressing FXR and treated with CDCA (data not shown). These data support the competitive role of FXR in the SF-1 binding site.

FXR Protein Binds to SF-1 RE in Vitro and in Vivo—On the basis of the evidence that the inhibitory effect of CDCA on aromatase requires the crucial presence of SF-1 RE, electrophoretic mobility shift assay experiments were performed using the SF-1 motif present in the aromatase promoter as probe. We observed the formation of a complex in nuclear extract from R2C cells (Fig. 6*A*, *lane 1*), which was abrogated by 100-fold molar excess of unlabeled probe (Fig. 6*A*, *lane 2*) demonstrating the specificity of the DNA binding complex. This inhibition was no longer observed when mutated oligodeoxyribonucleotide was used as competitor (Fig. 6*A*, *lane 3*). 50 μM CDCA for 6 h induced an increase in the DNA binding complex compared with control samples (Fig. 6*A*, *lane 4*). The inclusion of anti-SF-1 and anti-FXR antibodies in the reactions attenuated the specific bands, suggesting the presence of SF-1 and FXR proteins in the complex (Fig. 6*A*, *lanes 5* and *6*). Using SF-1 and FXR proteins transcribed and translated *in vitro*, we obtained complexes migrating at the same level as that of R2C nuclear extracts (Fig. 6*A*, *lanes 7* and *8*). Competition binding studies revealed that both transcribed and translated SF-1 and FXR DNA binding complexes were abrogated by 100-fold molar excess of unlabeled probe (Fig. 6*B*, *lanes 2* and *7*). Finally the specificity of these bands was proved by drastic attenuation of the complex in the presence of the anti-SF-1 antibody, whereas the inclusion of anti-FXR antibody completely immunodepleted the binding (Fig. 6*B*, *lanes 3* and *8*). IgG did not

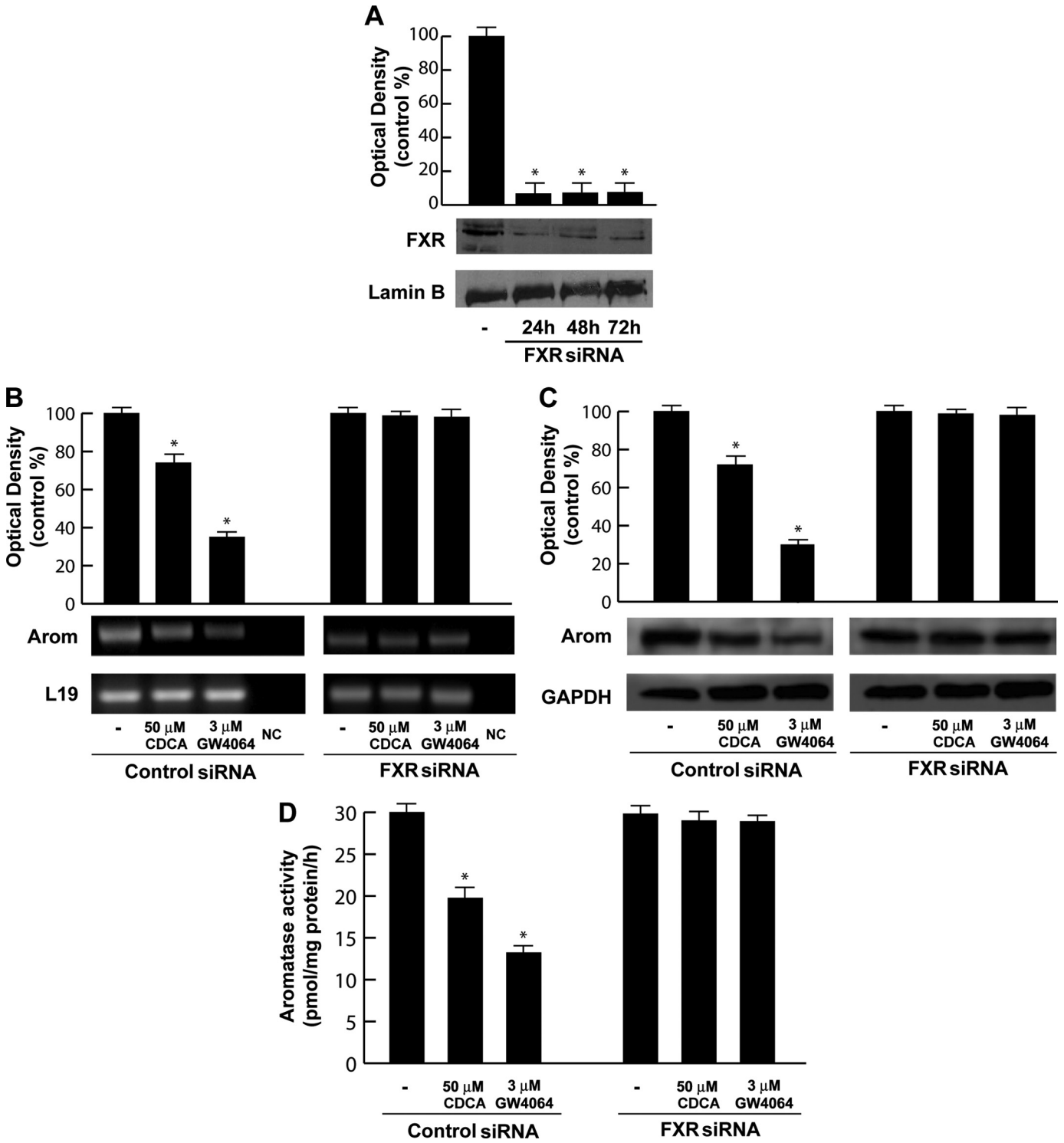

FIGURE 3. **Effects of FXR silencing on aromatase expression in R2C cells.** *A*, FXR protein in R2C cells that were not transfected (−) or transfected with siRNA targeted rat FXR mRNA sequence as reported under "Experimental Procedures" for 24, 48, and 72 h. GAPDH was used as loading control. The histograms represent the mean ± S.D. (*error bars*) of three separate experiments in which band intensities were evaluated in terms of optical density arbitrary units and expressed as percentages of the control, which was assumed to be 100%. *, $p < 0.01$ compared with not transfected cells. *B–D*, R2C cells were transfected with control siRNA or FXR siRNA for 24 h, and then treated with vehicle (−), 50 μM CDCA, or 3 μM GW4064 for 24 h. *B*, total RNA was extracted and reverse transcription-PCR analysis was performed to evaluate the expression of aromatase. L19 was used as loading control. *NC*, negative control, RNA sample without the addition of reverse transcriptase. *C*, total proteins were extracted and Western blotting analysis was performed. GAPDH was used as loading control. The histograms represent the mean ± S.D. of three separate experiments in which band intensities were evaluated in terms of optical density arbitrary units and expressed as percentages of the control, which was assumed to be 100%. *, $p < 0.01$ compared with vehicle. *D*, aromatase activity was performed as described under "Experimental Procedures." The results obtained were expressed as picomole of $[^3H]H_2O$/h of release and were normalized for milligrams of protein (pmol/mg of proteins/h). The values represent the mean ± S.D. of three different experiments each performed with triplicate samples. *, $p < 0.01$ compared with vehicle.

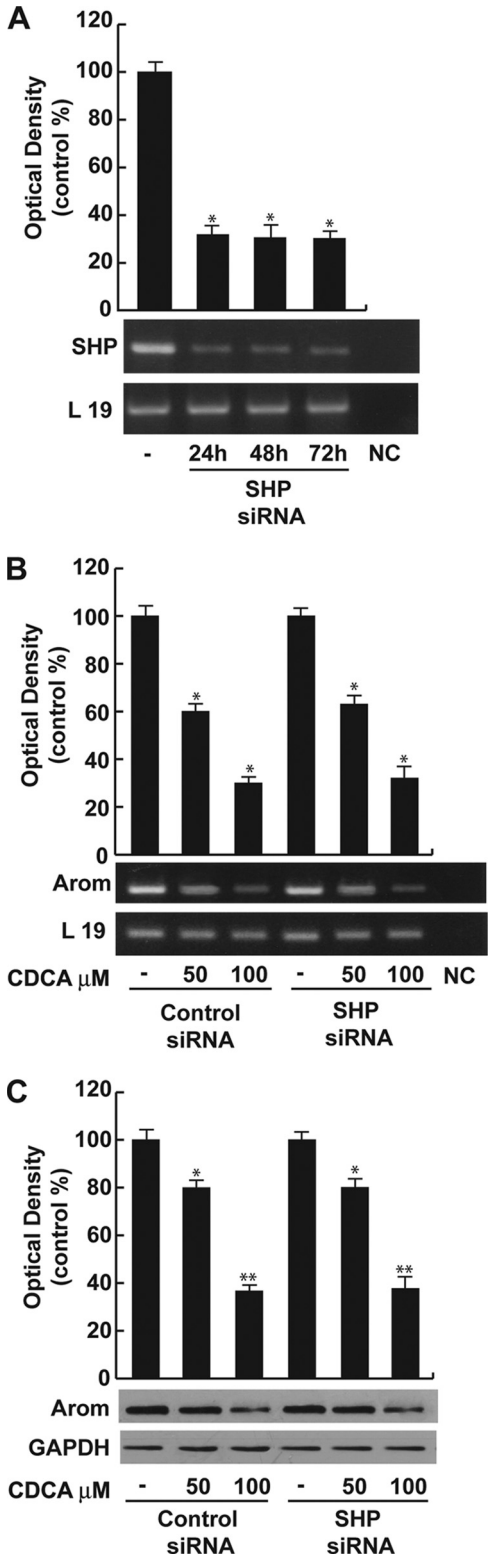

FIGURE 4. **SHP is not involved in CDCA-mediated down-regulation of aromatase.** *A*, SHP mRNA expression in R2C cells that were not transfected (−) or transfected with the siRNA-targeted rat SHP mRNA sequence as described under "Experimental Procedures" for 24, 48, and 72 h. L19 was used as loading control. *NC*, negative control, RNA sample without the addition of reverse transcriptase. The histograms represent the mean ± S.D. (*error bars*) of three separate experiments in which band intensities were evaluated in terms of optical density arbitrary units and expressed as percentages of the control, which was assumed to be 100%. *, $p < 0.01$ compared with not transfected cells. *B*, R2C cells were transfected with control siRNA or SHP siRNA for 24 h, and then treated with vehicle (−) or 50 and 100 μM CDCA for 24 h. Total RNA was extracted and reverse transcription-PCR analysis was performed to evaluate the expression of aromatase. L19 was used as loading control. The histograms represent the mean ± S.D. of three separate experiments in which band intensities were evaluated in terms of optical density arbitrary units and expressed as percentages of the control, which was assumed to be 100%. *, $p < 0.01$ compared with vehicle. *C*, in the same experimental condition as *B*, total proteins were extracted and Western blotting analysis was performed. GAPDH was used as loading control. The histograms represent the mean ± S.D. of three separate experiments in which band intensities were evaluated in terms of optical density arbitrary units and expressed as percentages of the control, which was assumed to be 100%. *, $p < 0.05$; **, $p < 0.01$ compared with vehicle.

affect either SF-1 or FXR complex formation (Fig. 6*B*, *lanes 4* and *9*).

The interaction of FXR with the aromatase gene promoter was further investigated by the ChIP assay. Using specific antibody against FXR and RNA-POL II, formaldehyde cross-linked protein-chromatin complexes were immunoprecipitated from R2C cells cultured with or without 50 and 100 μM CDCA. The resulting genomic DNA precipitated by using anti-FXR was then reprecipitated with the anti-SF-1 antibody. The results analyzed by PCR indicated that FXR was weakly constitutively bound to the aromatase promoter in untreated cells and this recruitment was increased upon CDCA treatment, which was correlated with a reduced association of RNA polymerase II (Fig. 6*C*). Interestingly, by a re-ChIP assay, we observed upon CDCA stimulation a significant reduction in SF-1 recruitment to the aromatase promoter (Fig. 6*C*). Moreover, as expected, no involvement of LRH-1 was observed in the re-ChIP experiment (data not shown). Next, the anti-FXR antibody did not immunoprecipitate a region upstream of the SF-1 site located within the aromatase promoter gene (Fig. 6*C*). The ChIP assay was quantified by real time PCR as shown in Fig. 6*D*.

CDCA Inhibits R2C Cell Proliferation through FXR Activation—Finally, we evaluated the effect of CDCA on growth of R2C cells by measuring changes in the rate of DNA synthesis ([^{3}H]thymidine incorporation). As shown in Fig. 7*A*, treatment with CDCA for 24 and 48 h reduced R2C cell proliferation in a dose- and time-dependent manner. The specific involvement of FXR in the antiproliferative response of R2C cells to CDCA was demonstrated by evidence that such inhibitory effects were completely reversed in the presence of the FXR dominant negative plasmid as well as after knocking down FXR with a specific siRNA (Fig. 7, *B* and *C*).

It is well known that aromatase overexpression in tumor Leydig cells leads to a consequent excess of *in situ* estradiol production that sustains tumor cell growth and proliferation (18). Because we demonstrated the ability of CDCA to down-regulate aromatase expression and activity in R2C cells, we wondered if CDCA was able to antagonize the effect of an aromatizable androgen androst-4-ene-3,17-dione (AD) on estradiol/ERα signaling in R2C cells. To this aim we performed a transient transfection experiment using the XETL plasmid, which carries firefly luciferase sequences under control of an estrogen response element upstream of the thymidine kinase promoter. As shown in Fig. 8*A* we observed that the exposure to CDCA (50 μM) *per se* did not elicit any changes in luciferase activity but completely reversed XETL activation induced by AD. CDCA antagonizes the effect of AD on estradiol/ERα sig-

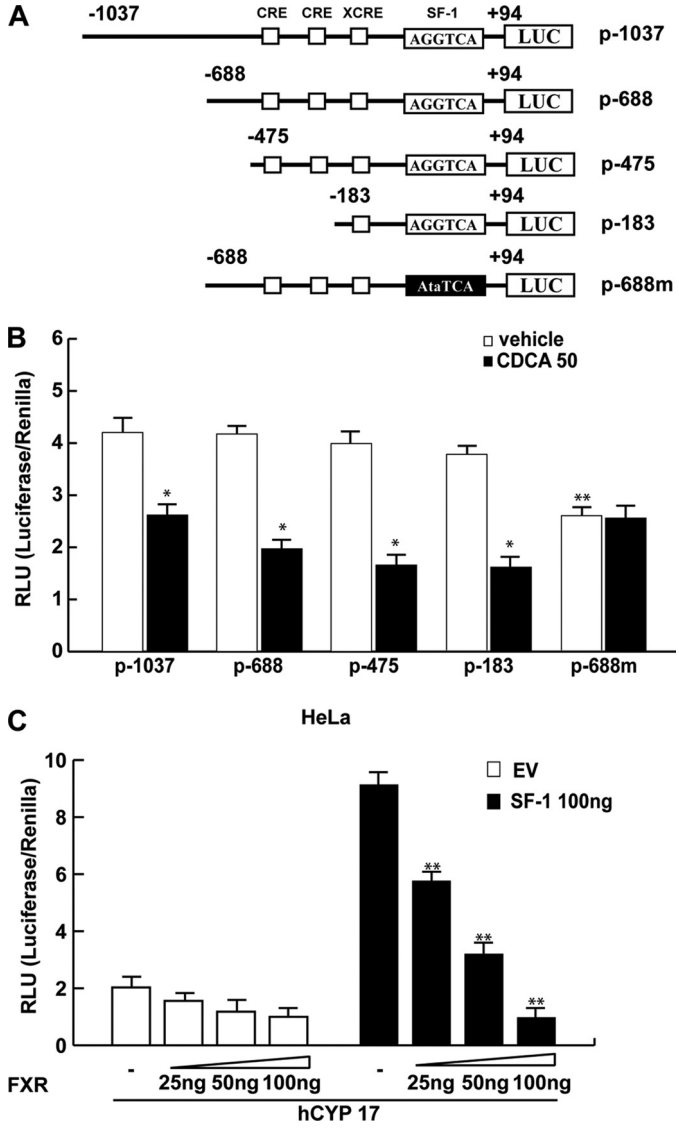

FIGURE 5. **Functional interaction between FXR and the SF-1 site.** *A*, schematic map of the P450arom proximal promoter PII constructs used in this study. All of the promoter constructs contain the same 3′ boundary (+94). The 5′ boundaries of the promoter fragments varied from −1037 to −183. Three putative CRE motifs (5′-CRE at −335; 3′-CRE at −231; XCRE at −169) are indicated as *squares*. The AGGTCA site (SF-1 RE at-90) is indicated as a *rectangle*. A mutated SF-1 binding site (SF-1 mut) is present in *p*-688m (*black rectangle*). *B*, aromatase transcriptional activity of R2C cells transfected with promoter constructs are shown. After transfection, cells were treated in the presence of vehicle (−) or 50 μM CDCA for 24 h. These results represent the mean ± S.D. (*error bars*) of three different experiments performed in triplicate. *, $p < 0.01$ with respect to the vehicle; **, $p < 0.01$ with respect to the control of p688. *C*, HeLa cells were transiently cotransfected with the *CYP17* promoter and SF-1 plasmid or empty vector (EV) in the presence of increasing amounts of FXR expression plasmid. These results represent the mean ± S.D. of three different experiments performed in triplicate. In each experiment, the activities of the transfected plasmids were assayed in triplicate transfections. *, $p < 0.01$ with respect to the EV; **, $p < 0.01$ with respect to the SF-1 alone.

naling by a FXR-dependent pathway because this effect was not observed when the FXR gene was knocked down (Fig. 8*A*). Moreover, we examined if CDCA was able to inhibit the effect of AD on R2C cell proliferation using two experimental approaches, thymidine incorporation and anchorage independent soft agar growth assay. As expected, treatment with 100 nM AD, through its conversion into estradiol, increased thymidine incorporation as well as the number of colonies present in soft agar (Fig. 8, *B* and *C*) concomitantly with increased levels of cell cycle regulators cyclin D1 and cyclin E (Fig. 8*D*). All these events were completely reversed by CDCA exposure (Fig. 8, *B–D*). Finally, we evaluated the effects of AD and/or CDCA on the R2C cell proliferation assay by thymidine incorporation after knocking down aromatase with a specific siRNA (Fig. 8*E*). As shown in Fig. 8*F*, as expected AD does not exert proliferative effects on R2C cells, whereas the addition of CDCA can only slightly decrease cell growth. These data demonstrated that the FXR ligand, through a down-regulation of aromatase activity, plays an important role in inhibiting R2C cell proliferation.

DISCUSSION

FXR is highly expressed in the enterohepatic system where it drives bile acid absorption and secretion, lipid, glucose metabolism, and immunological response to intestinal bacterial overgrowth (2, 4, 39–41). In hepatocytes, activation of FXR causes both feedback inhibition of cholesterol 7α-hydroxylase (CYP7A1), the rate-limiting enzyme in bile acid biosynthesis from cholesterol, and activation of intestinal bile acid-binding protein (42). In addition, several observations suggest that FXR may also be involved in control of steroid metabolism (13, 43). Indeed, FXR activation results in modulation of genes encoding androgen precursor-synthesizing enzymes, namely dehydroepiandrosterone sulfotransferase (SULT2A1), 5α-reductase, and 3β-hydroxysteroid dehydrogenase in the liver (44, 45). Recently, FXR was shown to inhibit androgen glucuronidation in prostatic cancer cell lines (46) and suppress the activity of aromatase in human breast cancer cells (13). The enzyme aromatase coded by the *CYP19* gene, converts androgens into estrogens and is involved in progression and growth of various estrogen hormonal-induced neoplasms. For instance, overexpression of aromatase plays a significant role in excessive estrogen production sustaining tumorogenesis in Leydig cells (18).

Here, we have documented that FXR is expressed in tissues of normal and tumor Fisher rat testis and in Leydig normal and tumor cell lines. In R2C cells, FXR activators CDCA and GW4064 down-regulate aromatase expression at both mRNA and protein levels, together with the inhibition of its enzymatic activity. Moreover, we demonstrated a direct involvement of FXR in regulating aromatase expression using a specific FXR siRNA.

One of the well characterized mechanisms by which FXR down-regulates gene expression is through induction of SHP (10), an atypical nuclear receptor lacking both a DNA-binding domain and the NH_2-terminal ligand-independent activation domain (8). This receptor interacts with other nuclear receptors, including peroxisome proliferator-activated receptor, RXR, ER, and LRH-1, preventing their activation of gene transcription (8–10). In preadipocytes of cancerous breast tissue, LRH-1 can regulate via an alternate promoter (II) the expression of aromatase induced by prostaglandin E_2 (47, 48). Moreover, SHP can inhibit LRH-1 induction of aromatase (49). LRH-1 is most homologous to SF1, which is essential for sex differentiation and develop-

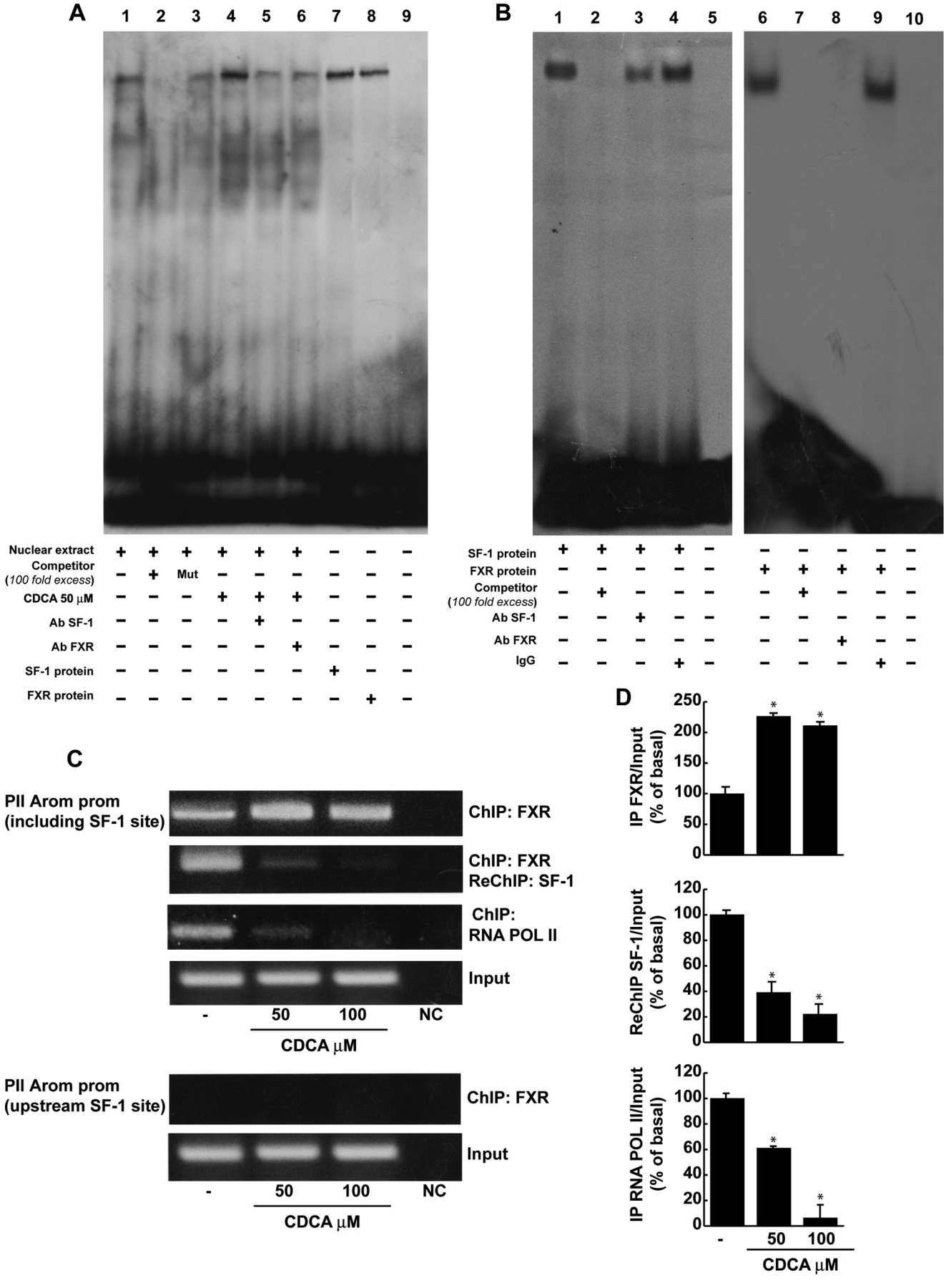

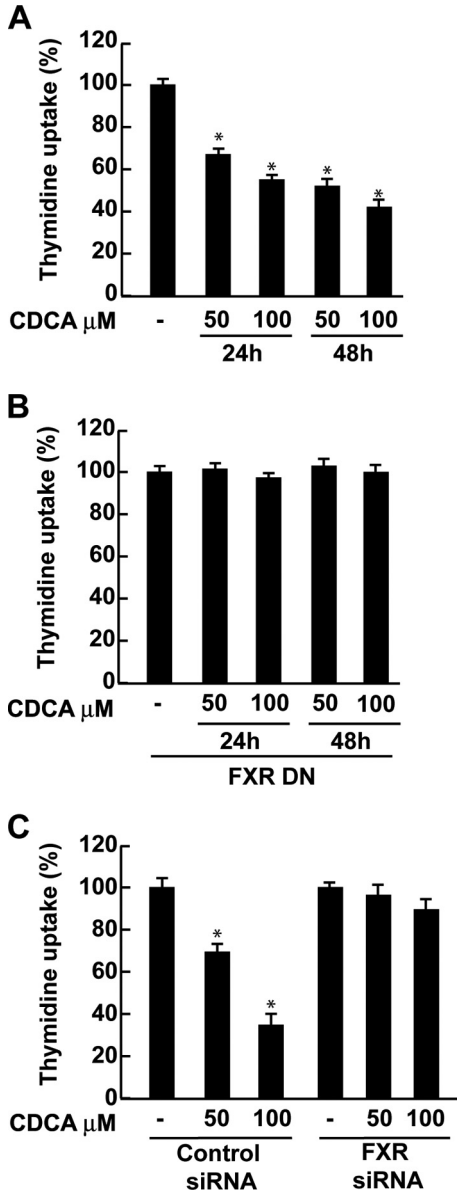

FIGURE 7. **CDCA effects on R2C cell proliferation.** *A*, R2C cells were treated with vehicle (−) or 50 and 100 μM CDCA for 24 and 48 h, or *B*, transiently transfected with FXR dominant negative (FXR-DN) for 24 h and then treated as reported above, or *C*, transfected with control siRNA or FXR siRNA for 24 h and treated for 24 h with 50 and 100 μM CDCA. Thymidine incorporation assay was performed. The results represent the mean ± S.D. (*error bars*) of three different experiments each performed with triplicate samples, and expressed as percentage of growth *versus* control, which was assumed to be 100%. *, $p < 0.01$ compared with vehicle.

ment of gonads (28), because they share a highly conserved DNA-binding domain (DBD) (>90% identity) and a moderately conserved ligand-binding domain (56% identity). SHP is detected in the interstitial cells of the adult testis and its expression has been shown to be induced by FXR (35).

Our current study revealed that FXR activation does not induce SHP expression in Leydig tumor cells in which inhibition of the aromatase protein by CDCA occurs even when this nuclear receptor was knocked down. These results suggest that SHP is not required for the effect of the FXR ligand to down-regulate aromatase expression, at least in R2C cells. On the basis of these observations, we focused our attention on the direct effect of FXR on the transcriptional activity of aromatase gene.

Distinctive tissue-specific promoters are employed to direct the expression of aromatase mRNA driving from a single aromatase gene. The promoter located immediately upstream of the transcriptional initiation site (PII) regulates aromatase expression in rat Leydig, Sertoli, and germ cells and in R2C Leydig tumor cells (23, 24). A number of functional motifs have been identified in the PII aromatase promoter: three motifs resembling CRE and an SF-1 binding site (27, 28).

We demonstrated by functional studies, using constructs containing different 5′-deleted regions of rat PII aromatase promoter, that CDCA treatment induces a decreased transcriptional activity. The observed inhibitory effect of CDCA was abrogated when a promoter fusion containing a mutated SF-1 element was employed. These results clearly suggest that the integrity of the SF-1 sequence is a prerequisite for the down-regulatory effects of the FXR ligand on aromatase promoter activity. These findings raise the possibility that FXR and SF-1 are competing for binding to a common site within this regulatory region. This assumption is further supported by the observation that FXR expression vector is able to abrogate the induction of SF-1 on the human *CYP17* promoter, which contains multiple SF-1 response elements. As a transcription factor, FXR binds to a specific consensus sequence (inverted repeat of 2 AGGTCA half-sites) either as a monomer or as a heterodimer with a common partner for NRs, as RXR to regulate the expression of various genes (6, 7).

Location of an AGGTCA sequence at the −90 position supports a possible binding of FXR to this promoter region, which we verified by electrophoretic mobility shift assay experiments. Nuclear extracts from R2C cells treated with CDCA revealed an increase in the DNA binding complex that was immunode-

FIGURE 6. **FXR binds to SF-1 site within the aromatase promoter region.** *A*, nuclear extract from R2C cells were incubated with a double-stranded SF-1-specific sequence probe labeled with [γ-^{32}P]ATP and subjected to electrophoresis in a 6% polyacrylamide gel (*lane 1*). Competition experiments were performed adding as competitor a 100-fold molar excess of unlabeled probe (*lane 2*) or a 100-fold molar excess of unlabeled oligonucleotide containing a mutated SF-1 RE (*lane 3*). *Lane 4*, nuclear extracts from CDCA (50 μM)-treated R2C cells. *Lanes 5* and *6*, CDCA-treated nuclear extracts were incubated with anti-SF-1 or anti-FXR antibodies, respectively. We used as positive controls transcribed and translated *in vitro* SF-1 (*lane 7*) and FXR (*lane 8*) proteins. *Lane 9* contains probe alone. *B*, SF-1 protein (*lane 1*) and FXR protein (*lane 6*) was incubated with a double-stranded SF-1 sequence probe labeled with [γ-^{32}P]ATP and subjected to electrophoresis in a 6% polyacrylamide gel. Competition experiments were performed adding as competitor a 100-fold molar excess of unlabeled probe (*lanes 2* and *7*). SF-1 and FXR proteins were incubated with anti-SF-1 antibody (*lane 3*), anti-FXR antibody (*lane 8*), or IgG (*lanes 4* and *9*). *Lanes 5* and *10* contain probe alone. *C*, R2C cells were treated in the presence of vehicle (−) or 50 and 100 μM CDCA for 1 h, then cross-linked with formaldehyde, and lysed. The precleared chromatin was immunoprecipitated with anti-FXR, and anti-RNA Pol II antibodies and normal mouse serum (*NC*) as negative control. Chromatin immunoprecipitated with the anti-FXR antibody was re-immunoprecipitated with anti-SF-1 antibody. The PII promoter sequence including the SF-1 site and that located upstream of the SF-1 site were detected by PCR with specific primers, as described under "Experimental Procedures," and *D*, a 5-μl volume of each sample and input were used for real time PCR. To determine input DNA, the PII promoter fragment was amplified from 30 μl of initial preparations of soluble chromatin before immunoprecipitations. Similar results were obtained in multiple independent experiments. *, $p < 0.01$ compared with vehicle.

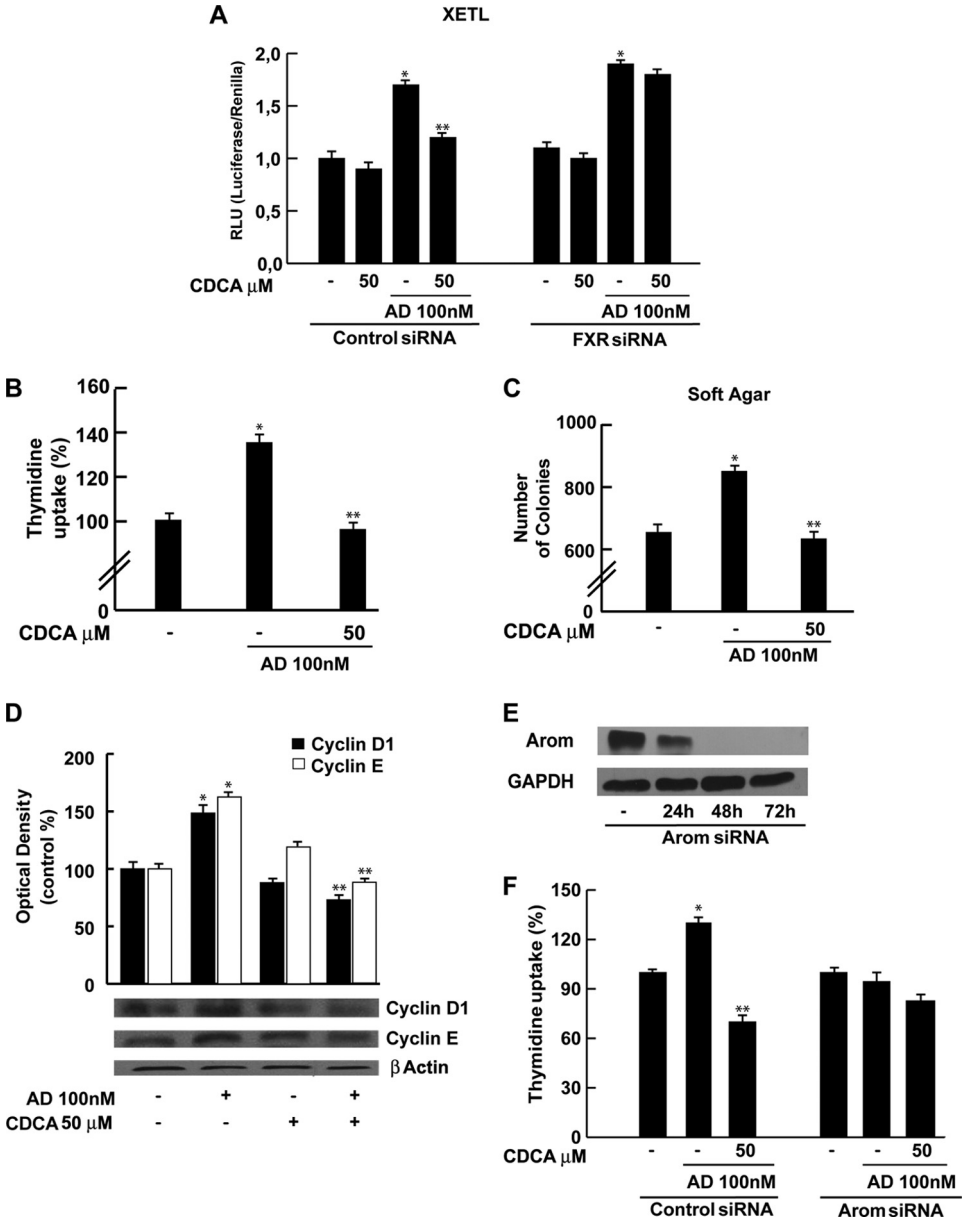

FIGURE 8. **CDCA reverses the effects of AD on R2C cell proliferation.** *A*, R2C cells were transfected with control siRNA or FXR siRNA for 24 h and then transiently transfected with the XETL promoter plasmid. Cells were treated with 50 μM CDCA in the with or without 100 nM AD for 24 h. These results represent the mean ± S.D. of three different experiments. In each experiment, the activities of the transfected plasmids were assayed in triplicate transfections. *, $p < 0.01$ with respect to the vehicle. **, $p < 0.01$ CDCA + AD treated *versus* AD alone. *B*, R2C cells were treated with 100 nM AD in the presence or not of 50 μM CDCA for 24 h. Thymidine incorporation assay was performed. The results represent the mean ± S.D. of three different experiments each performed with triplicate samples. *, $p < 0.01$ AD treated compared with vehicle. **, $p < 0.01$ CDCA + AD treated *versus* AD alone. *C*, R2C cells were seeded (10,000/well) in 0.5% agarose and treated as described above. Cells were allowed to grow for 14 days and then the number of colonies >50 μm were quantified and the results graphed. The results represent the mean ± S.D. of three different experiments each performed with triplicate samples. *, $p < 0.01$ AD treated compared with vehicle. **, $p < 0.01$ CDCA + AD treated *versus* AD alone. *D*, total proteins extracted from R2C cells treated with vehicle (−), 100 nM AD, 50 μM CDCA, and AD + CDCA for 24 h were used for immunoblot analysis of cyclin D1 and cyclin E. β-Actin was used as a loading control. The histograms represent the mean ± S.D. of three separate experiments in which band intensities were evaluated in terms of optical density arbitrary units and expressed as percentages of the control, which was assumed to be 100%. *, $p < 0.01$ AD treated compared with vehicle. **, $p < 0.01$ CDCA + AD treated *versus* AD alone. *E*, aromatase protein in R2C cells that were not transfected (−) or transfected with siRNA targeted rat aromatase mRNA sequence as described under "Experimental Procedures" for 24, 48, and 72 h. GAPDH was used as loading control. *F*, R2C cells were transfected with control siRNA or Arom siRNA for 48 h and then treated with 100 nM AD in the presence or not of 50 μM CDCA for 24 h. Thymidine incorporation assay was performed. The results represent the mean ± S.D. of three different experiments each performed with triplicate samples. *, $p < 0.01$ AD treated compared with vehicle. **, $p < 0.01$ CDCA + AD treated *versus* AD alone.

pleted by both anti-SF-1 and anti-FXR antibodies suggesting how the two proteins are able to bind the AGGTCA sequence located in the PII aromatase promoter. The specificity of the binding was proved by the attenuation, in the presence of anti-SF-1 and anti-FXR antibodies, of the DNA complex observed using SF-1 and FXR transcribed and translated in a cell-free system. In addition, the *in vivo* interaction between FXR and the aromatase promoter was further supported by ChIP assay, where upon CDCA treatment we observed a reduced recruitment of RNA-POLII to this promoter addressing a negative transcriptional regulation mediated by FXR. All together these data suggest that FXR is able to compete with SF-1 in binding to a common sequence within the PII promoter of aromatase interfering negatively with its activity. Finally, in our study we demonstrated that FXR activator CDCA induces growth inhibition in R2C cells, which was reversed in the presence of FXR dominant negative as well as after knocking down FXR with a specific siRNA addressing a FXR dependence of this event. However, it is worth mentioning, on the basis of our recent findings, that aromatase overexpression, in Leydig tumor cells, determines an excessive local estradiol production that is able to stimulate the expression of genes involved in cell cycle regulation sustaining cell proliferation (20).

Here, we evidenced the ability of CDCA to reverse the stimulatory effects of an aromatizable androgen AD at three different levels: 1) E2/ERα signaling; 2) an anchorage dependent and independent R2C cell growth proliferation; and 3) expression of cell cycle regulators cyclin D1 and cyclin E. Finally, knocking down aromatase enzyme reduces estradiol production by R2C cells upon AD exposure and exhibits as biological counterpart a decreased cell proliferation. In the same experimental condition the addition of CDCA can only slightly decrease cell growth demonstrating

that the FXR activator through an inhibition of aromatase expression exerts an important role in reducing R2C cell proliferation. In conclusion, our results elucidate, for the first time, a new molecular mechanism through which FXR antagonizes estrogen signaling and inhibits Leydig tumor growth and progression.

Acknowledgments—We thank Dr. T. A. Kocarek, Dr. D. J. Mangelsdorf, and Dr. W. E. Rainey for generously providing the FXR-responsive reporter gene, and FXR-DN, FXR, SF-1, and CYP17 gene reporter plasmids, respectively. We thank Dr. K. Morohashi for providing the anti-SF-1 antibody and Dr. Luc Belanger for the antibody anti-LRH-1.

REFERENCES

1. Forman, B. M., Goode, E., Chen, J., Oro, A. E., Bradley, D. J., Perlmann, T., Noonan, D. J., Burka, L. T., McMorris, T., Lamph, W. W., Evans, R. M., and Weinberger, C. (1995) *Cell* **81,** 687–693
2. Makishima, M., Okamoto, A. Y., Repa, J. J., Tu, H., Learned, R. M., Luk, A., Hull, M. V., Lustig, K. D., Mangelsdorf, D. J., and Shan, B. (1999) *Science* **284,** 1362–1365
3. Parks, D. J., Blanchard, S. G., Bledsoe, R. K., Chandra, G., Consler, T. G., Kliewer, S. A., Stimmel, J. B., Willson, T. M., Zavacki, A. M., Moore, D. D., and Lehmann, J. M. (1999) *Science* **284,** 1365–1368
4. Kalaany, N. Y., and Mangelsdorf, D. J. (2006) *Annu. Rev. Physiol.* **68,** 159–191
5. Ananthanarayanan, M., Balasubramanian, N., Makishima, M., Mangelsdorf, D. J., and Suchy, F. J. (2001) *J. Biol. Chem.* **276,** 28857–28865
6. Laffitte, B. A., Kast, H. R., Nguyen, C. M., Zavacki, A. M., Moore, D. D., and Edwards, P. A. (2000) *J. Biol. Chem.* **275,** 10638–10647
7. Claudel, T., Sturm, E., Duez, H., Torra, I. P., Sirvent, A., Kosykh, V., Fruchart, J. C., Dallongeville, J., Hum, D. W., Kuipers, F., and Staels, B. (2002) *J. Clin. Invest.* **109,** 961–971
8. Seol, W., Choi, H. S., and Moore, D. D. (1996) *Science* **272,** 1336–1339
9. Seol, W., Hanstein, B., Brown, M., and Moore, D. D. (1998) *Mol. Endocrinol.* **12,** 1551–1557
10. Goodwin, B., Jones, S. A., Price, R. R., Watson, M. A., McKee, D. D., Moore, L. B., Galardi, C., Wilson, J. G., Lewis, M. C., Roth, M. E., Maloney, P. R., Willson, T. M., and Kliewer, S. A. (2000) *Mol. Cell. Biol.* **6,** 517–526
11. Wang, Y. D., Chen, W. D., Moore, D. D., and Huang, W. D. (2008) *Cell Res.* **18,** 1087–1095
12. Journe, F., Laurent, G., Chaboteaux, C., Nonclercq, D., Durbecq, V., Larsimont, D., and Body, J. J. (2008) *Breast Cancer Res. Treat.* **107,** 49–61
13. Swales, K. E., Korbonits, M., Carpenter, R., Walsh, D. T., Warner, T. D., and Bishop-Bailey, D. (2006) *Cancer Res.* **66,** 10120–10126
14. Modica, S., Murzilli, S., Salvatore, L., Schmidt, D. R., and Moschetta, A. (2008) *Cancer Res.* **68,** 9589–9594
15. Hawkins, C., and Miaskowski, C. (1996) *Oncol. Nurs. Forum* **23,** 1203–1211
16. Carroll, P. R., Whitmore, W. F., Jr., Herr, H. W., Morse, M. J., Sogani, P. C., Bajorunas, D., Fair, W. R., and Chaganti, R. S. (1987) *J. Urol.* **137,** 420–423
17. Bosland, M. C. (1996) *Prog. Clin. Biol. Res.* **394,** 309–352
18. Fowler, K. A., Gill, K., Kirma, N., Dillehay, D. L., and Tekmal, R. R. (2000) *Am. J. Pathol.* **156,** 347–353
19. Carpino, A., Rago, V., Pezzi, V., Carani, C., and Andò, S. (2007) *Eur. J. Endocrinol.* **157,** 239–244
20. Sirianni, R., Chimento, A., Malivindi, R., Mazzitelli, I., Andò, S., and Pezzi, V. (2007) *Cancer Res.* **67,** 8368–8377
21. Aquila, S., Sisci, D., Gentile, M., Carpino, A., Middea, E., Catalano, S., Rago, V., and Andò, S. (2003) *Hum. Reprod.* **18,** 1650–1659
22. Inkster, S., Yue, W., and Brodie, A. (1995) *J. Clin. Endocrinol. Metab.* **80,** 1941–1947
23. Young, M., Lephart, E. D., and McPhaul, M. J. (1997) *J. Steroid Biochem. Mol. Biol.* **63,** 37–44
24. Lanzino, M., Catalano, S., Genissel, C., Ando, S., Carreau, S., Hamra, K., and McPhaul, M. J. (2001) *Biol. Reprod.* **64,** 1439–1443
25. Fitzpatrick, S. L., and Richards, J. S. (1994) *Mol. Endocrinol.* **8,** 1309–1319
26. Carlone, D. L., and Richards, J. S. (1997) *Mol. Endocrinol.* **11,** 292–304
27. Young, M., and McPhaul, M. J. (1998) *Endocrinology* **139,** 5082–5093
28. Parker, K. L., and Schimmer, B. P. (1997) *Endocr. Rev.* **18,** 361–377
29. Kocarek, T. A., Shenoy, S. D., Mercer-Haines, N. A., and Runge-Morris, M. (2002) *J. Pharmacol. Toxicol. Methods* **47,** 177–187
30. Lephart, E. D., and Simpson, E. R. (1991) *Methods Enzymol.* **206,** 477–483
31. Andrews, N. C., and Faller, D. V. (1991) *Nucleic Acids Res.* **19,** 2499
32. Coleman, G. L., Barthold, W., Osbaldiston, G. W., Foster, S. J., and Jonas, A. M. (1977) *J. Gerontol.* **32,** 258–278
33. Jacobs, B. B., and Huseby, R. A. (1967) *J. Natl. Cancer Inst.* **39,** 303–309
34. Nguyen, A., and Bouscarel, B. (2008) *Cell. Signal.* **20,** 2180–2197
35. Volle, D. H., Duggavathi, R., Magnier, B. C., Houten, S. M., Cummins, C. L., Lobaccaro, J. M., Verhoeven, G., Schoonjans, K., and Auwerx, J. (2007) *Genes Dev.* **21,** 303–315
36. Pezzi, V., Sirianni, R., Chimento, A., Maggiolini, M., Bourguiba, S., Delalande, C., Carreau, S., Andò, S., Simpson, E. R., and Clyne, C. D. (2004) *Endocrinology* **145,** 2186–2196
37. Sugawara, T., Holt, J. A., Kiriakidou, M., and Strauss, J. F., 3rd (1996) *Biochemistry* **35,** 9052–9059
38. Hanley, N. A., Rainey, W. E., Wilson, D. I., Ball, S. G., and Parker, K. L. (2001) *Mol. Endocrinol.* **15,** 57–68
39. Modica, S., and Moschetta, A. (2006) *FEBS Lett.* **580,** 5492–5499
40. Jung, D., Inagaki, T., Gerard, R. D., Dawson, P. A., Kliewer, S. A., Mangelsdorf, D. J., and Moschetta, A. (2007) *J. Lipid Res.* **48,** 2693–2700
41. Inagaki, T., Moschetta, A., Lee, Y. K., Peng, L., Zhao, G., Downes, M., Yu, R. T., Shelton, J. M., Richardson, J. A., Repa, J. J., Mangelsdorf, D. J., and Kliewer, S. A. (2006) *Proc. Natl. Acad. Sci. U.S.A.* **103,** 3920–3925
42. Chiang, J. Y. (2002) *Endocr. Rev.* **23,** 443–463
43. Lee, F. Y., Lee, H., Hubbert, M. L., Edwards, P. A., and Zhang, Y. (2006) *Trends Biochem. Sci.* **31,** 572–580
44. Pircher, P. C., Kitto, J. L., Petrowski, M. L., Tangirala, R. K., Bischoff, E. D., Schulman, I. G., and Westin, S. K. (2003) *J. Biol. Chem.* **278,** 27703–27711
45. Miyata, M., Matsuda, Y., Tsuchiya, H., Kitada, H., Akase, T., Shimada, M., Nagata, K., Gonzalez, F. J., and Yamazoe, Y. (2006) *Drug Metab. Pharmacokinet.* **21,** 315–323
46. Kaeding, J., Bouchaert, E., Bélanger, J., Caron, P., Chouinard, S., Verreault, M., Larouche, O., Pelletier, G., Staels, B., Bélanger, A., and Barbier, O. (2008) *Biochem. J.* **410,** 245–253
47. Clyne, C. D., Speed, C. J., Zhou, J., and Simpson, E. R. (2002) *J. Biol. Chem.* **277,** 20591–20597
48. Zhou, J., Suzuki, T., Kovacic, A., Saito, R., Miki, Y., Ishida, T., Moriya, T., Simpson, E. R., Sasano, H., and Clyne, C. D. (2005) *Cancer Res.* **65,** 657–663
49. Kovacic, A., Speed, C. J., Simpson, E. R., and Clyne, C. D. (2004) *Mol. Endocrinol.* **18,** 252–259

Journal of Cellular Physiology

A New Role of Anandamide in Human Sperm: Focus on Metabolism

SAVERIA AQUILA,[1,2] CARMELA GUIDO,[1,2] CHIARA LAEZZA,[3] ANTONIETTA SANTORO,[4] VINCENZO PEZZI,[1,5] SALVATORE PANZA,[1,2] SEBASTIANO ANDÒ,[1,2,5] AND MAURIZIO BIFULCO[4]*

[1]*Department of Pharmaco-Biology, University of Calabria, Arcavacata di Rende, Cosenza, Italy*

[2]*Centro Sanitario, University of Calabria, Arcavacata di Rende, Cosenza, Italy*

[3]*Institute of Endocrinology and Experimental Oncology, CNR Napoli, Italy*

[4]*Department of Pharmaceutical Sciences, University of Salerno, Fisciano, Salerno, Italy*

[5]*Faculty of Pharmacy, University of Calabria, Arcavacata di Rende, Cosenza, Italy*

The endocannabinoid system and the presence of CB1 receptor (CB1-R) target of the anandamide were identified in human sperm, however the anandamide action in this context needs to be further elucidated. At this purpose we analyzed the effects of anandamide on human sperm capacitation and motility. Afterwards, we focused on lipid and glucose sperm metabolism and also investigated the interrelationship between anandamide and insulin secretion by sperm. By intracellular free Ca^{2+} content assay and proteins tyrosine phosphorylation, we evidenced that anandamide did not induce capacitation process and a negative effect was obtained on sperm motility. The blockage of CB1-R by the specific antagonist SR141716 increased both capacitation and sperm motility suggesting an involvement of the CB1-R in the acquisition of sperm fertilizing activity. The evaluation of the triglycerides content, lipase and acyl-CoA dehydrogenase activities, suggest that anandamide exerts a lipogenetic effect on human sperm lipid metabolism. Concerning the glucose metabolism, anandamide increases GSK3 phosphorylation indicating that it is involved in the accumulation of energy substrates. G6PDH activity was not affected by anandamide. Interestingly, AEA is involved in insulin secretion by sperm. As insulin had been demonstrated to be an autocrine factor that triggers capacitation, the endocannabinoid might be inserted in the signaling cascade that induces this process. Altogether these findings highlight a pivotal involvement of the CB1-R in the control of sperm energy homeostasis and propose a new site of action for endocannabinoids in the control of energy metabolism.

J. Cell. Physiol. 221: 147–153, 2009.

Cannabinoids are the main constituents of the marijuana plant (*Cannabis sativa*), and it is well known that delta-9-tetrahydrocannabinol, the primary psychoactive substance in marijuana, has marked adverse effects on male and female reproductive systems (Habayeb et al., 2002; Wang et al., 2006). Beside cannabinoids, a family of unsaturated fatty acid derivatives, have been identified and are known as endocannabinoids (ECs); the main ones are anandamide (*N*-arachidonoylethanolamine, AEA), 2-arachidonoylglycerol (2-AG), and 2-arachidonoylglycerylether (noladin ether) (Hanus et al., 1993; Sugiura et al., 1995; Di Marzo et al., 1998, 2004). Cannabinoids and ECs exert their effects through the activation of specific cannabinoid receptors (CB-Rs), the brain-type CB1-R and the spleen-type CB2-R (Devane et al., 1988; Matsuda et al., 1990; Galiegue et al., 1995). CB-Rs are linked to inhibitory and stimulatory guanine nucleotide binding proteins (G_i and G_s proteins) and are widely distributed in many other tissues including placenta, uterus and testis (Schuel et al., 2002; Wang et al., 2006). They regulate several signal-transduction pathways in cells, by modulating ionic currents, activating focal adhesion kinase and mitogen-activated protein kinase (Mackie and Hille, 1992; Bouaboula et al., 1996; Glass and Felder, 1997).

Studies demonstrating the expression of functional CB-Rs in sea urchin sperm, provided the first evidence that cannabinoids could directly affect fertilization (Schuel et al., 1987; Wang et al., 2006). In sea urchin, it has been shown that sperm synthesizes AEA (Bisogno et al., 1997), AEA binds to CB-Rs and reduces fertilizing capacity of sperm (Schuel et al., 1994; Schuel and Burkman, 2005). Human seminal plasma contains nanomolar concentrations of AEA and human sperm expresses CB1-R (Wang et al., 2006). It has been shown that AEA reduces human sperm motility by reducing mitochondrial activity (Rossato et al., 2005). In addition, AEA inhibits acrosome reaction and its effects are prevented by the CB1 antagonist SR141716 (rimonabant, SR) (Rossato et al., 2005; Bifulco et al. 2007). Altogether, these findings suggest that the control of endogenous tone of ECs and its interaction with the CB-Rs are checkpoints in reproduction (Wang et al., 2006). To date the effects of ECs and the role of EC system in male fertility are still largely unexplored.

Abbreviations: 2-AG, 2-arachidonoyl glycerol; AEA, anandamide, *N*-arachidonoylethanolamine; CB-R, cannabinoid receptor; EC, endocannabinoid, Met-F-AEA, 2-methylarachidonyl-2′-fluoro-ethylamide; SR, SR141716, *N*-(piperidino-1-yl)-5-(4-chlorophenyl)-1-(2,4dichlorophenyl)-4-methyl-pyrazole-3-carboxamide; PPP, pentose phasphate pathway.

Contract grant sponsor: MURST (Ex 60%, 2008).
Contract grant sponsor: Associazione Educazione e Ricerca Medica Salernitana (ERMES).

*Correspondence to: Maurizio Bifulco, Via Ponte don Melillo, 84084 Fisciano, Salerno, Italy. E-mail: maubiful@unisa.it

Received 2 April 2009; Accepted 21 April 2009

Published online in Wiley InterScience (www.interscience.wiley.com.), 2 June 2009.
DOI: 10.1002/jcp.21837

In the present study we evaluated the effects of a stable analogue of AEA, Met-F-anandamide (2-methylarachidonyl-2′-fluoro-ethylamide, Met-F-AEA) on different aspects of human sperm biology, such as capacitation and motility. Sperm capacitation, a complex and not well-elucidated series of physiological changes, induces an increase of metabolism and energy expenditure, however the mechanisms through which these events occur are poorly understood (Andò and Aquila, 2005). Interestingly, we focused on lipid and glucose sperm metabolism since it was never investigated, in order to shed light on the possible pathophysiological role of the EC system in male fertility and to correlate the energy metabolism profile of human sperm with EC-induced events. With this respect we also investigated the interrelationship between AEA and insulin secretion by sperm.

Materials and Methods

Chemicals

BSA protein standard, Laemmli sample buffer, prestained molecular weight markers, Percoll (colloidal PVP coated silica for cell separation), Sodium bicarbonate, Sodium lactate, Sodium pyruvate, Earle's balanced salt solution (uncapacitating medium), stable analogue of anandamide, 2-methylarachidonyl-2′-fluoro-ethylamide (Met-F-AEA) and all other chemicals were purchased from Sigma Chemical (Milan, Italy). Acrylamide bisacrylamide was from Labtek Eurobio (Milan, Italy). Triton X-100, Eosin Y was from Farmitalia Carlo Erba (Milan, Italy). ECL Plus Western blotting detection system, Hybond^{TM} ECL^{TM}, Hepes Sodium Salt were purchased from Amersham Pharmacia Biotech (Buckinghamshire, UK). Triglycerides assay kit, lipase activity kit, calcium (Ca^{2+}) assay kit, Glucose-6-phosphate dehydrogenase (G6PDH) activity assay and insulin RIA kit were from Inter-Medical (Biogemina Italia Srl, Catania, Italy). Goat polyclonal actin antibody (Ab), monoclonal mouse anti-p-Tyr Ab, rabbit anti-insulin Ab, peroxidase-coupled anti-mouse, anti-rabbit and anti-goat IgG secondary Abs were from Santa Cruz Biotechnology (Heidelberg, Germany). CB1-R antagonist SR141716 (rimonabant, SR) was kindly provided by Sanofi-Aventis (Montpellier, France).

Semen samples and spermatozoa preparations

Human semen was collected, according to the World Health Organization (WHO) recommended procedure by masturbation from semen samples from healthy volunteer donors of proven fertility undergoing semen analysis in our laboratory. Spermatozoa preparations were performed as previously described (Aquila et al., 2006). Briefly, sperm samples with normal parameters of semen volume, sperm count, motility, vitality and morphology, according to the WHO Laboratory Manual (World Health Organization, 1999), were included in this study. For each experiment three normal samples were pooled. Washed pooled sperm were subjected to the indicated treatments and incubated for 30 min (min) at 37°C and 5% CO_2. Then, samples were centrifuged and the upper phase was used to determinate the insulin levels, while the pellet containing sperm was lysed to perform western blots, triglycerides assay, Ca^{2+} assay, acyl-CoA dehydrogenase assay, G6PDH activity, lipase activity. Prior the centrifugation several aliquots were used to perform sperm motility. The study was approved by the local medical-ethical committees and all participants gave their informed consent. MET-F-AEA was dissolved in ethanol (EtOH), while SR in dimethylsulfoxide (DMSO). EtOH (0.02% final concentration in culture) and DMSO (0.1% final concentration in culture) used as solvent controls did not induce any positive result in all in vitro assays.

Processing of ejaculated sperm

After liquefaction, normal semen samples were pooled and subjected to centrifugation (800 g) on a discontinuous Percoll density gradient (80:40%, v:v) (World Health Organization, 1999). The 80% Percoll fraction was examined using an optical microscope equipped with a 100× oil objective to ensure that a pure sample of sperm was obtained. An independent observer, who observed several fields for each slide, inspected the cells. Percoll-purified sperm was washed with unsupplemented Earle's medium (uncapacitating medium, Earle's balanced salt solution medium without supplementation with BSA sodium bicarbonate or calcium) and were incubated for 30 min at 37°C and 5% CO_2, without (control, NC) or with increasing MET-F-AEA (10 nM, 100 nM, and 1 μM). When the cells were treated with the CB1-R antagonist SR (1 μM), a pre-treatment of 15 min was performed, and then 100 nM MET-F-AEA were added.

Evaluation of Ca^{2+} in sperm

Intracellular Ca^{2+} concentration has been estimated spectrophotometrically with the indicator Arsenazo III using disrupted spermatozoa (Thomson and Wishart, 1989), according to the manufacturer instructions. At a neutral pH, the Ca^{2+} forms with arsenazo III a complex, the color intensity of which is directly proportional to the concentration of Ca^{2+} in the sample. Ca^{2+} content was measured at 600 nm. The Ca^{2+} standard used was 2.5 mM (100 mg/L). Inter- and intra-assay variation were 0.24% and 0.37%. Ca^{2+} results are presented as μM per 10×10^6 number of spermatozoa.

Western blot analysis of sperm proteins

Sperm samples, washed twice with Earle's balanced salt solution (uncapacitating medium), were incubated in the presence and absence of the test substances and then centrifuged for 5 min at 5,000*g*. The pellet was resuspended in lysis buffer as previously described (Aquila et al., 2002). An equal amount of protein (80 μg) were boiled for 5 min, separated on a 10% polyacrylamide gel electrophoresis, transferred to nitrocellulose membranes and probed with an appropriate dilution of the indicated primary antibody. The bound of the secondary antibody was revealed with the ECL Plus Western blotting detection system according to the manufacturer's instructions. As internal control, all membranes were subsequently stripped (glycine 0.2 M, pH 2.6 for 30 min at room temperature) and reprobed with anti-β actin antibody. The protein bands were quantified by scanning densitometry (Imaging Densitometer GS-700 Bio-Rad, Milan, Italy).

Evaluation of sperm motility

Sperm motility was assessed by means of light microscopy examining aliquots of each sperm sample in absence (NC) or in the presence of increasing concentrations of MET-F-AEA (10 nM, 100 nM, and 1 μM). Some samples were treated with 1 μM SR alone or combined with 100 nM MET-F-AEA. A blinded observer scored at least 200 cells. Sperm motility was expressed as percentage of total motile sperm.

Triglycerides assay

Triglycerides were measured in duplicate by a GPO-POD enzymatic colorimetric method according to manufacturer's instructions in sperm lysates and as previously described (Aquila et al., 2006). Sperm samples, washed twice by centrifugation with uncapacitating medium, were incubated in the same medium (control) for 30 min at 37°C and 5% CO_2. Other samples were incubated in the presence of the indicated treatments. At the end of the sperm incubation 10 μl of lysate were added to the 1 ml of buffer reaction and incubated for 10 min at room temperature. Then the triglycerides content was measured at 505 nm by using a spectrophotometer. Data are presented as μg/10^6 sperms.

Assay of acyl-CoA dehydrogenase activity

Assay of acyl-CoA dehydrogenase was performed on sperm, using a modification of the method described by Lehman et al. (1990). In brief, after protein lysis, 70 μg of sperm proteins were added to the buffer containing 20 mM Mops, 0.5 mM EDTA, and 100 μM FAD^+ at pH 7.2. Reduction of FAD^+ to FADH was read at 340 nm upon addition of octanoyl-CoA (100 μM) every 20 sec for 1.5 min. Data are expressed as nmol/min/mg protein. The enzymatic activity was determined with three control media: one without octanoyl-CoA as substrate, one without the coenzyme (FAD^+), and the third without either substrate or coenzyme (data not shown).

Lipase activity assay

Lipase activity was evaluated, by the method of Panteghini (Panteghini et al., 2001) based on the use of 1,2-*o*-dilauryl-rac-glycero-3-glutaric acid-(6′-methylresorufin) ester (DGGR) as substrate. Fifty micrograms of sperm extracts were loaded into individual cuvettes containing buffer for spectrophotometric determination. DGGR is cleaved by lipase, resulting in an unstable dicarbonic acid ester which is spontaneously hydrolyzed to yield glutaric acid and methylresorufin, a bluish-purple chromophore with peak absorption at 580 nm. The absorbance of samples was read every 20 sec for 1.5 min. The rate of methylresorufin formation is directly proportional to the lipase activity in the sample. Analysis of total imprecision gave a coefficient of variation of between 0.01% and 0.03%. The estimated reference interval was 6-38 U/L (μmol/min/mg protein). The enzymatic activity was determined with three control media: one without the substrate, one without the co-enzyme (colipase) and the third without either substrate or co-enzyme (data not shown).

G6PDH activity

The conversion of $NADP^+$ to NADPH, catalyzed by G6PDH, was measured by the increase of absorbance at 340 nm. Sperm samples, washed twice with uncapacitating medium, were incubated in the same medium (control) for 30 min at 37°C and 5% CO_2. Sperm samples, washed twice with uncapacitating medium, were incubated in the same medium (control) or in capacitating medium for 30 min at 37°C and 5% CO_2. Other samples were incubated in the presence of the indicated treatments. After incubation, 50 μl of sperm extracts were loaded into individual cuvettes containing buffer (100 mM triethanolamine, 100 mM $MgCl_2$, 10 mg/ml glucose-6-phosphate, 10 mg/ml $NADP^+$, pH 7.6) for spectrophotometric determination. The absorbance of samples was read at 340 nm every 20 sec for 1.5 min. Data are expressed in nmol/min/10^6 sperms. The enzymatic activity was determined with three control media: one without glucose-6-phosphate as substrate, one without the coenzyme ($NADP^+$), and the third without either substrate or coenzyme (data not shown).

Measurement of insulin secreted by human spermatozoa

A competitive RIA was applied to measure insulin in the sperm culture medium. Spermatozoa were washed twice with unsupplemented Earle's medium and incubated in the same medium for 30 min at 37°C in 5% CO_2. A final concentration of 10×10^6 sperm/500 ml was used. Sperm were treated with 10 nM, 100 nM, and 1 μM MET-F-AEA. Some samples treated with 1 μM SR alone or combined with 100 nM MET-F-AEA.

At the end of the sperm incubations, the culture media were recovered by centrifugation. Human insulin concentrations were determined in duplicate using an insulin RIA kit according to manufacturer's instructions. Insulin standards ranged from 0 to 300 μIU/ml. The limit of sensitivity for the assay was 0.01 μIU/ml. Inter- and intraassay variations were 4.4% and 5.1%, respectively.

Insulin results are presented as the original concentrations of the supernatants and are expressed as micro international units per milliliter.

Statistical analysis

The experiments for Western blot analysis were performed in at least four independent experiments. The data obtained from Ca^{2+} assay, Triglycerides Assay, G6PDH activity, acyl-CoA dehydrogenase activity, lipase activity, insulin assay, acrosin activity and motility (six replicate experiments using duplicate determinations), were presented as the mean ± SEM. The differences in mean values were calculated using analysis of variance (ANOVA) with a significance level of $P \leq 0.05$.

Results

MET-F-AEA effects on intracellular free Ca^{2+} content and on tyrosine phosphorylation of the proteins in human sperm

A first functional assessment of the sperm biological activities under increasing MET-F-AEA concentrations was performed on the capacitation process. To evaluate whether AEA was able to influence the sperm extratesticular maturation, we studied its potential action on intracellular free Ca^{2+} content and proteins tyrosine phosphorylation. Recently, it was demonstrated that internal sperm Ca^{2+} stores provide sufficient Ca^{2+} for the induction of hyperactivated motility (Kong et al., 2007), which is indicative of the capacitation status. It appears that 100 nM MET-F-AEA were able to produce an increase in the intracellular free Ca^{2+} while 10 nM and 1 μM did not (Fig. 1A). Surprisingly, the combined treatment of MET-F-AEA with 1 μM of the CB1-R antagonist SR, significantly increased the Ca^{2+} content.

Human sperm capacitation is correlated with an augment in intracellular cAMP levels that in turn induces an increase in tyrosine phosphorylation of a variety of substrates, while the AEA generally inhibits adenylate cyclase activity (Bifulco and Di Marzo, 2002). In order to assess this issue, the status of the proteins phosphorylation was investigated in human sperm after the treatment with increasing MET-F-AEA. A significant decrease in the sperm proteins phosphorylation (Fig. 1B) was observed by using different MET-F-AEA doses, while the treatment with 100 nM MET-F-AEA plus 1 μM SR induced a significant increase of tyrosine phosphorylated proteins.

MET-F-AEA has the ability to modulate human sperm motility

Motility is a critical sperm biological function that at the time of fertilization allows or at least facilitates passage of the sperm through the zona pellucida. A non-motile or abnormally motile sperm is not going to fertilize. Hence, assessing the fraction of a sperm population that is motile is perhaps the most widely used measure of semen quality. In our experiments, sperm motility decreased from 10 to 100 nM MET-F-AEA in a dose-dependent manner (Fig. 2), while it was enhanced by using 1 μM SR plus 100 nM MET-F-AEA.

MET-F-AEA effects on the triglycerides content in human sperm

During sperm extra-testicular maturation an overall increase in sperm metabolism occurs, however, the mechanisms that govern this event are still poorly understood. MET-F-AEA in somatic cells is an important lipid metabolism regulator (Wang et al., 2006) and in sperm its role in this issue was never evaluated. We first investigated triglycerides intracellular content. As shown in Figure 3, MET-F-AEA was able to significantly increase the triglycerides content and the

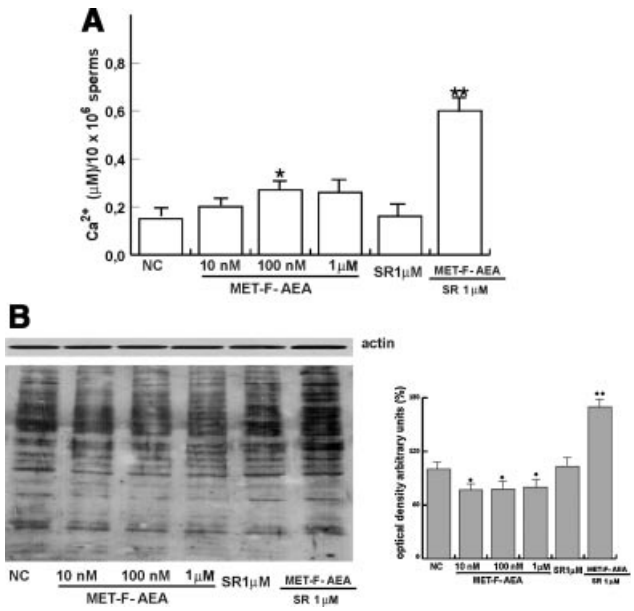

Fig. 1. MET-F-AEA influences free intracellular Ca^{2+} and protein tyrosine phosphorylations in sperm. Washed spermatozoa were incubated in the unsupplemented Earle's medium for 30 min at 37°C and 5% CO_2, in the absence (NC) or in the presence of increasing MET-F-AEA concentrations (10 nM, 100 nM, and 1 μM). Some samples were treated with 1 μM SR alone or combined with 100 nM MET-F-AEA. A: Free intracellular calcium was measured as reported in Materials and Methods Section. Columns represent mean ± SEM $^{*}P < 0.05$ versus control, $^{**}P < 0.02$ versus control. B: Eighty micrograms of sperm lysates were used for Western blot analysis performed to determine protein tyrosine phosphorylations. Actin was used as a loading control. On the right, quantitative representation after densitometry evaluation of the 95-kDa band. Autoradiograph presented is a representative example of experiments that were performed at least four times with repetitive results. $^{*}P < 0.05$ versus control, $^{**}P < 0.01$ versus control.

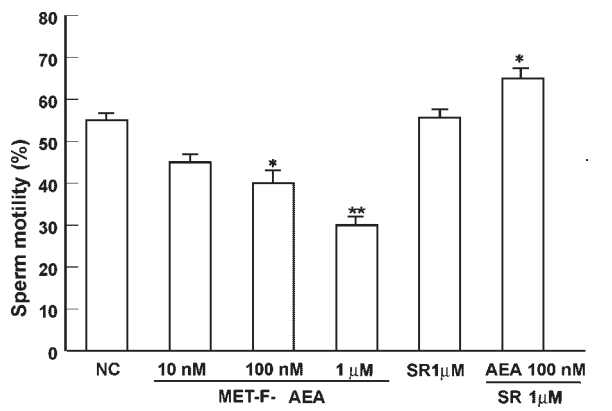

Fig. 2. MET-F-AEA effects on sperm motility. Washed spermatozoa were incubated in the unsupplemented Earle's medium for 30 min at 37°C and 5% CO_2, in the absence (NC) or in the presence of increasing MET-F-AEA concentrations (10 nM, 100 nM, and 1 μM). Some samples were treated with 1 μM SR alone or combined with 100 nM MET-F-AEA. Sperm motility was assessed as reported in Materials and Methods Section. Columns represent mean ± SEM. Data are expressed as % of sperm motility $^{*}P < 0.05$ versus control; $^{**}P < 0.02$ versus control.

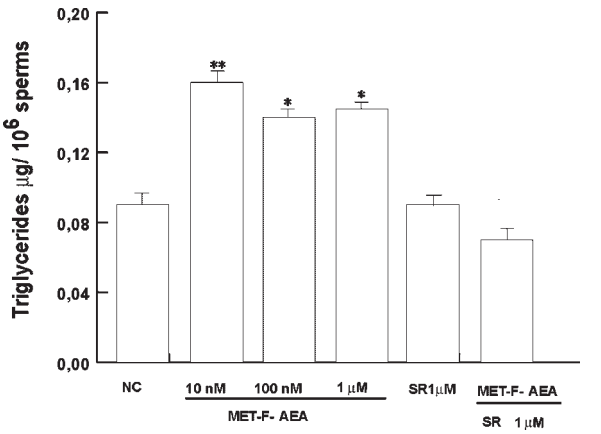

Fig. 3. MET-F-AEA effects on the triglycerides content in human sperm. Washed spermatozoa were incubated in the unsupplemented Earle's medium for 30 min at 37°C and 5% CO_2, in the absence (NC) or in the presence of increasing MET-F-AEA concentrations (10 nM, 100 nM, and 1 μM). Some samples were treated with 1 μM SR alone or combined with 100 nM MET-F-AEA. Triglycerides content was measured as reported in Materials and Methods Section. Columns represent mean ± SEM. $^{*}P < 0.05$ versus control, $^{**}P < 0.02$ versus control.

combination with SR was able to attenuate the effect of MET-F-AEA.

MET-F-AEA effects on acyl-CoA dehydrogenase and lipase activities

To further investigate the role of AEA in sperm lipid metabolism, we evaluated both acyl-CoA dehydrogenase and lipase activities. It appears that MET-F-AEA treatment alone did not produce effects on lipase activity (Fig. 4A) as well as on β-oxidation of the fatty acids (Fig. 4B). Interestingly, the combined treatment of 100 nM MET-F-AEA plus 1 μM SR increased both fatty acids-β oxidation and lipase activity.

MET-F-AEA effects on sperm glucose metabolism

It was recently demonstrated that human sperm express the GSK-3 and that the enzymatic activity is higher in uncapacitated than in capacitated sperm (Aquila et al., 2005a). In the present study, MET-F-AEA induced a dose-dependent increase in the GSK3 phosphorylation (Fig. 5A).

To gain insight into the MET-F-AEA regulation of sperm glucose metabolism we evaluated the G6PDH activity upon increasing MET-F-AEA concentrations. G6PDH, the rate-limiting enzyme in the pentose phosphate pathway (PPP), has been shown to be crucial in the acquisition of fertilizing capability as well as to mediate gamete fusion (Aquila et al., 2005b). From our results it emerges that MET-F-AEA was unable to significantly induce G6PDH activity (Fig. 5B).

MET-F-AEA effects on insulin secretion by sperm

In mouse pancreatic β-cells, cannabinoids inhibit insulin secretion via CB1-R (Nakata and Yada, 2008). In our recent study, we had shown that insulin is expressed in and secreted from human ejaculated spermatozoa, leading us to suppose an autocrine regulation of glucose metabolism according to the sperm energetic needs independently of the systemic insulin (Aquila et al., 2005b). In our cellular type, MET-F-AEA induced a very weak dose-dependent increase in insulin secretion reaching a maximal level of 0.6 μIU/ml of the hormone

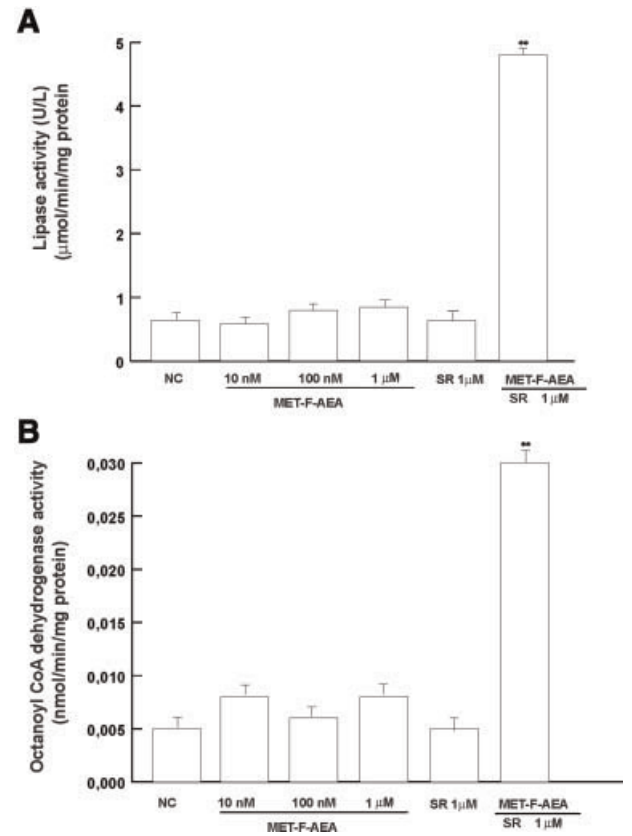

Fig. 4. MET-F-AEA effects on acyl-CoA dehydrogenase and lipase activities. Washed spermatozoa were incubated in the unsupplemented Earle's medium for 30 min at 37°C and 5% CO_2, in the absence (NC) or in the presence of increasing MET-F-AEA concentrations (10 nM, 100 nM, and 1 μM). Some samples were treated with 1 μM SR alone or combined with 100 nM MET-F-AEA. A: Lipase activity and (B) octanoyl-CoA dehydrogenase activity were performed as reported in Materials and Methods Section. Columns represent mean ± SEM. $^{**}P < 0.01$ versus control.

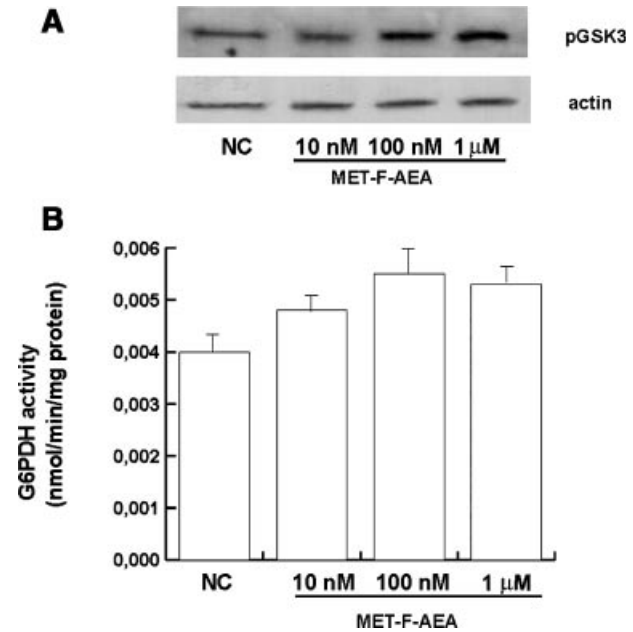

Fig. 5. MET-F-AEA effects on sperm glucose metabolism. Sperm samples, washed twice with uncapacitating medium, were incubated in the same medium (control) for 30 min at 37°C and 5% CO_2. A: Western blotting evaluating GSK3 phosphorylation. Actin was used as a loading control. Autoradiograph presented is a representative example of experiments that were performed at least four times with repetitive results. B: G6PDH activity was performed as reported in Materials and Methods Section. Columns represent mean ± SEM. $^{***}P < 0.01$ versus control.

concentration (Fig. 6A). These results indicate that in sperm, similarly to the endocrine pancreatic cells, CB1-R is involved in modulating insulin secretion. We also performed insulin western blot on sperm lysates to evidence that the increase in insulin secretion is related to a decrease in insulin sperm content (Fig. 6B).

Discussion

The EC system first emerged as a major neuromodulatory system in the brain, however, it has also been shown to play an important role in various peripheral organs, including testis. Recently, EC system was identified in boar sperm and CB1-R was demonstrated in human sperm (Rossato et al., 2005), suggesting a possible physiological role of the AEA in controlling male fertility. In our study, we evidenced the AEA role in different aspects of sperm biology, such as capacitation and motility. Particularly, we focused our researches on lipid and glucose metabolism and we also evaluated AEA action on insulin secretion by sperm.

The physiological changes that confer to the sperm the ability to fertilize a metaphase II-arrested egg are collectively called "capacitation." This extratesticular maturation is a complex process and a functional change that involves different sperm activities. During capacitation, spermatozoa become responsive to the stimuli that induce the acrosome reaction and prepare the male gamete to the penetration of the egg investments prior fertilization. Many gaps exist in our knowledge on the capacitation at molecular levels. It appears that the process involves modifications of intracellular Ca^{2+}, lipid remodeling in sperm plasma membrane as well as changes in proteins phosphorylation. Therefore, we first aimed to evaluate AEA action in some events that characterize the capacitation process, such as intracellular Ca^{2+} levels and tyrosine phosphorylation of sperm proteins.

Ca^{2+} signaling in sperm is critical for fertilization and recently it was demonstrated that internal Ca^{2+} stores provide sufficient Ca^{2+} for the induction of motility hyperactivation, whereas Ca^{2+} influx is required to maintain intracellular Ca^{2+} levels to sustain hyperactivation (Florman et al., 1998; Suarez and Ho, 2003). From our results it emerges that MET-F-AEA is able to slightly increase free intracellular Ca^{2+} levels and the inactivation of the CB1-R significantly enhanced this effect suggesting that the CB1-R status is implicated in the regulation of intracellular free Ca^{2+} and then in the induction of hyperactivated motility. Our data are not in agreement with previous studies concerning the AEA effects on Ca^{2+} levels in sperm (Rossato et al., 2005), however we may to take into account that different method and medium were used.

It has been demonstrated that proteins tyrosine phosphorylation is tightly associated to the initial stage the capacitation process (Visconti et al., 1995a,b). In somatic cells a major CB1-R-dependent signaling pathway involves the down-regulation of adenylate cyclase activity (Bifulco and Di Marzo, 2002). In our study, MET-F-AEA decreases sperm proteins tyrosine phosphorylation, while this effect was prevented by the CB1-R antagonist SR, leading to the

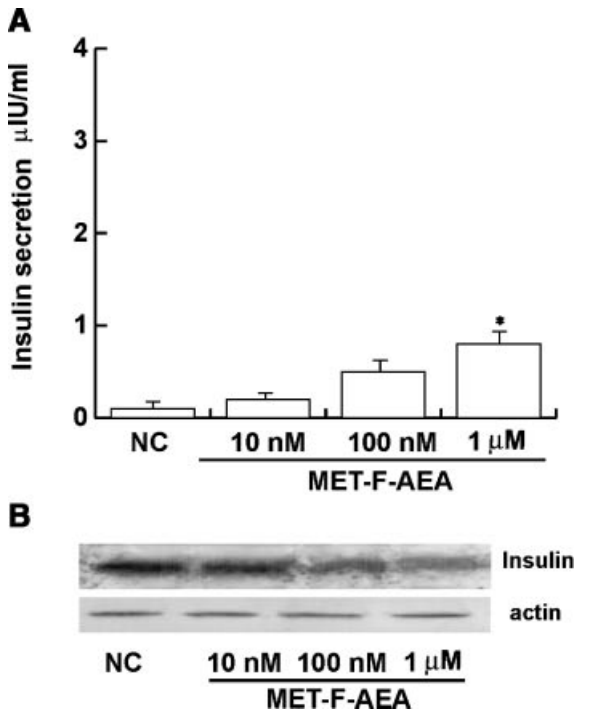

Fig. 6. MET-F-AEA effects on insulin secretion by sperm. Spermatozoa were washed twice with unsupplemented Earle's medium and incubated in the same medium for 30 min at 37 C in 5%CO_2. A final concentration of 10×10^6 sperm/500 ml was used. Sperm were treated with 10 nM, 100 nM, and 1 μM MET-F-AEA. At the end of the sperm incubations, the culture media were recovered by centrifugation. A: Human insulin concentrations were determined in duplicate using an insulin RIA kit according to manufacturer's instructions. Columns represent mean ± SEM, $^*P < 0.05$ versus control, $^{***}P < 0.01$ versus control. B: Western blotting to evaluate insulin inside sperm after the indicated treatment. Actin was used as a loading control. Autoradiograph presented is a representative example of experiments that were performed at least four times with repetitive results.

suggestion that this receptor is involved in the modulation of an important early event of the capacitation process. These results are in keeping with previous data demonstrating that the inhibitory effect of AEA on capacitation depends on its ability to reduce intracellular levels of cAMP (Bifulco and Di Marzo, 2002).

Sperm cell features comprise a high polarization of structure and functions, including motility that is a crucial requisite for the male gamete to reach the oocyte. In our study we observed that AEA induces a dose-dependent reduction of sperm motility and that SR was able to significantly enhance this effect addressing an important role of CB1-R in this sperm function. Our results confirm those of previous studies reporting that AEA negatively affects human sperm motility (Rossato et al., 2005). However, it deserves to be mentioned that different concentrations were used in our finding, in fact we have chosen the nanomalar doses of 10 nM to mimic the AEA levels observed in human seminal plasma (12.3 nM) and in mid-cycle oviductal fluid (10.5 nM) (Schuel et al., 2002), while 100 nM and 1 μM are supraphysiological levels. Particularly, we would like to point out that the spermatozoa used in our experiments are washed from seminal plasma and then they are deprived of the decapacitating factors, reproducing in some manner the sperm physiological conditions as they have in the female genital tract.

The mechanisms controlling the interaction between energy balance and reproduction are the subject of intensive investigations. Capacitated sperm display an increased metabolic rate and overall energy expenditure, presumably to affect the changes in sperm signaling and function during capacitation process. The EC system has been recognized as a new crucial player in energy balance control. In general the net effect at diverse sites in the brain and throughout the body is anabolic, facilitating increased energy intake, decreased energy expenditure and increased accumulation of body fat. An increase of the EC tone has been reported in the hypothalamus of obese animals and the administration of ECs has been shown to increase food intake and to promote weight gain (Després, 2007). In white adipocytes, CB1-R activation stimulates lipogenesis, while in contrast, CB1-R antagonists in vitro and in vivo reduce the expression of enzymes involved in lipogenesis (Pagotto et al., 2005). Similarly, MET-F-AEA seems to exert a lipogenetic effect on human sperm lipid metabolism, since the augment in the triglycerides content is compatible with the behavior of both lipase and acyl-CoA dehydrogenase activities. Our data clearly evidenced that the blockage of CB1-R induces an increase in the energy expenditure, corroborating the idea that the receptor activation in sperm is related to the uncapacitated status.

In the majority of the experiments performed, the 1 μM SR alone displayed a neutral antagonism, while in combination with MET-F-AEA it behaves as inverse agonist. SR has been shown to act as neutral antagonism, competitive antagonist and inverse agonist in host cells transfected with exogenous CB1 receptor, as well as in biological preparations endogenously expressing CB1 (Hurst et al., 2005; Pertwee, 2005). As inverse agonist, SR produces effects in some CB1 containing bioassay systems that are opposite in direction from those produced by agonists for these receptors. It was proposed that inverse agonism at the CB1 receptor may be explained in terms of a three-state model in which the receptor can switch between two receptor conformational states, a ground or inactive R state and an active R^* state, which are in equilibrium with each other (Leff, 1995). An agonist has higher affinity for R^* and agonist binding is thought to shift the equilibrium toward R^*, resulting in G protein activation with an increase in GDP/GTP exchange. An inverse agonist has higher affinity for R and its binding shifts the equilibrium toward R, resulting in a decrease in the activation of the signaling pathway. The binding of a neutral/null antagonist is thought not to alter the equilibrium between R and R^* because the neutral antagonist has equal affinity for both states. It is likely that the efficacy for the production of inverse cannabimimetic effects will be governed by the degree of ongoing endocannabinoid release onto CB1 receptors.

In our previous study, we demonstrated that sperm express and secrete insulin, the classical hormone involved in the body energy homeostasis (Aquila et al., 2005b). Moreover in uncapacitated sperm, insulin increased GSK-3 S9 phosphorylation, while during capacitation the kinase is not phosphorylated. These results suggested that the hormone modulates sperm energetic substrates availability on the basis of sperm energy needs (Ballester et al., 2000). We observed that under MET-F-AEA, GSK3 phosphorylation increases indicating that the endocannabinoid in uncapacitated sperm is involved in the accumulation of energy substrates, which would be spent during capacitation and thus mirroring the insulin behavior in this context. In fact, in uncapacitated sperm the GSK3 is tightly blocked, whereas during capacitation there is an activation of the enzyme. Intriguingly, glycogen deposits and GSK3 enzyme are present in the head and midpiece of spermatozoa where CB1-R is also localized and this support a physiological relevance of our finding. Although glycolysis is important for sperm functions this metabolic pathway does not appear to be responsible for successful gamete fusion (Urner and Sakkas,

1996; Travis et al., 2001). Instead, the beneficial effect of glucose on the acquisition of fertilizing ability as well as on gamete fusion is mediated by glucose metabolism through the PPP (Urner and Sakkas, 1999a; Urner et al., 2001) where G6PDH is the key rate limiting enzyme that regulates the production of NADPH (Urner and Sakkas, 1999b). Accordingly, with the above-mentioned results on GSK3, MET-F-AEA was unable to significantly increase the G6PDH activity.

In our previous study we have showed that sperm express and secrete insulin and we have demonstrated that a great difference in insulin secretion between incapacitated and capacitated sperm exists, therefore relating the hormone concentration to the different gamete physiological conditions. In mouse pancreatic islets it was shown that cannabinoids inhibit insulin secretion via CB1-R (Nakata and Yada, 2008). From the present work it emerges that MET-F-AEA induce an increase in insulin secretion, although the concentrations obtained are comprised in the typical range showed by sperm during uncapacitated status (0.1–0.73 μIU/ml). Insulin secretion is significantly higher in sperm during capacitation (4–12 μIU/ml), Our previous data lead us to speculate that insulin might be considered an endogenous factor involved in the autocrine induction of the capacitation, here we found that MET-F-AEA is able to modulate insulin secretion, therefore the EC could be considered a regulator of the capacitation process. On the other hand, the presence of AEA at higher concentration in seminal plasma prevents premature capacitation activating CB1-R, instead in the female genital tract spermatozoa are exposed to a progressively reduced concentration of AEA (Schuel et al., 2002) and sperm capacitation might occur as a consequence of reduced action of AEA on CB1-R. These observations, together with our findings, raise the possibility that defective AEA-signaling may likewise impair sperm acquisition of fertilizing ability and thus male fertility.

Apart from classical hormones like leptin and insulin, the AEA ability to modulate both lipid and glucose metabolism highlights also a pivotal involvement of this EC in the control of sperm energy homeostasis. Concluding, the present finding discovered a new site of action for ECs in the control of energy metabolism.

Acknowledgments

Our special thanks to Dr. Vincenzo Cunsolo (Biogemina SAS, Catania, Italy) for the technical and scientific assistance. We also thank Serena and Maria Clelia Gervasi for the English language review of the manuscript. This work was supported by MURST - Ex 60% -2008, and Associazione Educazione e Ricerca Medica Salernitana (ERMES).

Literature Cited

Andò S, Aquila S. 2005. Arguments raised by the recent discovery that insulin and leptin are expressed in and secreted by human ejaculated spermatozoa. Mol Cell Endocrinol 245:1–6.

Aquila S, Sisci D, Gentile M, Middea E, Siciliano L, Andò S. 2002. Human ejaculated spermatozoa contain active P450 aromatase. J Clin Endocrinol Metab 87:3385–3390.

Aquila S, Gentile M, Middea E, Catalano S, Morelli C, Pezzi V, Andò S. 2005a. Leptin Secretion by Human Ejaculated Spermatozoa. J Clin Endocrinol Metab 90:4753–4761.

Aquila S, Gentile M, Middea E, Catalano S, Andò S. 2005b. Autocrine regulation of insulin secretion in human ejaculated spermatozoa. Endocrinology 146:552–557.

Aquila S, Bonofiglio D, Gentile M, Middea E, Gabriele S, Belmonte M, Catalano S, Pellegrino M, Ando S. 2006. Peroxisome proliferator-activated receptor (PPAR)gamma is expressed by human spermatozoa: Its potential role on the sperm physiology. J Cell Physiol 209:77–986.

Ballester J, Fernandez-Novell JM, Rutllant J, Garcia-Rocha M, Jesus Palomo M, Mogas T, Pena A, Rigau T, Guinovart JJ, Rodriguez-Gil JE. 2000. Evidence for a functional glycogen metabolism in mature mammalian spermatozoa. Mol Reprod Dev 56:207–219.

Bifulco M, Di Marzo V. 2002. Targeting the endocannabinoid system in cancer therapy: A call for further research. Nat Med 8:547–550.

Bifulco M, Grimaldi C, Gazzerro P, Pisanti S, Santoro A. 2007. "Rimonabant: Just an antiobesity drug? Current evidence on its pleiotropic effects". Mol Pharmacol 71:1445–1456.

Bisogno T, Ventriglia M, Milone A, Mosca M, Cimino G, Di Marzo V. 1997. Occurrence and metabolism of anandamide and related acyl-ethanolamides in ovaries of the sea urchin Paracentrotus lividus. Biochim Biophys Acta 1345:338–348.

Bouaboula M, Poinot-Chazel C, Marchand J, Canat X, Bourrie B, Rinaldi-Carmona M, Calandra B, Le Fur G, Casellas P. 1996. Signaling pathway associated with stimulation of CB2 peripheral cannabinoid receptor. Involvement of both mitogen-activated protein kinase and induction of Krox-24 expression. Eur J Biochem 237:704–711.

Després JP. 2007. The endocannabinoid system: A new target for the regulation of energy balance and metabolism. Crit Pathw Cardiol 6:46–50.

Devane WA, Dysarz FA, Johnson MR, Melvin LS, Howlett AC. 1988. Determination and characterization of a cannabinoid receptor in rat brain. Mol Pharmacol 34:605–613.

Di Marzo V, Melck D, Bisogno T, De Petrocellis L. 1998. Endocannabinoids: Endogenous cannabinoid receptor ligands with neuromodulatory actions. Trends Neurosci 21:521–528.

Di Marzo V, Bifulco M, De Petrocellis L. 2004. The endocannabinoid system and its therapeutic exploitation. Nat Rev Drug Discov 3:771–784.

Florman HM, Arnoult C, Kazam IG, Li C, O'Toole CM. 1998. A perspective on the control of mammalian fertilization by egg-activated ion channels in sperm: A tale of two channels. Biol Reprod 59:12.

Galiegue S, Mary S, Marchand J, Dussossoy D, Carriere D, Carayon P, Bouaboula M, Shire D, Le Fur G, Casellas P. 1995. Expression of central and peripheral cannabinoid receptors in human immune tissues and leukocyte populations. Eur J Biochem 232:54–61.

Glass M, Felder CC. 1997. Concurrent stimulation of cannabinoid CB1 and dopamine D2 receptors augments cAMP accumulation in striatal neurons: Evidence for a Gs linkage to the CB1 receptor. J Neurosci 17:5327–5333.

Habayeb OMH, Bell SC, Konje JC. 2002. Endogenous cannabinoids: Metabolism and their role in reproduction. Life Sci 70:1963–1977.

Hanus L, Gopher A, Almong S, Mechoulam R. 1993. Two neu unsaturated fatty acid ethanolamides in brain that bind to the cannabinoid receptor. J Med Chem 36:3032–3034.

Hurst DP, Lynch DL, Barnett-Norris J, Hyatt SM, Seltzman HH, Zhong M, Song Z, Nie J, Lewis D, Reggio PH. 2005. N-(Piperidin-1-yl)-5-(4-chlorophenyl)-1-(2,4-dichlorophenyl)-4-methyl-1H-pyrazole-3-carboxamide (SR141716A) interaction with LYS 3.28(192) is crucial for its inverse agonism at the cannabinoid CB1 receptor. Mol Pharmacol 62:1274–1287.

Kong LJ, Yang YY, Wang GL. 2007. CatSper and sperm hyperactivation. Zhonghua Nan Ke Xue 13:164–167.

Leff P. 1995. The two-state model of receptor activation. Trends Pharmacol Sci 16:89–97.

Lehman TC, Hale DE, Bhala A, Thorpe C. 1990. An acyl-coenzyme A dehydrogenase assay utilizing the ferricenium ion. Anal Biochem 186:280–284.

Mackie K, Hille B. 1992. Cannabinoids inhibit N-type calcium channels in neuroblastoma-glioma cells. Proc Natl Acad Sci USA 89:3825–3829.

Matsuda LA, Lolait SJ, Brownstein MJ, Young AC, Bonner TI. 1990. Structure of a cannabinoid receptor and functional expression of the cloned cDNA. Nature 346:561–564.

Nakata M, Yada T. 2008. Cannabinoids inhibit insulin secretion and cytosolic Ca2+ oscillation in islet beta-cells via CB1 receptors. Regul Pept 14:49–53.

Pagotto U, Vicennati V, Pasquali R. 2005. The endocannabinoid system and the treatment of obesity. Ann Med 37:270–275.

Panteghini M, Bonora R, Pagani F. 2001. Measurement of pancreatic lipase activity in serum by a kinetic colorimetric assay using a new chromogenic substrate. Ann Clin Biochem 38:365–370.

Pertwee RG. 2005. Inverse agonism and neutral antagonism at cannabinoid CB1 receptors. Life Sci 76:1307–1324.

Rossato M, Ion Popa F, Ferigo M, Clari G, Foresta C. 2005. Human sperm express cannabinoid receptor Cb1, the activation of which inhibits motility, acrosome reaction, and mitochondrial function. J Clin Endocrinol Metab 90:984–991.

Schuel H, Burkman LJ. 2005. A tale of two cells: Endocannabinoid-signaling regulates functions of neurons and sperm. Biol Reprod 73:1078–1086.

Schuel H, Schuel R, Zimmerman AM, Zimmerman S. 1987. Cannabinoids reduce fertility of sea urchin sperm. Biochem Cell Biol 65:130–136.

Schuel H, Goldstein E, Mechoulam R, Zimmerman AM, Zimmerman S. 1994. Anandamide (arachidonylethanolamide), a brain cannabinoid receptor agonist, reduces sperm fertilizing capacity in sea urchins by inhibiting the acrosome reaction. Proc Natl Acad Sci USA 91:7678–7682.

Schuel H, Burkman LJ, Lippes J, Crickard K, Mahony MC, Giuffrida A, Picone RP, Makriyannis A. 2002. Evidence that Anandamide-signaling regulates human sperm functions required for fertilization. Mol Reprod Dev 63:376–387.

Suarez SS, Ho HC. 2003. Hyperactivation of mammalian sperm. Cell Mol Biol 49:351–356.

Sugiura T, Kondo S, Sukagawa A, Nakane S, Shinoda A, Itoh K, Yamashita A, Waku K. 1995. 2-Arachidonoyl-glycerol: A possible endogenous cannabinoid receptor ligand in brain. Biochem Biophys Res Commun 215:88–97.

Thomson MF, Wishart GJ. 1989. Elucidation of the mechanism responsible for the temperature-dependent reversible inactivation of the motility of fowl spermatozoa. Br Poult Sci 30:687–692.

Travis AJ, Jorgez CJ, Merdiushev T, Jones BH, Dess DM, Diaz-Cueto L, Storey BT, Kopf GS, Moss SB. 2001. Functional relationships between capacitation-dependent cell signaling and compartmentalized metabolic pathways in murine spermatozoa. J Biol Chem 276:7630–7636.

Urner F, Sakkas D. 1996. Glucose is not essential for the occurrence of sperm binding and zona pellucida-induced acrosome reaction in the mouse. Int J Androl 19:91–96.

Urner F, Sakkas D. 1999a. Characterization of glycolysis and pentose phosphate pathway activity during sperm entry into the mouse oocyte. Biol Reprod 60:973–978.

Urner F, Sakkas D. 1999b. A possible role for the pentose phosphate pathway of spermatozoa in gamete fusion in the mouse. Biol Reprod 60:733–739.

Urner F, Leppens-Luisier G, Sakkas D. 2001. Protein tyrosine phosphorylation in sperm during gamete interaction in the mouse: The influence of glucose. Biol Reprod 64:1350–1357.

Visconti PE, Baley JL, Moore GD, Pan D, Olds-Clarke P, Kopf GS. 1995a. Capacitation in mouse spermatozoa I. Correlation between the capacitation state and protein phosphorylation. Development 121:1129–1137.

Visconti PE, Moore GD, Bailey JL, Leclerc P, Connors SA, Pan D, Olds-Clarke P, Kopf GS. 1995b. Capacitation of mouse spermatozoa. II. Protein tyrosine phosphorylation and capacitation are regulated by a cAMP-dependent pathway. Development 121:1139–1150.

Wang H, Dey SK, Maccarrone M. 2006. Jekill and Hyde: Two faces of cannabinoid signaling in male and female fertility. Endo Rev 27:427–448.

World Health Organization. 1999. Laboratory manual for the examination of human semen and sperm-cervical mucus interactions. 4th edition. Cambridge, UK: Cambridge University Press.